Endocytosis and Trafficking of Polymer Therapeutics in Melanoma Cells

Friedrich Philipp Seib

BPharm (Hons), MSc (Hons), MRPharmS

A thesis submitted to Cardiff University in partial fulfilment of the requirements for the degree of Doctor of Philosophy

Centre for Polymer Therapeutics, Welsh School of Pharmacy

Cardiff University

United Kingdom

ProQuest LLC
789 East Eisenhower Parkway
P.O. Box 1346
Ann Arbor, MI 48106-1346

DECLARATION

This work has not previously been accepted in substance for any degree and is not being concurrently submitted in candidature for any degree.

Signed ..... (candidate)

Date .....7/3/05.....

STATEMENT 1

This thesis is the result of my own investigations, except where otherwise stated. Other sources are acknowledged by footnotes giving explicit references. A bibliography is appended.

Signed ..... (candidate)

Date .....7/3/05.....

STATEMENT 2

I hereby consent for my thesis, if accepted, to be available for photocopying and for inter-library loan, and for the title and summary to be made available to outside organisations.

Signed ..... (candidate)

Date .....7/3/05.....

Für meine Eltern und Geschwister

Acknowledgements

First and foremost I would like to thank my supervisor Prof. Ruth Duncan for her continued support, guidance, encouragement and enthusiasm over the past three years, which has shaped the research presented in this thesis. I also would like to thank Dr. Arwyn Jones for his tireless enthusiasm for this project, besides valuable suggestions to the thesis manuscript. I also want to thank Prof. Helmut Ringsdorf for his continued encouragement during the PhD.

Over the past three years many members at the Centre for Polymer Therapeutics and Cardiff University past and present have offered valuable advice, support and assistance and my thanks goes to all of them. Special thanks go to Dr. Maria Vicent for her endless optimism and encouragement with the chemistry. I am also in debt to Dr. Nicky Pattrick for introducing me to tissue culture and practical aspects of subcellular fractionation. I also extend my gratitude to Dr. Myrto Lee, Dr. Dirk Schmaljohann, Dr. Lorella Izzo, Dr. Maria Manunta, Dr. Vivian Diamanti, Dr. Ka-Wai Wan, Saly Al-Taei and Zeena Khayat who advised and introduced me to various aspects of the work presented in this thesis and showed me the ropes at CPT.

I also would like to thank Michelle Lazenby and Dr. Janette Davidge for the continued support and smooth running of the laboratory. I also extend my gratitude to Wendy Meeson for proof reading the manuscript. The Akademie der Wissenschaften und der Literatur, Mainz Germany and Cardiff University are gratefully acknowledged for their financial support.

Finally, I would like to thank my "old" and "new" personal friends, in particular Francesca Greco, Tom Kean, Lucile Dieudonne and Karen Phelps for their great support, encouragement and long discussions on "life in general" both in and outside work. Finally, I would like to offer my deepest thanks to my parents and sisters, since only with their amazing support and understanding has this thesis been made possible.

Abstract

Polymer therapeutics are often designed for lysosomotropic, endosomotropic or transcellular delivery. Thus routing to a specific intracellular compartment can be vital. For example, polymeric non-viral vectors for protein and gene delivery will never promote cytosolic access if they are rapidly trafficked to lysosomes, and polymer-drug conjugates designed for lysosomal activation will never deliver the drug payload unless they meet the appropriate enzyme. Therefore the first aim of this study was to establish a subcellular fractionation method to quantify intracellular trafficking of a polymeric anticancer conjugate (HPMA copolymer doxorubicin-PK1). B16F10 murine melanoma cells were chosen for this study as they have been widely used *in vitro* and *in vivo* to study the antitumour activity of PK1 and other polymer-drug conjugates. In the second part of this study the endocytic properties of polycations were studied.

It was first necessary to define a cell breakage assay. The cell cracker achieved a 90 % cell breakage efficiency which ensured that subsequent subcellular fractionation experiments were representative for the cell population. Next, markers for nuclei (DNA), mitochondria (succinate dehydrogenase), lysosomes (*N*-acetyl-β-glucosaminidase), plasma membrane (alkaline phosphatase) and cytosol (lactate dehydrogenase) were validated and used in due course for the quantitative characterisation of subcellular fractions. Finally, a differential centrifugation method was devised to separate and enrich nuclei (2.2 fold), mitochondria (4.1 fold), lysosomes (3.7 fold) and cytosol (2.5 fold). The intracellular trafficking of PK1 was studied by differential centrifugation and time-dependent accumulation in lysosomes was confirmed, in contrast to free doxorubicin which accumulated in the nucleus. Live cell fluorescence microscopy and confocal co-localisation studies corroborated these results.

In the second part of this study the endocytic properties of polycations used as non-viral vectors for gene delivery were examined. Linear and branched polyethylenimine (PEI, Mw = 25,000 g/mol) and polyamidoamine dendrimers (PAMAM) of generations (G) 2 – 4 were studied by flow cytometry using Oregon Green functionalised polymers. At non-toxic concentrations maximum internalisation was observed for PAMAM G4, followed by linear and branched PEI achieving 27 – 36 % of the maximum respectively. Lowest uptake was observed for PAMAM G2 and G3. Overall extent of extracellular binding was highest for branched PEI (58 % of total cell-association). For all dendrimers extracellular binding was between 16 – 26 % of total cell-association (G2 > G3 > G4). In preliminary studies PAMAM G4 and branched PEI were predominately internalised via cholesterol-dependent pathways, whereas internalisation of linear PEI appeared to be independent of clathrin and cholesterol.

Index

List of Figures

Chapter 3

Chapter 4

Chapter 5

List of Tables

Chapter 4

Chapter 5

Chapter 6

List of Abbreviations

ANOVA	Analysis of variance
AU	Arbitrary units
BCA	Bicinchoninic acid
BSA	Bovine serum albumin
CCV	Clathrin coated vesicles
CE	Caveosomes
CHO	Chinese hamster ovary
ci-MPR	Cation-independent manose-6-phosphate receptor
DAPI	4',6-Diamino-2-phenylindole
DB	Degree of branching
DMF	Dimethylformide
DMSO	Dimethyl sulphoxide
DNA	Deoxyribonucleic acid
DNM	Daunomycin
DOTAP	1,2-Diacyl-3-trimethylammonium propane
DTOMA	*N*-[1-(2,3-dioleyloxy)propyl]-*N,N,N*-tri-methylammoniumchloride
EA	Apparent cell-association
EAT	Ehrlich ascites tumour cells
ECV	Endocytic carrier vesicle
EE	Early endosome
EDTA	Sodium ethylenediaminetetraacetic acid
EI	Endocytic index
EN_{Total}	Total cell-association
EPR	Enhanced retention and permeability

List of Abbreviations continued

ER	Rate of polymer internalisation
ERC	Endocytic recycling compartment
EX_{K1}	Fast exocytosis kinetics
EX_{K2}	Slow exocytosis kinetics
FBS	Foetal bovine serum
FDA	Fluorescein diacetate
FITC	Fluorescein isothiocyanate
G	Generation
GAG	Glycosaminoglycans
GG	Glycine-Glycine
GPC	Gel permeation chromatography
$G_{V\ Control}$	Geometric mean of viable cell population of control cells
$G_{V\ Polymer}$	Geometric mean of viable cell population exposed to polymer
HeLa	Human epitheloid carcinoma
HEPES	N-2-hydroxyethylpiperazine-N'-ethanesulphonic acid
HIV	Human immunodeficiency virus
HPLC	High performance liquid chromatography
HPMA	N-(2-hydroxypropyl)metharcylamide
HSV	Herpes simplex virus
HTC	Cultured hepatoma cells
IC_{50}	Inhibitory concentration for 50 % of cell population
LAMP	Lysosomal membrane-associated glycoprotein
IL-2	Interleukin-2

List of Abbreviations continued

L	Lysosomal fraction
LDL	Low density lipoprotein
LDLR	Low density lipoprotein receptor
LE	Late endosome
M	Mitochondrial fraction
MβCD	Methyl-β-cyclodextrin
Mce_6	Mesochlorin e_6 monoethylenediame
MDCK	Madin-Darby canine kidney
MeOH	Methanol
Mic	Microsomal fraction
Mol%	Mole percent
MP	Macropinosome
MTT	(3-[4,5-dimethyl-thiazol-2-yl]-2,5-diphenyl-tetrazolium bromide
MTX	Methotrexate
Mn	Number-average molecular weight
Mw	Weight-average molecular weight
N	Nuclear fraction
NADH	Reduced β-nicotinamide adenine dinucleotide
NADPH	Reduced β-nicotinamide adenine dinucleotide phosphate
ND	Not determined
NLS	Nuclear localisation sequence
NMR	Nuclear magnetic resonance
NS	Not statistically significant
OG	Oregon Green

List of Abbreviations continued

OG-SE	Oregon Green succinimidyl ester
OND	Oligonucleotide
OVAR-3	Human ovarian adenocarcinoma
PAMAM	Polyamidoamine dendrimer (Starburst)
PEI	Polyethylenimine
PBS	Phosphate buffered saline
PDL	Poly-D-lysine
PEG	Polyethyleneglycol
PI	Propidium iodide
PLL	Poly-L-lysine
PMSF	Phenylmethylsulfonyl fluoride
PNS	Post nuclear supernatant
PVP	Polyvinylpyrrolidone
RI	Refractive index
RSA	Relative specific activity
S	Soluble fraction
SE	Sorting endosome
SEM	Standard error of the mean
SV	Simian virus
TAT	Transactivating factor
TEER	Transepithelial electrical resistance
TEM	Transmission electron microscopy
TGN	Trans Golgi network
TLC	Thin layer chromatography
Tris-HCl	Tris(hydroxymethyl)aminomethane hydrochloride
Tris-NaOH	Tris(hydroxymethyl)aminomethane

List of Abbreviations continued

UV	Ultraviolet
V_B	Bed volume
V_O	Void volume
wt%	Weight percent

Chapter 1

General Introduction

1.1 Introduction

The quest to improve health with the use of nano-sized (1 – 100 nm) medicinal products might seem like science fiction (LaVan et al., 2003; Whitesides, 2003), though research into "nanomedicines" (Duncan, 2004) has a long-standing history. In 1975 Ringsdorf proposed the concept of attaching a drug to a water-soluble polymer via a biodegradable linker and an optional targeting group (figure 1.1) (Ringsdorf, 1975). Since then a number of other polymer-based therapeutics have emerged, and Duncan coined the term polymer therapeutics to describe this family of nano-sized therapeutics (Duncan et al., 1996). The term polymer therapeutics encompasses polymer-protein conjugates and cationic polymer-based non-viral vectors, in addition to polymeric drugs, polymer-drug conjugates, and polymeric micelles where the drug is covalently linked to the polymer (figure 1.1) (Duncan, 2003a). Since the visionary proposal by Ringsdorf, a number of polymer therapeutics are now appearing in the marketplace and entering clinical trials (Duncan, 2003a; Harris & Chess, 2003). Polymers have been particularly successful for the delivery of proteins to extracellular targets, though intracellular delivery has proven more difficult (Brown et al., 2001). The intracellular delivery of small molecular weight drugs (Thanou & Duncan, 2003) is currently widely investigated with a number of compounds advancing towards the market (table 1.1). Intracellular delivery of biotechnology products, in particular oligonucleotides (ONDs), however is still a major challenge.

For both polymer-OND complexes (polyplexes) (Felgner et al., 1997) and polymer-drug conjugates, the process of "endocytosis" (see section 1.2) is the gateway into the cell (Duncan, 2000; Garnett, 1999). From the outset it has been known that routing of these polymer therapeutics to a specific intracellular compartment is vital (Duncan & Kopecek, 1984; Jones et al., 2003). For example, polymeric vectors for protein and gene delivery will never promote cytosolic access if rapidly trafficked to lysosomes and polymer-drug conjugates designed for

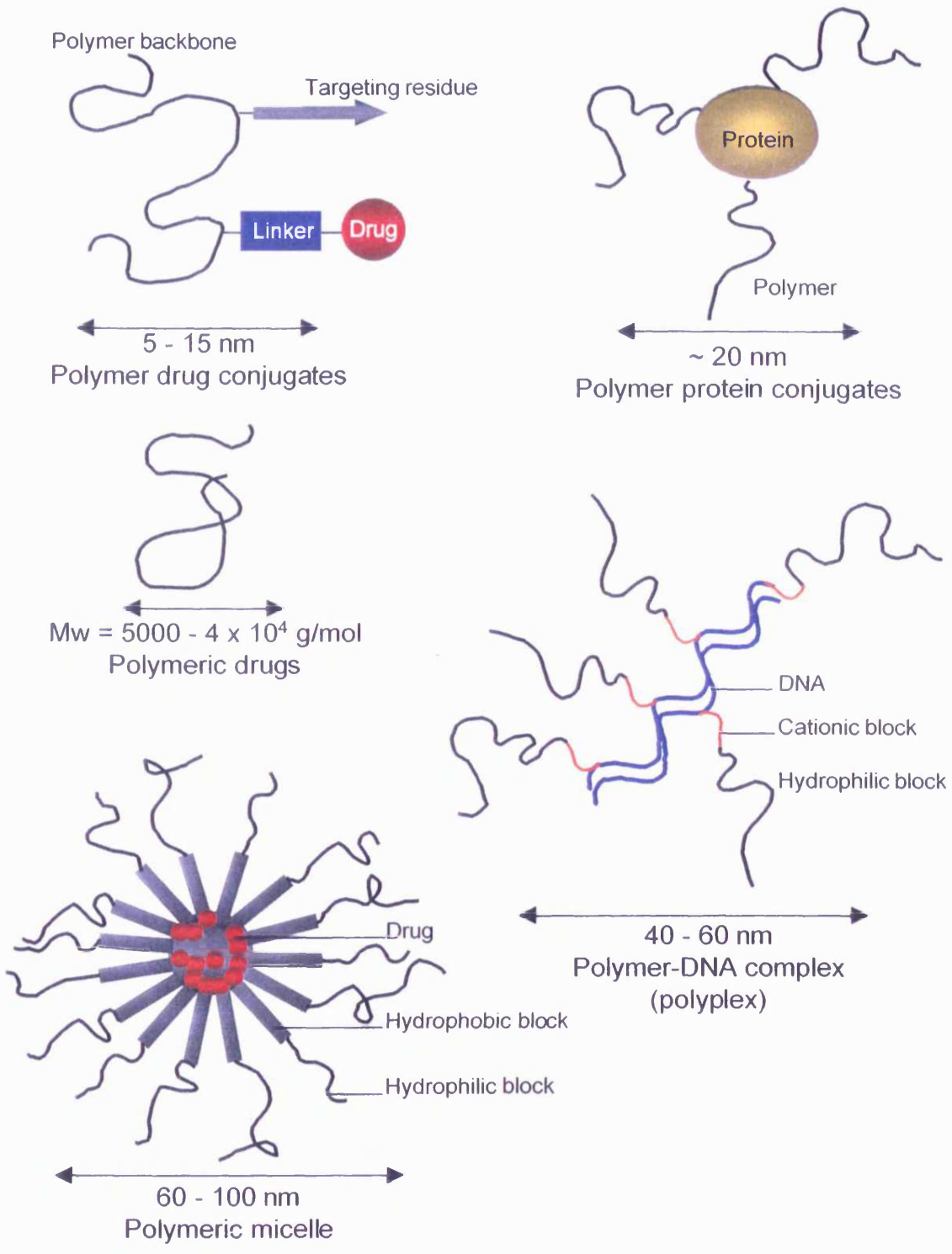

Figure 1.1 Schematic representation of polymer therapeutics. The multi-component nature of the constructs is clearly visible. Adapted from Duncan, 2003.

Table 1.1 Examples of polymer-drug conjugates and polymeric micelles in clinical trials as anticancer agents unless otherwise indicated. All conjugates are comprised of a linear polymer backbone with a covalently attached drug payload unless otherwise indicated.

Compound	Status of development	Reference
HPMA copolymer-doxorubicin	Phase II	(Vasey et al., 1999)
HPMA copolymer-doxorubicin-galactosamine	Phase I/II	(Duncan et al., 1986; Seymour et al., 2002)
HPMA copolymer-paclitaxel	Phase I†	(Terwogt et al., 2001)
HPMA copolymer-camptothecin	Phase I†	(Schoemaker et al., 2002)
HPMA copolymer-platinate	Phase I	(Gianasi et al., 2002)
Polyglutamic acid-paclitaxel	Phase III#	(Kudelka et al., 2002; Li et al., 1998; Sabbatini et al., 2002; Schulz et al., 2002; Singer, 2004; Sludden et al., 2001)
Polyglutamate-camptothecin	Phase I	(De Vries et al., 2001)
PEG-camptothecin	Phase II	(Shaffer et al., 2002)
PEG-aspartic acid-doxorubicin micelle	Phase I♦	(Kataoka et al., 1993; Nakanishi et al., 2001)
PEG-paclitaxel	Phase I	(Greenwald et al., 1994)
Dextran-doxorubicin	Phase I†	(Danhauser-Reidl et al., 1993)
Polysaccharide camptothecin	Phase I††	(Kumazawa & Ochi, 2004) (Suzuki et al., 2004)
Poly(L-lysine) generation 3 dendrimer with a benhydrylamine core and 32 naphthalene disodium disulfonate surface groups	Phase I*	(McCarthy et al., 2004) (Bernstein et al., 2003)

† Trial closed due to toxicity

†† Trial closed due to lack of tumour targeting

Accelerated approval designation by United States Food and Drug Administration

♦ Contains 45 % polymer bound doxorubicin, remainder is free drug (for all other conjugates free is usually < 2 %)

* First topical dendrimer based pharmaceutical product in clinical trials for the prevention of HIV and sexual transmitted infections

lysosomal activation (see section 1.4.4) will never deliver the drug payload unless they meet the appropriate enzyme (Duncan, 2003a).

However, there have been relatively few studies that have set out to design polymer therapeutics based on a biological rationale, which include systematic studies designed to quantify endocytosis and intracellular trafficking. Therefore the aim of this thesis was to quantify endocytosis and intracellular trafficking of polymer therapeutics in B16F10 mouse melanoma cells using both cell fractionation, fluorescence microscopy and flow cytometry-based techniques. With knowledge of the intracellular fate of different polymers and existing polymer therapeutics, it should be possible to aid the design of improved carriers for specific therapeutic applications. To understand the scope of this project it is important to have background knowledge of "endocytosis" (the many different uptake pathways and vesicular trafficking) which is described in the following section.

1.2 Endocytosis

The term "endocytosis" describes the mechanisms by which cells internalise macromolecules to control normal cell physiology and function (figure 1.2). Materials endocytosed include low-density lipoprotein (LDL) (Anderson et al., 1977), transferrin (Watts, 1985), membrane lipids and other substrates essential for cell function, but also xenobiotics such as polymer therapeutics (Duncan & Kopecek, 1984). Endocytosis describes the processes of phagocytosis (cell eating, i.e. internalisation of solid particles) and pinocytosis (cell drinking, i.e. internalisation of solutes) with the latter process occurring continuously in all cells (Cardelli, 2001; Mukherjee et al., 1997). Endocytosis is a highly dynamic process as demonstrated by macrophages and fibroblasts where more then 200 % of their entire surface is internalised every hour, and individual cell surface receptors mediate as much as 10 rounds of ligand uptake and recycling each hour (Steinman et al., 1983). To maintain cell function an elaborate endocytic machinery is required regulating cell surface

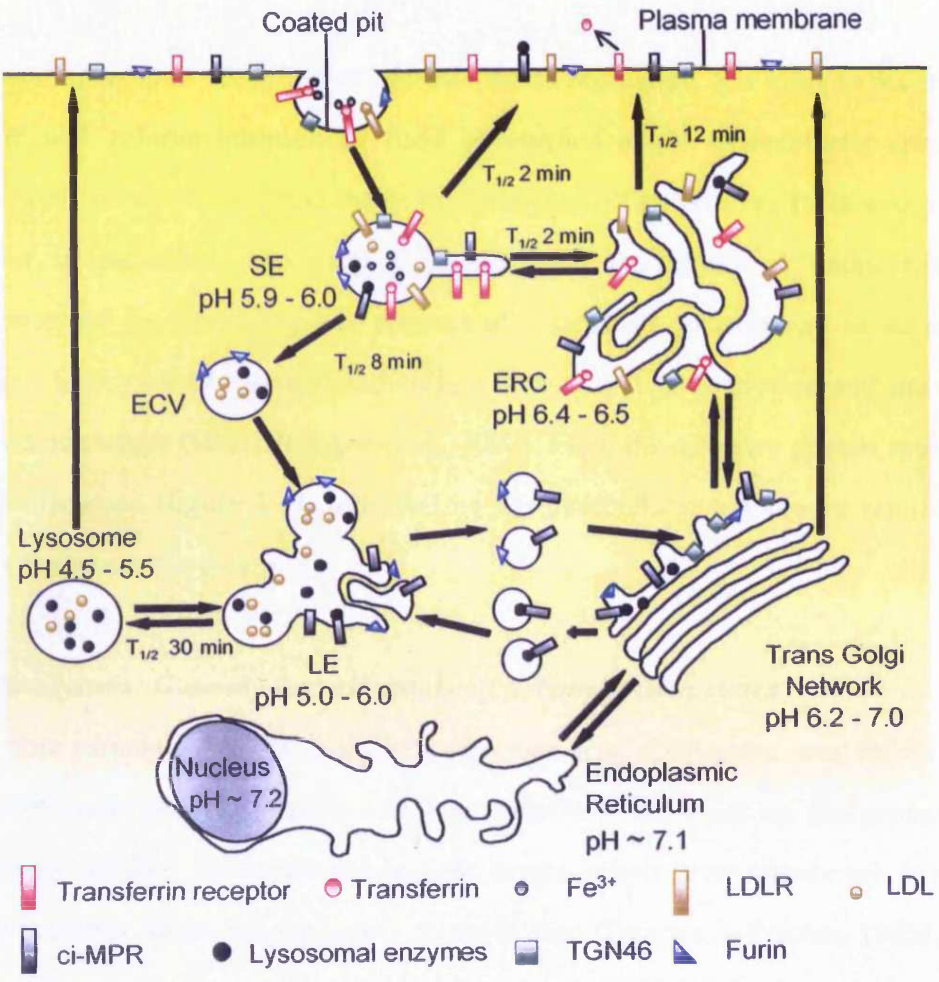

Figure 1.2 Endocytic trafficking in non-polarised cells of several membrane proteins which cluster in clathrin-coated pits and are initially delivered to sorting endosomes (SE). The low density lipoprotein receptor (LDLR) binds low-density lipoprotein (LDL); transferrin receptor binds diferric transferrin (transferrin and 2 x Fe^{3+}); and the cation-independent manose-6-phosphate receptor (ci-MPR) binds lysosomal enzymes (e.g. cathepsins). Upon internalisation most membrane proteins are swiftly returned to the plasma membrane or to the endocytic recycling compartment (ERC). Furin is trafficked from SE to late endosomes (LE), and subsequently to the Golgi. From the ERC, LDLRs and transferrin receptors recycle to the cell surface. Unlike most other ligands, transferrin is not released from its receptor in the acidic environment of the SE, though the two irons (Fe^{3+}) are released from differic transferrin at the acidic pH and released into the cytoplasm. Iron free transferrin remains bound to the receptor until it reaches the cell surface where the neutral pH triggers its release from the receptor. Most of internalised TGN46 and ci-MPR (~ 80 %) are also returned to the cell surface, the rest is trafficked to the Golgi. The ci-MPR can go from the Golgi to LE, where bound ligand can dissociate due the low pH of the compartment. From the LE free ci-MPR and furin can move to the Golgi, allowing delivery back to the plasma membrane. The $t_{1/2}$ values are approximate and cell-type dependent. Adapted from Maxfield & McGraw, 2004.

homeostasis, receptor recycling or receptor down regulation. For cells to maintain a constant cell volume internalised fluid is returned to the extracellular space by default. For the purpose of this thesis this process will be referred to as exocytosis. However, in specialised cells, such as neuronal cells, the process of "endocytosis" is complemented by the retrograde process of exocytosis in response to an action potential. Exocytosis in specialised cells will not be discussed here and has been reviewed elsewhere (Grundelfinger et al., 2003). First, the different portals into cells will be discussed (figure 1.3), followed by the intracellular machinery required to process the internalised cargo.

1.2.1 Pinocytosis: Gateway for cell uptake of polymer therapeutics

The rationale for the design of polymer-drug conjugates was to create a macromolecular prodrug that would be exclusively taken up by the process of pinocytosis unlike low molecular weight drugs, where transmembrane passage usually accounts for intracytoplasmic accumulation (Duncan & Pratten, 1985). The process of pinocytosis can be further classified into fluid-phase and adsorptive pinocytosis (figure 1.4). Fluid-phase pinocytosis of macromolecules is due to the capture of solubilised macromolecules and examples include *N*-(2-hydroxypropyl)methacrylamide (HPMA) copolymers (Duncan et al., 1981b), dextran (Ohkuma & Poole, 1978) and poly(vinylpyrrolidone) (PVP) (Williams et al., 1975). The degree of internalisation of those markers is directly proportional to their concentration in the medium and the internalised volume.

In the case of adsorptive pinocytosis two further possible mechanisms can be identified namely "non-specific" membrane interaction and receptor-mediated internalisation (figure 1.4). The former process leads to increased accumulation of solutes relative to fluid-phase pinocytosis, though receptor-mediated pinocytosis is the most efficient process of all, due to the ability to capture dilute solutes with high affinity receptors. So far indiscriminate electrostatic or hydrophobic interactions of

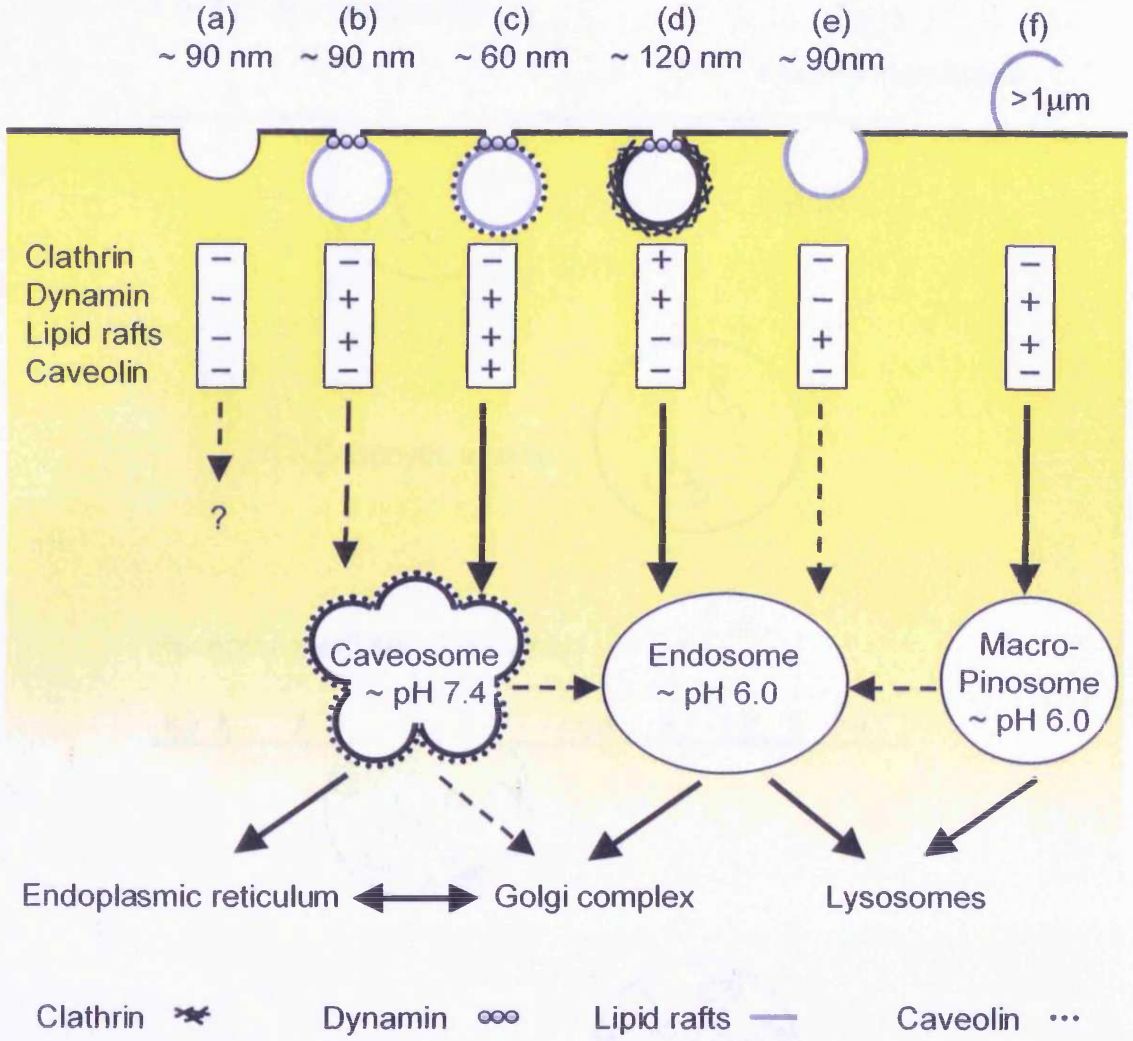

Figure 1.3 Potential entry routes for polymer therapeutics into mammalian cells. The range of pinocytic pathways described is cell-type dependent. Entry routes have been classified according to the requirements for clathrin, dynamin, lipid rafts and caveolin. Typical sizes of plasma membrane invaginations are shown. The best characterised are the clathrin-mediated pathway (d) and the caveolae pathway (c). Macropinocytosis (f) is actin driven and can be stimulated in many cells by growth factors or other signals. Dynamin may be involved in the process of macropinocytosis though the clear role has not been established. Dynamin has therefore been omitted form the diagram for clarity. The lipid raft-mediated pathways can be dynamin-dependent (b), or dynamin-independent (e). In addition, pathways have been described (a) that do not seem to depend on any of these factors. The initial intracellular trafficking of these pathways are indicated though with the exception of the clathrin mediated pathway, they are poorly defined (indicated by broken arrows). Adapted from Conner & Schmid, 2003; Pelkmans & Helenius, 2003; Swanson & Watts, 1995.

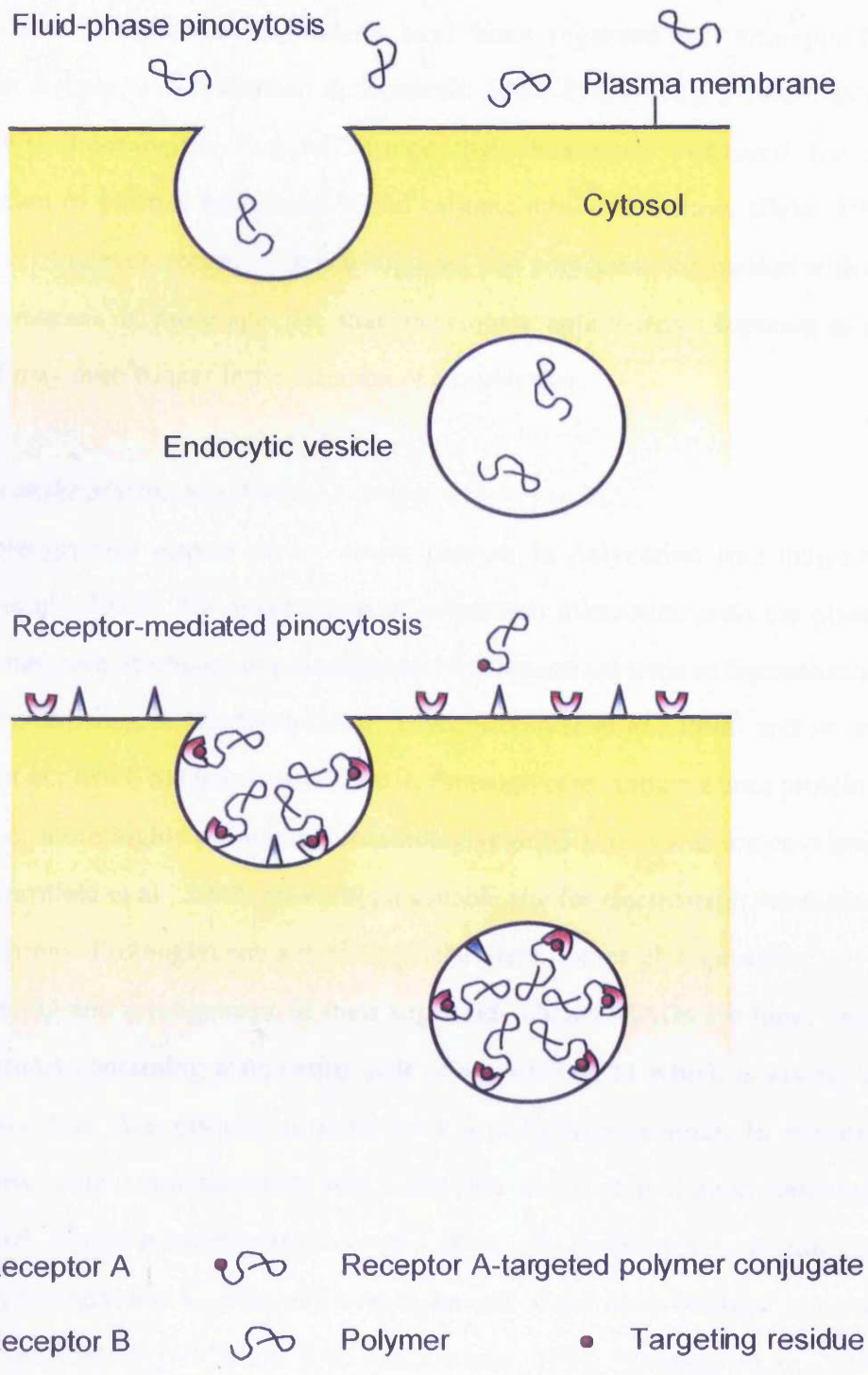

Figure 1.4 Fluid-phase and receptor-mediated pinocytosis. Note that the receptor-mediated uptake results in a greater efficiency of internalisation of polymers, despite low extracellular concentrations. In contrast, uptake of polymers by fluid-phase pinocytosis is concentration dependent.

polymers with the plasma membrane have been regarded as "non-specific" (Besterman & Low, 1983; Duncan & Kopecek, 1984; Pratten et al., 1980). In the early 1990s spontaneous "zipper" pinocytosis has been proposed for the internalisation of plasma membrane bound cationic non-viral vectors (Behr, 1993; Behr, 1994). However, recent evidence suggests that polycation interaction with the plasma membrane is more specific than previously anticipated (Ruponen et al., 2003), and may even trigger internalisation of the polymer.

Interaction at the plasma membrane: Adsorptive pinocytosis

Proteoglycans appear to be major players in polycation internalisation (Ruponen et al., 2003). The mechanism of polycation interaction with the plasma membrane has been attributed to proteoglycan binding and subsequent internalisation both *in vitro* (Mislick & Bladeschwieler, 1996; Mounkes et al., 1998) and *in vivo* (Mounkes et al., 1998; Sakharov et al., 2003). Proteoglycans contain a core protein to which one or more highly anionic glycosaminoglycan (GAG) chains are covalently attached (Bernfield et al., 1992) providing a suitable site for electrostatic interactions with polycations. Proteoglycans are distinguished from other glycoproteins by the nature, quantity and arrangement of their sugar side chains. GAGs are long, linear polysaccharides containing a repeating pair of sugars, one of which is always an amino sugar (i.e. *N*-acetylglucosamine or *N*-acetylgalactosamine). In contrast, glycoproteins contain comparatively few sugar side chains, which most commonly are branched oligosaccharides (Couchman, 2003). In recent years, membrane-associated proteoglycans have been found to be one of the main biological factors that affect gene delivery (Mislick & Bladeschwieler, 1996; Mounkes et al., 1998; Ruponen et al., 2001; Ruponen et al., 1999). Cell membrane-associated proteoglycans have been proposed as central binding sites for gene delivery complexes (Ruponen et al., 2001) and have been positively correlated to gene expression (Belting & Petersson, 1999; Kopatz et al., 2004; Mislick & Bladeschwieler, 1996). However, extracellular proteoglycans in the plasma (i.e. not membrane-associated) limit gene transfer of cationic lipids and polymers (Mislick &

Bladeschwieler, 1996; Mounkes et al., 1998; Ruponen et al., 2001; Ruponen et al., 1999). Ruponen and co-workers proposed altered cellular trafficking and cellular uptake for this phenomenon (Ruponen et al., 2001). Though GAGs function as membrane receptors, to date no polymer-based systems have been specifically designed to target them and only "classical" examples of receptor-targeted systems are described in the literature.

Interaction at the plasma membrane: Classical receptor-mediated pinocytosis

Cell surface receptors promote selective uptake of ligands and this is known as receptor-mediated pinocytosis. Unlike fluid-phase pinocytosis, receptor-mediated pinocytic uptake is a concentration-dependent process, which is saturable at high ligand concentrations (Mukherjee et al., 1997). Receptor-mediated uptake results in a rapid accumulation of the ligand leading to significant intracellular concentrations (Mukherjee et al., 1997). Much of the early work involving polyplexes utilised the concept of receptor-mediated pinocytic uptake by coupling a ligand to the polymer. A number of ligands such as asialoorosomucoid (Wu & Wu, 1987), transferrin (Cotten et al., 1990), folate (Mislick et al., 1995), monoclonal antibodies (Chen et al., 1994) and basic fibroblast growth factor (Sosnowski et al., 1996) have been conjugated to poly-L-lysine (PLL) to enhance the transfection ability of the polymer. Receptor-mediated uptake has also been exploited for the design of polymer-drug conjugates such as PK2, an HPMA copolymer doxorubicin-galactosamine conjugate designed to target the asialoglycoprotein receptor of hepatocytes (see section 1.5.1) (Duncan et al., 2001). PK2 is the only example to date of a targeted polymer-drug conjugate that has progressed to clinical trial (Seymour et al., 2002). Before harnessing pinocytosis for intracellular drug delivery, it is essential to examine pinocytosis with its underlying intracellular trafficking in greater detail.

1.3 Pinocytic portals of entry into cells

So far 6 different pinocytic pathways into cells have been identified which are diagrammatically represented in figure 1.3 (Conner & Schmid, 2003). Formation

of plasma membrane invaginations and subsequent internalisation uses a plethora of molecular components, though for the purpose of this thesis only a selected few will be considered and related to drug delivery. For comprehensive reviews on this topic see (Engqvist-Goldstein & Drubin, 2003; Mellman, 1996; Mukherjee et al., 1997; Pfeffer, 1996; Vale, 2003). The first intracellular compartments encountered by these vesicles are also presented, though to appreciate the versatility of this process figure 1.2 should serve as an example.

1.3.1 Coated vesicle-mediated pinocytosis

The formation of a morphologically characteristic bristle-coat around pinocytic vesicles was first observed by Roth and Porter in 1964 (Roth & Porter, 1964). Clathrin was subsequently identified as the major coat protein of coated vesicles, which are also referred to as clathrin-coated vesicles (CCVs) (Pearse, 1975). In cultured cells as much as half of membrane and fluid internalisation proceeds by this process (Maxfield & McGraw, 2004). Internalisation through a CCVs is a multi-step process occurring constitutively in all mammalian cells and it is tightly controlled by a number of cellular proteins. Recruitment of cytosolic coat proteins to the plasma membrane leads to the formation of a coated pit, which can concentrate receptors. For nutritive receptors, such as low-density lipoprotein receptor (LDLR) (Anderson et al., 1977) or transferrin (Watts, 1985), ligand binding is not a prerequisite for receptor clustering and internalisation. Epidermal growth factor receptor however, only clusters in coated pits when exposed to low concentrations of epidermal growth factor (Aguilar & Wendland, 2005; Sigismund et al., 2005). With continuing recruitment of coat proteins and the assembly of a "polygonal cage" (i.e. clathrin coat) (Fotin et al., 2004), the pit invaginates and eventually pinches off the plasma membrane mediated by dynamin and other effector proteins and rapidly loses its coat (Liu et al., 2001). Recently, lipoplex-mediated transfection in COS 7 cells (human pancreatic epitheloid) has been attributed to the internalisation through a cholesterol-dependent clathrin-mediated pathway (Zuhorn et al., 2002). Though the involvement of clathrin has here been discussed with

respect to plasma membrane-derived CCVs, clathrin is also used for the formation of transport vesicles at the trans Golgi network (TGN) and other intracellular sites (Schmid, 1997).

1.3.2 Caveolae-dependent pinocytosis

Caveolae-dependent uptake is not a universal process although seen in a number of cells types, most notably in capillary endothelial cells, lung epithelial cells, smooth muscle and adipocytes (Johannes & Lamaze, 2002). Electron microscopy reveals that caveolae are small (~ 50 nm ∅) flask shaped invaginations of the plasma membrane, which can constitute up to 10 – 20 % of cell surface in endothelial cells (Conner & Schmid, 2003). Formation of caveolae requires the cholesterol-binding protein caveolin, which is associated with glycolipid rich domains of the plasma membrane (i.e. lipid rafts) (Nichols, 2003). Interestingly, recent evidence suggests that caveolin might negatively regulate caveolae-dependent pinocytosis although further studies are needed to validate these findings (Le et al., 2002). In contrast to clathrin-mediated pinocytosis, the internalisation via caveolae is a triggered event (Pelkmans et al., 2002). For example the entry of the simian virus 40 (SV 40) and transcytosis (see below) of serum albumin is associated with caveolin-mediated uptake (Dautry-Varsat, 2001). In contrast to CCV, caveolae-derived vesicles do not lose the stabilising coat implicated in the selective delivery of cargo to other intracellular compartments (Pelkmans et al., 2004). For inhalation delivery of therapeutic proteins for systemic drug delivery caveolae-mediated uptake appears to be of critical importance. However, an inverse correlation between molecular size and rate of transport across lung epithelium could limit proteins delivered by this mechanism (Gumbleton, 2001; Patton, 1996). Although kinetics and contribution to total endocytic activity remains to be established, caveolae are only slowly internalised (e.g. 20 min – 3 h after SV 40 adsorption on the cell surface) (Pelkmans et al., 2002). Due to the low fluid-phase volume of caveolae, and the slow kinetics of the process, it is unlikely that this process contributes significantly to bulk fluid-phase uptake in non-endothelial cells (Conner & Schmid, 2003). Nonetheless,

caveolae-mediated uptake can have significant pharmacological effects as suggested by studies with cholera toxin (Nichols & Lippincott-Schwartz, 2001). Here, cell entry through the caveolae pathway was associated with toxicity due to Golgi trafficking of the toxin, which was not seen when taken up by CCVs (Orlandi & Fishman, 1998).

1.3.3 Clathrin- and caveolae-independent pinocytosis

Caveolae represents just one type of cholesterol rich micro-domain on the plasma membrane, and other ones are generally referred to as "lipid rafts" due to the lack of identified markers (Munro, 2003; Simons & Ikonen, 1997). However, due to the dependence of this uptake route on both lipid rafts and dynamin, the descriptor "caveolar" has been proposed to link this "lipid-mediated" mechanism with the caveolae-dependent uptake route (Nabi & Le, 2003). Nonetheless, for the purpose of this thesis this descriptor will not be used, and the processes will be differentiated and referred to as (a) caveolae- and (b) raft-mediated processes. Lipid rafts (~ 40 – 50 nm ∅) commonly contain cholesterol, sphingolipids and lipid anchored proteins (Anderson & Jacobson, 2002). Rafts freely diffuse on the cell surface and account for 10 – 15 % of the cell surface in macrophages (Gaus et al., 2003). Due to their specific lipid composition, rafts regulate protein sorting and internalisation (Edidin, 2001). Lymphocytes, which are naturally devoid of caveolae and caveolin, demonstrated constitutive interleukin-2 (IL-2) receptor internalisation by lipid rafts. The process is independent of caveolae and CCVs, but dependent on dynamin activity (Lamaze et al., 2001). Evidence from dominant-negative dynamin mutants points towards an alternative pinocytic mechanism independent from CCVs, caveolin or IL-2 containing lipid rafts, due to continuous fluid-phase internalisation (Damke et al., 1995). To date clathrin- and caveolae-independent pathways are only starting to emerge, and only with the availability of specific markers and ligands will it be possible to study them in greater detail. Identification of ligands could open new possibilities for directing ligand-targeted polymers via these routes.

1.3.4 Macropinocytosis

Macropinocytosis is accompanied by the formation of membrane ruffles, which collapse onto the plasma membrane and thereby internalise large volumes of extracellular solutes (Maniak, 2001). Macropinocytosis can occur constitutively in some tumour cells (Johannes & Lamaze, 2002), though in most cultured cells it is a triggered event, most notably following stimulation by epidermal growth factor or certain bacterial pathogens like *Salmonella* (Cardelli, 2001). Formation and collapse of membrane ruffles is an actin-dependent process and tightly controlled by a number of proteins (Engqvist-Goldstein & Drubin, 2003). Recent evidence suggests that dynamin is also involved in macropinocytosis, though its exact role remains to be elucidated (Cardelli, 2001).

1.3.5 Transcytosis: Transport across biological barriers

Certain vesicles forming at either the apical or basolateral domain subsequently carry material across the cell. This process is referred to as transcytosis (Mostov & Simister, 1985) and provides a means to overcome biological barriers. Transcytosis is of particular importance for the delivery of peptides and polymer therapeutics to the brain, lung, across capillary endothelial walls (Bickel et al., 2001; Schnitzer, 2001) and across the gut (Swaan, 1998). Pathogens such as HIV and HSV use the process of transcytosis to overcome the epithelial barrier to infect the host organism (Bomsel & Alfsen, 2003). The intracellular machinery used for vesicle internalisation and trafficking is reminiscent to the one seen in non-polarised cells and will not be discussed here. The process of transcytosis has recently been reviewed elsewhere (Apodaca, 2001; Mostov et al., 2000; Tuma & Hubbard, 2003).

1.4 The intracellular endocytic pathways

Once vesicles are formed from the plasma membrane, they mature and undergo fusion with other intracellular vesicles of the endocytic pathway (table 1.2); a process orchestrated by a number of proteins and membrane domains. The first compartment(s) these membrane-derived vesicles fuse with are shown in figure 1.3.

Table 1.2 Characteristics of acidic endocytic compartments*

	SE	ERC	LE	Lysosome
Half-life (min)	2 – 8	12	8	> 15
Morphology	Tubulo-vesicular	Tubular	Pleomorphic	Spherical
Dimensions°	250 – 400 nm vesicles 50 – 60 nm tubules	50 – 70 nm tubules	250 – 500 nm	500 – 2000 nm
Localisation	Peripheral	Variable	Perinuclear	Perinuclear
Markers	Rab 5, LDL, transferrin	Rab 4/11, LDL, transferrin	Rab 7/9 lysobisphosphatidic acid	LAMP 1/2 lysobisphosphatidic acid
Total surface area per cell (μm^2)#°	←	430 ± 105	→	370 ± 113
Volume per cell (μm^3) °		6.8 ± 1.6		36.8 ± 11.2
pH range (approximate)	5.9 – 6.0	6.4 – 6.5	5.0 – 6.0	4.5 – 5.5

Compiled from (Clague, 1998; Griffiths et al., 1989; Mukherjee et al., 1997; Seaman & Luzio, 2001)

* Values are cell type dependent and, where appropriate, reference to the cell line is made

Plasma membrane surface 2,200 μm^2 ± 470, coated pits 35 μm^2 ± 6

° Baby hamster kidney cells, cytoplasmic volume 1,050 μm^3

However, to illustrate intracellular trafficking pathways in more detail, only well-characterised ligands for clathrin-mediated pinocytosis are discussed (figure 1.2). Where appropriate, reference to analogous structures involved in non-clathrin-mediated pinocytosis is made. For the purpose of this thesis this rather simplified view will serve as a basis. However, to appreciate the versatility and complexity the reader is referred to comprehensive reviews on this topic (Clague, 1998; Luzio et al., 2000; Pfeffer, 2003; Rodman & Wandinger-Ness, 2000).

1.4.1 Early endosomes

The first compartments entered are the early endosomes (EEs) (Helenius et al., 1983). Internalised macromolecules appear in EEs within 1 – 5 min and are exposed to the organelle's mildly acidic (~ pH 6.5) environment (figure 1.2, table 1.2) (Seaman & Luzio, 2001). EEs are viewed as sorting organelles which select components for recycling to the cell surface or for delivery to other organelles such as late endosomes (see below) via endocytic carrier vesicles (also known as multivesicular bodies) (Gruenberg & Stenmark, 2004). EEs are not homogenous organelles but comprise at least two sub-units with sorting and recycling functions. For the purpose of this discussion, EEs will encompass both sorting endosomes (SEs) and the endocytic recycling compartments (ERCs). The small GTPases (essential for fusion of early endosomes with internalised vesicles (Tuvim et al., 2001) rab11 and rab5 are markers for ERC and SE, respectively (Clague, 1998). Recycling receptors such as transferrin and LDL are established markers for both ERC and SEs. Plasma membrane clustering of these receptors in coated pits is regulated by specific cytoplasmic motifs, though their recycling from EEs to the plasma membrane is a geometry-based process (Mukherjee et al., 1997). Following the fusion of the incoming vesicle with SEs, membrane is continuously removed from SEs by the formation of narrow-diameter tubules. Since the surface-area-to-volume ratio of tubules is greater than that of the vesicular portion of SEs, tubule formation preferentially sorts membrane associated components (e.g. receptors) from soluble molecules (Maxfield & McGraw, 2004). Therefore macromolecules, including

polymers, which do not interact with membrane components, could be expected to preferentially accumulate in SEs. Nonetheless, receptors destined for down-regulation (i.e. degradation) are also retained in SEs and are efficiently trafficked to late endosomes (see below) together with soluble macromolecules (Gruenberg & Stenmark, 2004, Conibear, 2002). Macromolecules internalised through caveolae-mediated pinocytosis are however trafficked differently. Studies with SV40 revealed delivery to specific early endosomes of neutral pH and devoid of the all typical EEs markers these were coined caveosomes (CE) (Pelkmans et al., 2001). Following the accumulation of SV40 in CEs over several hours, the virus was trafficked to the endoplasmic reticulum. Similarly, cholera toxin internalised via the caveolae-dependent pathway was also shown to pass through CE with subsequent Golgi trafficking (Nichols, 2002). Again, different trafficking is seen when macromolecules are internalised by the mechanism of macropinocytosis. With the collapse and fusion of the membrane ruffles, vesicles are formed at the plasma membrane termed macropinosome (MP). The intracellular fate of the MP is cell type-dependent and in macrophages, they move towards the centre of the cell, shrink and acidify all within 15 min. During this time, they change from a early-endosome-like organelle to a late endosome (see below), then merge completely with the lysosomal compartment (see below) (Swanson & Watts, 1995). In other cell types, the content of MPs is recycled back to the cell surface (Maniak, 2001). The implications of MP maturation on polymer trafficking is discussed in section 1.5.1.

1.4.2 Late endosomes

Late endosomes (LEs) (~ pH 5.5) are usually loaded within 4 – 30 min of uptake and receive material from EEs. The TGN also trafficks macromolecules to the endosome, namely proteins (e.g. endoprotease furin) and hydrolases bound to the cation-independent manose-6-phosphate receptor (ci-MPR) (figure 1.2) (Seaman & Luzio, 2001). LEs are viewed as the final sorting station of the endocytic pathway. At the LEs endocytosed materials are either recycled (e.g. ci-MPR), directed to lysosomes for degradation or of course function (e.g. cathepsin B) (Maxfield &

McGraw, 2004). Due to the enrichment of ci-MPR in late endosomes, the receptor is an established marker for this organelle in addition to rab7 and rab9 (Clague, 1998). Uptake into the LEs and formation of transport vesicles are an integral part of the sorting events. Escape of polymer therapeutics from these compartments into the cytosol is called endosomotropic delivery (see section 1.4.5) (Richardson et al., 1999a).

1.4.3 Lysosomes

Macromolecules destined for degradation from the endocytic pathway are directed from late endosome to lysosomes. By convention lysosomes are distinguished from late endosomes by virtue of their higher density on a Percoll gradient, the absence of ci-MPR and they are often the final site of accumulation of internalised macromolecules (Helenius et al., 1983; Mellman, 1996). Lysosomes are acidic (~ pH 4.8) organelles of vacuolar appearance (0.5 – 2.0 μm) and are characterised by a high concentrations of lysosomal membrane proteins (e.g. lysosomal membrane-associated glycoproteins, LAMP) and lysosomal hydrolases (e.g. cathepsins) (Sarafian et al., 1997; Seaman & Luzio, 2001). Though lysosomes are frequently regarded as the final endocytic compartment, they are dynamic structures as they interact and fuse with other cellular structures (e.g. endosomes, plasma membrane), and provide the cell with amino acids and oligosaccharides produced by the action of lysosomal hydrolases on internalised macromolecules (Luzio et al., 2000; Seaman & Luzio, 2001). Lysosomes, which serve both roles as secretory and degradative compartment, are known as secretory lysosomes. For a review see (Bainton, 1981; Blott & Griffiths, 2002). Delivery of polymer therapeutics via the lysosomal compartment has been coined lysosomotropic delivery (De Duve et al., 1974).

1.4.4 Lysosomotropic drug delivery

De Duve and co-workers introduced the term lysosomotropic delivery (De Duve et al., 1974) to describe compounds, which accumulate in the lysosomal

compartment of the cell with subsequent release of the drug to provoke a pharmacological response (Trouet et al., 1972). Polymer-drug conjugates designed for lysosomotropic drug delivery have been designed to include polymer-drug linkers that are substrates for specific lysosomal hydrolyses ensuring the release of drug only in the presence of these specific enzymes (figure 1.5). An example is the HPMA copolymer doxorubicin conjugate (PK1) and PK2 bearing the tetrapeptide drug-linker –glycine-phenylalanine-leucine-glycine (GFLG) which is susceptible to cleavage by the specific lysosomal hydrolase cathepsin B (Brocchini & Duncan, 1999; Duncan et al., 1996; Duncan & Kopecek, 1984). As the polymer-drug conjugate accumulates in lysosomes, liberated doxorubicin in its unprotonated form can then pass readily through the lysosomal membrane (Lloyd, 2000) and exhibit its pharmacological effect. Also pH-dependent linkers have been used as an alternative to peptide-based ones (Ulbrich & Subr, 2004).

1.4.5 Endosomotropic drug delivery

Endosomotropic delivery is particularly desirable when the drug payload (e.g. protein, OND) is sensitive to degradation by the hydrolytic enzymes and/or low pH present in lysosomes (figure 1.5). To achieve endosomotropic delivery, efforts have been made to design pH-responsive polymers that would permeabilise the endosomal membrane to permit cytosolic access. Examples of endosomolytic polymers and their intracellular trafficking is described in section 1.5.2 – 1.5.4. The ideal endosomolytic polymer for routine clinical use has so far not been found. Possibly the combination of membrane translocation features of natural macromolecules (e.g. toxins, transport proteins) with polymers could yield the ideal vector (Duncan, 2000; Wagner, 1999). Thus today's challenge is to mimic mother-nature with specifically designed polymers to produce purpose build biomimetics. To understand the scope of the project it is also essential to review the current understanding of polymer (therapeutic) trafficking in eukaryotic cells.

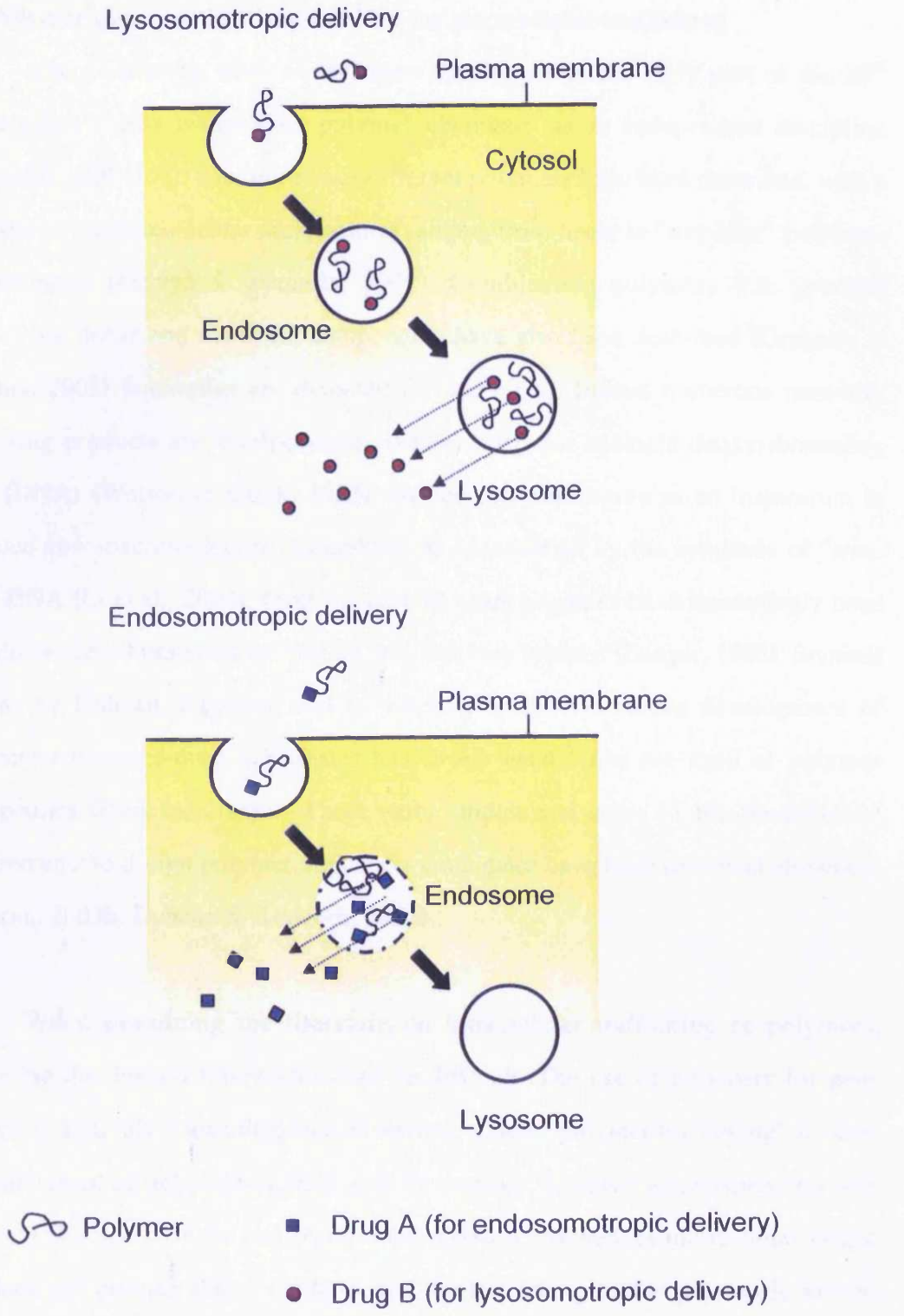

Figure 1.5 Schematic representation of endo- and lysosomotropic drug delivery. Desired route of delivery is dependent on drug-payload and requires the polymer therapeutic to response to intracellular stimulus.

1.5 Polymer therapeutics: Implications for intracellular trafficking

The pioneering work of Hermann Staudinger in the early part of the 20th century has firmly established polymer chemistry as an independent discipline (Ringsdorf, 2004). To date numerous different polymers have been described, with a plethora of macromolecular architectures ranging from linear to "tree-like'' polymers (dendrimers) (Esfand & Tomalia, 2001). Combination polymers (i.e. hybrids) employing linear and dendritic components have also been described (Grayson & Frechet, 2001) (examples are depicted in figure 1.6). Indeed numerous naturally occurring products are (bio)polymers (Elias, 1997) for example deoxyribonucleic acid (DNA) (Watson & Crick, 1953). Nature can often serve as an inspiration to produce new macromolecular assemblies as exemplified by the synthesis of "tree-like" DNA (Li et al., 2004). Over the past 30 years polymers have increasingly been used in the development of controlled drug delivery systems (Langer, 1998). Seminal studies by Duncan, Kopecek and co-workers on the systematic development of anticancer polymer-drug conjugates has firmly established the field of polymer therapeutics (Duncan, 2003a). These early studies and some of the fundamental requirements to design polymer anticancer conjugates have been reviewed elsewhere (Duncan, 2003b; Duncan & Kopecek, 1984).

When examining the literature on intracellular trafficking of polymers, extracting the desired information can be difficult. The use of polymers for gene therapy is a rapidly expanding area of interest, where "polymer trafficking" is often only addressed by determining final gene expression. However, gene expression only indicates that some of the payload has successfully reached its intracellular target, but does not provide direct evidence for the trafficking of the polymeric vector. Therefore for the purpose of this introduction only studies monitoring intracellular trafficking of polymers/polyplexes directly will be considered. To provide a background for the work presented in this thesis the focus of this introduction will be on the intracellular trafficking of dextran, HPMA copolymers, PEIs and PAMAM dendrimers. Linear, non-ionic polymers will be considered first.

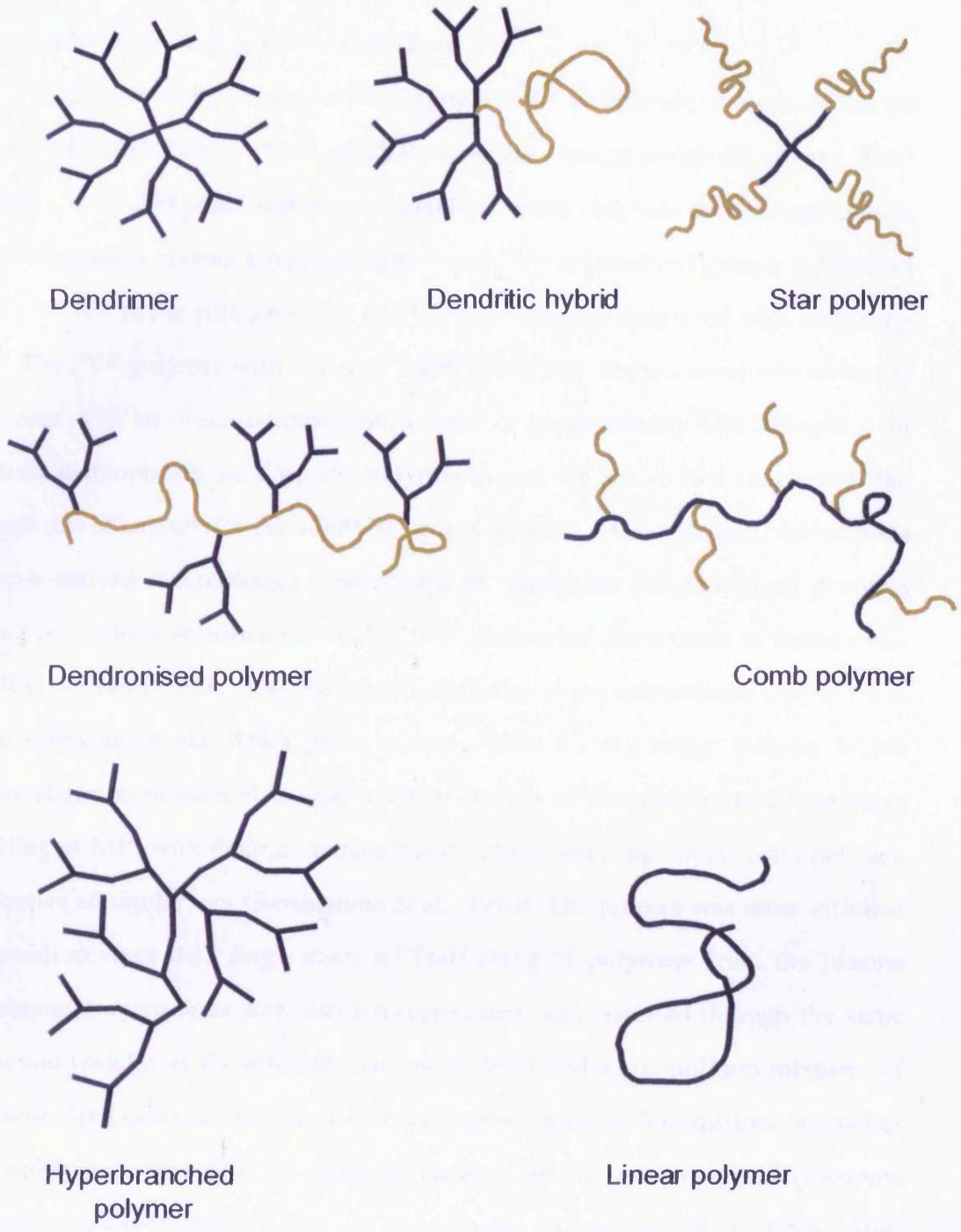

Figure 1.6 Schematic representation of some polymer architectures. Architectures resemble water-soluble polymers in an aqueous solvent. The multi-component nature of dendronised, grafted and star polymers is visible. Polymers are not drawn to scale.

1.5.1 Linear, non-ionic polymers

Intracellular trafficking of PVP and dextran

Experiments by Duncan *et al.* highlighted the importance of polymer size on pinocytosis as [^{125}I]iodide-labelled PVP of weight average molecular weight (Mw) 50,000 – 7,000,000 g/mol was pinocytosed by visceral yolk sacs and macrophages in a Mw-dependent manner (chemical structure of PVP depicted in figure 1.7) (Duncan et al., 1981a). In the yolk sacs, rate of PVP internalisation decreased with increasing Mw. The PVP polymer with a Mw of 7,000,000 g/mol was not accumulated by the yolk sacs with an observed molecular cut-off of approximately 100,000 g/mol. In contrast macrophages took up the polymer across the whole Mw range with the highest rate of capture for the 7,000,000 g/mol polymer. More recently, murine bone marrow-derived macrophages were shown to fractionate different sized dextrans during pinocytosis (Berthiaume et al., 1995). Following pinocytosis of fluorescein-labelled dextran (4,000 – 150,000 g/mol), recycling to the extracellular medium was more efficient for the 4,000 g/mol polymer than for the larger dextran, which preferentially accumulated in lysosomes. Induction of macropinocytosis and pulse labelling of MPs with dextran demonstrated optimal exchange of polymer between organelles of similar age (Berthiaume et al., 1995). The process was more efficient for small dextran than large dextran. Trafficking of polymers from the plasma membrane to lysosomes was also size-dependent, and occurred through the same endocytic vesicles as the efferent movement. Most strikingly, uniform mixtures of different-sized dextrans delivered into lysosomes separated into distinct organelles containing only one type of dextran. Differences in endosome and lysosome dynamics was proposed to segregate the dextrans (Berthiaume et al., 1995). Mw-dependent exocytosis/recycling via intermediate vesicles has also been reported for dextran in Chinese hamster ovary (CHO) cells, with highest rates of exocytosis for the low Mw dextran (4,200 $\approx$ 9,100 $>>$ 17,000 $>$ 42,000 g/mol) (Buckmaster et al., 1987). Recycling of dextran has also been reported in L929 cells (mouse fibroblasts), which accounted for ~ 50 % of pinocytosed dextran (Mw = 68,500 g/mol) to be delivered to the extracellular fluid within 15 – 30 min (Van Deurs et al., 1984). The

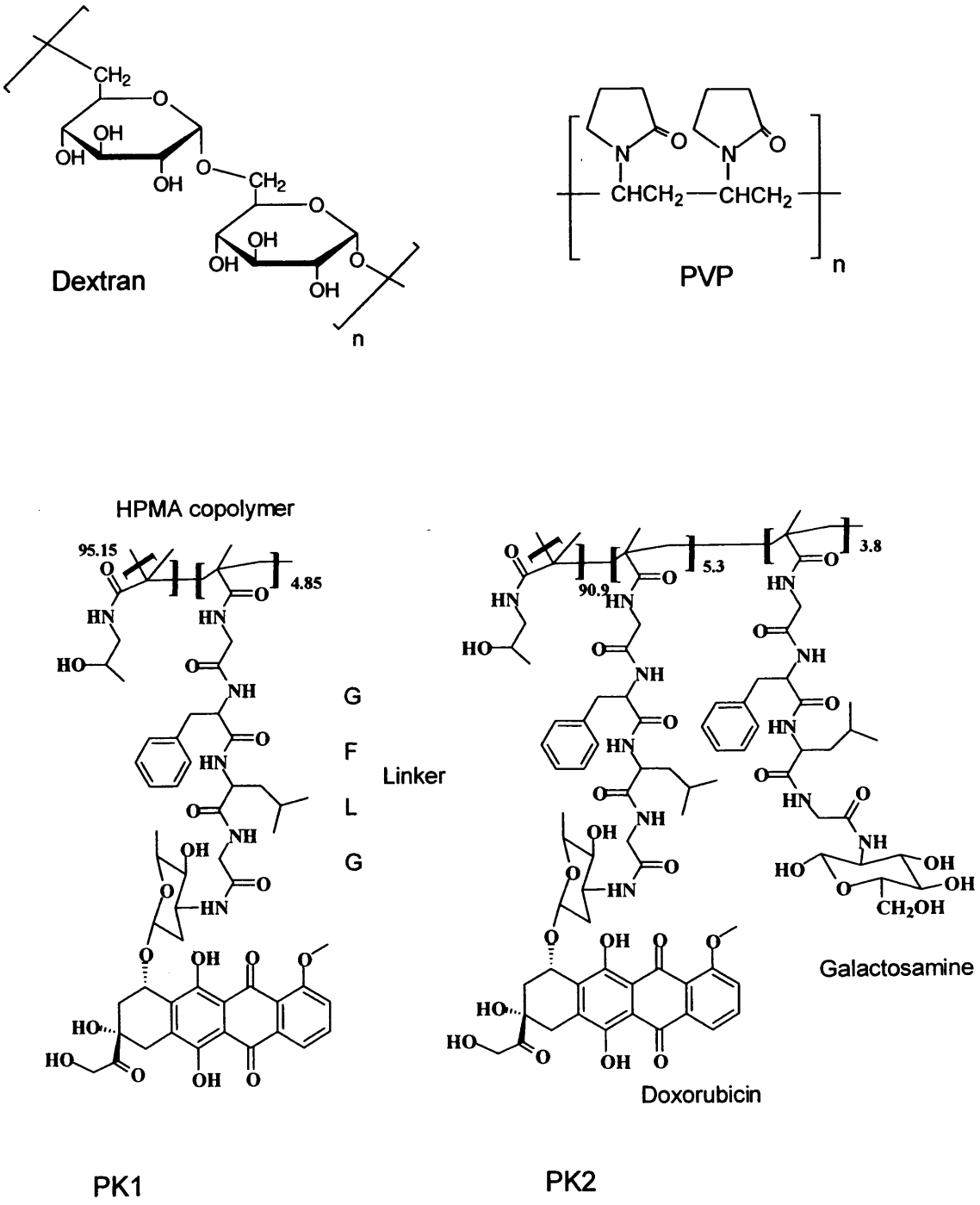

Figure 1.7 Chemical structures of fluid-phase markers and HPMA copolymer drug conjugates.

remaining dextran was trafficked into lysosomes (Van Deurs et al., 1984) as previously reported in mouse peritoneal macrophages (Ohkuma & Poole, 1978).

Intracellular trafficking of HPMA copolymers and polymer-drug conjugates

Linear HPMA copolymers have been the most widely studied polymers as a platform for polymer-drug conjugation. Though they are comprised of a linear polymeric backbone, the presence of hydrophobic groups, most notably doxorubicin, confers a unimolecular micellar conformation (Kean, 2002; Uchegbu et al., 1996). Polymer-drug conjugates with increasing doxorubicin loading (1, 5 and 10 mol%) exhibited a more condensed unimolecular conformation. The inclusion of the targeting ligand galactosamine increased the hydrophilicity of the conjugate which resulted in a more open polymeric coil (Vicent et al., 2004).

Whereas PK1 was devised for the uptake by fluid-phase pinocytosis (Duncan et al., 1981b), PK2 was designed for receptor-mediated uptake (figure 1.4 and 1.7) (Duncan & Kopecek, 1984; Duncan et al., 1986). High hepatic asialoglycoprotein receptor affinity was demonstrated for galactosamine (4 – 11.6 mol%) substituted HPMA copolymers, which were predominately internalised into hepatocytes and trafficked into lysosomes within 1 h of administration *in vivo* (Duncan et al., 1986). Also daunomycin bound to galactosamine-targeted HPMA copolymers demonstrated a 3 fold greater liver accumulation compared to free drug. Over the course of the experiment (48 h) subcellular fractionation experiments suggested lysosomotropic delivery of the conjugate (Wedge et al., 1991). Although these experiments demonstrated receptor-mediated uptake, no attention has been paid to the possible involvement of asialoglycoprotein receptor subclasses (Regoeczi et al., 1982). Subclasses display either delivery of the payload to lysosomes with receptor recycling to the plasma membrane (i.e. analogous to LDL trafficking, figure 1.2), or recycling of the intact receptor-ligand complex between endocytic compartments and the plasma membrane (Schwartz, 1991; Stockert, 1995). In rat liver a large fraction of receptor-bound ligand has been attributed to the latter process (~ 75 % of

internalised asialotransferrin type 3) (Regoeczi et al., 1982; Tolleshaug et al., 1981). Thus it remains to be seen if galactosamine-targeted HPMA copolymers provide the best way to maximise lysosomotropic delivery since it is not known what fraction of internalised polymer-drug conjugate participated in recycling. However, in *ex vivo* experiments lysosomes preloaded with the HPMA copolymer [^{125}I]iodo-L-tyrosine conjugate released 50 – 60 % of the conjugate associated radioactivity over 3 – 4 h. Thus HPMA copolymers reaching their intracellular target were able to liberate their payload due to cleavage of the model drug from the tetrapeptide linker (Duncan et al., 1986). The effectiveness of receptor-mediated pinocytosis has also been studied for galactosamine-targeted HPMA copolymers *in vitro* (Jensen et al., 2001). Although the study by Duncan *et al.* (Duncan et al., 1986) unequivocally demonstrated the lysosomotropic delivery of the linear polymer, recent evidence from fluorescence microscopy studies suggests that in particular conjugation of doxorubicin to the copolymer can have a significant effect on the intracellular distribution (see below) (Hovorka et al., 2002).

The intracellular distribution of PK1 and targeted with anti-Thy1.2 or anti-CD71 monoclonal antibodies have been investigated by fluorescence microscopy in EL-4 mouse T-cell lymphoma, SW620 human colorectal carcinoma and OVCAR-3 human ovarian adenocarcinoma cell lines. Here targeted and non-targeted polymer conjugates were only detectable in cytoplasmic structures even after 72 h of incubation, whereas doxorubicin control was always only detectable in the nucleus (Hovorka et al., 2002). Thus observations made by Omelyanenko with PK2, where intracellular distribution in endocytic vesicles, cytosol and the nucleus was reported could possibly be accounted for by (a) different cell lines, (b) different incubation times, (c) variable use of doxorubicin-equivalence, (d) use of a asialoglycoprotein-targeted polymer-drug conjugate and (e) fixed cells (Omelyanenko et al., 1998). Different intracellular distribution of PK1 and HPMA copolymer Texas red conjugates were observed following cell fixation, with diffuse cytoplasmic and typical endocytic labelling respectively (Hovorka et al., 2002). Possibly different

membrane affinities could be responsible for this behaviour. In live cells however, PK1 and the respective Texas red conjugate accumulate in vesicular structures (though less prominent for PK1). Overall these studies concluded that fixation lead to a re-distribution of the doxorubicin conjugate (Hovorka et al., 2002). Other studies describing HPMA copolymers are summarised in table 1.3. For a comprehensive summary of HPMA copolymers in drug delivery see recent review by Duncan (Duncan, 2005).

1.5.2 Cationic polymers for gene and drug delivery

Examples of linear, cationic polymers used for gene and drug delivery are summarised in table 1.4.

Linear amino acid polymers for gene delivery

PLL was one of the first cationic polymers studied as a gene delivery system (Wu 1987) (chemical structure of PLL depicted in figure 1.8), and is currently in a Phase I clinical trial to treat the monogenetic Canavan disease (i.e. inherited, degenerative brain disease) (OBA & RAC, 2004). Subcellular fractionation of rat liver by differential and isopycnic centrifugation has been used to follow the trafficking of polylysine complexed with [^{35}S]DNA. The different rate of trafficking of the PLL-DNA and poly-D-lysine-DNA (PDL-DNA) complexes was attributed to their different stereochemistries. Though both complexes were taken up to the same extent into Kupffer cells, intracellular degradation of the PLL-DNA complex was found to be markedly quicker than that of the PDL-DNA complex which was attributed to the susceptibility of the L-stereoisomer to peptidases (Laurent et al., 1999). Results indicated that DNA was more slowly transferred to lysosomes when complexed with PDL than with PLL. Therefore it has been suggested that digestion of the vector in the pre-lysosomal compartment is required for rapid DNA trafficking to lysosomes (Laurent et al., 1999).

Table 1.3 Subcellular distribution of HPMA conjugates *in vitro* and *vivo*

Polymer	Model system	Probe	Methodology used	Findings	Comment	Reference
HPMA daunomycin (DNM) conjugate with pendent galactosamine	Rat liver	^{3}H DNM	Subcellular fractionation	Demonstrated receptor-mediated uptake of conjugate. Prolonged retention of conjugate in hepatocytes with 62 % of the 1 h value at 48 h and lysosomal accumulation and release of drug.	Demonstrated lysosomotropic drug delivery. No evidence of nuclear accumulation.	(Wedge et al., 1991)
HPMA copolymer mesochlorin e_6 monethylenediamine (Mce_6)	Human ovarian carcinoma (A2780)	Mce_6	Subcellular fractionation	Lysosomal delivery and release of Mce_6 form tetrapeptide linker.	Poor characterisation and validation of fractionation method.	(Tijerina et al., 2001)
HPMA copolymer Mce_6 conjugated targeted with nuclear localisation sequence (NLS)	A2780	FITC Texas red, Mce_6	Confocal microscopy, subcellular fractionation	Enhance uptake for targeted conjugate compared to untargeted conjugate.	Fixed cell fluorescence microscopy prone to artefacts (Hovorka et al., 2002).	(Tijerina et al., 2003)

Table 1.3 Continued

Polymer	Model system	Probe	Methodology used	Findings	Comment	Reference
HPMA copolymer doxorubicin conjugate with trans-activating factor (TAT)	A2780	FITC Doxorubicin Texas red FITC	Confocal microscopy, flow cytometry, subcellular fractionation	Uptake and intracellular distribution attributed to non-endocytic uptake mechanism, subcellular fractionation by Tijerina et al., (2001) showed some cytosolic accumulation.	Typical vesicular labelling evident, flow cytometry did not include trypsin digestion invalidating the results (Richard et al., 2003).	(Nori et al., 2001; Nori et al., 2003b)
HPMA copolymer doxorubicin conjugates with polymer-drug linker: hydrazone/GFLG/GG/LL	Mouse 3T3 fibro-sarcoma, OVCAR-3	Doxorubicin	Epi-fluorescence microscopy	Uptake of hydrazone conjugates attributed to pinocytosis, uptake of other conjugates by translocating plasma membrane and localisation in major cellular organelles. Highest rate of uptake for GFLG conjugates (in seconds). No apparent differences of fixed and live cells.	Contradicts results reported previously on fixing artefacts. Possible use of epi-fluorescence limits study.	(Hovorka et al., 2004)

Table 1.4 Examples of cationic polymers for gene and drug delivery and their effect on pinocytosis

Polymer	Model system	Probe	Methodology used	Findings	Comment	Reference
PLL, polyornithin arginine-rich or lysine-rich histone	Sarcoma-180	^{125}I	Uptake of labelled albumin by S180 cells	All cationic polymers stimulated albumin uptake in the rank order of ornithin > arginine-rich histone > PLL > lysine-rich histone. Uptake rates of polycations were up to 1000 fold greater than for albumin.	First study to show that cationic polymers can stimulate pinocytic uptake of macromolecules.	(Ryser & Hancock, 1965)
Polyornithin PLL PDL	Sarcoma-180	^{125}I	Uptake of labelled albumin by S180 cells	Linear correlation between albumin uptake and Mw, minimum Mw of 900 g/mol required for stimulation.	First study to report Mw-dependent pinocytic stimulation.	(Ryser, 1967)
PLL methotrexate (MTX) conjugate (Mw = 70,000 g/mol)	CHO	^{3}H MTX	Uptake of ^{3}H-MTX into cells	Increased uptake of conjugate by drug-resistant cells	Demonstrated increased intracellular accumulation of conjugate .	(Ryser & Shen, 1978)

Table 1.4 Continued

Polymer	Model system	Probe	Methodology used	Findings	Comment	Reference
PLL (Mw = 6,700 g/mol) albumin conjugate	L929 mouse fibroblasts	^{125}I	Uptake of labelled albumin or horseradish peroxidase into cells	Increased uptake of proteins by 11 to 200 fold.	Conjugation significantly increased uptake above levels seen with mixtures of cationic polymers and probes.	(Shen & Ryser, 1978)
HPMA copolymer with cationic monomer at 12.5 wt% (Mw = 15,000 g/mol)	Rat visceral yolk sacs and rat liver	^{125}I	Pinocytic uptake in yolk sacs rat liver subcellular fractionation	In yolk sacs extensive binding of polymer to cellular surface which did not influence the basal rate of pinocytosis. In rats most of polymer accumulated in the liver and over 60 min was slowly transferred to lysosomes.	Transfer rate in liver much slower compared to galactosamine targeted polymer where accumulation in lysosomes was completed at 1 h.	(McCormick et al., 1986)

Table 1.4 Continued

Polymer	Model system	Probe	Methodology used	Findings	Comment	Reference
Polyarginine Polyornithine Polyhistine PLL	Human T-cells (Jurkat)	FITC	Flow cytometry confocal microscopy	D- and L-polyarginine showed optimum uptake, which was energy dependent but binding was not, polypeptide mimicked TAT.	Results suggest pinocytosis-mediated uptake.	(Mitchell et al., 2000)
Octaarginine-triclosan conjugate	*Toxoplasma gondii*	FITC	Flow cytometry confocal microscopy	Demonstrated effective delivery into the cytoplasm and nucleus of parasite.	Uptake mediated by number of processes but not characterised.	(Samuel et al., 2003)
Tertiary amine methacrylate homopolymers, tertiary amine methacrylate-ethylene glycol copolymers (block and comb-like)	Hep G2 A549 COS 7	YOYO	Transfection efficiency flow cytometry confocal microscopy	Positive correlation between uptake and transfection (homopolymers > block copolymers > comb-like copolymers).	Study does not address possibly limitations of flow cytometry for quantification. Comb-like polymer 3 x Mw than other ones. Homopolymer-DNA complexes >> larger than others.	(Deshpande et al., 2004)

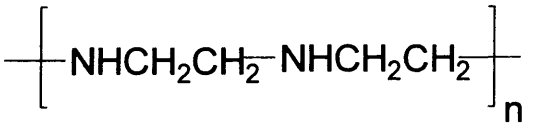

Linear PEI

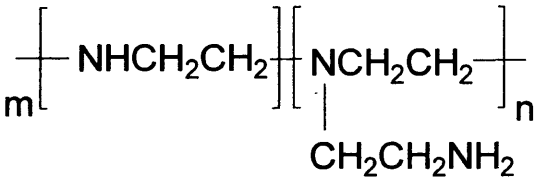

Branched PEI

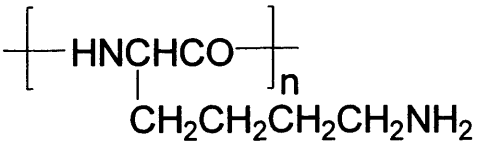

Poly-L-lysine

Figure 1.8 Chemical structure of cationic polymers used for gene and drug delivery.

Using ratiometric measurements of fluorophores, the intracellular journey of PLL polyplexes has been traced by monitoring changes in pH encountered during pinocytosis. In Hep G2 (human hepatocellular carcinoma) and HEK293 (human embryonic kidney) cells complexes remained in a mildly acidic compartment (pH ~ 6.0) over the course of the experiment (Forrest & Pack, 2002). Only in C2C12 cells (mouse myocytes) delivery of complexes to acidic organelles (pH < 5.0) was evident after 5 h. Nonetheless, transfection experiments with the polyplex did not show a correlation between trafficking and protein expression. Although trafficking of the polyplex was discussed, only the polymeric carrier was labelled with the fluorescent dyes (Forrest & Pack, 2002). Thus only the trafficking of the polymeric carrier was monitored. In a similar study by Akinc and Langer, both DNA and PLL were labelled. Here complexes were shown to reach lysosomal compartments in NIH 3T3 cells (pH ~ 4.5) within 2 h (Akinc & Langer, 2002).

Linear and branched amino acid copolymers for gene delivery

Studies with linear and branched histidine and lysine copolymers of different size and monomer arrangements were carried out in three different breast cancer cell lines, where highest transfection efficiency was observed for the branched copolymer (Chen et al., 2001). Recently, the same group found that optimal transfection efficacy was correlated to the degree of branching of the carrier and the pH of the encountered endocytic vesicle rather than the uptake of the complex *per se* (Chen et al., 2002). Optimum transfection levels of branched polymers were only observed in cell lines with a mildly acidic endocytic pH (6.2 – 6.9) where dissociation of DNA from the polymer was favoured. In turn, the highest transfection efficiency for linear polymers were observed in cell lines with low endocytic pHs, as the DNA was readily dissociated from the complex over the 6.5 – 4.5 pH range (Chen et al., 2002).

1.5.3 Linear and branched PEI for intracytoplasmic drug delivery

PEI is a cationic polymer synthesised in the linear and the branched form (Dermer & Ham, 1969). PEI has attracted considerable attention due to

unprecedented transfection levels with respect to other polymeric vectors (Boussif et al., 1995). It has been claimed that PEI exposure to the acidic environment allows for protonation of the polymer backbone resulting in an osmotic imbalance and subsequent bursting of the vesicle (i.e. proton sponge hypothesis) (Behr, 1997). However, recent evidence from other cationic polymers suggests endosomal escape due to polymer coil expansion leading to direct vesicle perturbation (Funhoff et al., 2004; Griffiths et al., 2004). Thus further studies are required to elucidate the precise mechanism of action of PEI. Since the focus of this introduction is on intracellular trafficking, the mechanism of endosomolytic polymers will not be discussed further. Despite the success of PEI as a vector, toxicity limits its use both *in vitro* (Boussif et al., 1995; Fischer et al., 1999; Godbey et al., 2001) and *in vivo* (Boussif et al., 1995; Wightman et al., 2001). A recent study by Wightman carefully compared the transfection efficiency of branched PEI (Mw = 25,000 g/mol and 899,000 g/mol) to linear PEI (Mw = 22,000 g/mol), with the linear form showing greater transfection efficiency and no toxicity *in vivo* (Wightman et al., 2001).

Despite the wealth of literature on PEI relatively little is known about the intracellular distribution and trafficking of the polymer. PEI (branched, Mw = 25,000 g/mol) complexed with DNA (120 nm ± 30) at a charge ratio of 10 : 1 was shown by live cell fluorescence microscopy to be pinocytosed into synchronised L929 cells (mouse fibroblasts) in less than 10 min. No signs of the formation of micrometric fluorescent clumps were observed on the outer surface of the plasma membrane, and uptake of PEI complexes was attributed to fluid-phase pinocytosis (Remy-Kristensen et al., 2001). PEI-DNA complexes localised in perinuclear vesicles and fusion occurred between these complex-loaded late endosomes. However, escape of the complex from endosomes was a major barrier to transfection. This limited the number of transfected cells to a few percent, despite the presence of pinocytosed PEI-DNA complexes within most cells. Entry of the complex into the nucleus for transfection was proposed to be dependent on mitosis (Remy-Kristensen et al., 2001). In contrast to the fluid-phase pinocytic uptake of PEI complexes in L929

cells, Godbey *et al.* reported the migration of PEI (branched, Mw = 25,000 g/mol) and PEI-DNA (7.5 : 1) complexes into clumps on the cell surface of live EA.hy929 cells (human endothelial hybridoma) 30 min post transfection, followed by the internalisation of the polyplex (Godbey et al., 1999b). Binding and subsequent clustering of the polymer was proposed to occur at discrete sites of the plasma membrane (Godbey et al., 1999b) and could thus involve cell surface proteoglycans. Adsorptive pinocytosis of PEI has also been suggested by others (Klemm et al., 1998). Thus observed differences could be related to the variable expression of cell-surface GAGs in L929 and EA.hy929 cells. Following pinocytosis of polyplexes by EA.hy929 cells, polymer loaded vesicles grew in size and occasionally lysed. Interestingly both PEI and PEI-DNA complexes underwent nuclear localisation in an ordered manner (Godbey et al., 1999b). Nuclear localisation of the polymer and polyplex is also supported by studies conducted by Pollard and co-workers (Pollard et al., 1998). Here, PEI (Mw = 25,000 g/mol, not specified if branched or linear) promoted gene trafficking from the cytoplasm to the nucleus followed by nuclear trans-gene expression (Pollard et al., 1998).

Nuclear localisation of PEI complexes (Mw = 25,000 g/mol at 6 : 1 polymer to DNA ratio) has also been demonstrated in COS 7 cells using live cell real-time multiple particle tracking (Suh et al., 2003). With this technique it was demonstrated that complexes were taken up by pinocytosis, and efficiently transported along microtubules towards the nucleus by a motor-driven process within minutes. Perinuclear localisation of complexes coincided with the intracellular localisation of the microtubule organisation centre. After 30 min, efferent polyplex movement was observed which was in equilibrium with the afferent transport processes. Stationary vesicles closest to the nucleus showed a change in movement from a sub-diffusive to diffusive transport following 1 – 4 h post-transfection. This transition may be caused by the escape of the polyplex from stationary endosomal carriers (Suh et al., 2003). Results reported by Clamme *et al.* support the notion of complexes diffusing out from late endosomes into the nucleus (Clamme et al., 2003b).

Direct experimental evidence for the escape of PEI-nucleic acid complexes (PEI Mw = 25,000 g/mol, not specified if branched or linear) from the endosomal/lysosomal compartments of SW 13 cells (adrenal gland carcinoma cells) was obtained with the aid of live cell confocal laser scanning microscopy (Merdan et al., 2001). Co-localisation of the lysosomal marker lysotracker blue and of the Oregon Green (OG) PEI conjugate indicated that the PEI complexes were directed to the lysosomal compartment. The confocal study revealed that release of the complex as a sudden event, suggesting bursting of the vesicle (Merdan et al., 2001). No lysosomal escape was observed with PEI polyplexes in the presence of bafilomycin A1, a drug which suppresses acidification of the lysosomal compartment. PEI polyplexes exhibited a high luciferase expression, which was reduced approximately 200 fold in the presence of bafilomycin A1 (Merdan et al., 2001).

Similar to the studies performed with PLL, Forrest and Pack demonstrated that branched PEI (Mw = 25,000 g/mol) was trafficked into acidic compartments in C2C12 cells (pH ~ 6.2), Hep G2 cells (pH ~ 4.5) and in HEK293 cells (pH ~ 5.0) in 1 – 5 h, though kinetics were highly cell type-dependent and no correlation between pH and transfection efficiency was evident (Forrest & Pack, 2002). The study by Akinc and Langer demonstrated in NIH 3T3 cells (murine fibroblasts) that linear PEI (Mw = 25,000 g/mol) and branched PEI (Mw = 25,000 g/mol) were exposed to pH values of 5.0 and 5.9 respectively, with a correlation between high pH values and increased transfection (Akinc & Langer, 2002).

Only one study has investigated the uptake and intracellular fate of PEI (branched, Mw = 25,000 g/mol) *in vivo* by differential and isopycnic centrifugation of rat liver (Lecocq et al., 2000). PEI was labelled with [^{125}I]iodide-tyramine cellobiose and injected intravenously into rats. In the liver, PEI accumulated predominately in hepatocytes (79.8 %) and to a lesser extent in endothelial and Kupffer cells (10.3 % and 9.9 % respectively). Early after injection (5 min), radioactivity exhibited a distribution pattern similar to that of the plasma membrane

marker. Thus it was concluded that PEI was internalised via adsorptive pinocytosis due to electrostatic interaction of the polymer with the plasma membrane, results which are in accordance with the fluorescence microscopy study by Godbey and co-workers (Godbey et al., 1999b; Lecocq et al., 2000). After 4 h and for up to 96 h, the distribution pattern was similar to that of cathepsin C, a lysosomal enzyme. Radioactivity and hydrolase distribution in a sucrose gradient were similarly modified by a pre-treatment of the rat with Triton-WR1339, a specific perturbant of lysosomes. These results indicated that PEI was pinocytosed, and most of the polymer was trafficked to lysosomes. Subcellular fractionation studies by the same group demonstrated that PEI (branched, Mw = 25,000 g/mol) complexed with DNA did not localise in the lysosomes 1 h after injection, whereas naked DNA did (Wattiaux et al., 2000). A similar phenomenon has been observed with 1,2-diacyl-3-trimethylammonium propane (DOTAP) lipoplexes (Wattiaux et al., 1996). The rate of polyplex transfer into lysosomes was attributed to size, thus explaining the different observations made in the two subcellular fractionation studies using PEI and PEI complexes (Wattiaux et al., 2000).

1.5.4 Dendritic polymers

Since the first report of dendritic polymer synthesis (Buhleier et al., 1978), there has been an increased interest in these structures due to their uniform Mw, large number of controllable peripheral functional groups for drug delivery applications and unique physico chemical characteristics (Bosman et al., 1999). There is a growing pipeline of therapeutics and diagnostic agents in pre-clinical and clinical development based on dendrimers (Aulenta et al., 2003; Stiriba et al., 2002). Most notably are a PLL dendrimer used for magnetic resonance imaging (Gadomer-17, Shering AG) (Herborn et al., 2003), and a modified PLL dendrimer with 32 naphthalene disodium disulfonate surface groups being explored as a vaginal (topical) virucide for prevention of HIV and sexual transmitted infections (Bernstein et al., 2003; McCarthy et al., 2004).

The intracellular trafficking of dendrimers has most widely been investigated in the context of gene delivery, due to their ability to condense DNA (table 1.5). However, increasingly dendrimers are also being investigated as potential drug carriers (for most recent examples see Chapter 6 table 6.1). The commercial availability of cationic polyamidoamine dendrimers (PAMAMs) (figure 1.9 and table 1.6), polypropylenimine diaminobutane dendrimers (DABs) and partially degraded or "fractured" PAMAM dendrimers (Superfect and Polyfect) has accelerated this field. Excellent transfection efficiency observed with "fractured" PAMAM dendrimers was attributed to the greater flexibility of the dendrons (Tang et al., 1996). Although, cationic dendrimers are cytotoxic in a generation-dependent manner (Brazeau et al., 1998; Malik et al., 2000; Roberts et al., 1996), dendrimers with carboxylate and malonate surface functionalities are less cytotoxic (Malik et al., 2000). Due to the highly defined architecture of these polymers, dendrimers are ideal tools to investigate the influence of topology on intracellular trafficking and distribution.

Antisense OND delivery by a fluorophore-conjugated PAMAM dendrimer generation (G) 5 was used to study the subcellular distribution of the construct in HeLa cells (human epitheloid carcinoma) (Yoo & Juliano, 2000). Surprisingly, the conjugation of the hydrophobic OG fluorophore to the dendrimer dramatically enhanced transfection efficiency of the construct to levels comparable to Lipofectin, Lipofectamine and Superfect. Dendrimer without OG showed only moderate activity and it was proposed that the presence of a hydrophobic small molecule like OG could possibly facilitate endosomal escape. Using an uncharacterised fractionation method approximately 5 % of functionally active dendriplexes were recovered in the "nuclear fraction" (Yoo & Juliano, 2000). The intracellular delivery of PAMAM dendriplexes (G3) were also investigated using flow cytometry and confocal microscopy. Intracellular delivery was enhanced (50 fold) with the use of PAMAM dendrimers compared to uncomplexed OND (De Long et al., 1997). Confocal analysis of live cells revealed primarily intra-cytoplasmic and nuclear accumulation,

Table 1.5 Examples of dendrimer-based drug delivery: transport and subcellular distribution

Polymer	Model system	Probe	Methodology used	Findings	Comment	Reference
PAMAM G2, 4 and 5	CHO	FITC	Flow cytometry	Concentration (2.5 – 20 μM) and generation-dependent uptake of dendrimers, dendriplex uptake was generation independent.	No evaluation of possible cell toxicity. Uptake only determined at 24 h.	(Poxon et al., 1996)
"Fractured" PAMAM	HeLa NIH 3T3	FITC	Flow cytometry confocal microscopy	Plasma membrane and intracellular labelling at 1 h, after 16 h chase only intracellular labelling, intracellular distribution was cell cycle-dependent with nuclear localisation for cells in the G2/M phase.	Only study addressing effect of cell cycle on dendrimer intracellular distribution.	(Helin et al., 1999a)
"Fractured" PAMAM	HeLa NIH 3T3	FITC	Flow cytometry confocal microscopy	At 4 h, 80 % of cells were fluorescent, perinuclear and nuclear localisation of dendriplexes at 1 – 24 h.	Limited information on methodologies used.	(Helin et al., 1999b)

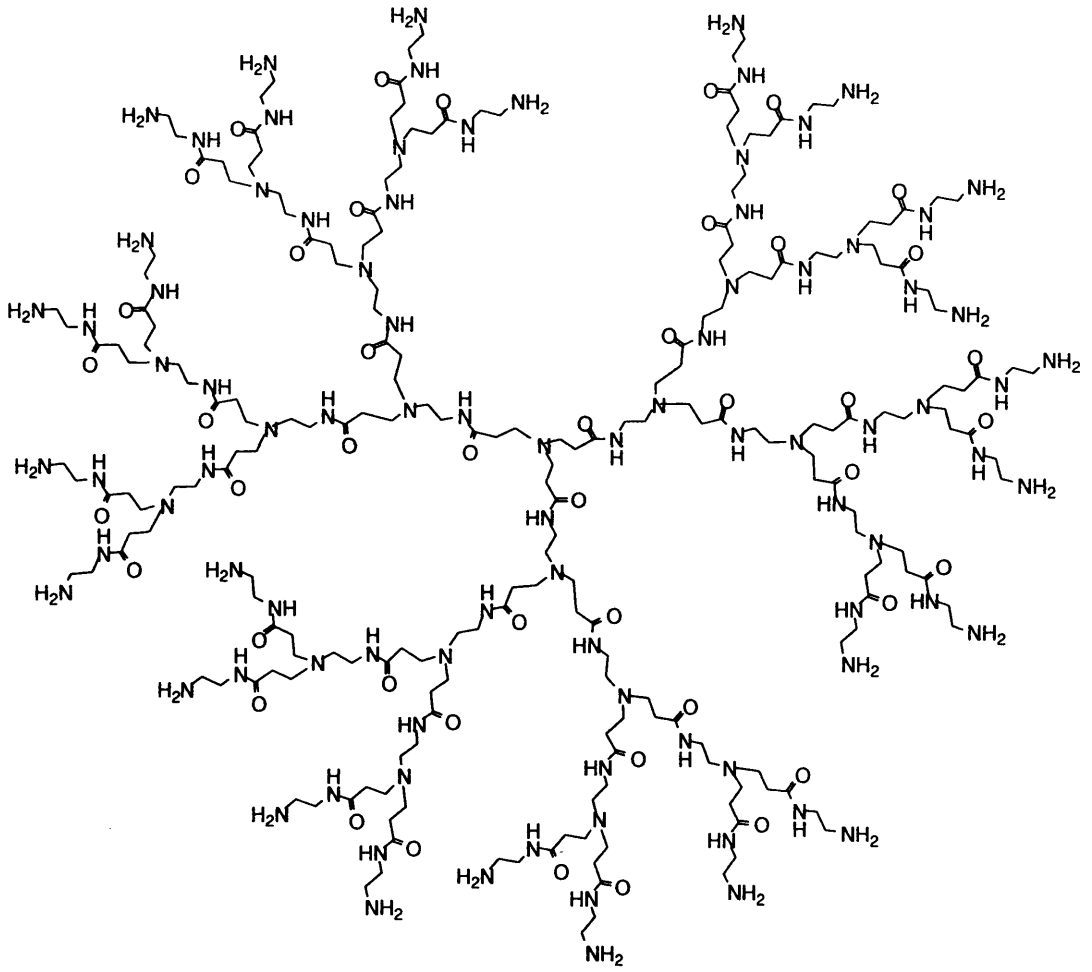

Figure 1.9 Chemical structure of PAMAM dendrimer G3 (NH_3 core).

Table 1.6 Physical chemical characteristics for PAMAM dendrimers (Eichman et al., 2000; Tomalia et al., 1990)

PAMAM (Ethylenediamine core)			PAMAM (NH_3 core)		
G	Mw	1° amine	G	Mw	1° amine
0	517	4	0	359	3
1	1,430	8	1	1,043	6
2	3,256	16	2	2,411	12
3	6,909	32	3	5,147	24
4	14,215	64	4	10,619	48
5	28,826	128	5	21,563	96

and the extent of delivery of PAMAM dendrimers was comparable to that seen using Lipofectamine (De Long et al., 1997).

One of the first studies to investigate PAMAM dendrimers as potential oral drug delivery systems was reported by Wiwattananpatapee and co-workers (Wiwattanapatapee et al., 2000). In this study the rate of transcytosis of different PAMAM dendrimers across the rat intestine using the inverted gut sac technique was evaluated. The study quantified the serosal transfer *in vitro* of [^{125}I]iodide-labelled PAMAM dendrimers (G 2.5, 3, 3.5, 4 and 5.5) in relation to dendrimer size and charge (Wiwattanapatapee et al., 2000). Fluid-phase pinocytosis has been suggested for the high serosal transfer rates (endocytic index (EI) of 3.4 – 4.4 µl/mg protein/h) observed for all investigated anionic dendrimers. Cationic dendrimers showed lower transfer rates (EI of 2.3 – 2.7 µl/mg protein/h) and extensive tissue binding. However, serosal transfer rates were still significantly greater than for fluid-phase markers PVP or HPMA (EI of 0.1 – 0.3 µl/mg protein/h) (Wiwattanapatapee et al., 2000). The defined molecular architecture of dendrimers could possibly play an important role for the rate of serosal transfer, although further studies are needed to substantiate these findings (Florence & Hussain, 2001).

1.6 Aims of this thesis

There have been relatively few studies that have set out to design polymer therapeutics based on a biological rationale, which include systematic studies designed to quantify pinocytosis and intracellular trafficking. Therefore the aim of this thesis was to establish a subcellular fractionation method in B16F10 mouse melanoma cells to quantify intracellular trafficking of polymer therapeutics and to systematically investigate the effect of selected polycations on pinocytosis. Due to the routine use of B16F10 cells in the development of polymer anticancer conjugates, quantitative methods in this cell line were of particular interest.

The first part of this thesis set out to establish a quantitative subcellular fractionation method in B16F10 mouse melanoma cells. First, it was necessary to select appropriate organelle markers, optimise and validate assays to allow their quantitative analysis in the respective subcellular fractions. Furthermore cell homogenisation and centrifugation conditions were tailored to maximise cell breakage and to achieve separation and enrichment of major cellular organelles/components (Chapter 3). The established fractionation method was then used to study the subcellular distribution of PK1 and doxorubicin which in part served to (a) validate the method due to the well documented subcellular distribution of doxorubicin, (b) enhance the current understanding of PK1 trafficking in B16F10 cells (Chapter 4).

However, it is clear that more studies are needed to define the endocytic and intracellular trafficking properties of polymers undergoing design as second-generation polymer therapeutics. Therefore a series of linear and branched PEI and PAMAM dendrimers (G2 – 4) were chosen which are commonly used as non-viral vectors for gene delivery. Polymer probes were labelled with OG, characterised and subjected to a cellular pharmacokinetics screen by flow cytometry (Chapter 5). The aim of the study was to identify polymers with favourable pharmacokinetics characteristics for gene delivery and to short list compounds for future fractionation studies.

Chapter 2

Materials & Methods

2.1 Materials

2.1.1 Linear, branched and dendritic polymers

PAMAM dendrimers G2 – 4 (ethylenediamine core), dextran (Mw = 10,000 g/mol), fluorescein isothiocyanate (FITC)-dextran (Mw 10,000 g/mol), branched PEI (Mw = 25,000 g/mol) and PVP (Mw = 1.3 x 10^6 g/mol) were from Sigma-Aldrich, UK. Linear PEI (Mw = 25,000 g/mol) was purchased from Polysciences Inc, UK. Polysaccharide standards (Mw = 738 – 47,300 g/mol) and PK1 (Mw ≈ 30,000 g/mol; total doxorubicin loading 6.6 wt% containing 0.39 % free doxorubicin) were purchased from Polymer Laboratories, UK. (For details of the polymer characteristics see table 5.3 in Chapter 5).

2.1.2 General chemicals and reagents

Methanol (MeOH), ethanol, acetone, ethyl acetate, hydrochloric acid, glacial acetic acid, boric acid, triethylamine, magnesium chloride, calcium chloride and paraformaldehyde were obtained from Fisher Scientific, UK. Deuteriumoxide (D_2O) was from Sigma-Aldrich, UK and 2,4,6-trinitrobenzensulfonic acid (TNBS) was obtained from Pierce, USA. Sodium chloride, sodium hydrogen carbonate, sodium carbonate, sucrose, sodium acetate, di-sodium hydrogen orthophosphate dodecahydrate and sodium dihydrogen orthophosphate monohydrate were obtained from BDH, Germany. Anhydrous dimethyl sulfoxide (DMSO) and diemthylformide (DMF) were from Sigma-Aldrich, UK, as were Triton X-100, lithium acetate, ninhydrin, hydrindantin, 4 %w/v copper (II) sulphate, bicinchoninic acid (BCA) solution, pentahydrate, 3-amino-1-propanol, sodium nitrate, succinic acid, ethylenediaminetetraacetic acid (EDTA), tris(hydroxymethyl)aminomethane hydrochloride (Tris-HCl), tris(hydroxymethyl)aminomethane (Tris-Base) and citric acid monohydrate. Sodium hydroxide pellets, *N*-2-hydroxyethylpiperazine-*N*'-ethanesulphonic acid (HEPES), 2-*p*-iodonitrotetrazolium violet (INT), 4',6-diamino-2-phenylindole (DAPI), calf thymus DNA, pyruvic acid (crystallised mono sodium salt), *p*-nitrophenyl phosphate, sodium borate, β-nicotinamide adenine dinucleotide

reduced disodium salt (NADH), 4-methylumbelliferyl, 4-methylumbelliferyl-*N*-acetamido-*β-D*-glucosaminide, leupeptin, aprotinin, pepstatin, chlorpromazine, wortmannin, methyl-*β*-cyclodextrin (MβCD), bovine serum albumin (BSA), BSA protein standards and phenylmethylsulfonyl fluoride (PMSF) were from Sigma-Aldrich, UK. Glycine and sodium metaborate were from ICN, USA.

2.1.3 Chemicals and reagents for fluorescence microscopy and flow cytometry

The 5'-isomer of the dye Oregon Green 488 succinimidyl ester (OG-SE) was obtained from Molecular Probes Inc, USA. Frosted microscope slides and ∅ 16 mm coverslips were purchased from Menzel, Germany and Chance Propper, UK respectively. Glass bottom culture dishes (∅ 35 mm) for live cell imaging were obtained from Matteck Co-operation, USA. Dako and Vectashield mounting medium with DAPI stain were obtained from Dakocytomation and Vector, USA respectively. Immersion oil with a 1.518 refractive index was obtained from Leica, Germany and clear nail polish from Number 17, UK. Fluorescein diacetate (FDA), fluorescein, and propidium iodide (PI) were purchased from Sigma-Aldrich, UK. FACS flow, -safe, -clean and Falcon tubes were purchased from Becton Dickinson, UK.

2.1.4 Cell culture

B16F10 murine melanoma cells were purchased from ATCC, USA. RPMI 1640 (L-glutamine) in the presence or absence of the pH indicator phenol red was obtained from Invitrogen Life Technologies, UK. Foetal bovine serum (FBS), and 0.05 %w/v trypsin/0.53 mM EDTA without magnesium and calcium chloride were obtained from Invitrogen Life Technologies, UK. Medical grade CO_2, N_2 (all 95 %v/v) and liquid nitrogen were supplied by BOC, UK. Trypan blue solution (0.4 %w/v), 3-(4,5-dimethylthiazol-2-yl)-2,5-diphenyl-2H-terazoliumbromide (MTT) and sterile DMSO were obtained from Sigma-Aldrich, UK and copper II sulphate from BDH, Germany.

2.2 Equipment

2.2.1 Analytical

Ultraviolet (UV) absorbance was measured with a Sunrise UV absorbance plate reader from Tecan, Austria, and a Cary 1G UV-visible spectrophotometer from Varian, Australia. Where indicated a Cary Win UV software package was used for data acquisition and analysis. Fluorescence was detected with an Aminco-Bowman Series 2 luminescence spectrophotometer from Spectronic Instruments, USA, and a Fluostar Optima fluorescence plate reader from BMG Labtechnologies, Germany. ^{13}C spectra were recorded either with a Brucker DPX 300 nuclear magnetic resonance (NMR) spectrometer at 75 MHz, and subsequently analysed with 3.6 XWin NMR software, or a Brucker Advanced 500 NMR spectrometer at 126 MHz and subsequently analysed with Topspin 1.3b software. Thin layer chromatography (TLC) silica plates coated with Alugram SIL-G/UV_{254} were from Macherey-Nagel, Germany and visualised under multiband UV lamp (254/365 nm) from Upland, USA. A Toledo 320 pH meter from Mettler Toledo, Switzerland or Hydrion pH indicator paper (Sigma-Aldrich, UK) were used for pH measurements.

Gel permeation chromatography (GPC) was carried out with Waters Ultrahydrogel 1000 and 250 columns (7.8 x 300 mm) in series, using a Gilson 133 refractive index (RI) detector (Gilson Inc, USA) and a Jasco PU-980 high-performance liquid chromatography pump (Jasco UK Ltd, UK). Samples were analysed with Caliber software (version 7.0.4) provided by Polymer Laboratories, UK. Gravitational GPC was performed with Sephadex G25 from Amersham Biosciences (Sweden) with PD10 columns or a 25 cm column with an internal diameter of 1 cm. Likewise Sephadex LH20 from Amersham Biosciences (Sweden) was used for gravitational GPC employing a 25 cm column with a 1.5 cm internal diameter.

Spectra/Pore 7-regenerated cellulose dialysis membrane (Mw cut-off 2,000

g/mol) was obtained from Spectrum Laboratories Inc, USA. Samples were freeze-dried with a Flexi Dry FD-1.540 freeze-dryer from FTS Systems, USA connected to a DD75 double stage, high vacuum pump from Javac, Australia.

2.2.2 Cell culture and subcellular fractionation

Costar cell culture consumables were purchased exclusively from Corning Inc, USA with the exception of serological pipettes, bejous and universal containers which were from Elkay, Ireland and 150 cm^2 petri dishes which were purchased from Nagel Nuc Inc, Denmark. Galaxy S incubators and a Procell incubator were supplied by Wolf Laboratories and Jencons-PLS, UK respectively whilst Bioair and Microflow class II laminar flow hoods were from Bioair (Italy) and Servicecare, UK respectively. For routine cell culture work an inverted DM IL Leica bright-field microscope was used (Leica, Germany), and a silver-stained Neubauer haemocytometer (Marienfeld, Germany) was used for cell counting. For cell scraping and homogenisation a tailor-made rubber policeman and a cell cracker with precision ball bearings were used, both from the European Molecular Biology Laboratory, Germany. A Varifuge 3.0 RS with swing out rotor buckets (type 8080, r_{max} 21.1 cm) and the Eppendorf 5417 R bench-top centrifuge with standard fixed angle rotor (model 5417 C/R) were from Heraeus Instruments and Eppendorf, Germany respectively. For ultracentrifugation studies thick-walled 6.5 ml polycarbonate centrifugation tubes were used in a Ti 50.4 fixed angel rotor (r_{max} 9.64 cm, r_{min} 6.57 cm), both supplied by Beckman, USA. Samples were ultracentrifuged with an Optima LE-80K centrifuge from Beckman Coulter, USA.

2.2.3 Flow cytometry, bright-field and fluorescence microscopy

A FACSCalibur flow cytometer (Becton Dickinson, UK) equipped with a single argon laser (excitation wavelength 486 nm) was used for all flow cytometry studies. Logarithmic-transformed data were acquired in 1024 channels with band pass filters FL-1 (530 nm ± 30 nm), FL2 (585 nm ± 42 nm) and FL-3 (670 nm long

pass filter) and subsequently processed with Cell Quest software (version 3.3). Epifluorescent images were viewed with an inverted Leica DM IRB fluorescence microscope (Germany) with an incident 450 nm – 490 nm and long pass filter 515 nm (i.e. for doxorubicin-associated fluorescence) and captured with a 12-bit cooled monochrome Retiga 1300 camera from Qimaging, Canada. Images were collected and handled using Openlab software (version 3.0.9) from Improvision, UK. The inverted Leica DM IRB microscope was also used to acquire bright-field images. Images were processed as described. For confocal fluorescence microscopy, images were captured with an inverted DM IRE2 microscope equipped with a λ-blue 60 x oil immersion objective and handled with a TCS SP2 system. Confocal images were acquired at a 0.33 μm or 0.84 μm section thickness for fixed and live cell images respectively. Fluorophores were excited with an argon laser (488 nm) and blue diode (405 nm) and emission wavelengths were collected at 425 nm – 473 nm (DAPI), 500 nm – 535 nm (OG/FITC) and 555 nm – 620 nm (doxorubicin). Each recorded image consisted of 4 line scans to improve image quality. Images were captured at an 8-bit grey scale and processed with LCS software (version 2.5.1347a, Leica Germany) containing multicolour, macro and 3D components. Stacked images were maximum projections composed of 10 – 16 single confocal slices.

2.3 Methods

Methods used in this thesis are described below, though where necessary specific details are given in the related experimental chapters. Where appropriate, buffers were made up in double distilled water as detailed in the Data for Biochemical Research reference book (Dawson et al., 1986).

2.3.1 General cell culture procedures

Cell culture was carried out according to guidelines by The United Kingdom Co-ordinating Committee on Cancer Research (UKCCCR, 2000), and all manipulations with the exception of the centrifugation step, were performed in a

class II laminar flow hood using sterilised consumables that had been decontaminated with 70 %v/v ethanol. Cells were incubated and maintained in incubators at 37 °C/5 % CO_2 with water humidifying trays containing copper II sulphate unless otherwise stated. Cell-culture techniques described here are for adherent cells.

Defrosting

Cells were obtained as a cryopreserved cell suspension from the supplier or from personal stocks. Cells were rapidly thawed at 37 °C and then placed in a universal container and centrifuged at 600 g for 4 min to remove the cryopreservative. After centrifugation, the supernatant was decanted and replaced with fresh medium containing 20 %v/v FBS (5 ml). The cell pellet was gently re-suspended and centrifuged as described above. After the centrifugation, the supernatant was decanted and the cells re-suspended by two passes through a 23 gauged needle in complete medium containing 10 %v/v FBS. The resulting cell suspension was placed in a flask (25 cm^2) and allowed to grow for 24 h. Cells were then washed and supplemented with fresh medium and maintained as described below.

Maintenance

Cells were maintained, subcultured and cryopreserved as summarised in table 2.1. Cells were subcultured twice weekly when they were > 70 % confluent by removing the culture medium from the flask, washing the cells twice with phosphate buffered saline (PBS 0.1 M; pH 7.4), and trypsinising the cells. Medium was added to the cells, and the cell suspension was centrifuged at 600 g for 4 min. The supernatant was decanted and the cells re-suspended in 10 ml of complete medium with a 23 gauged needle and syringe. The resulting cell suspension was then used to subculture the cells at the appropriate split ratio. Cell lines were kept for a maximum of 30 passages before starting up a new batch of cells to assure that the cells were

Table 2.1 Summary of culture conditions for B16F10 cells

Cell line	Origin	Medium#	Seeding density (cells/ml)	Split ratio	Freezing Medium
B16F10	Mouse melanoma	RPMI 1640 10 % FBS	1×10^4 1×10^5	1 : 10	90 % FBS 10 % DMSO

FBS sterilised by filtration

always within the same passage range for all studies.

Counting

Cells were washed, trypsinised, and re-suspended in a known volume of medium to form a cell suspension as described above. From this cell suspension, an aliquot (100 µl) was removed and diluted by half with a 0.2 %w/v trypan blue solution in PBS, mixed and allowed to stand for 1 min to stain dead cells. A coverslip was placed onto the haemocytometer. Following the appearance of Newtonian rings, the counting chamber was filled with the cell suspension and a total of eight 0.1 mm^3 squares were counted according to the manufacturers instructions excluding any non-viable cells stained with trypan blue. Taking into account the dilution factor, cell concentrations were determined.

Freezing

Cells were regularly frozen to maintain adequate stocks. The freezing medium used is specified in table 2.1. Following the cell count, cells were re-centrifuged and the resulting pellet was reconstituted as described above in freezing medium at 10^6 cells/ml. Then 1 ml of cell suspension was added to a cryogenic vial, wrapped in tissue paper and placed in a polystyrene box which was maintained at - 20 °C for 1 h, then at - 80 °C overnight, and finally in liquid nitrogen the next day.

2.3.2 Growth curves using the MTT assay

Before testing cellular cytotoxicity of polymers and drug(s), it was important to establish the growth rate of the cells to assure that studies were carried out during the exponential growth phase. Cell proliferation was assessed by monitoring the conversion of MTT to formazan. The reduction of MTT is catalysed by mitochondrial dehydrogenase enzymes and hence a measure for cell viability (figure 2.1) (Mosmann, 1983). Briefly, cells (100 µl/well) were seeded into 96 well microtitre plates and allowed to adhere for 24 h. Thereafter cellular viability was

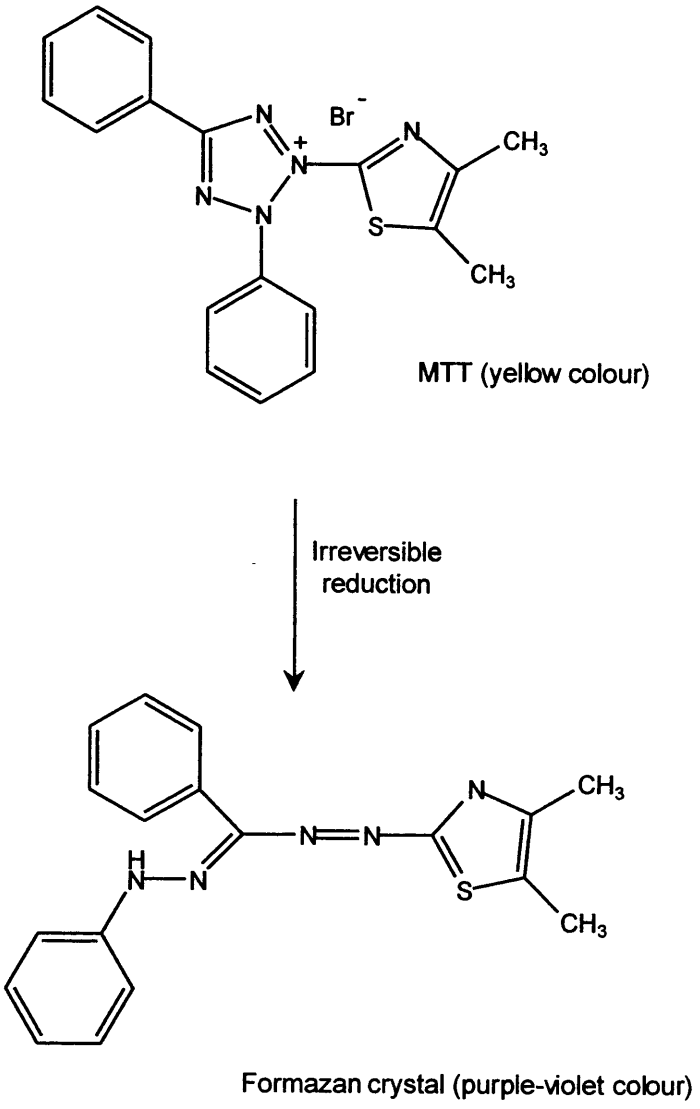

Figure 2.1 Outline of the reduction of MTT. Reduction of MTT to formazan is irreversible and catalysed by enzymes of the respiratory chain and thus an indicator for mitochondrial activity.

assessed on a daily basis by adding 20 µl of filter sterilised MTT (5 mg/ml in PBS) to a single row of six wells. Following a 5 h incubation period with MTT, wells were drained and the blue formazan crystals dissolved in sterile DMSO (100 µl) by incubating for 30 min and measuring the absorbance at 550 nm with an UV absorbance plate reader. Only the inner rows of the microtitre plate were used for these studies to minimise cell growth variations due to different medium evaporation rates. Growth curves were constructed by plotting absorbance, blanked with DMSO, against time. Typical growth curves for B16F10 cells are shown in figure 2.2.

2.3.3 Cytotoxicity assessment using the MTT assay

The previously described MTT assay for the *in vitro* screening of polymers and cytotoxic agents was used in Chapters 4 and 5 to evaluate cytotoxicity of polymers and drug(s) (Sgouras & Duncan, 1990). In brief, Cells (100 µl either 1 x 10^3 or 1 x 10^4) were seeded into 96 well microtitre plates as before and left to adhere for 24 h. The next day, the medium was removed from the wells and replaced with filter sterilised complete medium containing polymer or drug. The plates were then incubated with polymer solutions for either 67 h or 5 h. In the latter case medium was removed following the incubation period and replaced with medium only and further incubated. At 67 h, MTT (20 µl) was added to each of the wells and plates were incubated for a further 5 h. Then all the medium was removed and replaced with DMSO (100 µl), incubated for 30 min and read at 550 nm. Absorbance values were blanked with DMSO and cells exposed to medium only were taken as 100 % cell viability (i.e. control).

2.3.4 Cytotoxicity assessment using bright-field microscopy

Qualitative assessment of polymer cytotoxicity was made by bright-field microscopy at selected concentrations as described in Chapters 4 (section 4.2) and 5 (section 5.2.3). In brief, B16F10 cells were seeded (1 x 10^6) in glass bottom culture dishes and allowed to attach for 24 h. Cells were then washed 3 times with PBS (pH

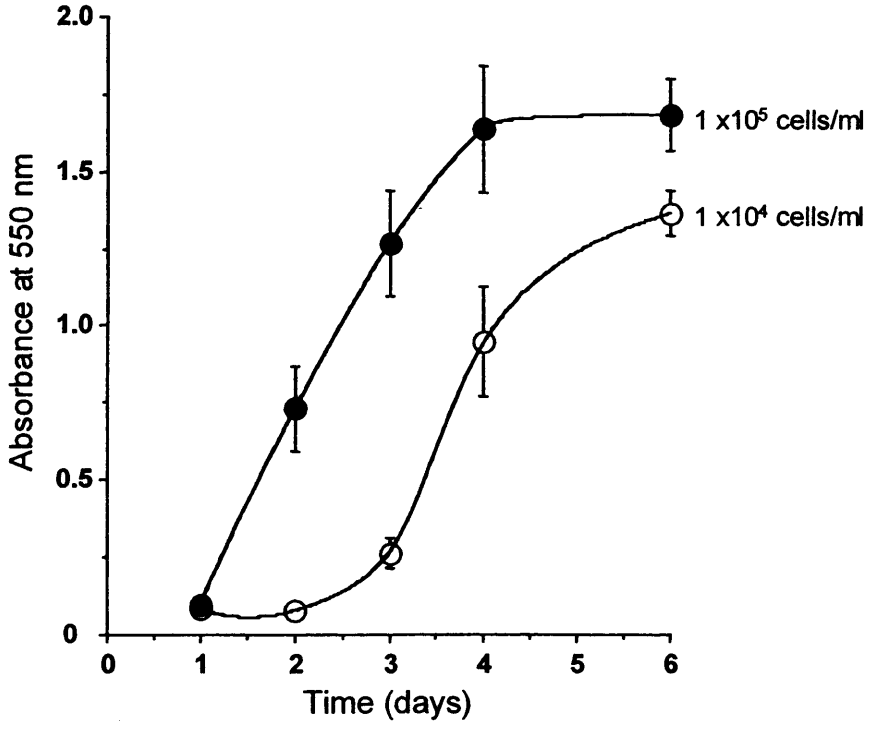

Figure 2.2 Cell proliferation of B16F10 cells measured with the MTT assay. Cells were seeded at a density of 1 x 10^5 cells/ml (●), and 1 x 10^4 cells/ml (O). (Data represents mean ± SEM n = 3, error bars are within plot symbols when not visible).

7.4) and 1 ml of clear complete medium was added containing polymer. Cells were incubated with polymer for 3 – 5 h under cell culture conditions and then visualised for a maximum of 10 min.

2.3.5 Optimisation of the cell breakage efficiency of B16F10 cells

Cell breakage was quantified first to ensure that most cells (> 80 %) had been homogenised in a controlled, uniform and reproducible manner (Chapter 3 section 3.2). Cells (1 x 10^6) were seeded in 150 cm^2 petri dishes and allowed to reach a ~ 80 – 90 % confluency over 2 – 3 days. (Cells were subsequently used for experiments as indicated). Cells were then washed three times with PBS and in the presence of 5 ml of fresh PBS cells were scraped off each petri dish. Cells were pooled and centrifuged at 600 g for 4 min and the pellet was washed with 10 ml of PBS and centrifuging again at 600 g for 4 min. The pellet was then washed with 5 ml of homogenisation buffer composed of 250 mM sucrose, 10 mM HEPES, 1 mM EDTA pH 7.4 and protease cocktail containing aprotinin (2 μg/ml), leupeptin (2 μg/ml), pepstatin A (1 mg/ml) and PMSF (1 mM). Cells were pelleted by centrifugation at 1000 g for 6 min. The resulting pellet was re-suspended in homogenisation buffer at 2.5 fold the wet cell weight. The resulting cell suspension was subjected to passes through the homogeniser (either syringe with 25 gauged needle or cell cracker with ball bearings of different diameters) (figure 2.3). After each pass a 5 μl sample was added to 1 μl of trypan blue and nuclei integrity assessed by bright-field microscopy. To quantify cell breakage, 50 μl of sample was added to 250 μl of 250 mM sucrose, vortexed for 30 s and centrifuged for 10 min at 2,000 g. To determine lactate dehydrogenase activity which served as the reference value for 100 % breakage efficiency, cells were vortexed and centrifuged in the presence of 0.1 %v/v Triton X-100. After centrifugation 50 μl of supernatant was used to determine lactate dehydrogenase activity as described (section 2.3.7). Determining the enzymatic activity of B16F10 post nuclear supernatant (PNS) in the presence and absence of 0.1

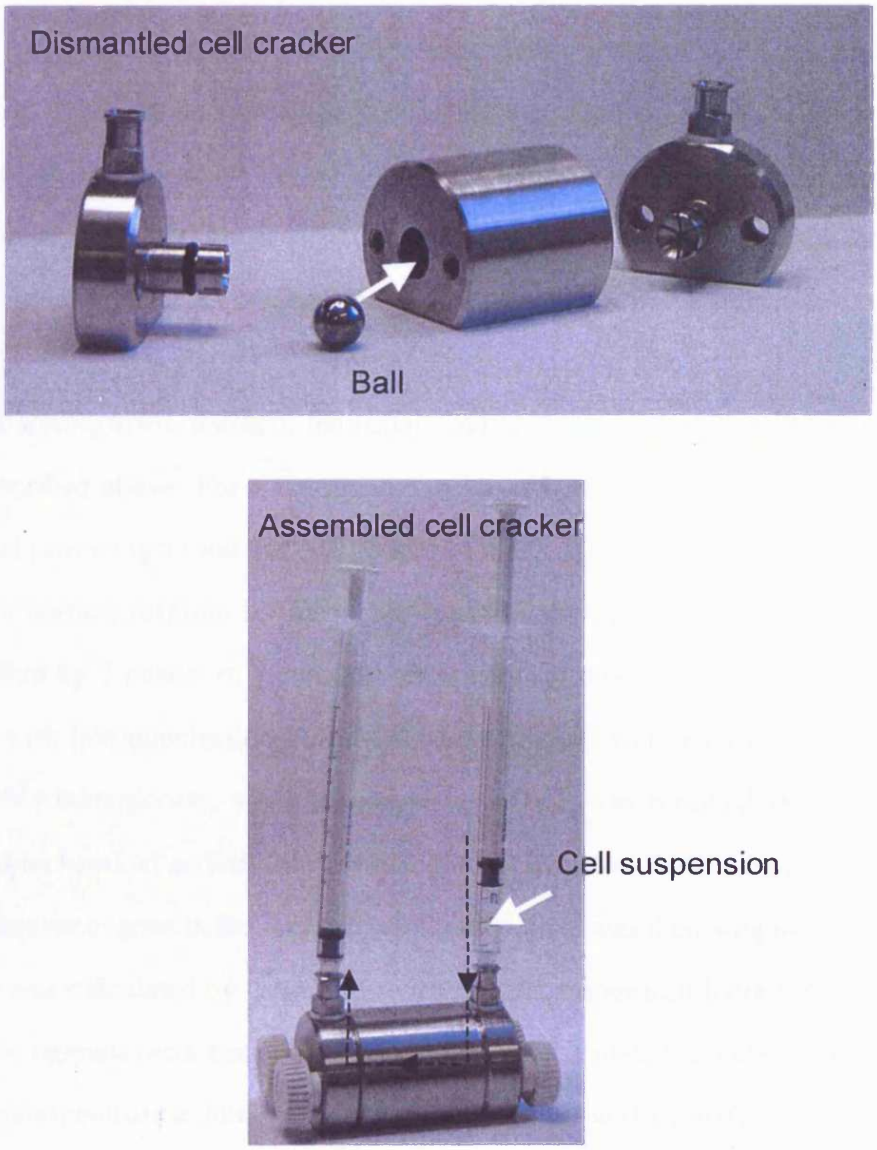

Figure 2.3 A cell cracker in its dismantled and assembled state.

%v/v Triton X-100 assessed the effect of surfactant on lactate dehydrogenase activity.

2.3.6 Differential centrifugation of B16F10 cell homogenate

The fractionation procedure is described below together with the marker assays used to characterise subcellular fractionations (figure 2.4). Details on the validation of the marker assays can be found in Chapter 3 section 3.2. The protein concentration of each fraction was between 0.11 – 1.79 mg/ml, with percentage distributions listed in table 3.4 in Chapter 3.

Cells were grown, washed, harvested and re-suspended in homogenisation buffer as described above. For fractionation studies 15 petri dishes (150 cm^2) were routinely used providing a total wet cell weight of 0.819 – 1.049 g. The pellet was re-suspended in homogenisation buffer at 2.5 fold the wet cell weight. After gentle homogenisation by 7 passes in a cell cracker (clearance 6 μm), the cell suspension was diluted with homogenisation buffer (4.2 fold original wet cell weight) (figure 2.4). From this homogenate, a small sample (~ 300 μl) was retained and used to estimate the biochemical activity of the homogenate. To allow for the calculation of enzyme marker recoveries in the factions, the homogenate was then weighed and the total volume was calculated by using the density of the suspension (detailed below). Next, the homogenate was centrifuged at 1,500 g for 2 min, the pellet was then washed in homogenisation buffer (2 fold pellet weight) and centrifuged again to obtain a nuclear pellet. The combined PNSs were subjected to a 3,000 g spin for 15 min. Again the pellet was washed with homogenisation buffer (2 fold pellet weight) and subjected to a further 15 min spin at 3,000 g and denoted the mitochondrial fraction. The combined supernatants were further centrifuged in sequence, first at 22,000 g for 10 min to obtain the lysosomal pellet, then at 100,000 g for 30 min to obtain the microsomal pellet and the soluble fraction. (N.B. The microsomal pellet commonly refers to vesiculated endoplasmic reticulum fragments and other pelleting

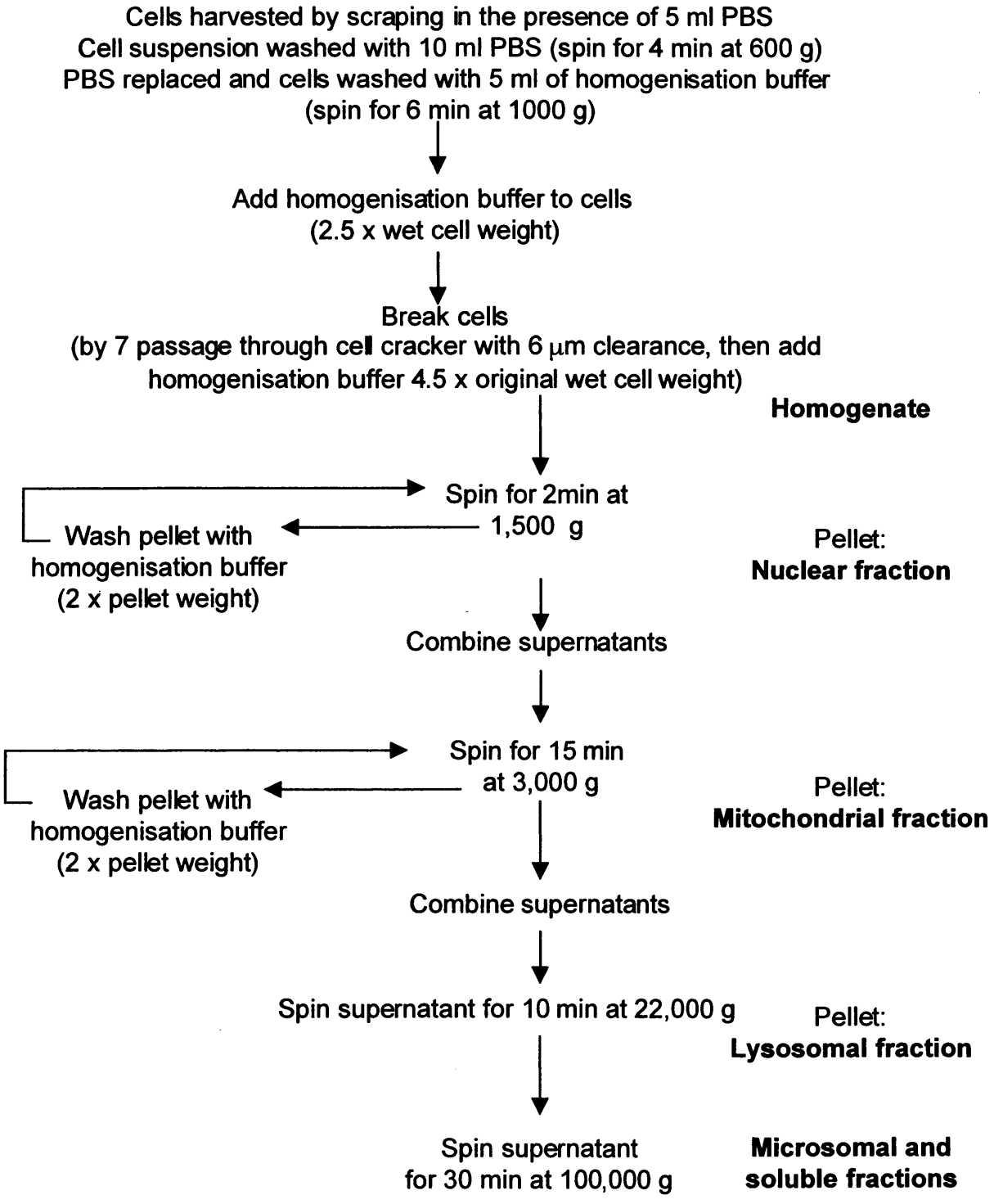

Figure 2.4 Fractionation scheme for B16F10 cells.

vesicles of variable origin). Using pre-weighed tubes, all pellets were re-suspended in homogenisation buffer, and subsequently analysed for marker assays described in 2.3.7. The final volume was calculated by dividing the total sample weight by 1.05, which is the estimated density of such suspensions in 250 mM sucrose (De Duve et al., 1955). All homogenisation, fractionation and washing procedures were carried out at 4 °C.

2.3.7 Marker assays for characterising subcellular fractions

Protein assay: bicinchoninic acid (BCA)

The protein content of cell homogenates was determined to establish the specific catalytic activity of enzyme markers and to estimate the recovery of protein in subcellular fractions. Furthermore the protein content of subcellular fractions served as an indicator to estimate the enrichment of markers in subcellular fractions. The BCA procedure reported previously was used and scaled accordingly (Smith et al., 1985). BCA reagent was added to a $CuSO_4$ pentahydride solution (4 %w/v) at a ratio of 1 : 50 respectively, and 200 µl of this reagent was added to 20 µl of sample (5 µl of fraction and 15 µl of homogenisation buffer) and incubated at 37 °C for 25 min. The absorbance of the copper-I-BCA complex was measured at 550 nm. Calibration standards of BSA in homogenisation buffer treated identical to samples were used to quantify the amount of protein in the fractions. The concentration range test can be deduced from the calibration curve shown in figure 2.5 (panel a).

Nuclear marker DNA

DAPI binding to DNA was used to establish the subcellular distribution of nuclei. Upon DAPI binding to A-T base pairs of DNA the fluorescence is enhanced about 20 fold as compared with the fluorescence of the dye alone. The method developed by Kapuscinski was used (Kapuscinski & Skoczylast, 1977) and scaled accordingly. Briefly, 50 µl of DAPI (20 µg/ml in 250 mM sucrose) was added to each fraction (25 µl) and the mixture diluted to 3 ml with 12 mM NaCl containing 5

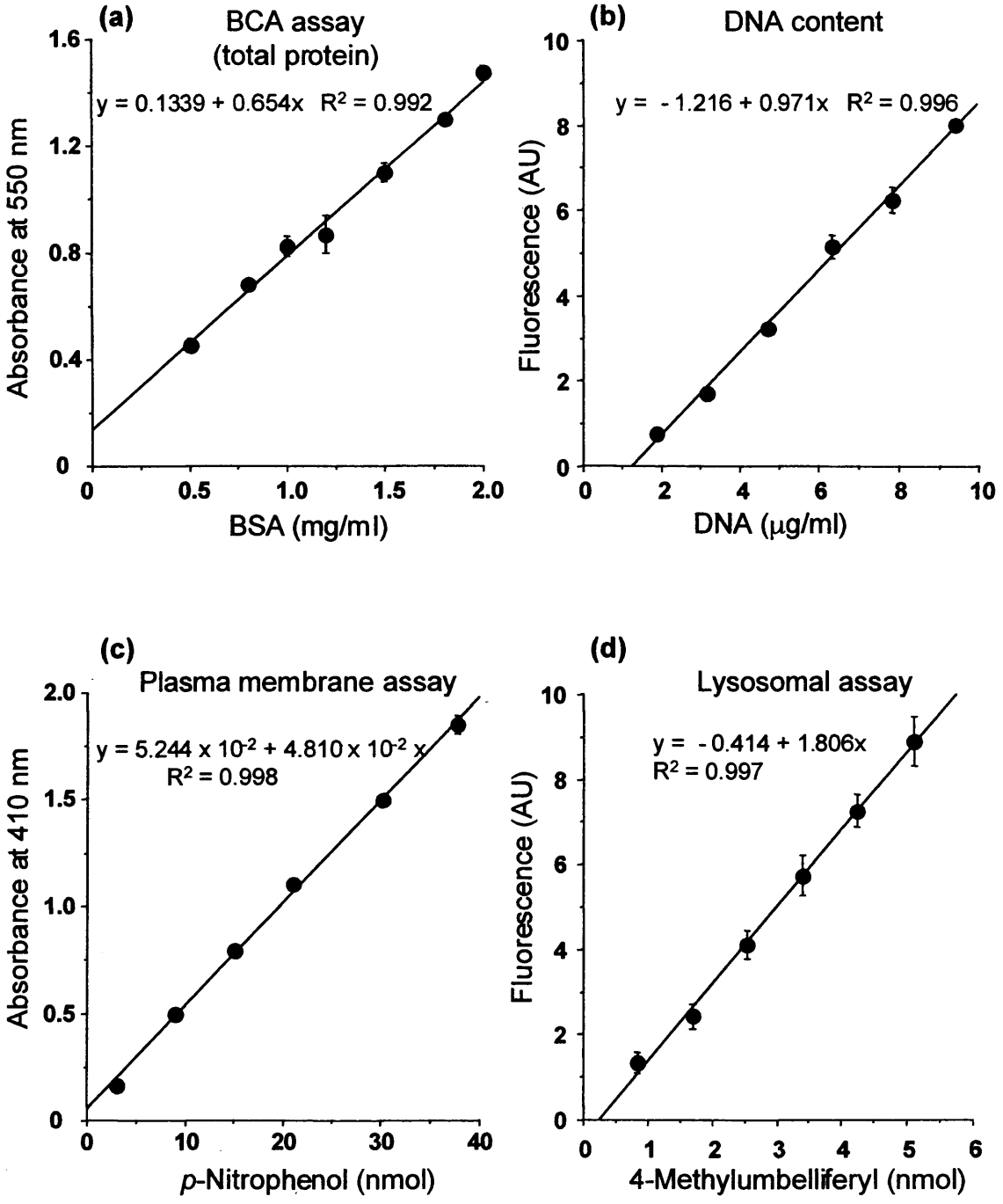

Figure 2.5 Calibration curves for the protein assay, DNA assay, plasma membrane assay and lysosomal assay. (Data represents mean ± SEM n=3, error bars are within plot symbols when not visible).

mM HEPES (pH 7.0). Fluorescence was excited at 358 nm and detected at 454 nm. The amount of DNA was estimated with the calibration curve shown in figure 2.5 (panel b) using calf thymus DNA.

Plasma membrane marker alkaline phosphatase (EC 3.1.3.1)

Alkaline phosphatase activity was used to establish the subcellular distribution of plasma membrane fragments. The substrate nitrophenyl phosphate is hydrolysed at alkaline pH to nitrophenol which gives an intense absorption signal at 410 nm (Bretaudiere & Spillman, 1984). The method described previously was used and scaled accordingly (Graham, 1993). Briefly, to each 5 ml of *p*-nitrophenyl phosphate (16 mM) and sodium borate-NaOH (50 mM; pH 9.8) 20 µl of $MgCl_2$ (1 M) was added. To 200 µl of this assay mixture 25 µl of sample was added and incubated at 37 °C for exactly 30 min and stopped with 1 ml of NaOH (250 mM). Samples were centrifuged at 8,000 g for 2 min and the absorbance of the supernatant was measured at 410 nm. The amount of nitrophenol produced was calculated with the calibration curve shown in figure 2.5 (panel c). For enzyme kinetics experiments, the amount of *p*-nitrophenyl produced was monitored over fixed time points at 5 – 70 min at a (homogenate) protein content of 0.04 – 0.17 mg. For each amount of protein, the enzyme activity was calculated in milli-Units (nmol of substrate transformed per min). All determined activities have then been plotted against protein content and a straight line of best fit was applied. From this line the slope was determined, which represented the specific enzyme activity (expressed as milli-Units per mg of protein).

Lysosomal marker N-acetyl-β-glucosaminidase (EC 3.2.1.30)

N-acetyl-β-glucosaminidase activity was used to establish the subcellular distribution of lysosomes. The substrate 4-methylumbelliferyl-*N*-acetamido-β-*D*-glucosaminide is hydrolysed by the enzyme to yield highly fluorescent 4-methylumbelliferone, which can readily be quantified (Stirling, 1983). The assay described previously (Klemm et al., 1998) was slightly modified. To 50 µl of each

fraction 250 µl of citrate phosphate buffer (200 mM; pH 5.0) was added followed by 75 µl of 250 mM sucrose containing 0.1 %v/v Triton X-100. To this 100 µl of 4-methylumbelliferyl-*N*-acetamido-*β-D*-glucosaminide (5 mM) in 250 mM sucrose was added and the solution was incubated for 1 min exactly. Following the incubation period, 2.5 ml of glycine-NaOH (0.25 M; pH 10.4) was added to stop the reaction. Liberated 4-methylumbelliferyl was quantified by exciting the fluorophore at 357 nm and measuring the emission at 444 nm. Fluorescence values were blanked with control samples containing either no biological material or substrate. The amount of 4-methylumbelliferyl produced was calculated with the calibration curve shown in figure 2.5 (panel d). For enzyme kinetics experiments the amount of 4-methylumbelliferone produced was monitored over fixed time points at 0.25 – 2 min at a (homogenate) protein content of 0.09 mg, 0.17 mg and 0.35 mg. The specific enzymatic activity was calculated from the activity associated with 0.17 mg of protein. This was done by fitting a straight line of best fit to the data points (product formed vs. time). From this line the slope was taken as the specific enzyme activity (expressed as milli-Units per mg of protein). For completeness, the enzyme activities were also calculated at a 0.09 mg and 0.35 mg protein content and also included in the plot.

Mitochondrial marker succinate dehydrogenase (EC 1.3.99.1)

Succinate dehydrogenase activity was used to establish the subcellular distribution of mitochondria. The reduction of INT to formazan is catalysed by mitochondrial dehydrogenase enzymes present at the inner mitochondrial membrane (Schomburg et al., 1993). The basis of the tetrazolium-based assay is analogues to MTT assay depicted in (figure 2.4). The assay described previously (Rickwood, 1992) was used and scaled accordingly. Briefly, to 250 µl of 20 mM Tris-HCl containing 100 µM EDTA (pH 7.4), 50 µl of 200 mM succinic acid (adjusted to pH 7.4 with 5 M NaOH) was added, followed by 50 µl of freshly prepared INT (2.5 mg/ml in DMF). Finally 50 µl of each fraction was added and incubated at 37 °C for

exactly 25 min. The reaction was stopped with the addition of 1 ml of ethyl acetate/ethanol/trichloroacetic acid (5 : 5 : 1 v/v). Samples were centrifuged for 2 min at 8,000 g and the absorbance of the pink supernatant was measured at 490 nm. Product concentration was determined by using the extinction coefficient for INT derived formazan ($\varepsilon = 1.941$ l x mmol^{-1} x mm^{-1}) (Möllering et al., 1978). For enzyme kinetics experiments, the amount of formazan produced was monitored over fixed time points at 5 – 40 min at a (homogenate) protein content of 0.10 – 0.38 mg. Data were analysed as detailed for alkaline phosphatase.

Cytosolic marker lactate dehydrogenase (EC 1.1.1.27)

Lactate dehydrogenase activity was used to establish the subcellular distribution of cytosol. The assay also formed the basis to quantify cell breakage by monitoring lactate dehydrogenase leakage. Lactate dehydrogenase catalyses the oxidation of NADH to NAD^+ by consuming pyruvate, which is converted to lactate. The enzymatic reaction can thus be followed by monitoring the disappearance of NADH at 339 nm (Schomburg & Stephen, 1995). The procedure described previously was used (Vassault, 1984). A freshly prepared solution containing 81 mM Tris-NaOH (pH 7.2), 203 mM NaCl, 244 µM NADH and 10 mM pyruvate (pyruvic acid sodium salt) was allowed to equilibrate at 30 °C. Next, 3 ml of this solution was added to a thermostatically controlled cuvette (30 °C) followed by 50 µl of sample. The solution was mixed and the decrease in absorbance was continuously recorded over 1 min at 339 nm. The decrease in absorbance over the linear region of the curve (0 – 25 s) was used to determine breakage efficiency (section 2.3.5), lactate dehydrogenase activity in the fractions and specific enzyme activity. The specific enzyme activity was assessed as detailed for alkaline phosphatase at a 0.04 – 0.25 mg (homogenate) protein concentration range (expressed as milli-Units per mg of protein) and the amount of NADH consumed was calculated by using the extinction coefficient for NADH ($\varepsilon = 0.631$ l x mmol^{-1} x mm^{-1}).

Presenting marker distribution in fractions

Histograms were plotted with the five fractions presented on the abscissa in the order they were isolated with the length of the blocks proportional to their protein content. The ordinate displayed the enrichment of the respective marker, which was expressed as the relative specific activity (RSA). RSA is the percentage of activity/content recovered in the fraction over the percentage of protein of the same fraction. Enrichment of the marker is indicated by a RSA > 1.

2.3.8 Measurement of PK1 and doxorubicin in subcellular fractionations

Direct measurements of doxorubicin-associated fluorescence

These experiments aimed at investigating fluorescence quenching in subcellular fractions and are detailed in Chapter 4 section 4.2. B16F10 cells were grown as described in section 2.3.5. Culture medium was aspirated and replaced with 10 ml of fresh medium containing PK1 at 0.1 mg/ml (6.6×10^{-3} mg/ml of doxorubicin-equivalence) and incubated for either 15 min or 5 h. Following the incubation period, cells were placed on ice and processed as described in 2.3.6. Fractions were analysed for doxorubicin-associated fluorescence by direct measurements and by serial dilutions of subcellular fractions in PBS (pH 7.4). Measurements were performed with a fluorescence plate reader with an excitation set at 480 nm and emission at 590 nm.

Quantification of doxorubicin-associated fluorescence by extraction

A previously described extraction procedure for doxorubicin (Bachur et al., 1970) was employed to estimate drug concentrations in subcellular fractions (Chapter 4, section 4.2). Cells were cultured, incubated with drug (6.6×10^{-3} mg/ml doxorubicin-equivalence), and subsequently processed as described above. Drug was extracted from fractions using a 0.3 N HCl 50 %v/v ethanolic solution at a 1 : 2 v/v sample : buffer ratio, samples were vortexed for 20 s and centrifuged at 10,000 g for 5 min. The supernatant was aspirated and the biological sample was subjected to a

second extraction procedure using the same volume of extraction buffer as before. The supernatants were combined and measurements were performed with a fluorescence plate reader with an excitation set at 480 nm and emission at 590 nm. Drug content was estimated by constructing appropriate calibration curves using the same buffer composition as for biological samples (figure 2.6). Recovery was calculated by analysing the amount of drug in the homogenate and in the fractions. To determine the suitability of the method to quantify doxorubicin-associated fluorescence, B16F10 cell homogenate was spiked with doxorubicin or PK1 to a final concentration of 0.2 – 212 μg doxorubicin-equivalence/mg protein. From this homogenate samples were subsequently extracted as detailed above. Recovery was estimated using standards prepared in homogenisation buffer, which were subjected to same extraction procedure.

2.3.9 Confocal and epifluorescence microscopy

The subcellular distribution of fluorescently labelled polymers was qualitatively assessed in Chapter 4 (section 4.2) and Chapter 5 (section 5.3.2), where specific experimental conditions can be found. Autoclaved glass coverslips were flamed and placed into 6 well plates. Cells were then seeded (1 x 10^6 cells/well) and left to adhere to the coverslips for 24 h. To assess the subcellular localisation of polymers, cells were incubated for either 15 min, 1 h or 5 h with 1 ml of clear complete medium containing the fluorescent probe. Following the incubation period, cells were placed on ice and washed three times with ice cold PBS (~ 4 ml). Cells were then fixed for 20 min on ice with 3 %w/v paraformaldehyde in PBS (1 ml). Following fixation, cells were washed a further three times with PBS (~ 4 ml). Coverslips were then lifted out of the wells, dipped in PBS and then H_20 and mounted on microscope slides with 6 μl of Dako mounting medium. To stain nuclei, Vectashield mounting medium containing DAPI was diluted with Dako mounting medium at 1 : 10 %v/v ratio. Slides were then sealed with clear nail polish and stored at 4 – 8 °C and viewed within 24 h. For live cell imagining, 1 x 10^6 cells were seeded

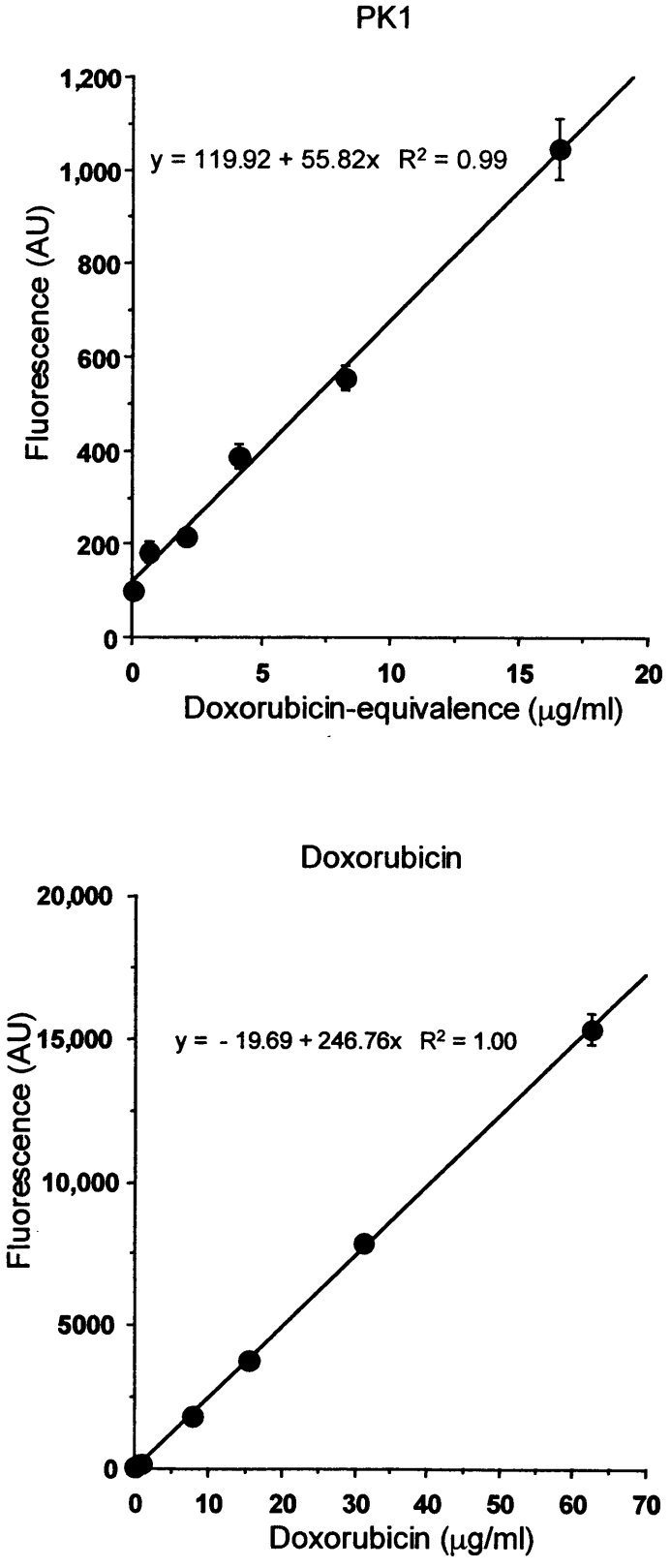

Figure 2.6 Standard curves for PK1 and doxorubicin to determine drug concentrations in biological samples. (Data represents mean ± SEM n=3, error bars are within plot symbols when not visible).

in glass bottom culture dishes. Cells were treated as described above, though omitting the fixation steps and performing all washing steps at 25 °C. Finally clear complete medium was added to the dish and cells were subsequently visualised for a maximum of 30 min. Cells were viewed with either an inverted epifluorescence microscope with the appropriate filter settings and by manually adjusting the gain or by confocal laser scanning microscopy.

2.3.10 Flow cytometry: determination of cell viability using fluorescent probes

To allow for the exclusion of non-viable cells and debris from the analysis by flow cytometry, the viable cell population had to be determined first. Since viable cells have different scatter characteristics to non-viable cells, the scatter plot was used to select the viable cell population. To aid this process, viable and non-viable cells were labelled with fluorescein and PI respectively. Following the diffusion of FDA into cells, non-specific cellular esterases convert the non-fluorescent FDA substrate into fluorescein (figure 2.7). The green fluorescent fluorescein is charged at the cytosolic pH and thus trapped and detected within cells containing an intact plasma membrane (i.e. viable cells). Conversely, PI does not gain access into cells with an intact plasma membrane and hence is excluded from viable cells. However, the fragmenting plasma membrane of dead or dying cells allows access of PI, which upon binding to nucleic acid fluoresces red. The method described by Ormerod served as a basis to determine viable cells in the scatter plot (Ormerod, 2000). Briefly, cells were seeded in 6 well plates, allowed to attach and reach a cell density of 1 x 10^6 cells/well. Cells were then washed three times with PBS (~ 4 ml), and in the presence of 1 ml of PBS cells were scraped off each well and placed into Falcon tubes. Detached cells were centrifuged at 600 g for 4 min and the supernatant was decanted. To each pellet 100 µl of FDA (stock of 100 µg/ml prepared in acetone and diluted in PBS pH 7.4 to a working stock of 100 ng/ml) and 100 µl of PI (100 µg/ml in PBS pH 7.4) was added. The pellet was then gently re-suspended with a pipette and the cell suspension was incubation for 15 min under cell culture conditions.

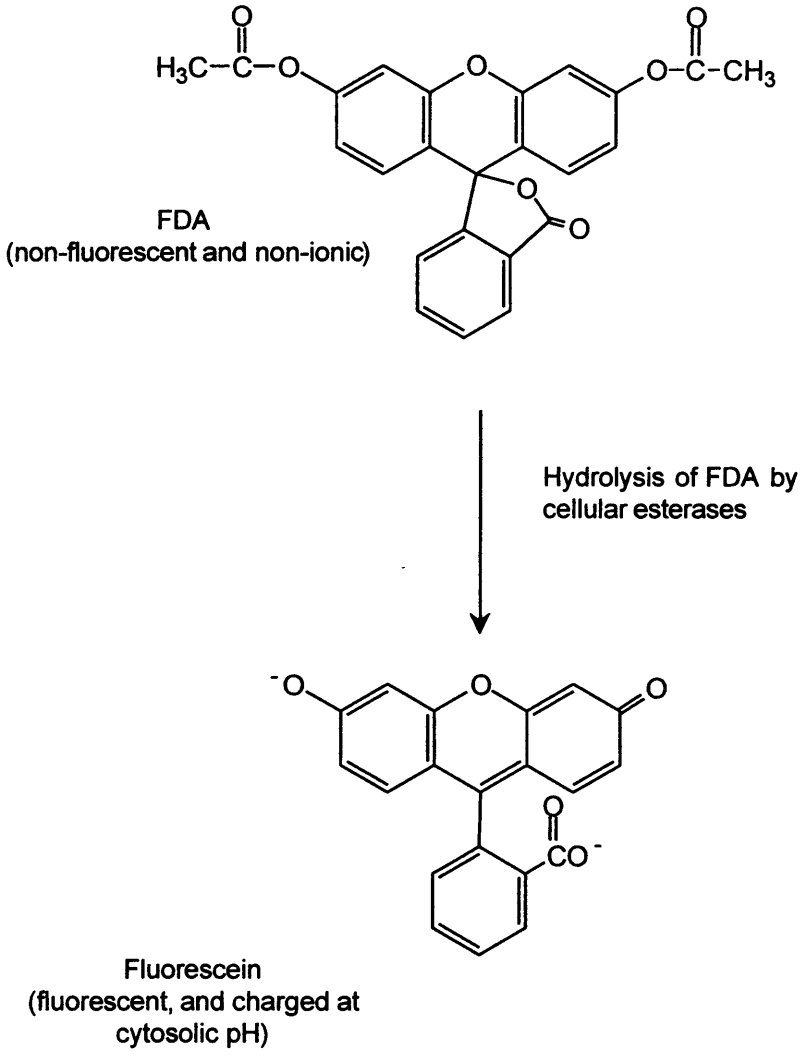

Figure 2.7 Hydrolysis of FDA to fluorescein. Fluorescein is charged at the cytosolic pH and hence retained by viable cells.

Following the incubation period cells were immediately analysed by flow cytometry. For B16F10 cells, forward and side scatter was always set to 290 and E-1 respectively and a total of 10^4 events were counted. Fluorescence emission was detected at 530 nm (FL-1) and 630 nm (FL-3) for fluorescein and PI cell-associated fluorescence respectively using logarithmic signal amplification. In the scatter plot, only viable cells were selected (i.e. gated) to exclude non-viable cells. A plot of green fluorescence (viable cells) versus red fluorescence (non-viable cells) confirmed the suitability of the gate to identify viable cells (figure 2.8). This gate was used for all uptake and exocytosis studies in B16F10 cells.

2.3.11 Uptake of fluorescently labelled polymers

Flow cytometry was used in Chapters 4 and 5 to assess cell-association and cellular pharmacokinetics of selected polymers. Incubation times and polymer concentrations used are detailed in sections 4.2 and 5.2.3 of the respective Chapters. Cells were always grown in 6 well plates and incubated with 1 ml of medium as described above. Polymer samples were dissolved in complete medium and allowed to reach 37 °C or 4 °C for studies under cell culture conditions or ice respectively. For uptake studies performed at 37 °C, cells were maintained under cell-culture conditions during the incubation period. To determine external binding, cells were pre-chilled on ice for 25 min before commencing the study. At the start of the study cells were then washed with PBS (1 ml) and 1 ml of polymer solution was added per well. Following the incubation period at either 37 °C or 4 °C, cells were always maintained at 4 °C for the rest of the experiment. Cells were harvested as described above (2.3.10) and detached cells were centrifuged at 600 g for 4 min, the supernatant was decanted, replaced with 200 µl of PBS and the pellet gently re-suspended with a pipette. Within 30 min of sample preparations cell-associated fluorescence was measured. Control cells were used each time to account for cell auto-fluorescence. Besides the inclusion of untreated cells in every experiment, control experiments for all polymers were carried out with unlabelled polymers (i.e.

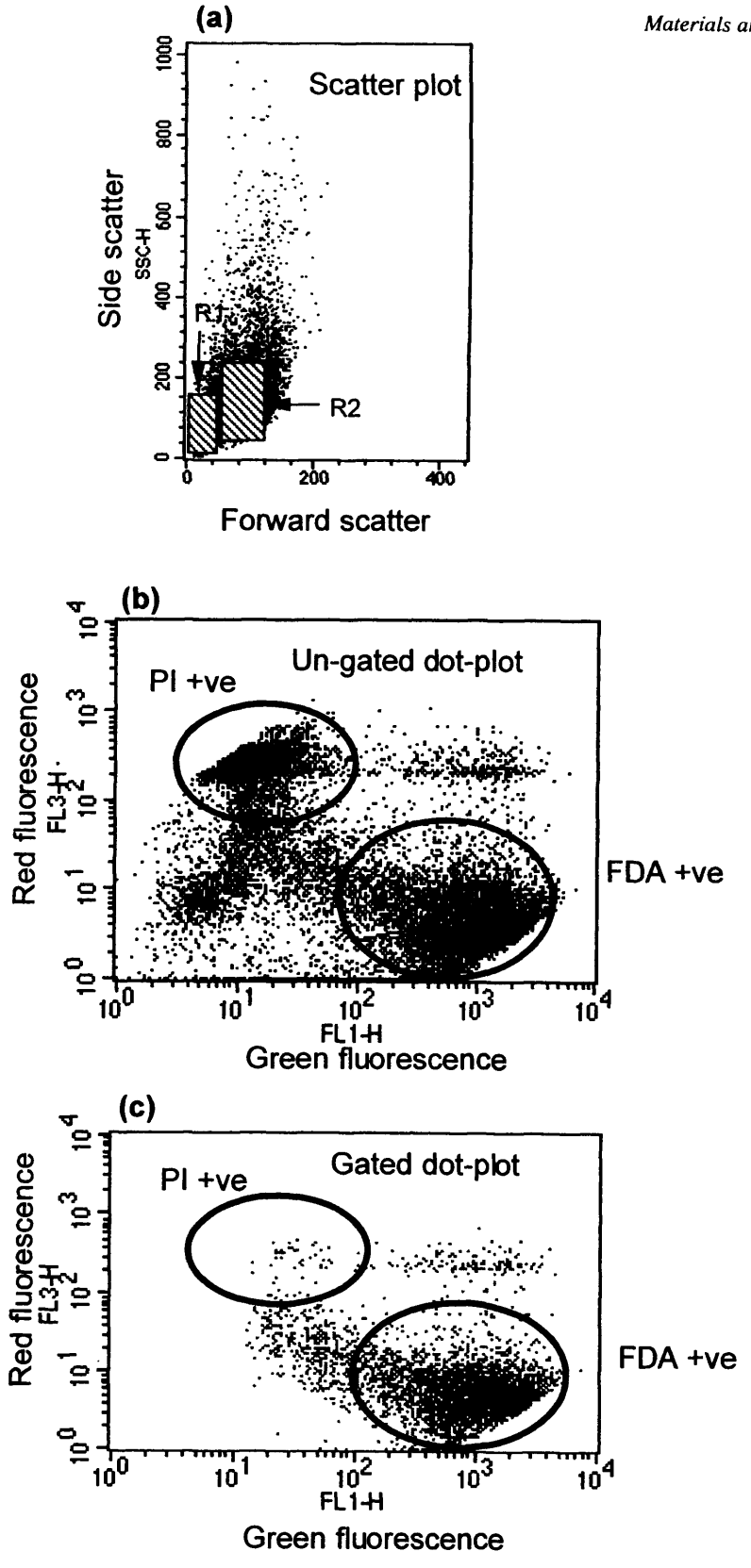

Figure 2.8 Flow cytometry plots of B16F10 cells incubated with FDA and PI to assess cell viability. Panel (a) dot plot with gates (R1 = non-viable cells; R2 = viable cells). Panel (b) dot plot of green fluorescein derived fluorescence versus red PI derived fluorescence (no gate applied). Panel (c) dot plot following gating (R1) of cells in the scatter plot. Note the disappearance of PI positive cells.

not fluorescent) to assess possible changes in cell granularity, size and autofluorescence. Forward and side scatter was set to 290 and E-1 and a total of 10^4 events were counted in the viable gate. Fluorescence emission was detected at 530 nm (FL-1) and 590 nm (FL-2) for OG/FITC and doxorubicin cell-associated fluorescence respectively using logarithmic signal amplification. Data were analysed as described below.

2.3.12 Analysis of flow cytometry data

For all flow cytometry experiments, cell-associated fluorescence was acquired using log amplification to improve peak symmetry and to accommodate large differences in cell-associated fluorescence. Due to log transformation of the signal, data analysis was also required to be carried out on the transformed data (Daly & Bourke, 2000). Thus to establish the central location of the population the geometric mean was used, which equates to the median of the original data (providing that the distribution of the log-transformed data is perfectly symmetrical) (Daly & Bourke, 2000). The use of the median as a measure of uptake was considered preferable to the arithmetic mean, due to its true mid-point measure of the total population. More specifically, the geometric mean of the viable cell population exposed to polymer ($G_{V\ Polymer}$) was used to assess uptake/binding. For each experiment, the geometric mean of viable control cells ($G_{V\ Control}$) (i.e. not exposed to polymer) was also determined. Therefore by correcting for background fluorescence, cell-associated fluorescence was determined according to equation (1).

$$\text{Cell-associated fluorescence (AU)} = G_{V\ Polymer} - G_{V\ Control} \qquad \text{Equation (1)}$$

2.3.13 Exocytosis of fluorescently labelled polymers

Exocytosis experiments were used in Chapter 5 to determine the overall cellular pharmacokinetics of polymers. Briefly, cells were prepared as described, and incubated with polymers for 2 h. Following the 2 h "loading period", cells were rinsed three times with PBS (1 ml) and immediately incubated for 5 – 60 min with

complete medium only. Cells were then prepared for analysis as described above.

2.3.14 Inhibitor assays for macropinocytosis, clathrin-mediated and cholesterol-dependent pinocytosis

Preliminary experiments investigating the route(s) of polymer internalisation into B16F10 cells have been described in Chapter 5 section 5.2.3 and were based on the method described previously (Manunta et al., 2004). The pharmacological inhibitors MβCD, chlorpromazine and wortmannin were selected to block mainly cholesterol-dependent (Rodal et al., 1999), clathrin-mediated (Orlandi & Fishman, 1998; Wang et al., 1993) and phosphoinositide 3-kinase-dependent (Araki et al., 1996; Shepherd et al., 1995) macropinocytosis respectively. Although MβCD is commonly used to inhibit cholesterol-dependent uptake (Hailstones et al., 1998; Orlandi & Fishman, 1998; Puri et al., 2001), inhibition of clathrin-mediated pinocytosis has also been reported (Rodal et al., 1999; Subtil et al., 1999). Chlorpromazine is thought to inhibit coated pit assembly at the plasma membrane (Wang et al., 1993), whereas MβCD selectively extracts cholesterol from the plasma membrane (Ilangumaran & Hoessli, 1998) and wortmannin by interfering with the completion of macropinocytosis (Araki et al., 1996). Stocks of wortmannin (1 mM) were prepared in DMSO and stored at – 20 °C until use, and a fresh stock of chlorpromazine (1 mg/ml) in MeOH was prepared each time before use. Before each experiment working stocks (10 ml) were prepared with ice cold, serum-free RPMI medium at a final concentration of 100 nM for wortmannin (Wang et al., 1993) and 10 μg/ml for chlorpromazine (Goncalves et al., 2004). Serum was not included to eliminate possible interference with the assays. Likewise MβCD was prepared with serum-free medium at final concentration of 10 mM (Rodal et al., 1999). B16F10 cells were grown in 6 well plates as described above. To pre-incubated cells with one of the inhibitors, cells were washed three times with PBS (pH 7.4) and 1 ml of the respective (working) stock solution was added per well. Plates were transferred to a 37 °C water bath for 30 min. Thereafter cells were washed once with PBS, and 1 ml

of serum-free medium was added and cells were transferred to an incubator for 30 min. Following the incubation period, medium was replaced with serum free media (1 ml) containing polymer conjugates. Cells were incubated for 1 h and then prepared for analysis by flow cytometry as described above. Background fluorescence was assessed using control cells exposed to inhibitor treatment only and data were analysed as described in 2.3.12.

2.3.15 Characterisation of polymers

All polymers used in this thesis were subjected to a preliminary characterisation, which included the determination of the weight and number average molecular weights (Mn) to estimate polymer polydispersity. Where applicable, cationic polymers were also assayed for their 1°, 2° and 3° amine content using inverse-gated ^{13}C NMR, and colorimetric tests described below. Further details of the methods and a summary of polymer characteristics (tables 5.3 and 5.4) can be found in Chapter 5.

Aqueous GPC for characterisation of polymers

All cationic polymers were analysed using an aqueous 0.5 M acetic acid (NaOAc/OHAc) mobile phase (pH ~ 4.5). The mobile phase was first filtered through a 0.22 μm Micropore filter and then sonicated for 30 min to remove dissolved 0_2. For dextran, PBS (0.1M; pH 7.4) was used as the mobile phase and subjected to filtration and sonication as described above. The system was purged with the appropriate mobile phase and the baseline was allowed to stabilise before polysaccharide standards (Mw = 738 – 47,300 g/mol), 250 mM sucrose, and samples (5 mg/ml) were injected through a 20 μl sample loop. All injected materials were dissolved in the mobile phase, and passed through a 0.22 μm filter. The flow rate was set to 1.0 ml/min and the run time was 30 min. PVP (1.3 x 10^6 g/mol) and sucrose were used to identify the void (V_0) and bed (V_B) volumes of the column respectively. Polysaccharide standards were used to construct a standard curve of Mw against

retention time and samples were subsequently analysed using Caliber software (figure 2.9).

Characterisation of cationic polymers with the ninhydrin assay

The ninhydrin reagent reacts with primary amines to produce an aldehyde blue complex (figure 2.10, panel a) that can be quantified spectrophotometrically (Moore, 1968). Thus the assay has here been used to quantify the amount of primary amine groups present in commercial PAMAM dendrimers and PEI. In brief, a 4 M aqueous lithium acetate buffer was freshly prepared and the pH adjusted to 5.2 with glacial acetic acid. Ninhydrin reagent (ninhydrin 2.0 %w/v, hydrindantin 0.3 %w/v) was freshly prepared in DMSO/lithium acetate buffer at a 3 : 1 ratio and protected from light. Aqueous samples and calibration standards (3-amino-1-propanol) were mixed with the ninhydrin reagent at equivolumes in glass test tubes and boiled at 100 °C for 15 min. The test tubes were then cooled on ice and 3 ml of an ethanolic solution (50 %v/v) was added to the mixtures and the absorbance measured at 570 nm. Readings were background corrected with water, which otherwise had been treated identically to the samples. Using a standard curve of 3-amino-1-propanol (figure 2.10, panel a), the number of terminal amine groups of polymers and PAMAM dendrimers were identified and compared with the theoretical number.

Characterisation of cationic polymers with the TNBS assay

TNBS reacts with primary amines to produce a highly chromogenic derivative that can be readily quantified by measuring its absorbance at 420 nm (figure 2.10, panel b). In the present study the assay was used to quantify the content of primary amines of PEI and PAMAM dendrimers using the previously described method (Snyder & Sobocinski, 1975). Briefly, polymers and 3-amino-1-propanol calibration standards were dissolved in MeOH and to 20 µl of sample, 10 µl of TNBS (17 mM) was added followed by 200 µl of borate buffer (0.1 M sodium tetraborate adjusted to pH 9.3 with boric acid). Samples were incubated at 25 °C for

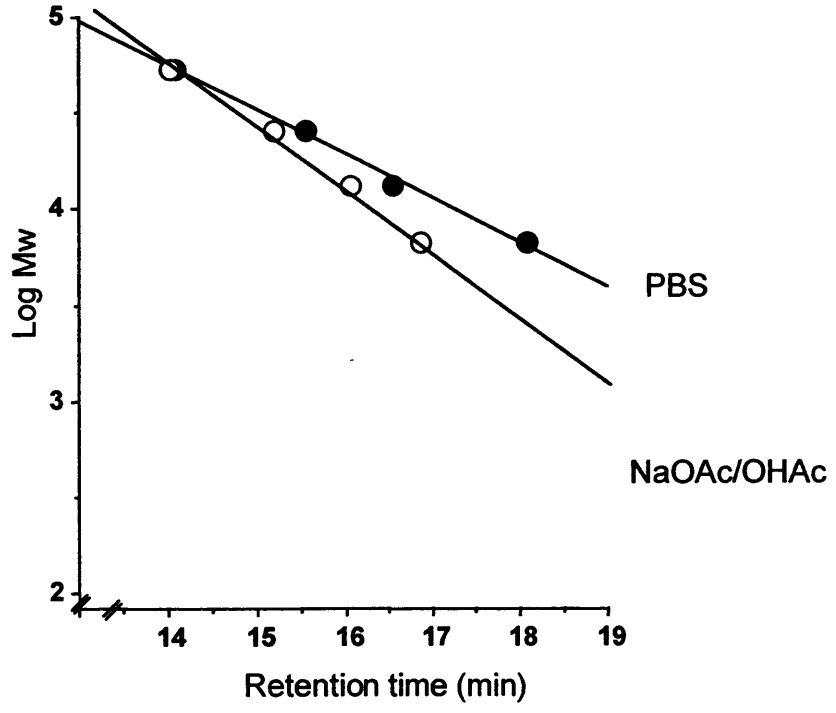

Figure 2.9 Typical GPC calibration curves for polysaccharide standards using PBS and NaOAc/OHAc as mobile phase.

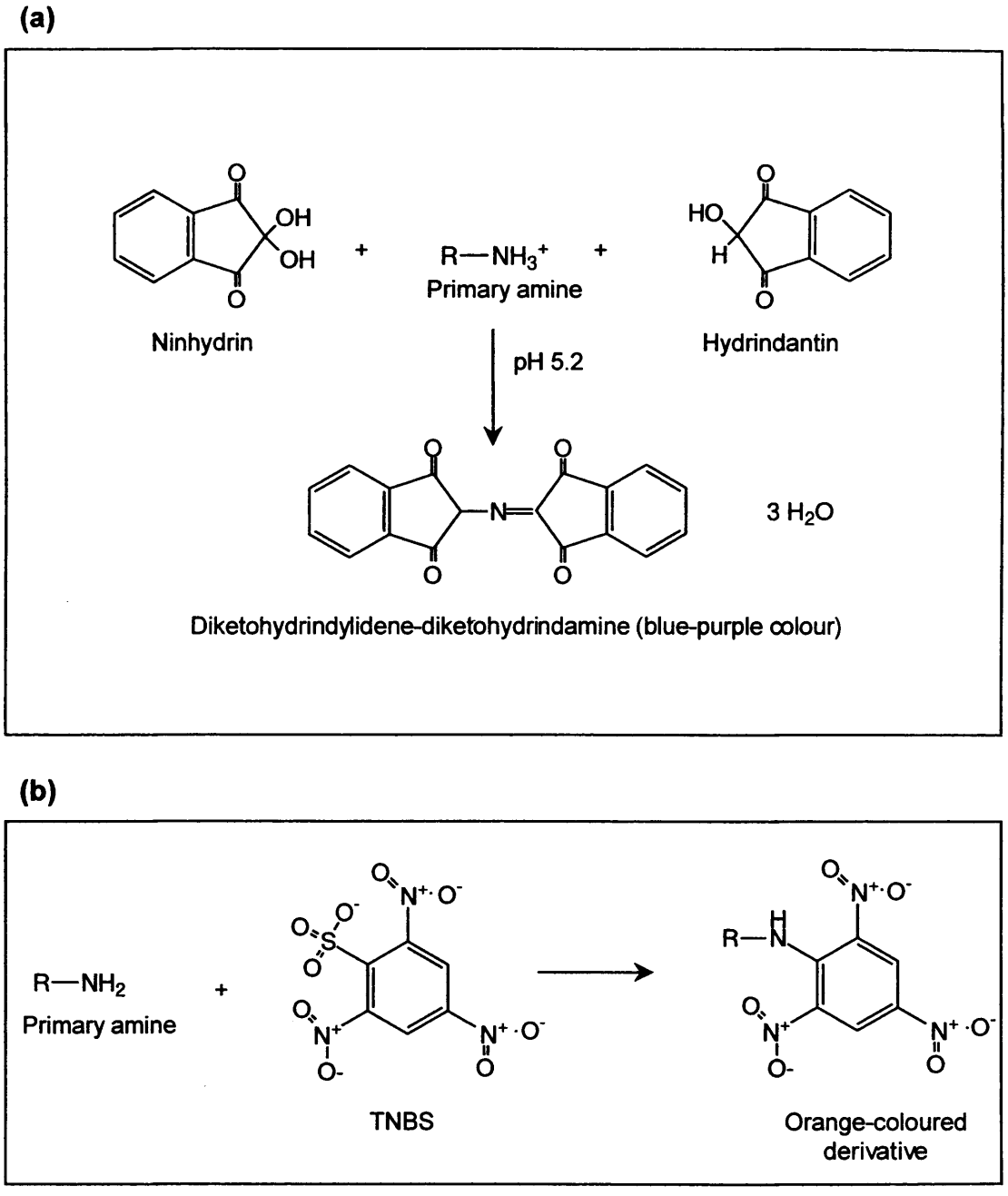

Figure 2.10 Outline of the ninhydrin and TNBS reaction where primary amines are detected due to the formation of highly coloured derivatives. Primary amines can originate form small organic molecules (e.g. 3-amino-1-propanol) or polymers (e.g. PAMAM G4). Panel (a) ninhydrin reaction, panel (b) TNBS reaction.

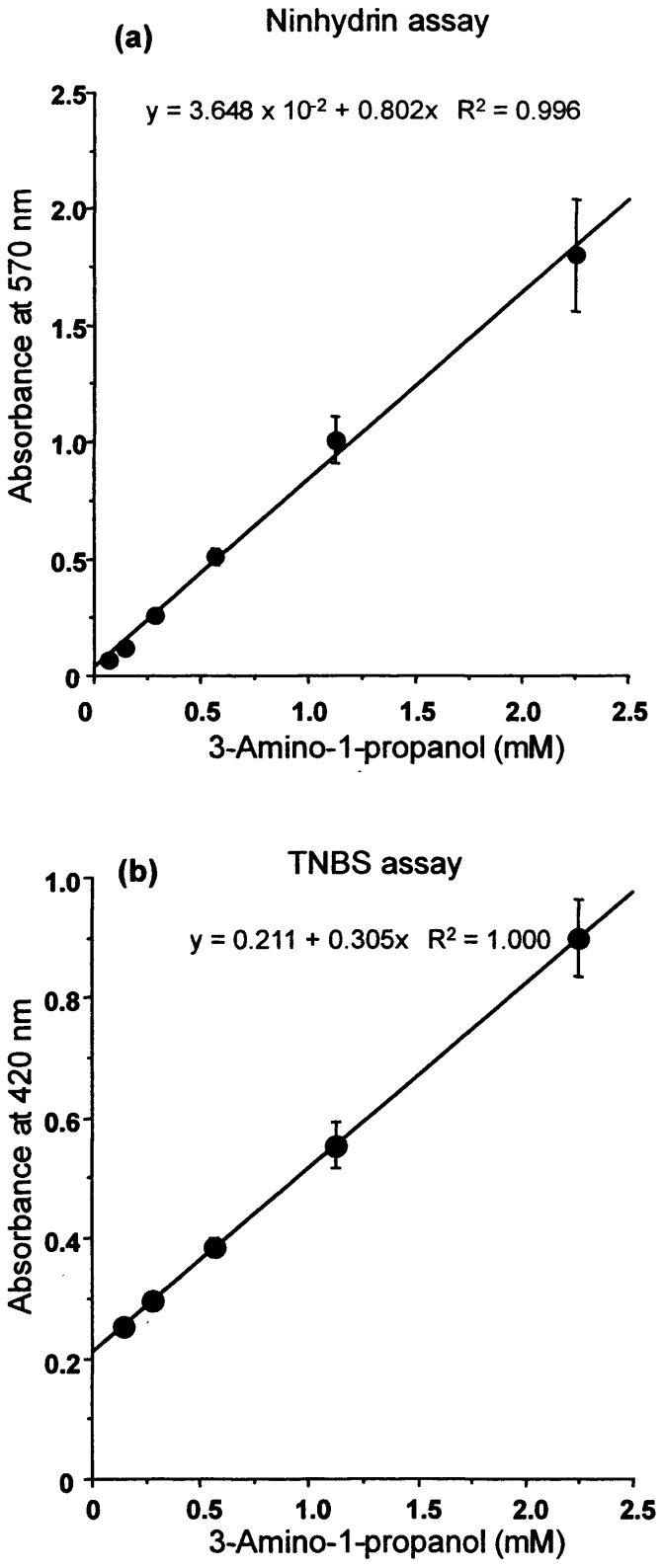

Figure 2.11 Calibration curves for the ninhydrin and TNBS assay using 3-amino-1-propanol as a standard. (Data represents mean ± SEM n=3, error bars are within plot symbols when not visible).

30 min and the absorbance was measured at 420 nm. Readings were background corrected with MeOH, which otherwise had been treated identically to the samples. Using the standard curve for 3-amino-1-propanol, the number of primary amine groups per polymer was estimated (figure 2.10, panel b).

Characterisation of cationic polymers by inverse-gated ^{13}C NMR

Inverse-gated ^{13}C NMR was also used to provide quantitative information for 1°, 2° and 3° amines. The experimental conditions chosen were based on those previously used for branched PEI (Pierre & Geckle, 1985; Von Harpe et al., 2000) and PAMAM dendrimers (Meltzer et al., 1992). In brief, NMR analysis at 75 MHz was performed at room temperature using 50 mg of PAMAM G2 and G3 and 25 mg of PAMAM G4 in D_2O. To provide better spectral resolution, branched PEI (100 mg in D_2O) was analysed at 40 °C at 126 MHz. All samples were subjected to an inverse-gated ^{13}C zgig30 pulse sequence. A spin lattice relaxation time (T_1) of 5 s was used to minimise the nuclear Overhauser effect since the longest T_1s were 700 ms and 665 ms for PAMAM G2 and PEI respectively. By doing so, quantitative signal accumulation was achieved and spectra were recorded with a minimum of 7000 scans. From ^{13}C NMR spectra the content of amine groups for PEI and PAMAMs was calculated using signal intensities (A) for the corresponding ^{13}C, according to equation (2) and (3) respectively. (Subscript numbers correspond to the assigned chemical shifts of the spectrum as shown in the Results section of Chapter 5). It is noteworthy that the two identical carbons bonded to each 2° amine resonate, raising the intensity to twice that of actual content of 2° amines. Thus the intensity is corrected by dividing by a factor of 2. Likewise, for 3° amines the direct linkage of three identical carbons per amine gives a 3 fold rise in signal so values are corrected by a factor of 3.

$$1° : 2° : 3° = (A_7 + A_8) : [(A_4 + A_5 + A_6)/2] : [(A_1 + A_2 + A_3)/3] \quad \text{Equation (2)}$$

For PAMAM dendrimers, the amine ratios were calculated with formula (3) using signal intensities of the corresponding carbons:

$$1° : 2° : 3° = A_3 : 0 : [(A_2 + A_1)/3] \quad \text{Equation (3)}$$

2.3.16 Statistics

Statistical significance was assigned to $p \leq 0.1 - 0.01$ and calculated using a two-tailed Student's t-test (paired/unpaired as indicated) for the comparison of two samples, and one-way analysis of variance (ANOVA) when more than two samples were compared followed by Bonferroni post-hoc analysis. Where indicated, standard error of the mean (SEM) for data points was calculated and the number (n) of experiments/replicates are given as indicated.

Chapter 3

Establishing a subcellular fractionation method in B16F10 cells

3.1 Introduction

Although pioneering work of Trouet and co-workers in the 1970s and '80s employed fractionation methods for murine L1210 leukaemic cells (Zenebergh et al., 1981) and rat embryo fibroblasts (Tulkens et al., 1974) to quantify intracellular trafficking of doxorubicin/daunorubicin-DNA complexes for lysosomotropic delivery (Peterson et al., 1979; Noel & Trouet, 1976) (reviewed in Trouet & Jolles, 1984), subcellular fractionation has rarely been used in drug delivery (table 3.1). To date most studies investigating the intracellular trafficking of polymers and polymer therapeutics have used confocal microscopy (table 1.3 and 1.5). Nonetheless, fluorescence-based microscopy techniques have major limitations. In particular, quantification is limited by small sample size, optical resolution of the microscope and not least use of fluorescent probe. This can be subject to photo bleaching, concentration and pH-dependent fluorescence quenching. In general conventional confocal microscopy has a resolution limit ~ 180 nm, though new specialised techniques are providing now a resolution of ~ 28 nm in live cells (Hell, 2003).

The simplicity and quantitative nature of subcellular fraction by differential centrifugation makes it an ideal tool to monitor the intracellular trafficking of polymer therapeutics since it can overcome the limitations associated with fluorescence microscopy. However, the main disadvantages of the technique include the need to tailor and characterise the method to each cell line. Furthermore detailed kinetic analysis of polymer therapeutics are laborious due to the discontinuous nature of the method and the need for large cell numbers. Despite the disadvantages associated with fractionation studies, it was considered important to establish a method for the subcellular quantification of polymer therapeutics. Key points to a meaningful fractionation method in B16F10 cells are considered below. However, the rationale for selecting B16F10 murine melanoma cells for these studies is considered first (Fidler, 1973; Fidler, 1975).

Table 3.1 Summary of subcellular fractionation studies used to monitor the trafficking of macromolecular drug delivery systems

Monitoring trafficking of	Fractionation methodology	Cell line/organ	Findings & Comment	Reference
HPMA copolymer Mce_6 conjugated targeted with NLS	Percoll* density centrifugation	A2780	Enhance uptake for targeted conjugate compared to untargeted conjugate.	(Tijerina et al., 2003)
HPMA copolymer with TAT	Percoll* density centrifugation	A2780	There appears to be a cytoplasmic and nuclear accumulation of polymer conjugate, though study does not take into account possible re-distribution of probe during subcellular fractionation. Method reported by Zaro & Shen (2003) would be more appropriate.	(Nori et al., 2003b)
HPMA copolymer with TAT	Percoll* density centrifugation	A2780	No specific data presented in paper	(Nori et al., 2003a)
HPMA copolymer Mce_6	Percoll* density centrifugation	A2780	Lysosomal delivery and release of Mce_6 form tetrapeptide linker. Poor characterisation and validation of fractionation method, since used in a number of additional studies.	(Tijerina et al., 2001)

Table 3.1 Continued

Monitoring trafficking of	Fractionation methodology	Cell line/organ	Findings & Comment	Reference
Polyamidoamine (ISA 1 and 4)	Differential pelleting	Rat liver	Time (30 – 60 min) and dose-dependent disruption of lysosomes.	(Pattrick et al., 2001)
Branched (Mw = 25,000 g/mol) PEI-^{35}S-DNA	Sucrose gradient# centrifugation	Rat liver	Lysosomal transfer reduced by complexing DNA with PEI. Smaller complexes more rapidly trafficked to lysosomes than larger ones.	(Wattiaux et al., 2000)
Branched PEI (Mw = 25,000 g/mol)	Differential and sucrose gradient# centrifugation	Rat liver	Early after injection (5 min) PEI exhibits distribution pattern similar to plasma membrane, later (4 h – 4 days) there is lysosomal accumulation. First study to investigate subcellular distribution of PEI by isopycnic and differential centrifugation.	(Lecocq et al., 2000)

Table 3.1 Continued

Monitoring trafficking of	Fractionation methodology	Cell line/organ	Findings & Comment	Reference
^{35}S-DNA ± PDL or PLL (Mw = 75,000 – 150,000 g/mol)	Differential and sucrose gradient# centrifugation	Rat liver	Same extent of polyplex uptake of D- and L-stereoisomers into Kupffer cells. Retention of D-polyplex in non-lysosomal compartment for longer (4 – 14 h) than L-polyplexes, where significant degradation occurred after 4 h. First paper to address importance of stereochemistry for polymer therapeutics and intracellular trafficking.	(Laurent et al., 1999)
^{35}S-DNA ± 6 different lipids♦	Differential and sucrose gradient# centrifugation	Rat liver	Intracellular trafficking of all lipoplexes to lysosomes significantly reduced over 1 – 5 h time course when compared to ^{35}S-DNA only. At 14 h, lipoplexes exhibited similar profile as ^{35}S-DNA.	(Wattiaux et al., 1996)
^{35}S-DNA ± DOTAP	Differential and sucrose gradient# centrifugation	Rat liver	No differences in uptake of ^{35}S-DNA ± DOTAP; intracellular trafficking of lipoplexes to lysosomes significantly reduced over experimental time course (60 min) when compared to ^{35}S-DNA only.	(Wattiaux et al., 1995)

Table 3.1 Continued

Monitoring trafficking of	Fractionation methodology	Cell line/organ	Findings & Comment	Reference
Free and polymer (HPMA) bound daunomycin	Differential centrifugation	Rat liver	Demonstrated lysosomal accumulation of polymer drug conjugate.	(Wedge et al., 1991)
HPMA copolymers with pendent galactosamine residues (1.0 – 11.6 mol%)	Percoll* density centrifugation	Rat liver	The most highly substituted polymer (11.6 mol%) accumulated in the liver (80 – 90 % of initial dose) and was trafficked into lysosomes within 60 min.	(Duncan et al., 1986)
Cationic HPMA copolymer	Percoll* density centrifugation	Rat liver	Extensive accumulation in the liver with a slow transfer to lysosomes (58 % over 60 min).	(McCormick et al., 1986)
Daunorubicin, doxorubicin and respective DNA complexes	Differential and sucrose gradient# centrifugation	Rat ventricles	Accumulation of free and DNA complexed daunorubicin in nucleus and to a lesser extent in lysosomes. Free or DNA complexed doxorubicin only found in the nucleus. Study does not differentiate between free and complexed drug.	(Blanchard et al., 1981)

Table 3.1 Continued

Monitoring trafficking of	Fractionation methodology	Cell line/organ	Findings & Comment	Reference
Daunorubicin-DNA complexes	Differential pelleting and sucrose gradient# centrifugation	Cultured rat embryo fibroblasts	Localisation of daunorubicin in lysosomes and nuclei, though no differentiation between free and complexed drug.	(Peterson et al., 1979) (Noel & Trouet, 1976)

* Percoll used for isopycnic gradient centrifugation.

Isopycnic equilibrium centrifugation where separation is dependant on the buoyant densities of the particles.

♦ Perfect transfection kit, nature of lipids not given by Invitrogen.

Rationale for selecting B16F10 cells

B16F10 cells have been used over the last 20 years in our laboratory as an *in vitro* and *in vivo* model to study the anticancer effects of a large number of polymer anticancer conjugates. For example, this was one of the preclinical screening models used to determined the *in vivo* antitumour activity and pharmacokinetics of PK1 (Duncan et al., 1992; Seymour et al., 1994), and the characteristics of the enhanced permeation and retention (EPR) effect with tumour size (Sat, 1999) and Mw (Seymour et al., 1995). PK1 subsequently progressed into clinical trial (Vasey et al., 1999). This murine melanoma model was also used to evaluate HPMA copolymer platinates, assisting the selection of 2 compounds (Gianasi et al., 2002; Gianasi et al., 1999) for Phase I clinical testing (Nowotnik, 2004), and the first dendrimer anticancer agent, a PAMAM G 3.5 – platinate (Malik et al., 1999). B16F10 cells are currently also used to elucidate the subcellular distribution and activity of poly-L-glutamic acid paclitaxel (Shaffer & Singer, 2004), which is destined to be the first polymer-drug conjugate to reach the market. In addition to the strong track record of B16F10 cells in the development of clinical candidates, they have also been used to study polymer cytotoxicity (Malik et al., 2000), transfection efficiency (Mounkes et al., 1998; Ogris et al., 1998; Wightman et al., 2001) and intracellular trafficking *in vitro* (Rejman et al., 2004).

Development of a subcellular fractionation method by differential centrifugation

Cell breakage, fractionation and characterisation of subcellular fractions are three key steps in the development of a subcellular fractionation procedure. Cell breakage will be considered first. A number of techniques are available to accomplish cell breakage, which either utilise liquid shear (e.g. Dounce, Potter-Elvehjem, cell cracker, needle attached to syringe), mechanical shear (e.g. Polytron) or gaseous shear (e.g. "nitrogen bomb") (Evans, 1992). Although homogenisation methods are ultimately dictated by cell type and amount, liquid shear is most commonly used for homogenisation of cultured cells and "soft" tissues (e.g. liver,

brain) (table 3.2) (Graham, 1997). In the present study disruption by liquid shear was selected, as B16F10 cells have previously been homogenised by this mechanism (Rozhin et al., 1987; Seiji et al., 1963; Wade et al., 2001). Adequate cell breakage (> 80 %) is an absolute requirement for quantitative studies to provide data representative for the cell population. However, homogenisation conditions must be gentle enough to avoid excessive damage to subcellular membranes. Thus homogenisation conditions need to be standardised and tailored to each cell line to ensure the reproducibility and suitability of the method (Evans, 1992). Following cell breakage major cellular components can be readily separated by differential centrifugation. Both the time and the magnitude of the gravitational force acting on those particles in suspension dictates whether a stable pellet can be formed (Graham, 1997; Spragg & Steensgaard, 1992). In practice, successively smaller cellular components are pelleted (nuclei > mitochondria > lysosomes/endosomes > microsomes) by increasing the centrifugal force and possibly run times. Examples of differential centrifugation conditions are summarised in table 3.2 and served as a basis for the present study.

Following differential centrifugation fractions need to be characterised. Frequently organelle specific markers, such as enzymes, are used to quantify the distribution in the fractions (table 3.3). For historic reasons (Bainton, 1981) the specificity of these enzymes has been well documented in rat liver (Amar-Costesec et al., 1974b; Appelmans et al., 1955; Beaufay et al., 1974; Beaufay et al., 1964; Claude, 1946; De Duve et al., 1955; Leighton et al., 1968). However, subcellular distribution of those markers might be altered in other biological systems, in particular when dealing with neoplastic tissues. The lysosomal enzyme cathepsin B for example is also associated with the plasma membrane in human breast carcinomas (Poole & Tiltman, 1978), colorectal adenoma (Talieri et al., 2004) and B16 variants (Rozhin et al., 1987; Sloane et al., 1982; Sloane et al., 1986). However, there appears to be a number of universal markers such as DNA, succinate

Table 3.2 Examples of homogenisation and differential centrifugation methods reported in literature

Cell line/ organ	Homogenisation method	Number of fractions*	Washing of fractions♦	Centrifugal forces & run times	Method derived form	Comment	Reference
Rat liver	Potter-Elvehjem	5	1 – 4	1,500 g 4 min# 3,000 g 11 min# 25,000 g 10 min# 100,000 g 30 min#	-	Basis of numerous subcellular fractionation methods, wide range of enzyme assays used.	(De Duve et al., 1955)
B16 mouse melanoma grown in C57 mice	Potter-Elvehjem	5	2	700 g 10 min 11,000 g 10 min 15,000 g 10 min 105,000 g 60 min	-	Separation and characterisation of melanosomes.	(Seiji et al., 1963)
Cultured HTC cells	Dounce	5	1 – 5	See above	(De Duve et al., 1955)	Seminal study for cultured cells.	(Lopez-Saura et al., 1978; Lopez-Saura et al., 1972)

Table 3.2 Continued

Cell line/ organ	Homogenisation method	Number of fractions*	Washing of fractions♦	Centrifugal forces & run times	Method derived form	Comment	Reference
Cultured rat embryo fibroblasts	Dounce	5	1 – 4	See above	(De Duve et al., 1955)	Seminal study for cultured cells. In some experiments only 4 fractions or cytosolic extract.	(Tulkens et al., 1974)
EAT cells grown in CD1 mice	Dounce tight pestle	5	2 – 5	See above	(De Duve et al., 1955)	Differences in RSA in the two publications. Possible indicator for high inter-experimental variation.	(Londos-Gagliardi et al., 1980; Londos-Gagliardi et al., 1979)
Murine leukaemia L1210 cells	Dounce with loose pestle	5	1 – 4	See above	(De Duve et al., 1955)	Seminal study for cultured cells.	(Zenebergh et al., 1981)

Table 3.2 Continued

Cell line/ organ	Homogenisation method	Number of fractions*	Washing of fractions♦	Centrifugal forces & run times	Method derived form	Comment	Reference
Cloudman S91 melanoma, B16a mice, mouse liver	Tekmar	4	1 – 3	530 g 11 min 6,800 g 7 min 15,100 g 19 min	-	Subcellular fractions assayed for lysosomal and plasma membrane, enzymes only.	(Sloane et al., 1986)
B16-BL6 B16-B15b B16-013 B16a B16F1 B16F10 Mouse liver A2058	Potter-Elvehjem	4	1 – 3	500 g 11 min 7,000 g 7 min 15,000 g 19 min	-	Subcellular fractions assayed for lysosomal, plasma membrane, endoplasmic reticulum, Golgi apparatus enzymes.	(Rozhin et al., 1987) (Rozhin et al., 1989)

Table 3.2 Continued

Cell line/ organ	Homogenisation method	Number of fractions[+]	Washing of fractions[♦]	Centrifugal forces & run times	Method derived form	Comment	Reference
Cultured MCF-7 (human breast carcinoma)	Dounce with tight pestle	3	-	700 g 10 min 150,000 g 30 min	-	Nuclear, particular and soluble fractions only..	(Aboud-Pirak et al., 1988)
Rat liver	Potter-Elvehjem	5	2 – 5	See above	(De Duve et al., 1955)	Subcellular distribution of PK2 studied.	(Wedge et al., 1991)
Rat liver	Potter-Elvehjem	5	2 – 5	See above	(De Duve et al., 1955)	Density of lysosomes perturbed to investigated lysosomal transfer.	(Laurent et al., 1999; Lecocq et al., 2000; Wattiaux et al., 1995; Wattiaux et al., 1996)

Table 3.2 Continued

Cell line/ organ	Homogenisation method	Number of fractions♣	Washing of fractions♦	Centrifugal forces & run times	Method derived form	Comment	Reference
Cultured Hep G2	Dounce	4	1	See above	(De Duve et al., 1955)	It appears that Hep G2 cells are not easily homogenised using a Dounce homogeniser♥. No enzymatic characterisation of fractions obtained by differential pelleting.	(De Diesbach et al., 2000; De Diesbach et al., 2002)

Total average centrifugal force in the middle of the centrifuge tube.

♣ Including final supernatant.

♦ Denotes fractions where pellet has been washed with homogenisation buffer and re-centrifuged to improve purity of fraction.

♥ To produce a nuclear fraction, cells were repeatedly homogenised and subjected to 1000 g for 10 min (once) and 1400 g for 5 min spin (4 x). At each step the resulting PNS was removed and pooled and the pellet re-homogenised.

Table 3.3 Marker enzymes and biochemical assays used to quantify major cell organelles in subcellular fractions (1)

Organelle/ component	Enzyme/marker	Cell lines/organs studied	References
Cytosol	Lactate dehydrogenase	Rat liver	(Wedge, 1991)
		Rat hepatocytes	(Kopitz et al., 1990)
		HTB44 (human renal epithelial carcinoma)	(Schröter et al., 1999)
		HaCaT (human keratinocyte)	
		Cox (human B cell)	
		BSM (human B cell)	
Nucleus	DNA	Rat liver	(Wedge, 1991)
		Ehrlich ascites tumour cells (EAT)	(Londos-Gagliardi et al., 1979)
		HTC	(Lopez-Saura et al., 1978;
		L1210	Lopez-Saura et al., 1972)
			(Zenebergh et al., 1981)
Lysosomes	*N*-Acetyl-β-glucosaminidase	Rat liver	(De Duve et al., 1955)
		Cultured rat embryo fibroblasts	(Tulkens et al., 1974)
		HTC	(Lopez-Saura et al., 1978;
		L1210	Lopez-Saura et al., 1972)
		Murine liver (2)	(Zenebergh et al., 1981)
		B16-013 (2)	(Rozhin et al., 1987)
		B16F1 (2)	(Sloane et al., 1981)

Table 3.3 Continued

Organelle/ component	Enzyme/marker	Cell lines/organs studied	References
Lysosomes	*N*-Acetyl-β-glucosaminidase	B16F10 (2)	(Sloane et al., 1981)
		B16B15b (2)	(Blanchard et al., 1981)
		B16BL6 (2)	(Londos-Gagliardi et al., 1980; Londos-Gagliardi et al., 1979)
		B16a (2)	
		Rat heart ventricles	
		EAT	
Mitochondria	Succinate dehydrogenase/ cytochrome c oxidase	HTC	(Lopez-Saura et al., 1978; Lopez-Saura et al., 1972)
		Cultured rat embryo fibroblasts	
		Rat liver	(Tulkens et al., 1974)
		MCF7	(Amar-Costesec et al., 1974a)
		L1210	(De Duve et al., 1955)
		Rat heart ventricles	(Aboud-Pirak et al., 1988)
		EAT cells	(Zenebergh et al., 1981)
			(Blanchard et al., 1981)
			(Londos-Gagliardi et al., 1980; Londos-Gagliardi et al., 1979)

Table 3.3 Continued

Organelle/ component	Enzyme/marker	Cell lines/organs studied	References
Plasma membrane	Alkaline phosphatase (3)	Rat liver HTC Rat heart ventricles	(Amar-Costesec et al., 1974a) (Blanchard et al., 1981; Lopez-Saura et al., 1978; Lopez-Saura et al., 1972)
Plasma membrane	5'-Nucleotidase (3)	Cultured rat embryo fibroblasts MCF7 HTC (4) L1210 (4)	(Aboud-Pirak et al., 1988; Tulkens et al., 1974) (Lopez-Saura et al., 1978; Lopez-Saura et al., 1972) (Zenebergh et al., 1981)

(1) Refers to references in the literature where the subcellular distribution of the marker has been studied. For generic protocols to study those markers refer to (Eisenthal & Danson, 1992; Graham, 1993; Rickwood, 1992).

(2) Activity in murine liver was only associated with lysosomes following Percoll gradient centrifugation, however in other melanoma cell lines subcellular distribution was partially altered to include plasma membrane association (i.e. B16-F1 = 1.7 RSA > B16a = 1.5 RSA > B16F10 ~ 1.2 RSA) (Rozhin et al., 1987).

(3) The distribution in polarised cells can in some instances be related to the type of plasma membrane involved.

(4) Not detectable.

dehydrogenase, alkaline phosphatase, *N*-acetyl-β-glucosaminidase and lactate dehydrogenase for nuclei, mitochondria, plasma membrane, lysosomes and cytosol respectively. The subcellular distribution of these specific markers has been well documented and there appears to be little variation between different cell types and tissues (table 3.3). These markers were therefore used in the present study to characterise subcellular fractions.

To date the only subcellular fractionation studies in B16F10 cells were devised to study the biosynthesis of melanin (Seiji et al., 1963) and localisation of cysteine proteases (Rozhin et al., 1987; Rozhin et al., 1989). Thus there was the need to establish a new method to quantify the intracellular trafficking of polymer therapeutics. Therefore the aims of the studies described in this Chapter were (a) to optimise cell breakage, (b) to validate marker assays in B16F10 cells (c) to devise a differential centrifugation protocol to fractionate the homogenate to separate and enrich nuclei, mitochondria, lysosomes and cytosol.

3.2 Methods

For the validation of biochemical and marker assays, procedures described in section 2.3.7 were used with the exception of the lysosomal assay, where also sodium bicarbonate (1 M) was tested as a stopping buffer. For the validation of biochemical marker assays, cells were harvested as described in section 2.3.6 and homogenised by 6 successive freeze-thaw cycles at -196 °C – 4 °C to ensure complete cell breakage. Lactate dehydrogenase activity was assessed with an homogenate containing 4.20 mg/ml of protein, for all other assays the protein content was 3.48 mg/ml. Enzyme activities were calculated as described in section 2.3.7. Next, it was considered important to optimise breakage efficiency with the quantitative method detailed in section 2.3.5. Following the optimisation of the homogenisation method, subcellular fractionation was performed as outlined in section 2.3.6. Biochemical analysis of subcellular fractions was conducted at protein

concentrations within the validated range. This protein range can be deduced from figure 3.2 and is also detailed in section 2.3.6. For fluorescence-based assays, samples were routinely diluted (2 fold) to assess possible quenching effects.

3.3 Results

3.3.1 Validation of marker assays

The suitability of each particular stopping buffer to halt enzyme activity was assessed first. For *N*-acetyl-β-glucosaminidase sodium bicarbonate was found to be inadequate to stop the enzyme catalysed reaction, whereas glycine-NaOH was found to be superior and was thus used for all subsequent studies (figure 3.1, panel a – b, note differences in scale). All other stopping buffers tested for the remaining enzyme catalysed reactions proved appropriate under experimental conditions (figure 3.1). Next, enzyme kinetics were estimated to ensure that assays could serve as a direct indicator for the subcellular distribution of organelles/cellular components. Linear reaction kinetics for all investigated enzymes under both variable incubation times and protein content was observed (figure 3.2). *N*-acetyl-β-glucosaminidase showed only linearity at lower protein concentrations (figure 3.2, panel b). Deviation from linearity was observed when protein content was raised above ~ 0.2 mg/ml. Possible quenching was excluded by diluting samples and reanalysis (data not shown). It was thought important to also assess lactate dehydrogenase activity in the presence of Triton X-100 since the surfactant was included to establish a reference value for 100 % breakage efficiency. Triton X-100 did not change the enzyme kinetics (figure 3.2, panel c). Following the validation of enzyme assays, the methodology for detecting DNA was validated. First the effect of DNA concentration on fluorescence was determined using two DAPI concentrations. A linear relationship between protein concentration and fluorescence was observed under optimised conditions (figure 3.3).

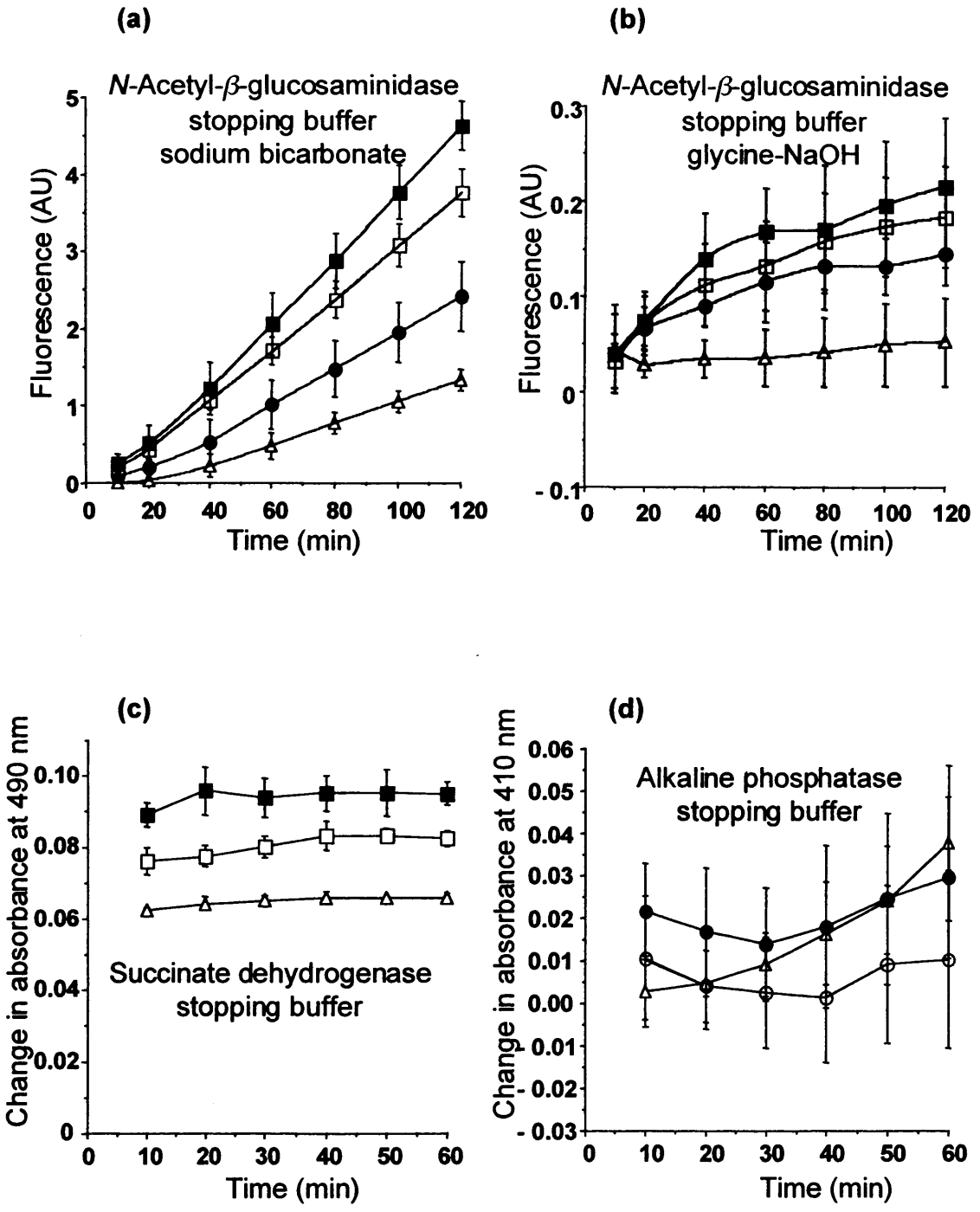

Figure 3.1 Evaluation of stopping buffers used to halt enzyme catalysed reactions. Panel (a - b) effect of sodium bicarbonate and glycine-NaOH buffer on *N*-acetyl-β-glucosaminidase activity, panel (c) stopping buffer for succinate dehydrogenase and panel (d) stopping buffer for alkaline phosphatase. Protein content for assays was as follows: 0.35 mg (■), 0.26 mg (□), 0.17 mg (●), 0.09 mg (△) and 0.04 mg (○). (Data represents mean ± SEM n=3, error bars are within plot symbols when not visible).

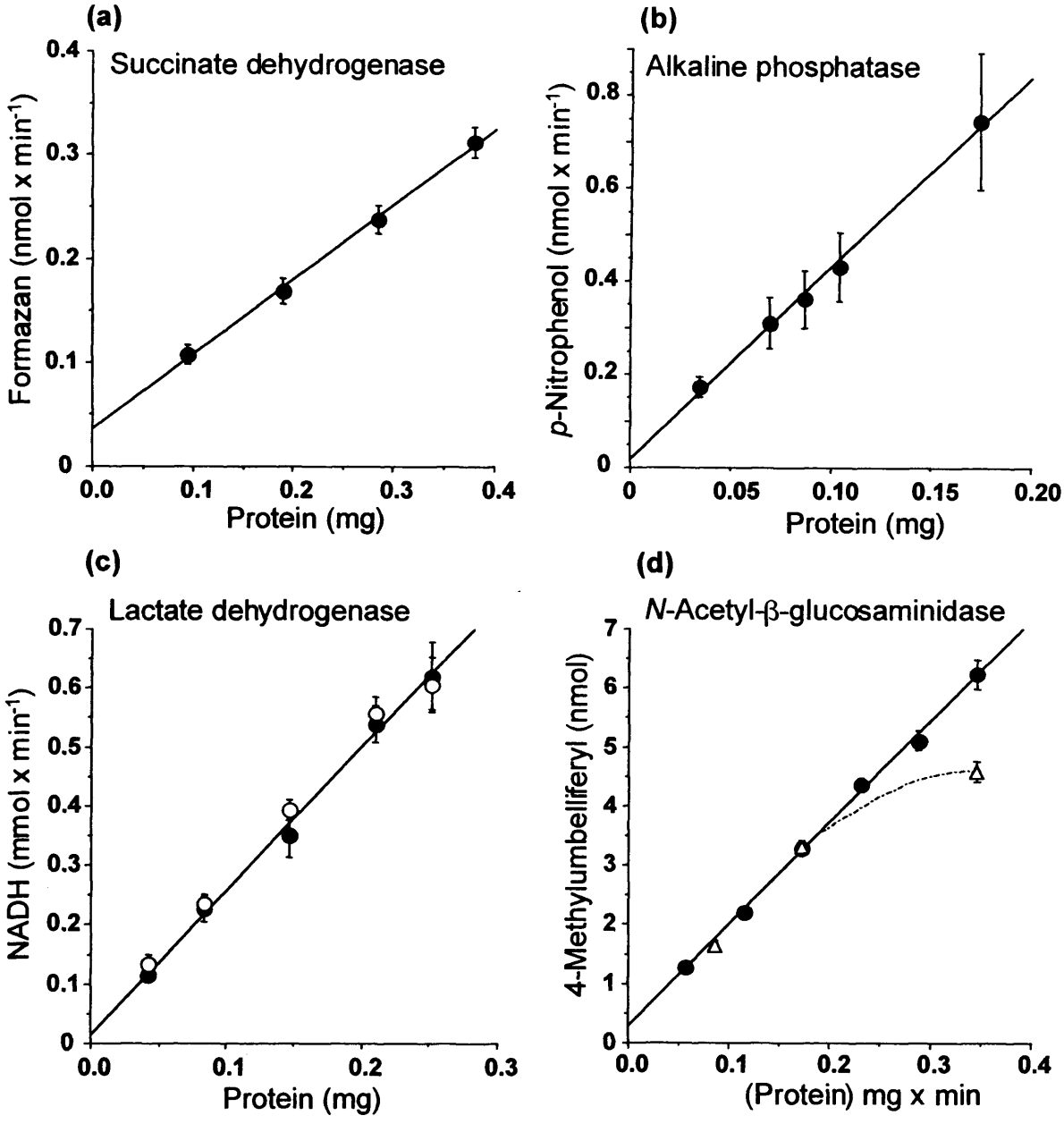

Figure 3.2 Enzymatic activities of B16F10 homogenate. Succinate dehydrogenase (panel a), alkaline phosphatase (panel b), lactate dehydrogenase (panel c) and *N*-acetyl-β-glucosaminidase (panel d) catalytic activities are shown. Lactate dehydrogenase activity was determined in the absence (●) and presence (○) of 0.1%v/v Triton X-100. For *N*-acetyl-β-glucosaminidase (panel d) activities were determined at either constant amount of protein (0.17 mg) and varied incubation times (●), or at a variable amount of cell protein (△) with a fixed 1 min incubation period. The ordinate of each graph is the amount of reaction product released. (Data represents mean ± SEM n=3 error bars are within plot symbols when not visible).

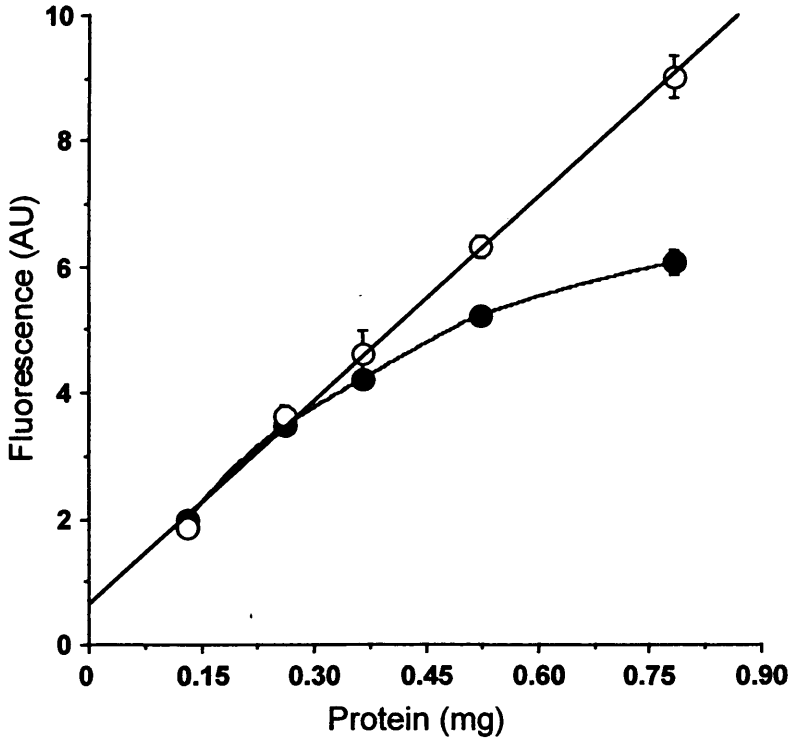

Figure 3.3 Effect of concentration on DAPI fluorescence in B16F10 homogenate. Plot symbols correspond 0.5 μg (O) and 1 μg (●) of DAPI. (Data represents mean ± SEM n=3, error bars are within plot symbols when not visible).

3.3.2 Optimisation of cell breakage

It was considered important to optimise cell breakage to ensure that subsequent fractionation studies were representative for the cell population. Therefore a quantitative method was developed by monitoring the release of the cytosolic marker lactate dehydrogenase (for methodology see section 2.3.5). Due to the small sample size (~ 0.9 mg of wet tissue) two homogenisation methods were evaluated, namely the cell cracker and a 25 gauged needle attached to a syringe. The optimum internal clearance for the cell cracker was determined to be 6 μm, with gaps of 5 μm and 7 μm at the extremes of the cell breakage efficiency (figure 3.4, panel b). The cell cracker with a 6 μm internal clearance was then directly compared to a 25 gauged needle. Seven passes through the cell cracker gave a cell breakage efficiency of 90 % compared to 50 % for a 25 gauged needle (figure 3.4, panel a).

3.3.3 Differential centrifugation and characterisation of fractions

Following the homogenisation of cells with the optimised method, cells were subjected to differential centrifugation, and subcellular fractions were assayed for biochemical markers. In particular the excellent mass balance of protein (82 %) ensured that no significant loss occurred during the subcellular fractionation procedure with recoveries for DNA, succinate dehydrogenase and lactate dehydrogenase in excess of 75 % (table 3.4). However, for *N*-acetyl-β-glucosaminidase and alkaline phosphatase, recoveries were somewhat lower with values of 58 % and 47 % respectively (table 3.4). Subcellular fractions were characterised and nuclei were typically enriched in the first fraction (RSA 2.2) (RSA has been defined in section 2.3.7), (figure 3.5, panel b). Enrichment of mitochondria (RSA 4.2) was only seen in the mitochondrial fraction (figure 3.6). Good lysosomal enrichment was obtained in the lysosomal fraction and somewhat lower levels were detected in the mitochondrial fraction with RSA values of 3.7 and 1.9 respectively. Distribution of plasma membrane was enriched in both the mitochondrial and lysosomal fractions, a general distribution pattern mirroring the one of *N*-acetyl-β-

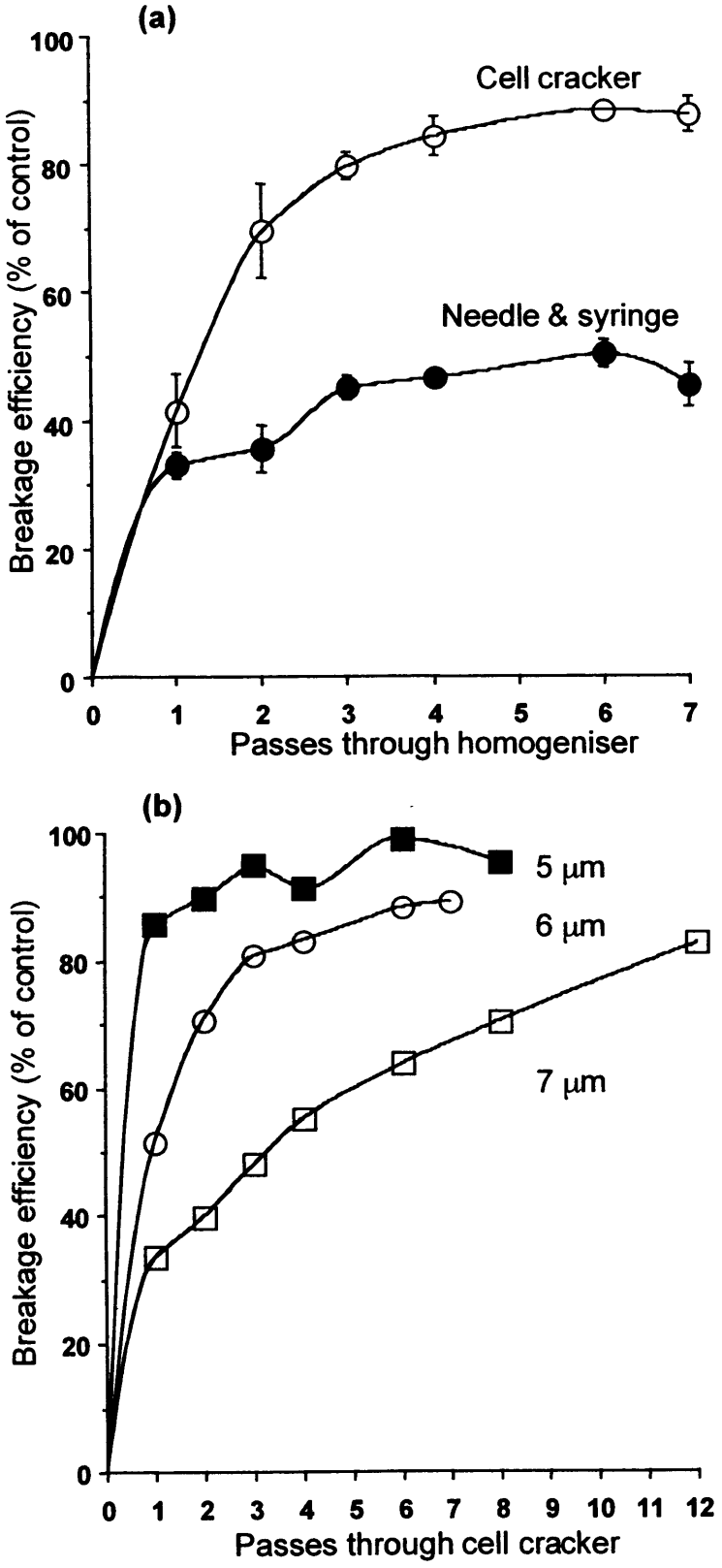

Figure 3.4 Comparison and effect of cell cracker passage number on B16F10 breakage efficiency. Panel (a) comparison of a 25 gauged needle attached to a syringe (●) with cell cracker (○) with a 6 μm gap (data represents mean ± SEM n=3, error bars are within plot symbols when not visible). Panel (b) selection of ball size for cell cracker with gaps of 5 μm (■), 6 μm (○) and 7 μm (□) (n=1).

Table 3.4 Distribution of enzymes, protein and DNA in the fractions following differential centrifugation. Results are given as percentages (± SEM) of the total amount recovered in the five fractions. Recoveries have been calculated by determining the total activity in the five fractions and the activity of the homogenate which served as 100 %.

Constituents	Number of experiments	Fractions N	M	L	S	Mic	Recovery (%)
Protein	4	36.58 (±1.46)	16.93 (±1.35)	10.31 (±1.35)	25.89 (±2.33)	10.29 (±1.60)	82.1 (±2.75)
DNA	5	78.76 (±2.75)	11.55 (±1.67)	5.33 (±0.72)	0.82 (±0.33)	3.54 (±0.53)	75.2 (±5.11)
Succinate dehydrogenase	4	17.02 (±2.89)	70.14 (±3.46)	8.11 (±1.34)	2.95 (±0.68)	1.80 (±0.35)	75.3 (±9.45)
Alkaline phosphatase	4	24.91 (±1.94)	32.56 (±4.94)	25.10 (±0.21)	8.65 (±2.32)	8.78 (±0.95)	47.3 (±3.45)
Lactate dehydrogenase	4	6.70 (±1.28)	3.44 (±0.71)	13.70 (±1.33)	64.63 (±3.94)	11.70 (±1.56)	112.1 (±3.90)
N-Acetyl-β-glucosaminidase	4	18.69 (±1.72)	32.82 (±4.55)	37.82 (±2.60)	1.21 (±0.28)	9.44 (±2.89)	57.7 (±3.45)

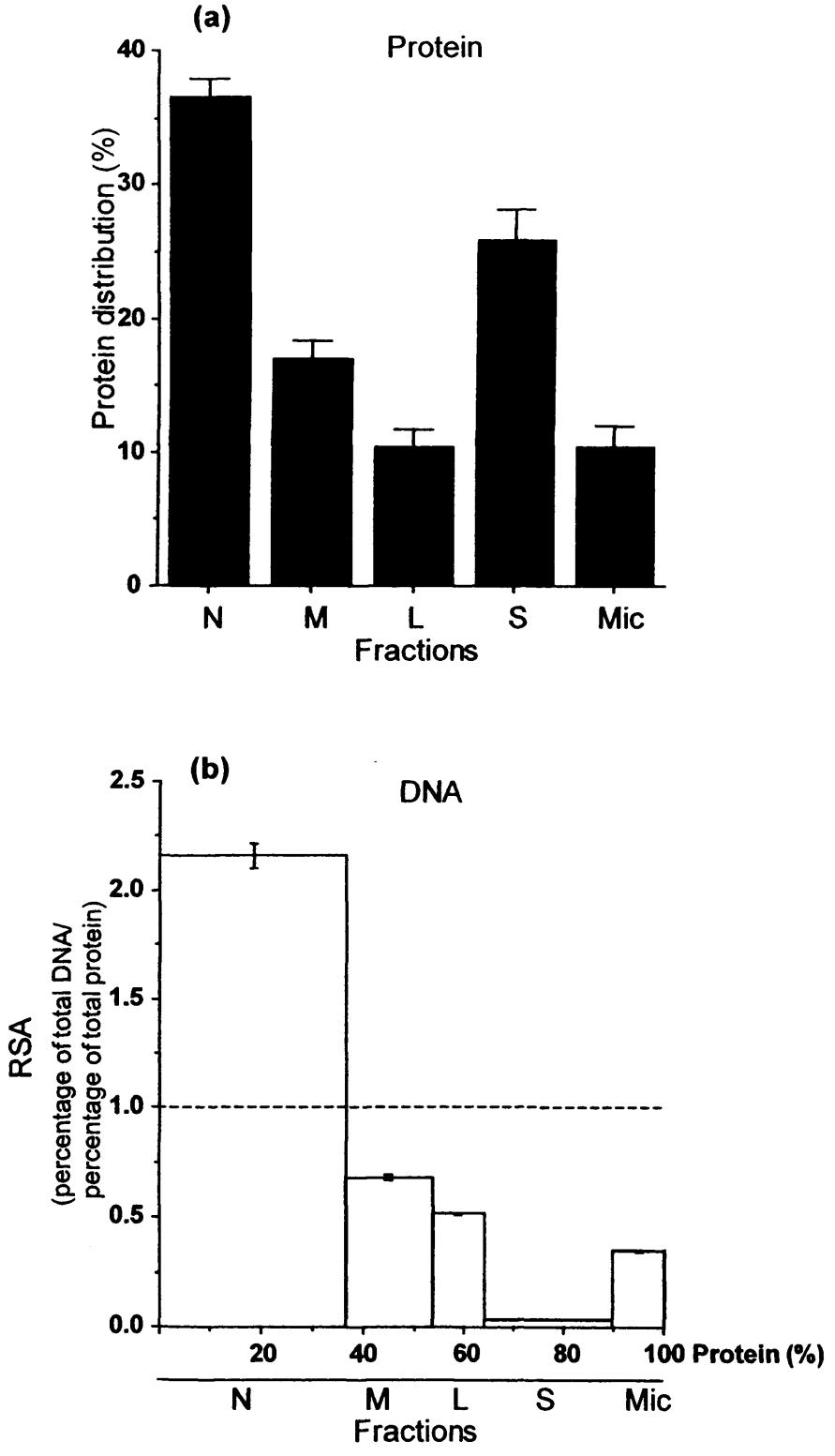

Figure 3.5 Distribution of protein and DNA in subcellular fractions. Panel (a) protein and panel (b) DNA distribution. Key: Nuclear (N), mitochondrial (M), lysosomal (L), soluble (S) and microsomal (Mic) fraction. An RSA > 1 indicates enrichment of DNA in fraction. (Data represents mean ± SEM n=4, error bars are within plot symbols when not visible).

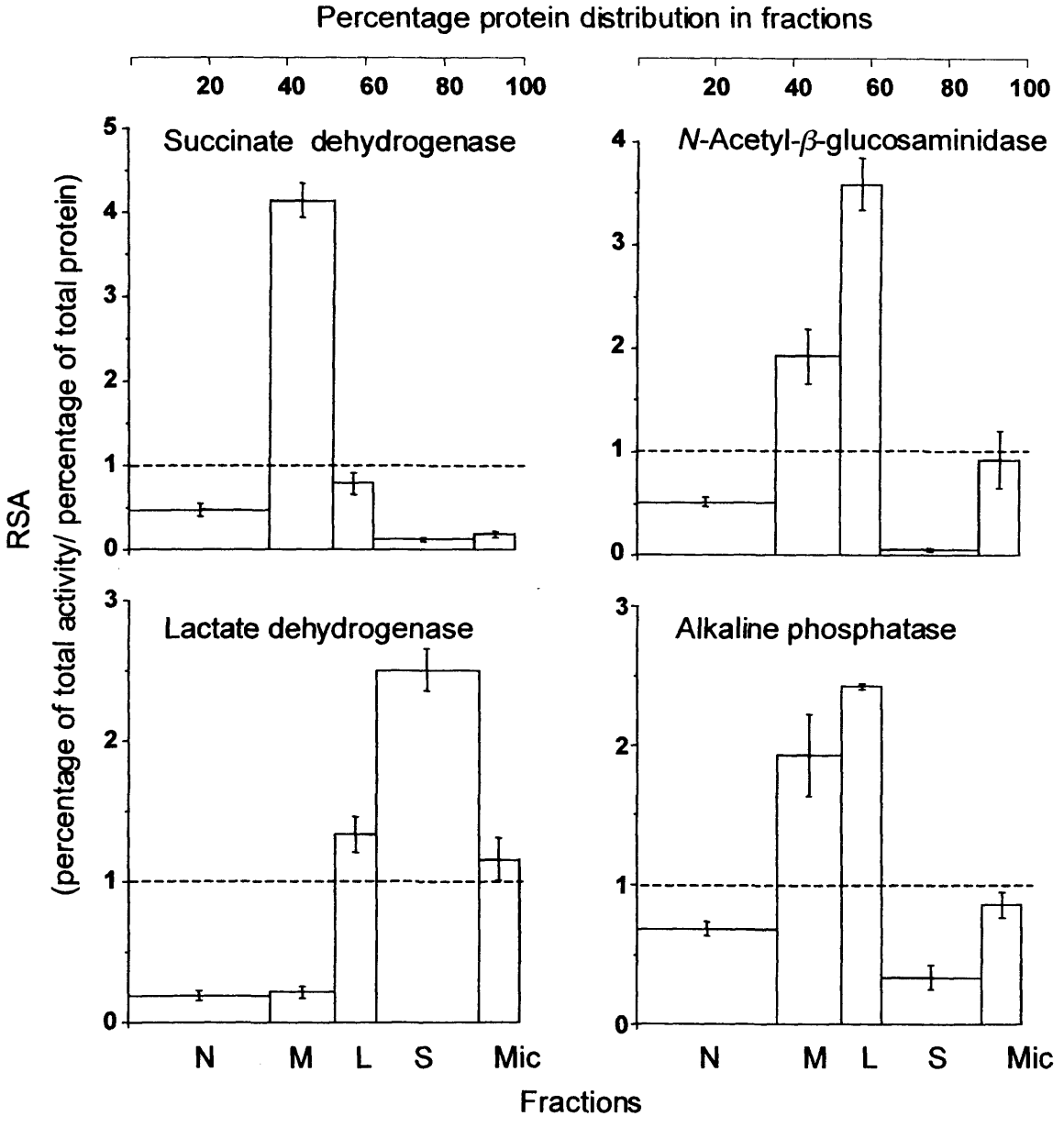

Figure 3.6 Distribution of marker enzymes in the subcellular fractions. Key: Nuclear (N), mitochondrial (M), lysosomal (L), soluble (S) and microsomal (Mic) fraction. An RSA > 1 indicates enrichment of marker in the fraction (Data represents mean ± SEM n=4, error bars are within histograms when not visible).

glucosaminidase (figure 3.6). The majority of lactate dehydrogenase activity was found in the soluble fraction with a RSA of 2.5.

3.4 Discussion

3.4.1 Validation of marker assays

To date few investigations have quantified the intracellular trafficking of polymer therapeutics using subcellular fractionation (table 3.1). Thus a simple differential centrifugation method was devised. The preliminary kinetic study was performed for all enzymes, in order to validate them in B16F10 cells (figure 3.2). When setting up subcellular fractionation studies, careful evaluation of enzymatic characteristics as reported here are common place (Appelmans et al., 1955; De Duve et al., 1955; Londos-Gagliardi et al., 1979; Lopez-Saura et al., 1972; Tulkens et al., 1974; Zenebergh et al., 1981) and indispensable (Tipton, 1992). A number of subcellular fractionation studies published recently in drug delivery however lack these data (Nori et al., 2003a; Nori et al., 2003b; Tijerina et al., 2001; Tijerina et al., 2003). It was thought important to study these enzyme catalysed reactions as they served as the basis for the characterisation of subcellular fractions. In particular, for enzyme catalysed reactions, identical specific enzyme activities under both varied incubation time and protein content ensured that biochemical analysis of subcellular fractions could serve as a direct indicator for organelle enrichment. The only exception was *N*-acetyl-β-glucosaminidase; here possibly the presence of some endogenous inhibitors in the homogenate reduced enzymatic activity, which was most notable with high protein concentrations. Samples were therefore routinely diluted to fall within the linear range of the assay taking into account the possible enrichment of the enzyme.

Secondary was the possibility to compare specific enzyme activities with other cells and tissues. Determined activities were very different to those observed either in cultured HTC cells or rat liver (table 3.5). Differences in basic physiological

Table 3.5 Comparison of the specific content of enzymes and DNA in the homogenates of B16F10 cells, cultured HTC cells and rat liver.

Enzyme or constituent	B161F10 cells	HTC cells#	Rat liver#
N-Acetyl-β-glucosaminidase	18.7 (± 1.1)	215.0	31.4
Succinate dehydrogenase	77.1×10^{-2} ($\pm 4.1 \times 10^{-2}$)	3.8	131.0
Alkaline phosphatase	4.1 (± 0.9)	79.9	79.9
Lactate dehydrogenase	2440.8 (± 0.2)	Not determined	1531.0
DNA	157.3 (± 13.9)*	67.1	13.1

Results are means ± SEM (n=3) in milli-Units (enzymes) and μg (DNA) per mg of protein.

Values for HTC and rat liver from references (Amar-Costesec et al., 1974a; Knox, 1976; Lopez-Saura et al., 1978).

* The amount of DNA is only an estimate since calf thymus DNA was used as a standard.

functions between melanocytes and hepatocytes, would be expected to give rise to significant differences in biochemical activities and contents.

3.4.2 Homogenisation and fractionation of B16F10 cells

Quantifying the extent of cell breakage was highly desirable, as this ensured that marker distributions were genuine for B16F10 cells and subsequent trafficking experiments were representative for the cell population. Reproducible cell breakage was highly encouraging since adequate homogenisation is recognised as a one of the major obstacles when dealing with cultured cells (Evans, 1992). The use of lactate dehydrogenase to optimise and monitor cell breakage has not been reported previously, and was a unique feature of the current study (Seib et al., 2003).

Good cell breakage made it feasible to devise a differential centrifugation method. It is worth reiterating that the final pellet was denoted as the microsomal fraction, which is commonly used to describe vesiculated endoplasmic reticulum fragments. However, the microsomal fraction in the present study also contained plasma membrane fragments and contaminating lysosomes besides uncharacterised cellular components. However, some degree of cross contamination of the fractions is inevitable due to (a) entanglement of organelles in the cytoskeleton, (b) inherent organelle heterogeneity, (c) entrapment of organelles by sedimenting cellular components, (d) fragmentation of organelles, reducing the sedimentation coefficient and hence sedimentation behaviour. Thus by means of differential centrifugation it is not possible to purify single cellular components (Spragg & Steensgaard, 1992). However separation of mitochondria or nuclei is readily achieved due to an approximate 1,000 fold difference in their sedimentation coefficients (Hinton & Mullock, 1993). Therefore it is usual to achieve an excellent separation of nuclei and mitochondria (typically ~ 4.5 RSA) (De Duve et al., 1955; Lopez-Saura et al., 1978). However, separation of cellular components of similar sedimentation coefficients (e.g. lysosomes, peroxisomes) requires isopycnic gradient centrifugation where

differences in buoyant density can be exploited for separation. Therefore to provide high purity fractions, the PNS could be subjected to gradient fractionation (Hinton & Mullock, 1993).

3.4.3 Characterisation of subcellular fractions

Enrichment of DNA in the nuclear fraction and low levels in the mitochondrial fraction indicated that nuclear integrity was preserved during the homogenisation procedure due to little cross contamination of other fractions by raptured nuclei (figure 3.5, panel b). Since mitochondrial DNA only contributes ~ 1 % of total DNA content in hepatocytes, similar observations made in both HTC cells (i.e. hepatocytes) and in the current study suggested, that DAPI binding closely resembled nuclei distribution (Lopez-Saura et al., 1978). Enrichment of mitochondria was only seen in the mitochondrial fraction (RSA 4.2), results comparable to those obtained with EAT cells (Londos-Gagliardi et al., 1979).

As expected lactate dehydrogenase activity was enriched in the soluble fraction (RSA 2.5), with residual activities in the lysosomal and microsomal fractions (figure 3.6). Enzymatic activities in the latter two fractions can be attributed to the incomplete removal of the soluble components from the pellet. Washing of these fractions with homogenisation buffer would most probably avoid this problem. Additional washing steps were however not included in the fractionation procedure to avoid excessive organelle damage. The presence of lactate dehydrogenase activity in the lysosomal fraction could also, in part be related to the autophagic sequestration of the cytosolic protein by lysosomes, as demonstrated in isolated rat hepatocytes where ~ 3.5 % of enzyme was found in lysosomes (Kopitz et al., 1990).

Alkaline phosphatase was used as the marker for plasma membrane, since 5'-nucleotidase activity assayed according to the method described by Avruch and Hoelzl Wallach (Avruch & Hoelzl Wallach, 1971) did not yield detectable levels in

B16F10 homogenates. 5'-Nucleotidase activity is most commonly associated with the apical membrane of polarised cells (Evans, 1992). Hence undetectable levels in B16F10 cells were not surprising with similar observations reported previously (Lopez-Saura et al., 1978; Zenebergh et al., 1981). Plasma membrane fragments were enriched in the mitochondrial and lysosomal fraction (figure 3.6), results which are comparable to those reported for L1210 cells, cultured rat embryo fibroblasts and HTC cells (Lopez-Saura et al., 1978; Tulkens et al., 1974; Zenebergh et al., 1981). Fractionated B16a cells also showed the mitochondrial-lysosomal distribution pattern for plasma membrane, with additional enrichment in the nuclear fraction (Rozhin et al., 1987). In fractionated rat liver, alkaline phosphatase was however only "nuclei-microsomally" distributed (Amar-Costesec et al., 1974a). Different distribution patterns of plasma membrane in B16F10, B16a and rat liver subcellular fractions was not unexpected, since the results of cell disruption may differ, depending on sample size and homogenisation method.

As mentioned in the introduction to this Chapter, the selection of appropriate markers for the characterisation of fractions can be demanding (Evans, 1992). Although the specificity of commonly used markers has been amply illustrated by analytic fractionation of liver, their use in cultured cells can be challenging. Previous studies by Rozhin and co-workers demonstrated that commonly used lysosomal markers cathepsin B and L were associated with the plasma membrane in B16F10 cells. *N*-Acetyl-β-glucosaminidase was therefore a more representative marker for lysosomes (Casciola-Rosen & Hubbard, 1991), with only little plasma membrane association (Rozhin et al., 1987; Rozhin et al., 1989). This was corroborated by differential centrifugation studies in B16F10 cells where identical distribution patterns of *N*-acetyl-β-glucosaminidase and β-glucuronidase were observed (Sloane et al., 1981). Nonetheless, a possible better alternative to *N*-acetyl-β-glucosaminidase would have been cathepsin H or β-glucuronidase, due to the absence of any plasma membrane association in B16 variants (Rozhin et al., 1987). However, classic

lysosomal markers in melanocytes are not only found in lysosomes, but can also be present in melanosomes (Orlow, 1995). Naturally, B16F10 cells contain a large number of melanosomes (Novikoff et al., 1968). Melanosomes are lysosome-related organelles and thus share many features commonly associated with lysosomes (Marks & Seabra, 2001; Raposo & Marks, 2002; Stinchcombe et al., 2004). For instance, melanosomes contain typical lysosomal markers such as LAMPs (Zhou et al., 1993) and hydrolytic enzymes such as cathepsin B and *N*-acetyl-β-glucosaminidase (Diment et al., 1995). It might therefore be deduced that melanosomes could obscure the subcellular distribution of lysosomes. However, it is strongly believed that the subcellular distribution pattern of *N*-acetyl-β-glucosaminidase is representative for the actual distribution of lysosomes. This view is supported by findings that lysosomes and melanosomes co-migrate during subcellular fractionation of B16F10 cells by differential centrifugation (Seiji et al., 1963), leading to a similar distribution pattern in fractions as reported for cultured rat fibroblasts and HTC cells (Lopez-Saura et al., 1978; Tulkens et al., 1974). Satisfactory separation of *N*-acetyl-β-glucosaminidase activity associated with lysosomes and melanosomes is only achieved following Percoll density gradient fractionation (Diment et al., 1995; Orlow et al., 1993).

So far only a handful of cellular components have been discussed, but it is clear from the general introduction that an array of endocytic compartments are involved during pinocytosis (section 1.4, table 1.2). Although endocytic compartments and transient hybrid organelles are characterised by different morphology, size, and buoyant densities (Mullock et al., 1998), it is suffice to say that separation by differential centrifugation is inadequate, since differences in sedimentation coefficients as large as 1,000 fold are needed for good separation (Hinton & Mullock, 1993). It is therefore reasonable to predict that the majority of endocytic compartments pelleted in the lysosomal and microsomal fractions. The

lysosomal and microsomal fraction could therefore be regarded as a descriptor to encompass endocytic organelles.

3.5 Conclusions

The systematic development of a quantitative subcellular fractionation study in B16F10 cells has been described. First, enzyme markers and biochemical assays were validated and used in due course for the quantitative characterisation of subcellular fractions. Next, cell homogenisation was optimised to achieve a 90 % cell breakage efficiency with the cell cracker, ensuring that subsequent subcellular fractionation experiments were representative for the cell population. Finally, a differential centrifugation method was devised to separate and enrich nuclei (2.2 fold), mitochondria (4.1 fold), endosomes/lysosomes (3.7 fold) and cytosol (2.5 fold). The involvement of those cellular components is of particular importance for the design of new endosomolytic carriers for cytosolic and nuclear delivery and lysosomotropic anticancer polymer-drug conjugates. The method was therefore used to follow the intracellular trafficking of polymer-bound (PK1) and free doxorubicin as described in the following Chapter.

Chapter 4

Subcellular trafficking of PK1 and doxorubicin

4.1 Introduction

Using the differential centrifugation method established in the previous Chapter, it was possible to monitor the intracellular trafficking of PK1. Despite the wealth of literature on PK1, no studies have investigated the intracellular trafficking of PK1 by subcellular fractionation. Only the intracellular fate of the asialoglycoprotein receptor targeted HPMA copolymer conjugate PK2 (bearing galactosamine) has been studied in rat liver (Duncan et al., 1986; Wedge et al., 1991). All trafficking studies with PK1 have used fluorescence microscopy (summarised in table 1.3). However, interpretation of these results can be difficult with artefacts arising from cell fixation and changes in fluorescence of polymer-bound and free doxorubicin. Therefore the fractionation method established in Chapter 3, was used to study the intracellular fate of PK1 over time with the hope of providing insight into its mechanism of action. The subcellular distribution of free doxorubicin was also studied as a reference control experiment for these studies. The intracellular distribution of free doxorubicin is well known in a panel of other cell lines employing subcellular fractionation (Noel et al., 1978; Peterson & Trouet, 1978; Zenebergh et al., 1984) and could therefore validate the fractionation method. Fractionation studies were underpinned by careful fluorescence microscopy studies of live and fixed cells to visualise the intracellular localisation of PK1 and doxorubicin in B16F10 cells with time. However, it is important to have background knowledge of the subcellular distribution of PK1 in patients, animal models and *in vitro* systems to appreciate the opportunities and limitations of the present study.

PK1 trafficking in patients

As discussed in Chapter 1, a number of polymer-drug conjugates have now entered clinical development (table 1.1). Many are designed to release their drug payload when exposed to lysosomal thiol-dependent proteases (Duncan, 2005). For examples of such polymer conjugates in the clinic see summary of compounds in table 1.1. Widely discussed has been the design of the HPMA copolymer-GFLG doxorubicin conjugates (PK1/PK2) and polyglutamic paclitaxel today (Duncan,

2003a; Kopecek et al., 2000). The correct intracellular trafficking of these polymer-drug conjugates is a key requirement if drug is to be released from the carrier in an active form inside cells, and pharmacological response attained. Intracellular trafficking may be a key determinant of the pharmacokinetic-pharmacodynamic relationship. Although PK1 was designed for lysosomal activation, it is important to realise that cathepsin B (thiol protease) is often secreted from tumours (Kos & Lah, 1998; Yan et al., 1998) and could allow for drug activation outside the cell. It remains to be seen if extracellular activation of PK1 will be of any importance. In its Phase I evaluation PK1 administered to chemotherapy refractory patients produced 4 responses (2 partial and 2 minor) in breast, non-small cell lung and colorectal cancer patients (Vasey et al., 1999). However, no clinical response was observed in head/neck, pancreas, ovary, urinary and biliary tract cancers (Vasey et al., 1999). As elevated extracellular and intracellular cathepsin B levels have been associated with the majority of these cancers (Kos & Lah, 1998), the observed differences could point to ineffective intracellular trafficking in certain tumour types (and/or tumour stage).

PK1 trafficking in animal models

Similar considerations also apply to *in vivo* data, where a variable response to PK1 has been observed in a number of tumour models. No response was seen in resistant Lovo tumours (Duncan, 2005), a partial response in P388R (resistant) (Wedge, 1991) and excellent activity in P388 (Wedge, 1991), L1210 (Duncan et al., 1989), A2780 (doxorubicin sensitive), A2780/AD (doxorubicin resistant) (Minko et al., 2000) and B16F10 tumour models (Seymour et al., 1994). Drug release was always required, since therapeutic response was only attained with conjugates designed for lysosomotropic activation (Duncan, 2005). Therefore release of the drug must have been triggered by the lysosomal enzyme cathepsin B. Improved survival following PK1 administration was in part attributed to altered pharmacokinetics. In particular increased extravasation of the conjugate at the tumour site and reduced lymphatic drainage (EPR effect) (Duncan, 1999; Maeda, 1994), provided high

conjugate levels at the target site (Seymour et al., 1994). Although tumour accumulation is a prerequisite for activity, data from experimental colon tumour models suggested that activity for PK1 was primarily dependent on drug activation (Loadman et al., 1999). Therefore variable *in vivo* activity of PK1 could be due to a number of factors including (a) ineffective intracellular trafficking, (b) variable cathepsin B levels, (c) variable tumour vascular properties. Due to a number of contributing factors for *in vivo* response, *in vitro* studies could provide a useful tool to delineate these factors and are particularly well suited for studying intracellular trafficking events.

PK1 trafficking in vitro

Although no quantitative data is available on the subcellular distribution of PK1, a number of studies have investigated the intracellular trafficking of PK1 by fluorescence microscopy (section 1.5.1 and table 1.3). However, only a few studies have monitored PK1 trafficking in live cells (Hovorka et al., 2002; Nori et al., 2003b). Vastly different trafficking has been observed in live cells, which might be cell type related. The study by Hovorka and co-workers showed in a panel of cell lines PK1 accumulation in pinocytic vesicles with minimal doxorubicin release from the polymer and complete absence of nuclear staining at 48 h (Hovorka et al., 2002). Different observations have been reported by Jensen for HPMA copolymer doxorubicin conjugates with the stable GG polymer-drug linker. In Hep G2 cells cytoplasmic and nuclear accumulation (> 8 h) was demonstrated, in addition to vesicular labelling. The authors suggested a possible endosomal/lysosomal escape of the polymer conjugate (Jensen et al., 2001).

A major challenge for *in vitro* model systems is to mimic *in vivo* conditions. Since all studies detailing PK1 trafficking employed either methodologies known to introduce artefacts (e.g. cell fixation) or cell lines not used for screening PK1 activity *in vivo*, it remains to be seen if observations made in these *in vitro* studies can ever be related to *in vivo* performance of PK1. Therefore the aims of the studies described

in this Chapter were to use B16F10 cells to (a) trace the intracellular path of PK1 with time, (b) validate the fractionation method with the use of doxorubicin (c) compare the results from fractionation with fluorescence microscopy studies.

4.2 Methods

First it was necessary to determine the effect of buffer composition and pH on fluorescence. Therefore calibration curves were constructed using a range of doxorubicin and PK1 concentrations (5.0×10^{-4} – 1.0 mg/ml doxorubicin-equivalence) in either PBS (0.1 M; pH 7.4 or 6.4) or citrate phosphate buffer (0.1M; pH 5.4). Before undertaking the subcellular fractionation studies it was necessary to define non-toxic drug concentrations. The cytotoxicity of PK1 and doxorubicin was determined using the MTT assay (see section 2.3.3) at cell seeding densities of 1×10^4 cells/ml and 1×10^5 cells/ml. The incubation period for these studies was 5 h or 72 h. The 72 h incubation period was chosen to maximise possible polymer-associated toxicities and provide a more clinically relevant incubation period (approximate elimination half-life of PK1) (Vasey et al., 1999). The 5 h incubation period was selected to reflect the incubation time used in this study. In addition, qualitative assessment of polymer cytotoxicity was made (see section 2.3.4) by visualising cells using bright-field microscopy at a single PK1 concentration (6.6×10^{-3} mg/ml doxorubicin-equivalence) after a 5 h incubation period.

Before examining the cellular uptake of PK1 (and FITC-dextran which was used as a control) using flow cytometry, it was considered important to determine its stability in the presence of tissue culture medium and cells. B16F10 cells were exposed to PK1 (6.6×10^{-3} mg/ml doxorubicin-equivalence) or FITC-dextran (1.0 mg/ml) in complete culture medium for 5 h. The cell culture medium was then aspirated, 3 ml dried under vacuum and the residue re-dissolved in 0.5 ml of MeOH and applied to a 6 cm LH20 column. FITC-dextran was prepared in the same way but dissolved in PBS and applied to a PD10 column (Sephadex G25). Samples were fractionated (0.5 ml) and analysed for doxorubicin or FITC-associated fluorescence

with an excitation wavelength set at 485 nm and emission wavelengths at 590 nm and 520 nm respectively. GPC profiles were constructed by plotting fluorescence versus fraction volume.

To guide the choice of time points for the subcellular fractionation studies the cell-association of PK1 over 5 h was assessed using flow cytometry. For these studies a non-toxic PK1 concentration (6.6 x 10^{-3} mg/ml doxorubicin-equivalence) was used. The methods used for flow cytometry are described in detail in section 2.3.11 – 2.2.12. To assess the extent of doxorubicin release from the polymer backbone B16F10 cells were pre-incubated with leupeptin (20 – 100 μg/ml) for 10 min. Fresh medium with leupeptin was then added and cells exposed to PK1 (6.6 x 10^{-3} mg/ml doxorubicin-equivalence) for 5 h under tissue culture conditions. For comparative purposes, cells exposed to culture medium only were incubated with PK1 as indicated. After 5 h, cells were analysed by flow cytometry as described above. Leupeptin itself might alter cell autofluorescence, so as a control cells were incubated with the drug and subsequently used to determine cell-associated background fluorescence. In addition, the basal rate of pinocytosis was monitored in B16F10 cells using FITC-dextran (Mw = 10,000 g/mol; 0.1 mg/ml) as a marker in the presence and absence of leupeptin. Cell-association of FITC-dextran was assessed by flow cytometry as described above.

To visualise the intracellular localisation of PK1 and doxorubicin epifluorescence and confocal laser scanning microscopy was conducted as described in section 2.3.9. PK1 or doxorubicin (6.6 x 10^{-3} mg/ml doxorubicin-equivalence) was added to cells and images were acquired in both live and fixed cells. Live cell microscopy was performed in the present study to exclude possible fixation artefacts. The subcellular distribution of doxorubicin was monitored by epifluorescence microscopy, whereas all PK1 studies were performed by confocal microscopy. For confocal co-localisation studies, PK1 was co-incubated with 1.0 mg/ml of FITC-

dextran (Mw = 10,00 g/mol) for 5 h. FITC-dextran was included to label the endocytic pathway. All confocal images are maximum projections.

The subcellular fractionation method described in Chapter 3 was used to study the intracellular distribution of PK1 or free doxorubicin in B16F10 cells, and an early (15 min) and late (5 h) time point were selected. Cells were incubated with PK1 (6.6 x 10^{-3} mg/ml doxorubicin-equivalence) at both time points and doxorubicin (6.6 x 10^{-3} mg/ml) at the 5 h time point only. Following the incubation, cells were kept at 4 °C, harvested, broken with the cell cracker and fractionated according to the method described in section 2.3.6. Doxorubicin-associated fluorescence was either determined by direct measurements of the fractions, which were routinely subjected to serial dilutions to assess possible fluorescence quenching (section 2.3.8). Alternatively, drug was extracted from fractions and quantified as described in section 2.3.8. The suitability of the extraction method was verified as described in section 2.3.8.

4.3 Results

Doxorubicin fluorescence in its free and polymer-bound form displayed concentration-dependent quenching between 0.04 – 1 mg/ml (figure 4.1). Doxorubicin fluorescence was independent of pH (7.4 – 5.4) and conjugated drug exhibited a lower fluorescence quantum yield (~ 3.5 fold) than free drug.

4.3.1 Cytotoxicity of PK1 and doxorubicin in B16F10 cells

The cytotoxicity of PK1 in B16F10 cells (seeding density of 1 x 10^4 cells/ml) was greatest after 72 h than at 5 h (figure 4.2, summarised in table 4.1). When seeding density was increase from 1 x 10^4 to 1 x 10^5 cells/ml, PK1 cytotoxicity was significantly reduced ($p < 0.01$). It should be noted that since PK1 contains ~ 0.39 wt% free doxorubicin, this free contaminant could theoretically contribute to the seen cytotoxicity. When its contribution is estimated, a close correlation between the theoretical toxicity attributable to free doxorubicin present in the preparation and

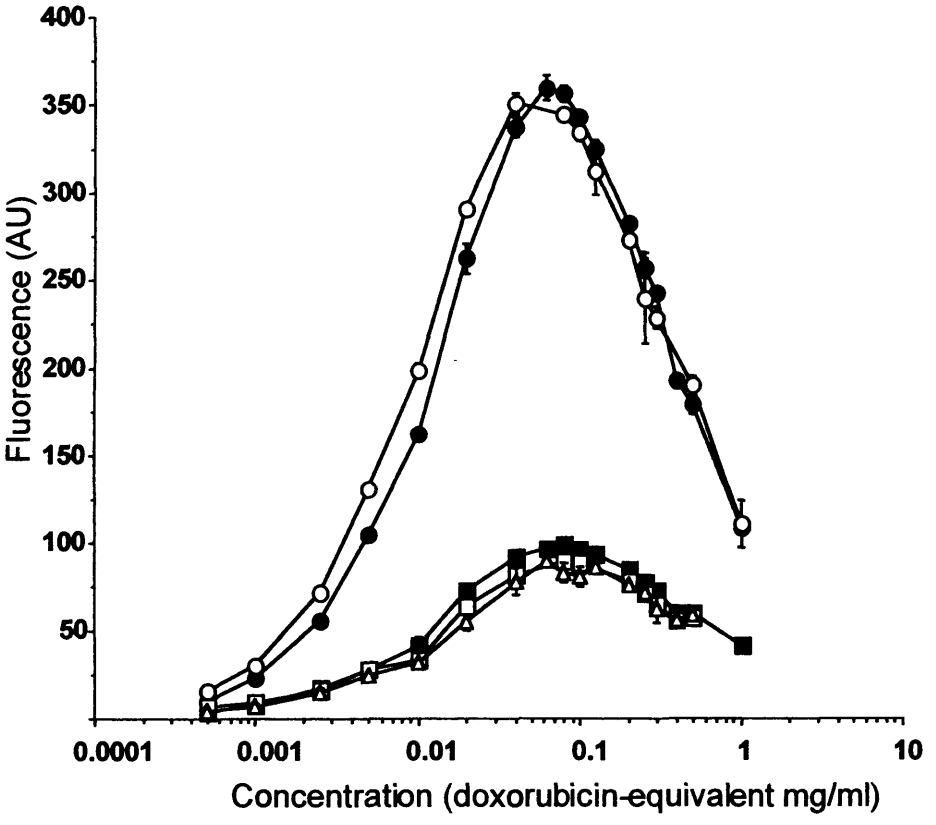

Figure 4.1 Effect of concentration and buffer pH on fluorescence of free and polymer-bound doxorubicin (PK1). Values for free doxorubicin were obtained at pH 7.4 (●) and pH 5.4 (○), and for PK1 at pH 7.4 (■), pH 6.4 (□) and pH 5.5 (△). (Data represents mean ± SEM n=3, error bars are within plot symbols when not visible).

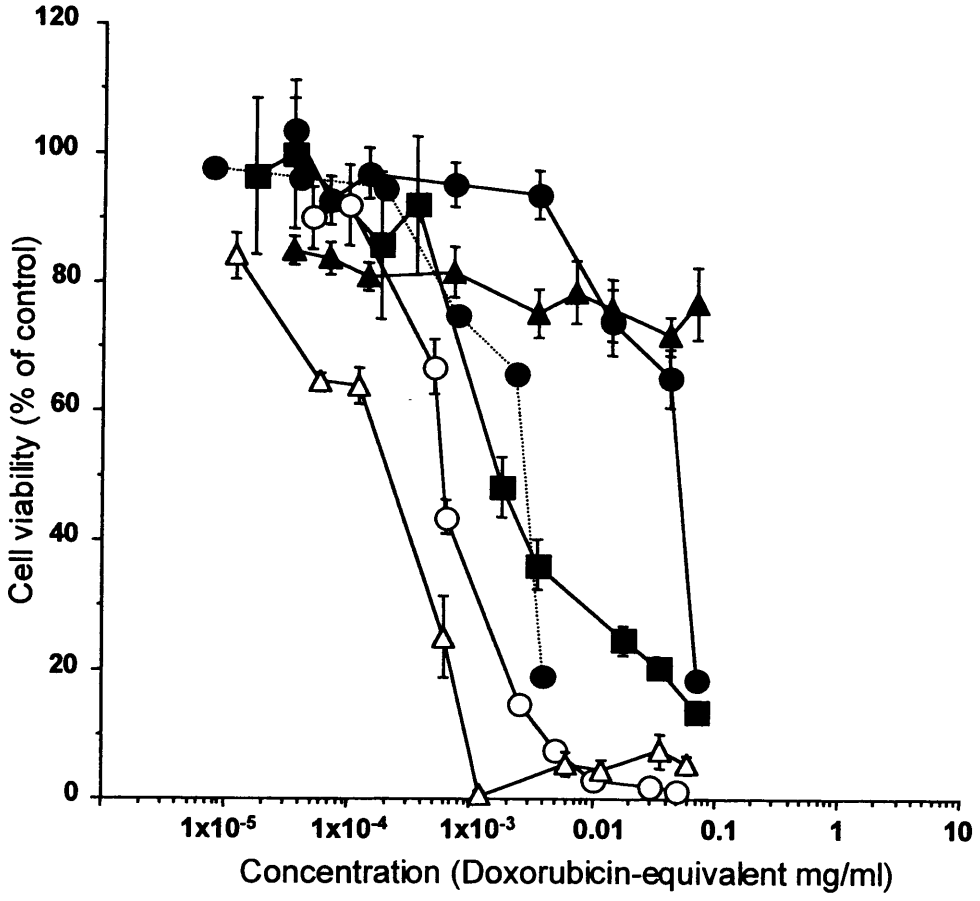

Figure 4.2 Cytotoxicity of PK1 and doxorubicin in B16F10 cells. Key: 1 x 10^4 cells/ml exposed to PK1 for 5 h (●), 1 x 10^4 cells/ml exposed to doxorubicin for 5 h (○), 1 x 10^4 cells/ml exposed to PK1 for 72 h (■), 1 x 10^5 cells/ml exposed to PK1 for 72 h (▲), 1 x 10^5 cells/ml exposed to doxorubicin for 72 h (△). Since 0.39 % of total doxorubicin in PK1 is in its free form, cytotoxicity attributable to free drug can be calculated using (●) as a reference curve. This theoretical profile is shown as (····). (Data show cell viability as percentage of untreated control cells and represent mean ± SEM n=18, error bars are within plot symbols when not visible).

Table 4.1 Summary of IC_{50} values for PK1 and doxorubicin in B16F10 cells.

Seeding density (cells/ml)	Exposure time (h)	Compound	IC_{50} (μg/ml)*
1×10^4	5	Doxorubicin	3.9×10^{-1}
1×10^5	72	Doxorubicin	3.0×10^{-1}
1×10^4	5	PK1	48.6
1×10^4	72	PK1	1.6
1×10^5	72	PK1	> 66.0

* IC_{50} Doxorubicin-equivalence required to inhibit 50 % of cell growth

actual toxicity for PK1 was evident (figure 4.2). Doxorubicin was consistently more cytotoxic than PK1, with a greater cytotoxicity at 72 h than at 5 h. B16F10 cells exposed to PK1 (6.6 x 10^{-3} mg/ml doxorubicin-equivalence) for 5 h showed no signs of drug-induced toxicity by either MTT assay or bright-field microscopy (figure 4.3), therefore this concentration was chosen for subcellular fractionation studies.

4.3.2 B16F10 association of PK1 and FITC-dextran measured by flow cytometry

Before assessing cell-association of PK1 in B16F10 cells, the stability of PK1 and FITC-dextran was assessed using GPC. It can be seen, that following the exposure of PK1 and FITC-dextran to B16F10 cells for 5 h, no obvious signs of released fluorescent low Mw products could be detected (figure 4.4). The cell association of PK1 with B16F10 cells at 37 °C displayed a biphasic behaviour (figure 4.5). A rapid linear increase in cell-associated fluorescence was seen over the first 15 min, followed by a much slower increase in fluorescence over the remaining incubation period. At 4 °C, PK1 cell-associated fluorescence was always significantly lower ($p \leq 0.05$) than seen at 37 °C. When PK1 and FITC-dextran uptake was assessed at 5 h in the presence and absence of the protease inhibitor leupeptin (figure 4.6), at a 20 μg/ml leupeptin concentration no statistically significantly difference in uptake was seen. However, at a leupeptin concentration of 100 μg/ml, the PK1 cell-associated fluorescence was marginally but statistically lower ($p \leq 0.05$) in the presence of leupeptin, whereas the FITC-dextran cell-associated fluorescence was unchanged .

4.3.3 Fate of PK1 and doxorubicin in B16F10 cells monitored by subcellular fractionation

First it was established that both PK1 and doxorubicin could be extracted over a wide concentration range from cell homogenate (figure 4.7). When B16F10 cells were exposed to doxorubicin (6.6 x 10^{-3} mg/ml) for 5 h (figure 4.8) most doxorubicin was recovered from the nuclear fraction (86 %). Doxorubicin was also detected in the lysosomal fraction (57 μg/mg protein) and the remainder was

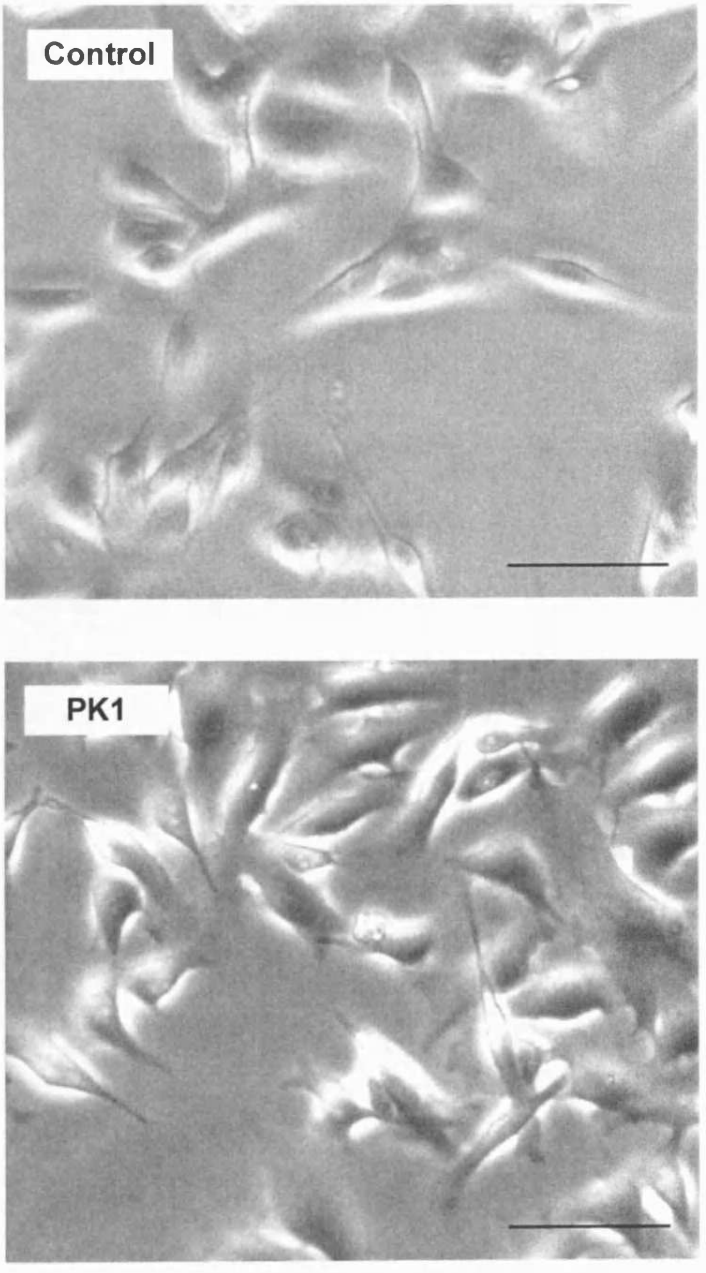

Figure 4.3 Effect of PK1 exposure on B16F10 morphology. Panel (a) control cells, panel (b) cells incubated with PK1 (6.6×10^{-3} mg/ml doxorubicin-equivalence) for 5 h. Scale bar 20 μm.

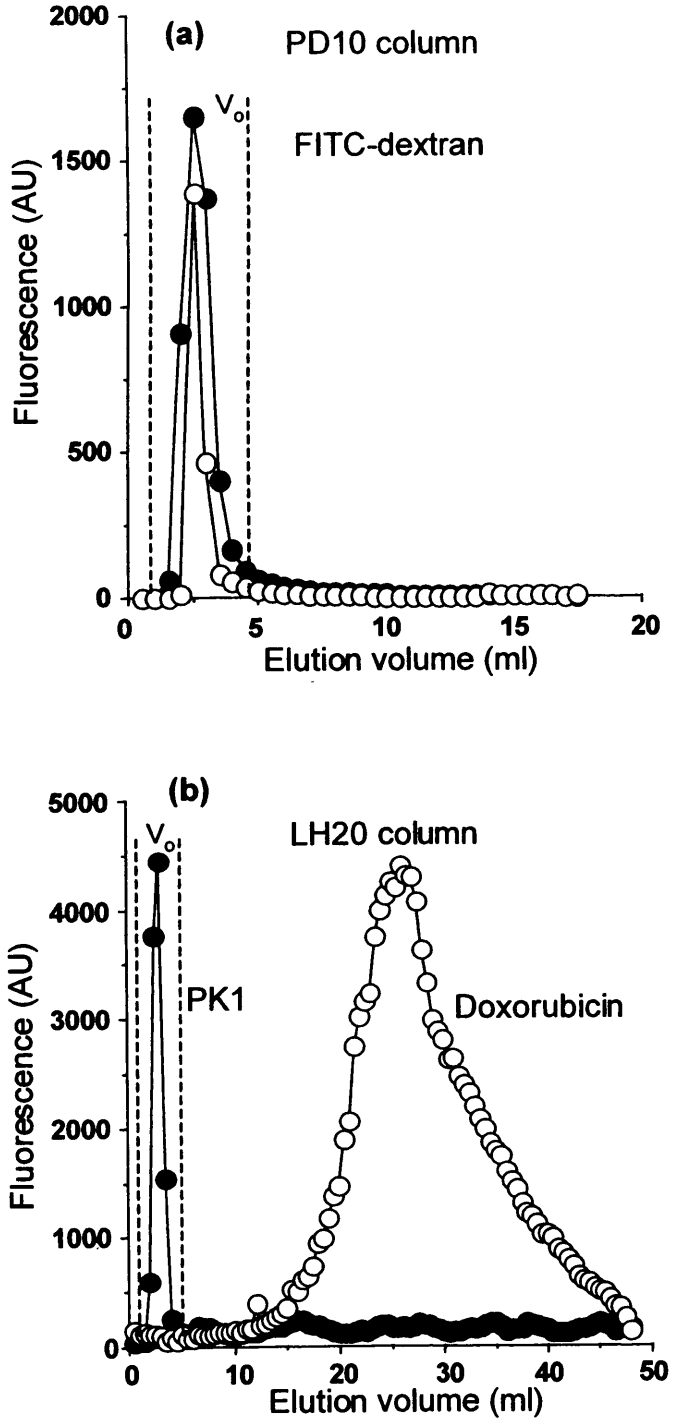

Figure 4.4 Stability of PK1 and FITC-dextran during incubation with B16F10 cells (5 h). Panel (a) FITC-dextran at 0 h (O) and 5 h (●), panel (b) profiles for doxorubicin at 0 h (O) and PK1 at 5 h (●). (Data from single representative experiment).

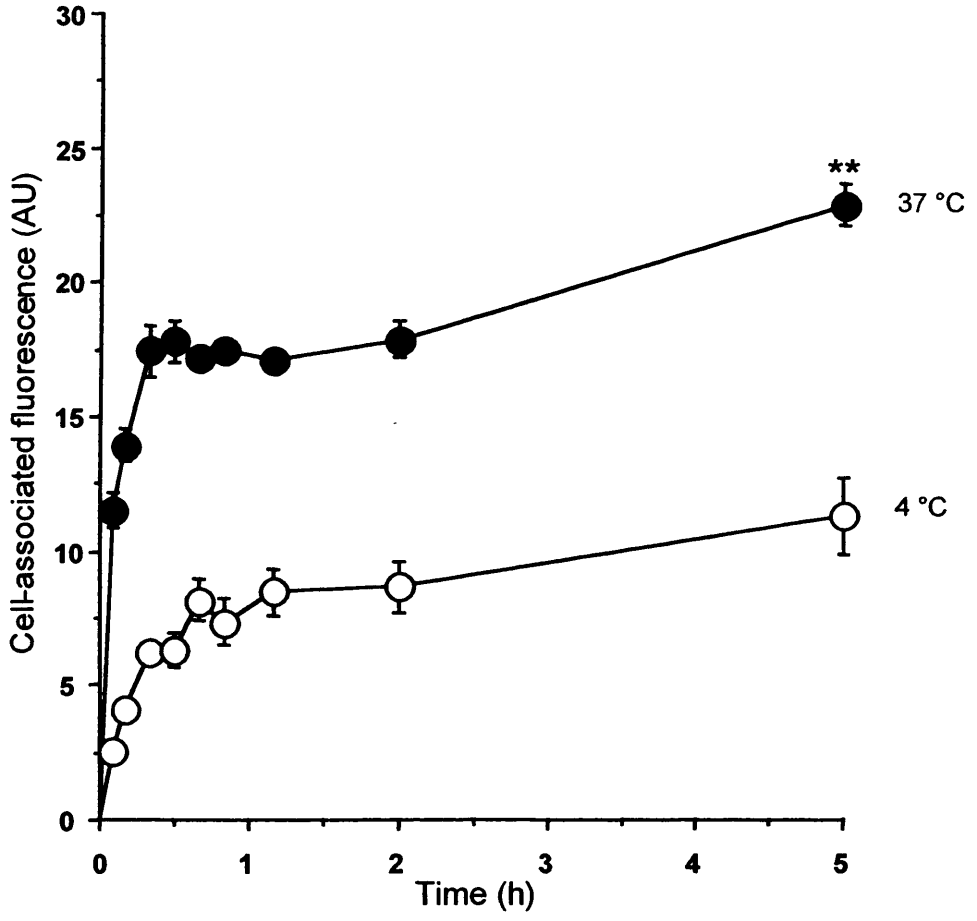

Figure 4.5 Time-dependent cell-association of PK1 in B16F10 cells measured by flow cytometry. Cells were incubated with PK1 at 37 °C (●) or 4 °C (○). Statistical difference at 37 °C between cell-associated fluorescence at 15 min and 5 h was determined at $p \leq 0.05$ (**) using a student's t-test. (Data represents mean ± SEM n=6, error bars are within plot symbols when not visible).

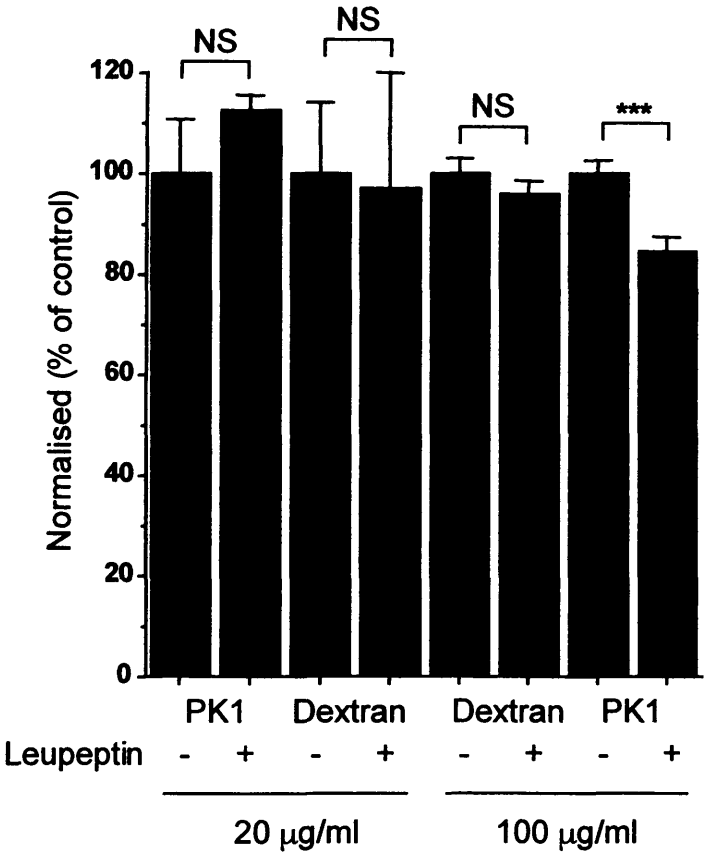

Figure 4.6 Effect of leupeptin on PK1 and FITC-dextran B16F10 cell-associated fluorescence. Cells were exposed to either PK1 or FITC dextran for 5 h in the presence or absence of leupeptin of either 20 μg/ml or 100 μg/ml. Statistical differences between sample and corresponding control (cell-associated fluorescence for corresponding polymer in absence of leupeptin) were determined at $p \leq 0.10$ or $p \leq 0.01$ (***) using a paired student's t-test. (Data represents mean ± SEM n=3).

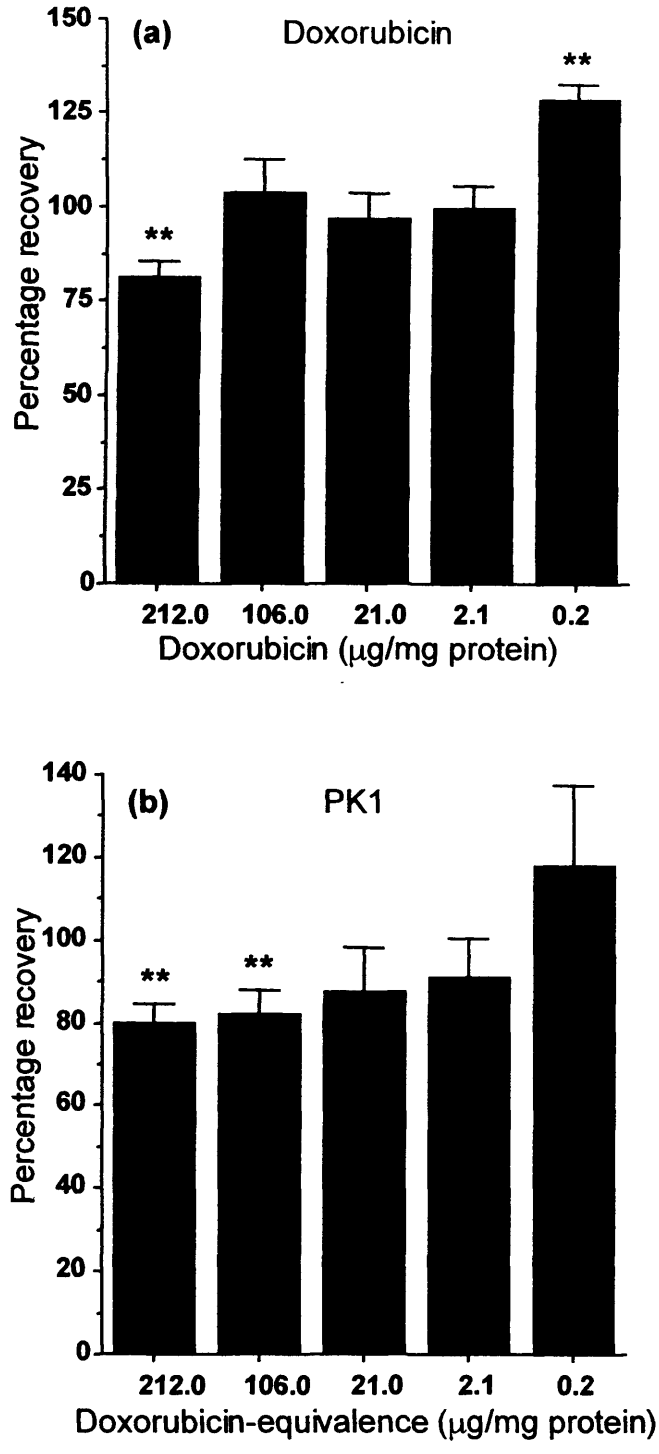

Figure 4.7 Extraction efficiency for doxorubicin and PK1 from spiked B16F10 cell homogenate. Drug was extracted form homogenate and assayed for doxorubicin-associated fluorescence. Results are expressed as percentage recovery. Statistical differences were determined at $p \leq 0.05$ (**). (Data represents mean ± SEM n=3).

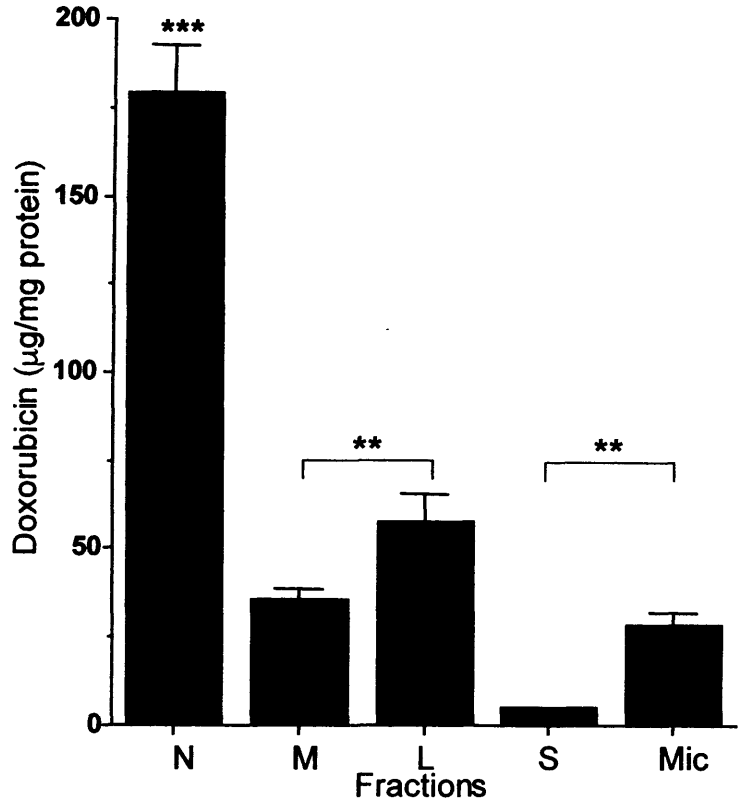

Figure 4.8 Distribution of doxorubicin in the subcellular fractions of B16F10 cells (5 h). Key: nuclear (N), mitochondrial (M), lysosomal (L), microsomal (Mic) and soluble (S) fractions. Statistical differences between fractions were determined at $p \leq 0.10$ (*), $p \leq 0.05$ (**) and $p \leq 0.01$ (***) using one-way ANOVA and Bonferroni post hoc test. (Data represents mean ± SEM n=3, error bars are within plot symbols when not visible).

distributed between the mitochondrial and microsomal fractions with lowest levels in the soluble fraction. The overall recoveries were between 75 % – 84 %. In contrast, PK1 showed a totally different distribution (figure 4.9). PK1-associated fluorescence was detected at both 15 min and 5 h in the mitochondrial, lysosomal and microsomal fractions. At 5 h drug levels in the mitochondrial and lysosomal fractions were significantly higher ($p \leq 0.01$) than at 15 min. Only at 5 h could drug levels be detected in the nuclear fraction, although levels were > 350 fold lower than for free doxorubicin. At no time could drug be detected in the soluble fraction. Serial dilution of fractions obtained after a 5 h incubation period with PK1 demonstrated a general decrease of fluorescence upon dilution. Drug naïve nuclear and mitochondrial fractions from cells not exposed to PK1 did show some signs of increased fluorescence upon dilution (figure 4.10).

4.3.4 Fate of PK1 and doxorubicin in B16F10 cells monitored by fluorescence microscopy

B16F10 cells incubated with PK1 for 15 min, 1 h or 5 h and fixed using paraformaldehyde showed extensive fluorescent labelling of the plasma membrane and a hazy cytosolic labelling (figure 4.11 – 4.12) (N.B. all fluorescent images are also presented in an electronic format to aid visualisation. The CD can be found at the back of the thesis in Appendix II). There was no evidence of nuclear or vesicular labelling at any time point. Absence of nuclear localisation was confirmed by confocal microscopy following DAPI staining of the nucleus of fixed cells (figure 4.11, panel b). Confocal microscopy images of live B16F10 cells exposed to PK1 were very different. In this case there was considerable reduction of both the extensive cytosolic haziness and also plasma membrane labelling. In live cells, distinct vesicular labelling was already evident at 15 min with often a perinuclear localisation (figure 4.11, panel c – d). After 1 h, the PK1 fluorescence appeared similar to that seen at 15 min. However, after 5 h vesicular labelling was more pronounced (figure 4.12, panel b – c). When examining both fixed and live cells, highly fluorescent blebs (~ 0.2 – 1.0 μm ∅) were evident, which were most abundant

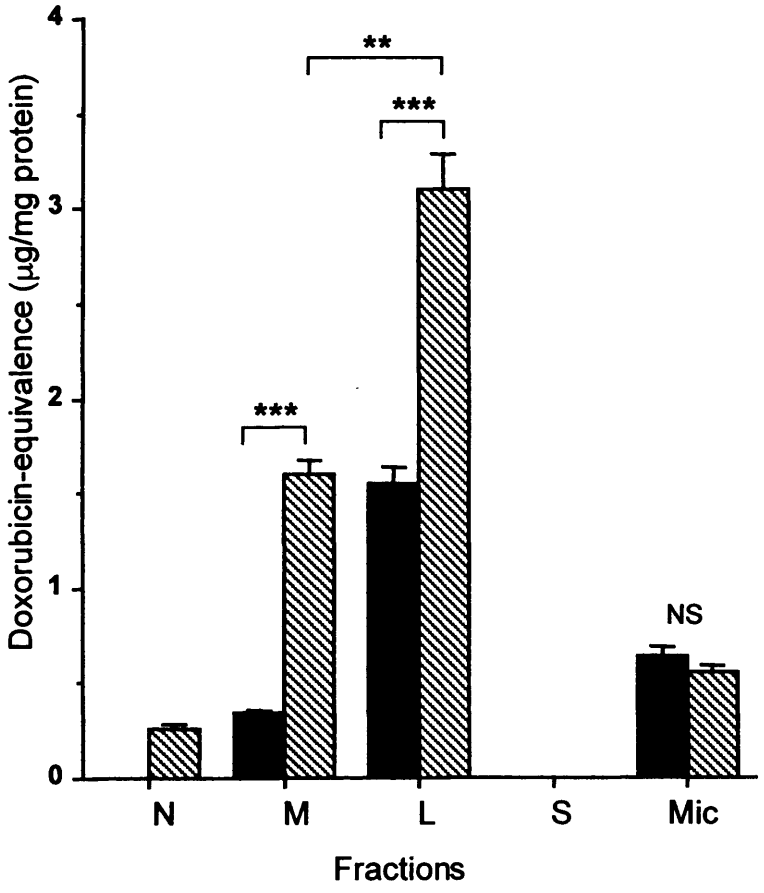

Figure 4.9 Distribution of PK1-associated fluorescence in the subcellular fractions of B16F10 cells. Key: nuclear (N), mitochondrial (M), lysosomal (L), microsomal (Mic) and soluble (S) fractions, 5 h (hatched bars) or 15 min (filled bars). Statistical differences between fractions were determined at $p \leq 0.1$ (*), $p \leq 0.05$ (**) and $p \leq 0.01$ (***) using one-way ANOVA and Bonferroni post hoc test. Undetectable drug levels in the nuclear fraction at 15 min, likewise at 15 min and 5 h in the soluble fraction. (Data represents mean ± SEM n=3, error bars are within plot symbols when not visible).

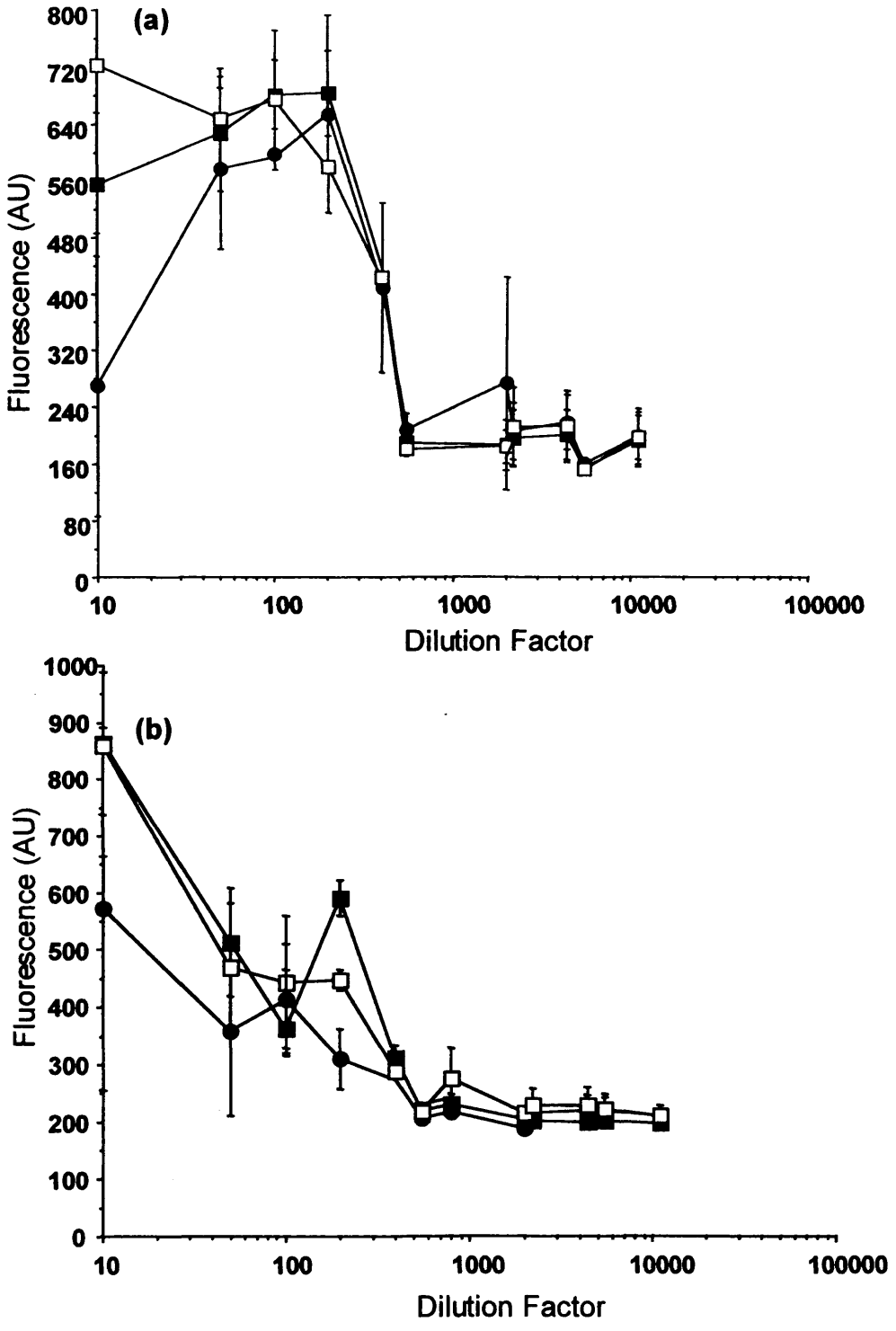

Figure 4.10 Effect of serial dilution in PBS (pH 7.4) on subcellular fraction fluorescence. Key: nuclear (●), mitochondrial (■) and lysosomal (□) fractions. Panel (a) fluorescence of diluted fractions obtained from B16F10 cells that have not been exposed to polymer, (b) fluorescence of fractions obtained from cells after a 5 h incubation period with PK1. (Data represents mean ± SEM n=3, error bars are within plot symbols when not visible).

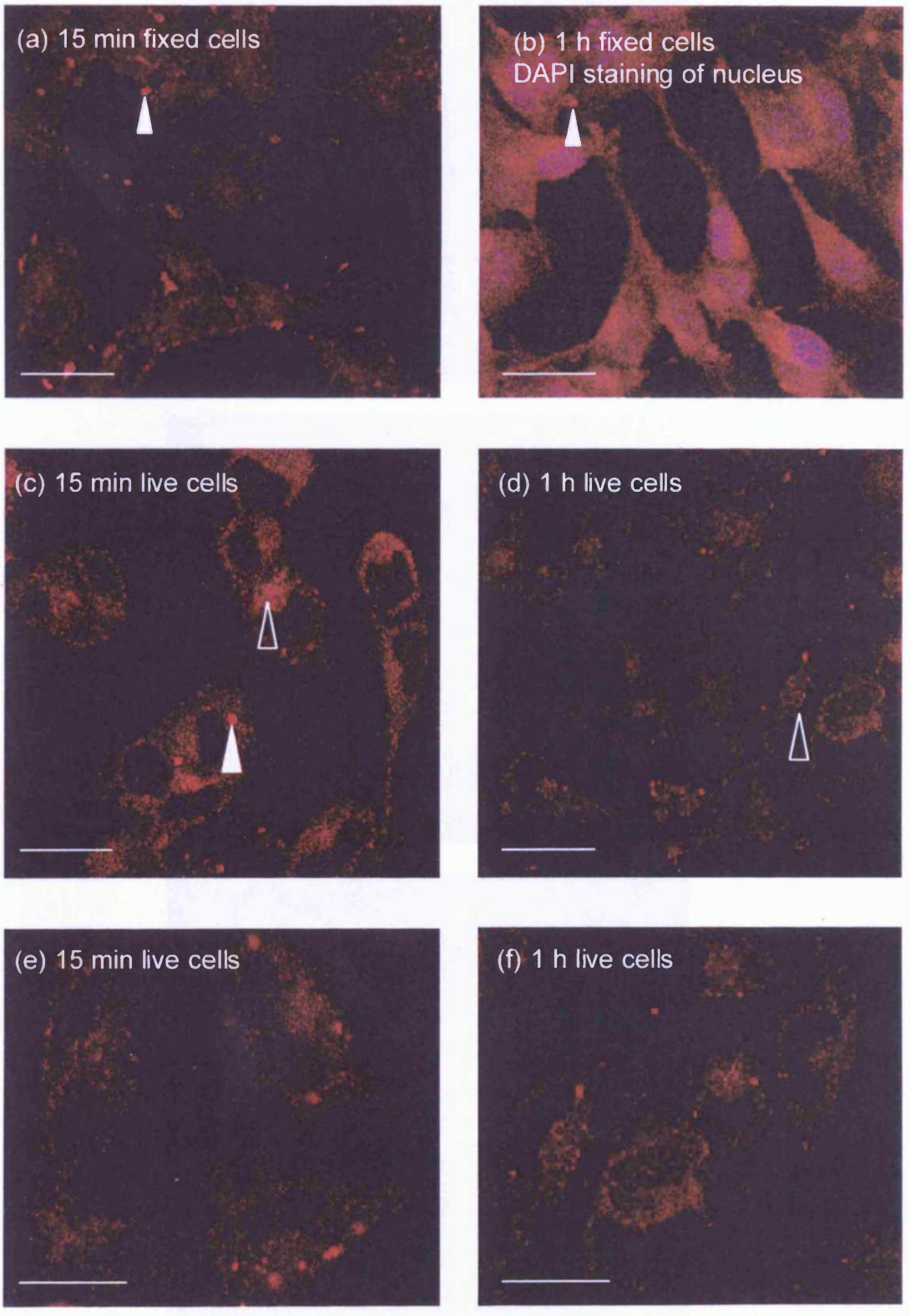

Figure 4.11 Representative confocal images of the subcellular distribution of PK1 in fixed and live B16F10 cells. Cell were incubated with drug for either 15 min or 1 h. Examples of blebs and intracellular vesicles are marked by filled and open arrows respectively. Images are maximum projections of confocal slices. Scale bar 10 μm.

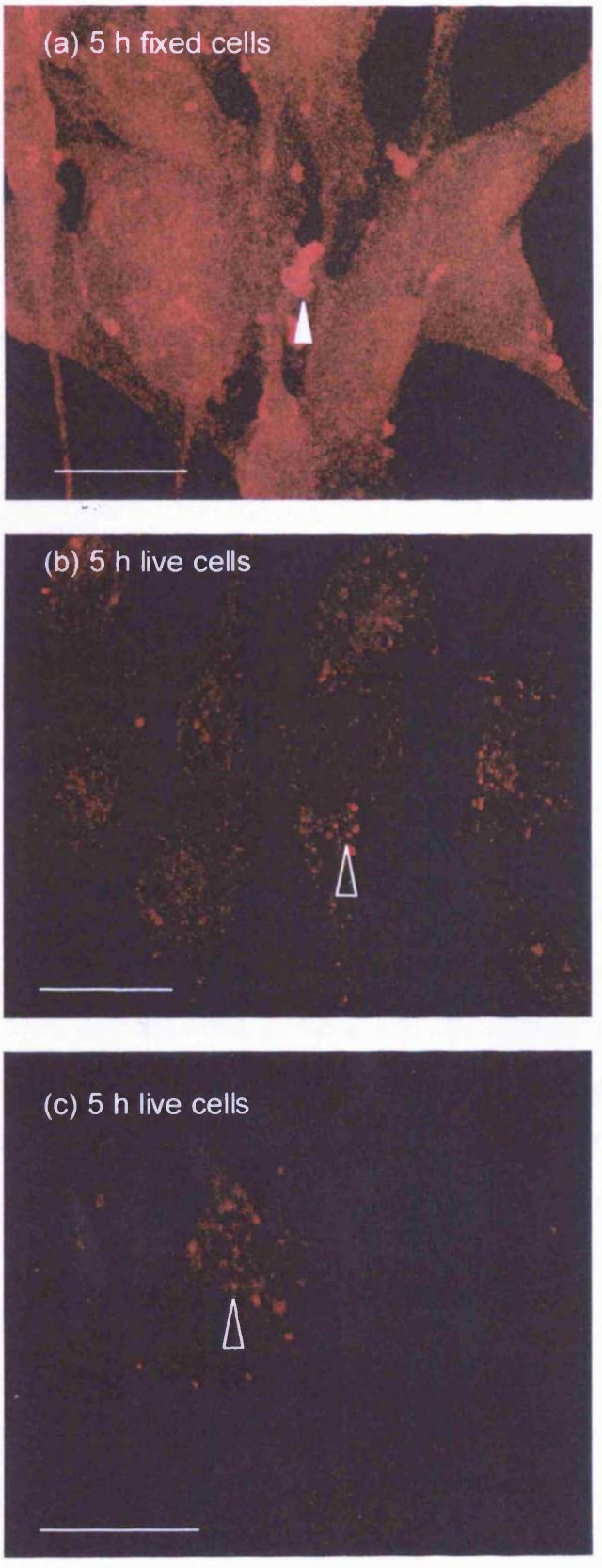

Figure 4.12 Representative confocal images of the subcellular distribution of PK1 in live and fixed B16F10 cells at 5 h. Examples of blebs and intracellular vesicles are marked by filled and open arrows respectively. Images are maximum projections of confocal slices. Scale bar 10 μm.

in fixed cells (figure 4.11, panel a – c). When B16F10 cells were co-incubated with FITC-dextran and PK1, there was clear co-localisation of both markers in vesicular structures (figure 4.13).

Subcellular distribution of free doxorubicin was only assessed at 5 h by epifluorescence microscopy of both fixed and live cells (figure 4.14). Following chemical fixation of cells, diffusive staining of the cell with distinctive nuclear localisation was observed, but little vesicular/punctate labelling (figure 4.14, panel a). In live cells, besides clear nuclear staining, vesicular labelling was evident (figure 4.14, panel b – d).

4.4 Discussion

Although fractionation studies are most commonly used to monitor the intracellular trafficking of macromolecules, this technique has also been used to monitor the intracellular distribution of low molecular weight drugs, for instance cytotoxic and antibacterial antibiotics (Ahmed, 1985; Masquelier et al., 1980; Trouet & Tulkens, 1981; Vasanthakumar & Ahmed, 1986). Most importantly, subcellular fractionation has been demonstrated to be a suitable method to quantify the intracellular distribution of doxorubicin (Zenebergh et al., 1984; Noel et al., 1978). However before the subcellular distribution of polymer-bound and free doxorubicin could be monitored, it was considered necessary to determine non-toxic concentrations for PK1 and doxorubicin.

4.4.1 Cytotoxicity of PK1 and doxorubicin

In preliminary cytotoxicity experiments PK1 was clearly less toxic than free doxorubicin displaying similar IC_{50} values reported previously for L1210, P388 and A2780 cells employing the same methodology (Duncan et al., 1991; Duncan et al., 1992; Minko et al., 1998). Differences in cytotoxicity between free and polymer-bound drug are not surprising due to the different cellular uptake mechanism, cellular pharmacokinetics and intracellular distribution, with free doxorubicin readily gaining

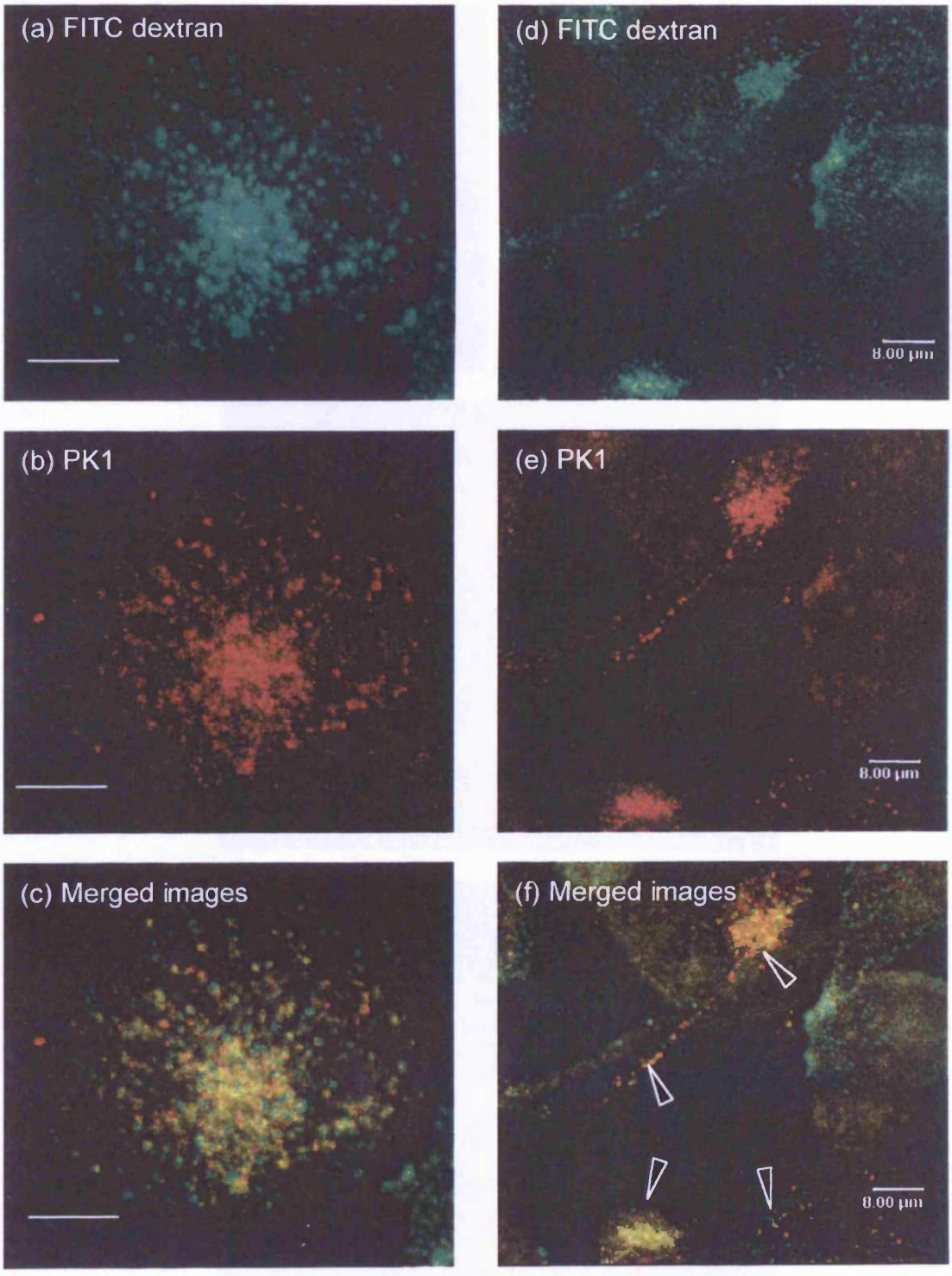

Figure 4.13 Subcellular distribution of PK1 and FITC-dextran in live B16F10 cells at 5 h. Examples for the co-localisation of PK1 and FITC-dextran in intracellular vesicles are marked by open arrows. Images are maximum projections of confocal slices. Scale bar 8 µm.

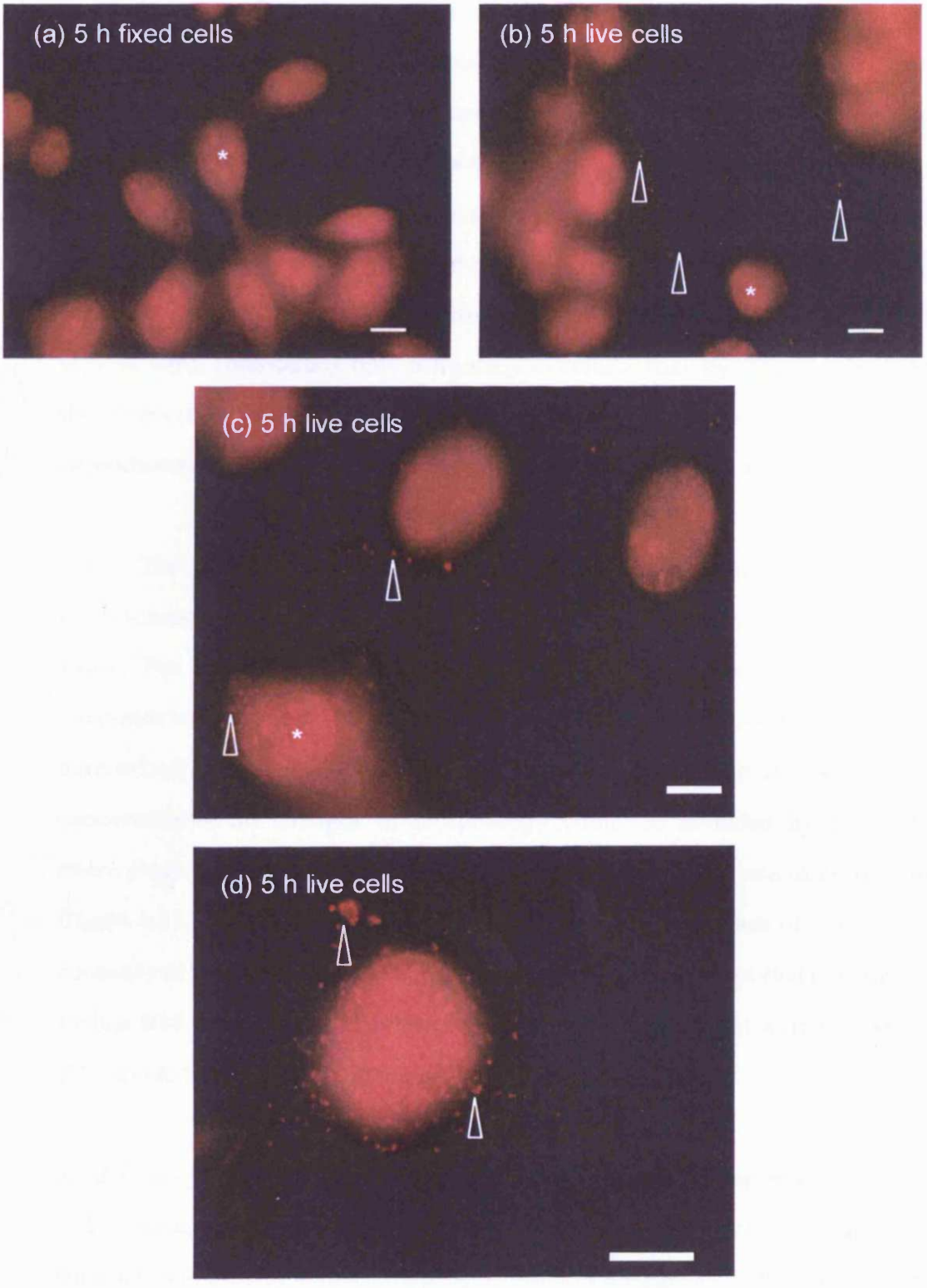

Figure 4.14 Representative epifluorescent images of the subcellular distribution of doxorubicin in fixed and live B16F10 cells (5 h). Examples of vesicular sequestration and nuclear accumulation shown by arrows and asterisks respectively. Scale bare 10 μm.

access into the cell. Although only 0.39 % of the total doxorubicin content of PK1 was in the free form, this small amount of active drug could be accountable for the cellular toxicity (figure 4.2). Since uptake of PK1 into B16F10 cells is restricted to fluid-phase pinocytosis and requires the presence of active lysosomal enzymes to liberate doxorubicin, cellular accumulation and drug activation would be expected to be slow. Thus it might be deduced that release of doxorubicin during the 72 h incubation period from the polymer backbone and subsequently from lysosomes was slow *in vitro*, contributing only marginally to cellular toxicity. This is supported by the observation that in B16F10 cells the cytotoxic effect of doxorubicin is directly proportional to intracellular drug concentration (Bhuyan et al., 1981).

The selected PK1 concentration per cell for fractionation, flow cytometry and fluorescence microscopy experiments was > 100 fold less than the determined IC_{50} value. For experiments employing free drug only, a doxorubicin-equivalent concentration was used where drug exposure per cell was also > 8 fold less than the determined IC_{50} value. Following the exposure of cells to the selected PK1 concentration, no changes in morphology could be revealed by bright field microscopy (figure 4.3) and blebs reported in fluorescence microscopy studies (figure 4.11, panel a – c) could not be visualised. Possibly the lack of resolution and contrast could account for this. Gross morphological changes reported previously for variant B16 melanoma cells following exposure to doxorubicin were not observed (Mariani & Supino, 1990; Supino et al., 1992).

4.4.2 Flow cytometry of PK1 in the presence and absence of leupeptin

To aid the selection of appropriate time points for subcellular fractionation studies and to provide a more complete picture of PK1 kinetics in B16F10 cells, flow cytometry was used to monitor both total uptake (37 °C) and extracellular binding (4 °C) (figure 4.5). The biphasic accumulation reported here at 37 °C has also been reported in mouse 38C13 B-cell lymphoma cells (Kovar et al., 2004) and could be related to the physico chemical properties of PK1. Namely, the unimolecular micellar

conformation of PK1 in solution driven by the hydrophilicity and hydrophobicity of polymer and drug respectively (Uchegbu et al., 1996). The rapid increase in cell-associated fluorescence during the first 15 min would be expected to arise from a PK1-plasma membrane interaction mediated by conjugated doxorubicin, besides the cellular accumulation of free drug present in the preparation. However, the exact nature of the drug-membrane interaction would be dependent on the nature of lipids present in B16F10 cells and the steric hindrance of the polymer backbone (Tritton, 1991). The kinetics during the rest of the study could be explained by equilibrated surface binding, and pinocytic capture of PK1 with lysosomal trafficking. Since free doxorubicin is ~ 3.5 fold more fluorescent than polymer-bound drug, increasing cell-associated fluorescence (> 2 h) could suggest drug release from the polymer. However, it is important to realise that the design of these experiments did not provide a comprehensive picture of all pinocytic processes and only showed, that increased cell-association occurred over the time course of the experiment.

The proposed sequence of events suggested lysosomotropic delivery of PK1. It was considered possible to investigate this indirectly due to the higher fluorescence yield of free doxorubicin to polymer-bound drug. Therefore cells were exposed to PK1 in the presence and absence of the competitive protease inhibitor leupeptin to specifically inhibit cathepsin B activity responsible for the release of doxorubicin from the tetrapeptide linker (Duncan et al., 1982; Subr et al., 1992). With sufficient inhibition of cathepsin B activity, a small but significant difference in cell-associated fluorescence between inhibitor treated and untreated cells was evident (figure 4.6). Increased cell-associated fluorescence in the absence of the inhibitor was consistent with the cleavage of the drug from the polymeric carrier, suggesting lysosomotropic delivery of PK1 since changes in basal pinocytic rates could be excluded with the use of the FITC-dextran control. It is worth noting that studies investigating the *in vitro* stability of PK1 did not demonstrate release of doxorubicin from the polymer (figure 4.4). The study was however potentially flawed due to the high binding affinity of

any free doxorubicin for DNA and sequestration in acidic organelles (Gewirtz, 1999), precluding its detection in the tissue culture medium.

4.4.3 Subcellular fractionation studies in B16F10 cells with PK1 and doxorubicin

Subcellular fractionation studies for PK1 were performed at 15 min and 5 h since flow cytometry experiments provided evidence for equilibrated cell-surface binding and lysosomotropic delivery. It was considered important to assess possible quenching and dilution profiles for fractions obtained after a 5 h incubation period with PK1 demonstrated a general decrease of fluorescence up on dilution. This would suggest that doxorubicin-associated fluorescence was not quenched (figure 4.10). Thus performed measurements were a good indicator for the subcellular distribution of PK1, though the absolute values should be treated with caution.

At 5 h, drug levels in the mitochondrial and lysosomal fractions were significantly higher than those seen after 15 min, which was consistent with the lysosomotropic delivery of PK1 (figure 4.9). At first sight even higher levels might have been expected. However, intracellular retention with subsequent lysosomal trafficking is essential to maximise lysosomotropic delivery, and it is not known what fraction of internalised PK1 is trafficked to lysosomes and to which extent PK1 participates in exocytosis/recycling. It is essential to realise that exocytosis impedes intracellular drug accumulation. For fluid-phase markers, such as dextran or lucifer yellow, only ~ 20 % of internalised marker is retained by cells due to extensive exocytosis (Swanson et al., 1985; Van Deurs et al., 1984). Therefore it is not surprising that the inefficient process of fluid-phase pinocytosis did not yield higher intracellular PK1 concentrations at 5 h. Progressive accumulation of PK1 in lysosomes would be expected to increase lysosomal density as reported for dextran (Lopez-Saura et al., 1972). Therefore lysosomes could possibly be pelleted more readily thus explaining the high drug levels seen in the mitochondrial fraction at 5 h. In an attempt to estimate lysosomal drug concentration the methodology reported previously was used (Noel et al., 1978). (The basis of this calculation is briefly

detailed in scheme 4.1). Lysosomal drug concentrations were estimated to be 3 fold greater than the concentration present in the incubation medium (table 4.2) or as high as 5 fold, taking into account the possible "lysosomal" contribution of the mitochondrial fraction. These rather crude calculations reinforce that drug was concentrated in lysosomes, but also emphasises that fluid-phase pinocytosis limits drug accumulation.

Doxorubicin-associated fluorescence in the nuclear fraction at 5 h was also consistent with lysosomotropic delivery of PK1 due to the release of the drug from the polymer and subsequent nuclear accumulation (figure 4.9). Since only free and uncharged doxorubicin would be able to escape from lysosomes (Lloyd, 2000), both release kinetics of the drug from the polymer and lysosomal trapping of predominately protonated doxorubicin (pKa = 8.22) (Vigevani & Williamson, 1980) would be expected to impede nuclear accumulation leading to relatively low drug levels. However, the nuclear fraction also contained contaminating lysosomes. This cross contamination could have greater significance at 5 h than at 15 min, due to time-dependent lysosomal accumulation of PK1. Although only free drug is able to reach the nucleus, differentiating between free doxorubicin-associated fluorescence in the nuclear fraction and fluorescence derived from polymer-bound drug from contaminating lysosomes was impossible. It might be concluded that doxorubicin-associated fluorescence detected in the nuclear fraction was due to contaminating lysosomes, since fluorescence microscopy experiments showed no signs of nuclear accumulation. However, results from flow cytometry studies (discussed above) might indicate, that nuclear fluorescence was indeed due to free doxorubicin. Further studies are required to address the contribution of contaminating lysosomes on nuclear drug levels. In particular experiments examining the distribution of lysosomes in subcellular fractions following a 5 h incubation period with PK1 could prove conclusive.

Methodology to calculate drug levels in lysosomes and nucleus

By assuming that 1 μg of protein corresponds to 5 μl of cell volume (Tulkens & Trouet, 1978), the theoretical cellular volume for the corresponding fraction can be calculated based on the protein concentration determined. Since the volume of lysosomes and the nucleus were estimated to occupy 3 % (Tulkens & Trouet, 1978) and 20 % of the total cellular volume respectively, the theoretical concentrations determined in the nucleus and lysosomes can be deduced and compared to the extracellular concentration to estimate the extent of sequestration. A sample calculation for doxorubicin is shown below:

Protein concentration of lysosomal fraction:	2.0 mg/ml
Amount of doxorubicin in lysosomal fraction:	0.14 mg/ml
Concentration of doxorubicin in incubation medium:	6.6×10^{-3} mg/ml

Based on the protein content of the lysosomal fraction, the theoretical cellular volume would thus be 10 ml (2 x 5). Since 0.14 mg of doxorubicin was **not** present in the cellular homogenate but in the **lysosomal** fraction, the estimated lysosomal volume would be 0.3 ml ([10 ml x 3]/100), and thus the lysosomal concentration would equate to 0.47 mg/ml (0.14 mg/0.3 ml). Therefore when the lysosomal concentration of doxorubicin would be compared with the extracellular concentration a ~ 71 fold (0.47 mg ml^{-1}/6.6×10^{-3} mg ml^{-1}) higher concentration would prevail reflecting lysosomal drug sequestration.

Scheme 4.1 Methodology and worked example to calculate drug levels in lysosomes and nucleus.

Table 4.2 Summary of calculated intracellular concentrations of PK1 and doxorubicin at 15 min and 5 h. Where applicable extent of drug sequestration is shown in brackets.

Site	Doxorubicin (μg/ml)	PK1 (doxorubicin-equivalence μg/ml)	
	5 h	5 h	15 min
Nucleus	178.8 (27)	0.3	Not detected
Lysosomes	385.1 (58)	20.7 (3.1)	10.3 (1.6)
Total cell	19.1 (3)	0.2	0.1

At 5 h, the subcellular distribution of doxorubicin was markedly different when compared to PK1 (figure 4.8). A typical nuclear drug distribution was seen accounting for ~ 85 % of total intracellular doxorubicin. Similar values have been reported in L1210 cells and cultured rat embryo fibroblasts (Noel et al., 1978; Zenebergh et al., 1984). Nuclear accumulation of doxorubicin would be expected, due to the high binding affinity of doxorubicin for DNA (Gewirtz, 1999). Levels determined here were significantly higher than reported in a number of cell lines. Possibly the polyploidic nature of B16F10 cells could provide more doxorubicin binding sites (Baroja et al., 1998) since the amount of DNA present in B16F10 cells was found to be > 2 – 10 fold greater than for instance for hepatocytes (Chapter 3 table 3.5). High levels of doxorubicin in the lysosomal fraction, accompanied by drug sequestration, correlates well with the literature (Blanchard et al., 1981; Noel et al., 1978; Peterson & Trouet, 1978; Skovsgaard, 1977; Zenebergh et al., 1984). The observation that doxorubicin is sequestered in lysosomes (table 4.2) might be related to its weakly basic nature (Schindler et al., 1996; Simon et al., 1994), since the acidic environment facilitates its protonation producing charged doxorubicin to which the lysosomal membrane is less permeable (De Duve et al., 1974; Duvvuri et al., 2004). Doxorubicin sequestration in melanosomes would also be expected as they share many features associated with lysosomes including an acidic pH (pHs of 3.0 – 4.6) (Bhatnagar et al., 1993). Overall intracellular accumulation of doxorubicin in B16F10 cells could be expected to follow similar kinetics as in rat embryo fibroblasts, where rapid and saturable drug levels in the nucleus were observed and continuous accumulation of drug in lysosomes (Gieseler et al., 1994; Peterson & Trouet, 1978). The presence of doxorubicin in the mitochondrial and microsomal fraction could in part be due to contaminating DNA (results shown in table 3.4 Chapter 3).

4.4.4 Fluorescence microscopy studies to visualise subcellular distribution of PK1 and doxorubicin

Fluorescence microscopy was used to assess qualitatively the subcellular distribution of PK1 and doxorubicin in B16F10 cells. Fluorescent blebs were observed following PK1 exposure, in particular in fixed cells and to a lesser extent in live cells (figure 4.11, panel a – c). Blebbing has previously been reported in hepatocytes and L1210 cells when incubated with microspheres containing covalently attached doxorubicin (Rogers et al., 1983; Tokes et al., 1982). Possibly changed cellular pharmacokinetics at the plasma membrane and the multivalent nature of polymer-bound doxorubicin, could facilitate blebbing in B16F10 cells. In the present study it could be clearly demonstrated that cell fixation dramatically changed the subcellular distribution of both free doxorubicin and polymer-bound drug (figures 4.12 and 4.14). It is believed that differences between fixed and live cell images were related to the physico chemical properties of doxorubicin and would thus be applicable to other cell lines. The majority of studies comparing the subcellular distribution of free doxorubicin to PK1 have been conduced with fixed cells and should therefore be treated cautiously (Nori et al., 2003a; Nori et al., 2003b; Tijerina et al., 2003). However, to make valid conclusions about the subcellular distribution, only data obtained from live cells will be discussed here (figure 4.11 – 4.13). For PK1 vesicular labelling was already evident at 15 min, suggesting localisation of PK1 in early endocytic compartments such as endosomes (i.e. in particular the perinuclear localisation points to the involvement of the endocytic recycling/sorting compartments; see table 1.2). At 5 h, labelling appeared to be more punctate and the nature of vesicles was evaluated by co-incubating cells with FITC-dextran (figure 4.13). Co-localisation of PK1 and dextran labelled vesicles was evident, indicating that at least some PK1 reached its intended intracellular destiny. However, no nuclear accumulation was evident and the subcellular distribution was very different from free doxorubicin. Here, clear nuclear accumulation was evident besides sequestration of the drug in acidic vesicles.

4.4.5 Fluorescence microscopy versus subcellular fractionation

The prospects of fractionation studies to overcome limitations associated with fluorescence microscopy have been a major driving force for establishing a fractionation method and quantifying the subcellular distribution of polymer-bound and free doxorubicin. It is therefore interesting to directly compare the results obtained with both techniques. From fractionation studies the lysosomal PK1 concentration was calculated as 0.02 mg/ml (doxorubicin-equivalence) suggesting the absence of significant quenching (table 4.2), since quenching was only evident at > 0.04 mg/ml (figure 4.1). It might therefore be deduced that live cell images provided a representative picture for the intracellular distribution of PK1. For free doxorubicin extensive sequestration of drug in both acidic organelles (0.39 mg/ml) and the nucleus (0.18 mg/ml) suggested that fluorescent pictures only provided a "glimpse" of the intracellular drug distribution due to quenching.

4.5 Conclusions

Quantitative data have been presented on the intracellular trafficking of PK1, which support lysosomal delivery of the drug, though further studies are needed to unequivocally demonstrate lysosomotropic delivery. Results reported in this Chapter could suggest that *in vivo* activity of PK1 might be influenced by factors other than intracellular trafficking. For example, the activation of PK1 in the tumour tissue (i.e. extracellular) due to secreted cathepsin B. However, it has long been recognised that predicting *in vivo* performance from *in vitro* data is particularly difficult for polymer-drug conjugates (Duncan, 2003b). Therefore additional fractionation studies are needed using excised tumours to provide a direct comparison to *in vitro* studies to establish the importance of intracellular trafficking on therapeutic outcome.

The subcellular distribution of doxorubicin followed the expected nuclear-lysosomal distribution, and demonstrated the suitability of the established fractionation method to follow the intracellular distribution of (macromolecular)drugs. Direct comparison of PK1 with free doxorubicin highlighted

the fundamental differences in subcellular fate of free and polymer-bound drug. Quantitative data from fractionations studies also demonstrated that even the qualitative nature of fluorescence microscopy could be limited by fluorescence quenching.

As already stressed in this Chapter, cellular retention of polymers is of particular importance to maximise lysosomotropic or endosomotropic delivery. Therefore in the next Chapter pinocytosis of selected polycations has been studied.

Chapter 5

Pinocytosis of linear, branched and dendritic polycations

5.1 Introduction

The previous Chapter used the subcellular fractionation technique established in Chapter 3 to give a quantitative snap shot of intracellular trafficking of free and polymer-bound doxorubicin (PK1). Whereas doxorubicin has been used clinically for many years as an antitumour agent and PK1 entered clinical development, it is clear that more studies are needed to define the endocytic and intracellular trafficking properties of polymers undergoing design as second-generation polymer therapeutics (Duncan, 2003a).

Need to study pinocytosis and trafficking of polymers

There have been relatively few studies that have set out to design polymer therapeutics based on a biological rationale, which include systematic studies designed to quantify pinocytosis and intracellular trafficking. Historically, linear polymers of neutral and charged nature have been used in an attempt to improve drug delivery and therefore studies quantifying pinocytosis and trafficking have most often been conducted with these polymers (section 1.5.1 – 1.5.2, table 1.4). Polymers studied include, PVP (Duncan et al., 1981b), HPMA copolymers (Duncan, 2005), dextran (Berthiaume et al., 1995, Ohkuma & Poole, 1978) and PLL (Ryser, 1967; Ryser & Hancock, 1965; Ryser & Shen, 1978; Shen & Ryser, 1979). Until now linear polymers have formed the basis for all clinically investigated polymer therapeutics (table 1.1). However, modified poly(L-lysine) dendrimers as anti-infective gels for topical application (McCarthy et al., 2004) and dendrimers used as magnetic resonance imaging agents (Gadomer 17) (Herborn et al., 2003) are recent examples of dendrimer-based polymer therapeutics in clinical development. So far very few studies have quantified pinocytosis of dendrimers and further investigations are needed to provide a sound biological rationale for their use (summarised in section 1.5.4, table 1.5) (Wiwattanapatapee et al., 2000; Xyloyiannis, 2004; Xyloyiannis et al., 2003).

However, pinocytosis is only a descriptor for a range of uptake routes into cells, and it is clear from pathogens that route of internalisation dictates intracellular trafficking and clinical outcome (section 1.3). Polycations of linear, branched and dendritic topology are commonly used in the development of new polymer therapeutics, but little is known about their (pinocytosis or) uptake routes. Polycations could act as biomimetics by binding to a cell surface "receptor(s)", which dictates their route of internalisation (detailed in section 1.2.1). Only a handful of studies have investigated "adsorptive pinocytosis" of polymers to identify uptake routes. Recent examples include the uptake of lysine-based polyplexes into Hep G2 cells, which was attributed to a number of processes, including macropinocytosis and clathrin-mediated pinocytosis (Goncalves et al., 2004). In contrast, a cholesterol-dependent uptake mechanism has been proposed for polyplexes employing branched PEI (Mw = 25,000 g/mol) or "fractured" PAMAM dendrimers (Kopatz et al., 2004; Manunta et al., 2004). Therefore the overall aim of this Chapter was to quantify and compare pinocytosis and trafficking of linear, branched and dendritic polycations.

Selection of polymer probes

Cationic polymers commonly used as non-viral vectors were selected (Garnett, 1999). Linear and branched PEI (Mw = 25,000 g/mol) were chosen due to their common use as vectors and their excellent transfection capabilities both *in vitro* and *in vivo* (section 1.5), besides their progress towards clinical evaluation (Behr, 2004). PAMAM dendrimers have also been used in transfection studies (Kukowska-Latallo et al., 1996) and their physico chemical properties have been well documented (Tomalia & Durst, 1993; Tomalia et al., 1990) making them ideal probes for the purpose of this study. PAMAM G4 was the largest dendrimer investigated, since polymer-associated toxicity for PAMAM dendrimers is positively correlated with generation (Brazeau et al., 1998; Malik et al., 2000). Due to similar monomer units of PAMAMs and PEIs, extrapolating results from one polymeric class to the other could be attempted. The fluid-phase marker FITC-Dextran was

included as a control (Pratten et al., 1980), but could also serve as a model compound for polymer-drug conjugates.

Labelling of polymers to allow detection in biological systems

To follow the cellular and intracellular fate of polymers, it was necessary to label them with a suitable probe. A number of probes have been used historically to label polymers most notably [^{125}I]iodide (Duncan, 1987; Malik et al., 2000; Richardson et al., 1999b), ^{3}H (Ryser & Shen, 1978; Wedge et al., 1991), biotin and organic fluorophores such as FITC or more recently OG (Helin et al., 1999a; Helin et al., 1999b; Poxon et al., 1996; Yoo & Juliano, 2000). An alternative to organic fluorophores are quantum dots (inorganic semiconductors of 5 – 650 nm ∅), which most recently have been used for *in vivo* (Larson et al., 2003; Voura et al., 2004) and live cell imaging (Jaiswal et al., 2004) due to unprecedented photo-stability and unique spectral properties (Jaiswal & Simon, 2004). However, their large size and limited conjugation chemistry eliminated them as potential tags. Instead labelling with an organic fluorophore was chosen, to allow the detection of the polymer in live cells by laser scanning microscopy and flow cytometry. OG was selected due to excellent photostability and pH independence at pH 5.0 – 7.4. Hydrophobicity and a Mw close to 500 g/mol makes OG an excellent model compound to mimic commonly used drug molecules. Standard conjugation chemistry (the activated ester of OG to a primary amine of the selected polymer) was used to prepare conjugates (Hermanson, 1996). Such amine reactive probes are commonly used for fluorescent labelling (Banks & Paquette, 1995), and the amide bond formed between the fluorophore and the polymer is extremely stable in a wide range of buffer systems for > 10 days at 37 °C (Banks & Paquette, 1995). This is of particular importance since trafficking of polymers was assessed indirectly with the detection of fluorescence.

The aims of the studies described in this Chapter were (a) to fluorescently label and characterise linear and branched PEI, PAMAMs G2 – 4, (b) to quantify

their pinocytosis in B16F10 cells, (c) to provide preliminary data in B16F10 cells on their route of internalisation.

5.2 Methods

To assess purity and molecular weight distribution all parent polymers were subjected to GPC analysis as described in section 2.3.15. In addition both the ninhydrin and TNBS assays were used to determine the content of 1° amine groups. Inverse-gated ^{13}C NMR was also used to provide quantitative information for branched PEI (1°, 2° and 3° amines) and PAMAM dendrimers (1°, 3° amines). The experimental conditions are detailed in section 2.3.15. Theoretical amine content was subsequently used to calculate the degree of branching (DB) of the polymers according to Frey (formula 1), where D, and Li are the fractions of dendritic and linear incorporated monomers respectively (Hölter et al., 1997). The DB was determined according to Frey, due to the ability to differentiate between truly linear polymers and polymers with a low degree of branching or Mw (Schmaljohann et al., 1999).

$$DB = 2\,D/(2D + Li) \qquad \text{Equation (1)}$$

5.2.1 Synthesis and purification of fluorescently labelled polymers

Reaction conditions were optimised using PAMAM G4 as a model compound using first an aqueous solvent and then MeOH. The optimised conditions were subsequently used for all other OG-conjugations without further modification. The conjugate was protected from light whenever possible during sample preparation and storage. First reaction conditions were explored based on previously reported methods for polyester dendrons (Xyloyiannis, 2004) and PEI (Godbey et al., 1999b). These conjugation reactions were carried out in a 0.1 M sodium bicarbonate buffer. Briefly, PAMAM G4 (20 mg) was dried under vacuum and re-dissolved in sodium bicarbonate buffer (0.1 M; pH 8.4). One molar equivalence of OG-SE was dissolved in DMSO and added to the polymer solution and stirred in the dark at room temperature under N_2 for 1 h. The reaction was monitored by TLC using MeOH as a

mobile phase (Rf for free OG ~ 0.7, polymer remains at base line). The solvent was evaporated and the crude product dissolved in 2 ml of purifying PBS (0.1 M; pH 7.4) and fractionated with a 25 cm Sephadex G25 column using PBS pH 7.4 as the mobile phase (fraction volume 1 ml). A second GPC profile was obtained using 25 μl of crude reaction mixture and PD10 desalting column (Sephadex G25) with PBS pH 7.4 as the mobile phase (fraction volume 0.5 ml). Fractions were analysed for OG-associated fluorescence in a black 96 well microtitre plate with a fluorescence plate reader. Chromatograms were subsequently constructed by plotting fluorescence against fraction volume and used to estimate labelling efficiency (detailed below). To improve labelling efficiency and to minimise non-specific hydrolysis of OG-SE in the aqueous buffer system, the reaction was repeated in MeOH. A 1 molar equivalence of OG-SE : PAMAM G4 (20 mg) was dissolved in MeOH and reacted for 2 h under N_2 at room temperature in the dark. Sample purification was carried out as before using a 25 cm G25 column. Fractions were routinely analysed by TLC for the absence of free OG. Pooled fractions were subjected to a final analysis by GPC to confirm the purity of the sample. To estimate fluorophore loading, a small sample (25 μl) of the crude reaction mixture was retained and analysed by GPC using a PD10 column. As before, peak area ratios were used to estimate loading (see below). To recover the conjugate from solution and to remove PBS salts, the conjugate was extensively dialysed (Mw cut-off 2000) against distilled H_20 and subsequently freeze-dried and stored at – 20 °C until use. All subsequent reactions to label polymers with OG were carried out in MeOH and analysed as detailed above. Though when necessary, the pH of the reaction mixture was adjusted with triethylamine to pH ~ 8.5. For conjugate purification (bulk) and profiling (to estimate loading), 25 cm and 6 cm GPC columns were used respectively, with experimental conditions detailed in table 5.1.

Table 5.1 Purification methods employed for fluorescently labelled polymers

Polymer	Fluorophore	Stationary phase for GPC	GPC mobile phase
PAMAM G4	OG	G25	PBS pH 7.4 (0.1M)
PAMAM G3	OG	G25	PBS pH 7.4 (0.1 M)
PAMAM G2	OG	G25	PBS pH 7.4 (0.1M)
PEI branched	OG	LH20	MeOH/$H_2$0 60 : 40 (0.36 M NaCl in aq. phase)
PEI linear	OG	G25	Citrate buffer pH 5.0 (0.1 M)
Dextran	FITC	G25	PBS pH 7.4 (0.1M)

The amount of covalently linked OG was estimated by integrating peak areas of polymer-bound and free fluorophore using GPC chromatograms. Total peak areas of bound and free OG served as 100 % labelling efficiency. Labelling efficiency was then converted into the amount of OG bound (μg) per mg of polymer by using formula (2). To estimate the maximum amount of free OG present in the conjugate the detection limit of the employed TLC system was established by using known concentrations of OG. By spotting identical volumes of sample/standard the amount of free OG could be estimated and was expressed as a percentage of total OG.

$$\text{Labelling efficiency} = \frac{\text{OG (μg) added to reaction mixture x fraction of bound OG}}{\text{Amount of polymer added to reaction mixture (mg)}} \quad \text{Equation (2)}$$

(μg of OG/mg of polymer)

5.2.2 Characterisation of polymer-fluorophore conjugates

All polymer conjugates were characterised to ensure that spectral properties of OG were unchanged following polymer conjugation and to evaluate fluorescence quantum yields. The fluorescence spectrum for each polymeric probe was determined by exciting the fluorophore at 485 nm using a 4 nm band pass filter and recording an emission spectrum (420 nm – 650 nm). Effect of polymer concentration, buffer composition and pH on fluorescence yield at equivalent molar concentrations of conjugate was determined (8.75 – 350 nM). Two buffer systems were used namely, PBS (0.1 M) at pH 7.4 and 6.4 and citrate phosphate buffer (0.1 M) at pH 5.4 and 4.0. Identical sample preparation, sensitivity, excitation and emission wavelengths allowed direct comparison between polymer conjugates.

5.2.3 Biological evaluation of polymer conjugates

Cytotoxicity of all cationic polymers (only unlabelled parent compounds were used due to the need of comparatively large amounts) was evaluated using a 72 h incubation time and a MTT assay as outlined in section 2.3.3. A B16F10 cell seeding density of 1 x 10^5 cells/ml was used. To exclude possible fluorophore-associated cytotoxicity, toxicity of OG alone was assessed at levels well above maximum molar concentrations used in the form of polymer-OG conjugates.

Qualitative assessment of polymer cytotoxicity was made by bright-field microscopy as detailed in section 2.3.4. Only PAMAM G4 and linear PEI were tested at a 1.4 $x10^{-7}$ M concentration and a 3 h incubation period. All subsequent studies were performed with cationic polymers at this molar equivalent concentration (1.4 x 10^{-7} M) to allow direct comparison between probes (summarised in table 5.2).

Before examining the cellular uptake of OG-labelled polymers, it was considered important to determine their stability in the presence of tissue culture medium and cells. OG-PAMAM G4 and linear OG-PEI were chosen as models to establish the stability of polymer conjugates. B16F10 cells were exposed to linear OG-PEI and OG-PAMAM G4 (1.4 x 10^{-7} M) in complete culture medium for 3 h. Cell culture medium was then aspirated and 3 ml dried under vacuum. Linear OG-PEI residue was re-dissolved in 0.5 ml of citrate phosphate buffer (0.1 M; pH 5.0) and OG-PAMAM G4 was re-dissolved in PBS (0.1 M; pH 7.4). Samples were fractionated (0.5 ml) with a PD10 column and analysed for OG-associated fluorescence with an excitation wavelength set at 485 nm and emission wavelengths at 520 nm respectively. GPC profiles were constructed by plotting fluorescence versus fraction volume.

Live cell confocal laser scanning microscopy was used to visualise cell binding and uptake of fluorescently labelled polymers at 1 h (see section 2.3.9). A summary of the polymer concentrations used is shown in table 5.2. Flow cytometry was used to measure extracellular binding (4 °C), pinocytosis (37 °C) and exocytosis of polymer probes. Experiments were conducted as described in section 2.3.11 and 2.3.13 and data were analysed as described in section 2.3.12. A 5 – 120 min incubation period was used for binding and pinocytosis studies, and polymer concentrations are listed in table 5.2. The potential route of internalisation of PEIs and PAMAM G4 was also examined by flow cytometry as described in section 2.3.14 using a 1 h incubation period with polymers. FITC-dextran was used as a reference marker for these studies to assess whether inhibitor treatments induced

Table 5.2 Summary table of polymer concentrations used for flow cytometry and microscopy experiments

Polymer	Nominal Mw (g/mol)	Fluorophore	Flow cytometry (M)	Fluorescence microscopy (M)	Bright-field microscopy (M)
Dextran	10,000	FITC	4.0×10^{-6}	1.0×10^{-4}	-
PEI linear	25,000	OG	1.4×10^{-7}	1.4×10^{-7}	1.4×10^{-7}
PEI branched	25,000	OG	1.4×10^{-7}	1.4×10^{-7}	-
PAMAM G2	3,256	OG	1.4×10^{-7}	-	1.4×10^{-7}
PAMAM G3	6,909	OG	1.4×10^{-7}	-	-
PAMAM G4	14,215	OG	1.4×10^{-7}	1.4×10^{-7}	-

changes in basal pinocytic rates. To assess the effect of free fluorophore on cell-associated fluorescence, the model compound fluorescein (3.5 μM) was incubated with cells for 2 h at either 37 °C or 4 °C, followed by sample preparation as detailed in section 2.3.11 (denoted as washed cells). Alternatively, washing steps were omitted and cells were left in the incubation medium during harvesting and pelleting. Immediately before analysis, incubation medium was decanted and the cell pellet was re-suspended in PBS and analysed (denoted as unwashed cells).

5.2.4 Interpretation of flow cytometry data to estimate pinocytosis

Mathematical analysis was based on the principles reported previously for fluorescent pinocytic substrates (Swanson et al., 1985) to provide a common basis for interpreting binding, uptake and exocytosis data. Figure 5.1 has been included to clarify the approach.

- To allow for inter-sample comparison, data from uptake experiments (total cell-association at 37 °C for 10 – 40 min time points) were normalised for variable quantum yield. From the appropriate calibration curve, the fluorescence at 350 nM (pH 5.4) was used to correct readings. For studies with FITC-dextran values were also normalised by taking into account the 29 fold higher concentration used.
- A straight line of best fit was applied to the normalised data points from uptake experiments.
- From this line the rate of **apparent cell-association** (EA) was deduced according to formula (3) (i.e. internal and external retention of polymer).

$$EA = \frac{\text{Change in cell-associated fluorescence at 37 °C}}{\text{Time (min)}} \qquad \text{Equation (3)}$$

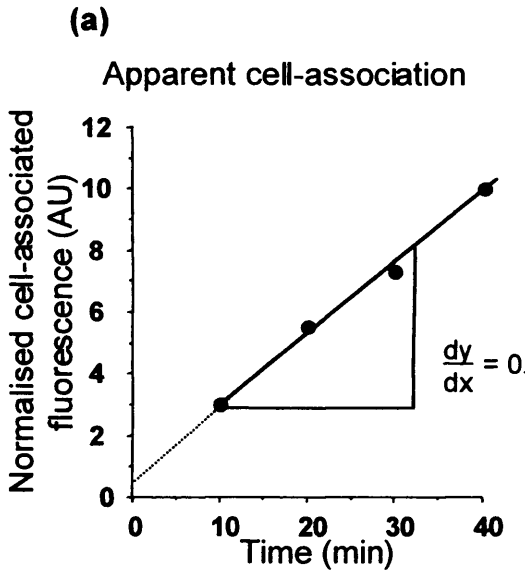

Data points form flow cytometry profiles at 37 °C were normalised by taking into account fluorescence yield of respective polymer at pH 5.4 at a 350 nM concentration.

Apparent uptake was determined from straight line fit using normalised data points (10 - 40 min) (panel a). Thus EA would be 0.15 (normalised change in fluorescence/min).

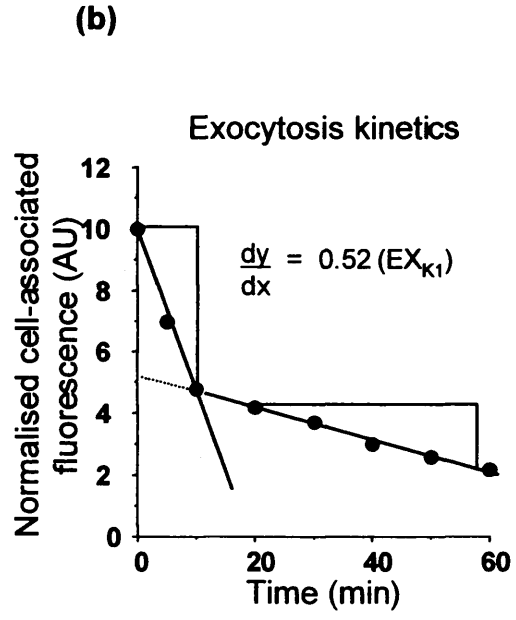

Exocytosis kinetics were determined for the fast and slow release kinetics as 0.52 (EX_{K1}) and 0.05 (EX_{K2}) respectively (panel b).

Fast = EX_{K1}

Slow = EX_{K2}

Thus total endocytosis kinetics was calculated according to:

$$EN_{Total} = EA + EX_{K1}$$

$$EN_{Total} = 0.15 + 0.52$$

$$EN_{Total} = 0.67 \text{ (Normalised change in fluorescence/min)}$$

Figure 5.1 Method of data transformation performed to determine cell-association and exocytosis kinetics.

- Data points from exocytosis experiments were corrected using calibration curves as detailed above. Where obvious signs of exocytosis were evident, straight lines of best fits were applied to describe both **fast** (EX_{K1}) and **slow** (EX_{K2}) **exocytosis** rates.
- From the fitted lines the rate change of cell-associated fluorescence was estimated using equation (4).

$$EX_K = \frac{\text{Change in cell-associated fluorescence at 37 °C}}{\text{Time (min)}} \qquad \text{Equation (4)}$$

- Due to limitations of the current studies to differentiate between intracellular sequestration and/or release, the slow kinetic process EX_{K2} was not used for rate calculations.
- Exocytosis rate and EA were used to calculate the rate of **total cell-association** (EN_{Total}) according to formula (5).

$$EN_{Total} = EX_{K1} + EA \qquad \text{Equation (5)}$$

- The influence of binding on total cell-association was estimated with the use of the 4 °C data by calculating the average contribution of external binding to total cell-associated fluorescence at 37 °C over the first 10 – 40 min. It was assumed that binding characteristics would be independent of temperature.
- The **rate of internalisation** (ER) for polymers demonstrating surface binding was therefore deduced according to formula (6a) and according to formula (6b) in the absence of surface binding.

$$ER = EN_{Total} \times (\text{average fraction of surface bound polymer}) \qquad \text{Equation (6a)}$$

$$ER = EN_{Total} \qquad \text{Equation (6b)}$$

- The determined ER served as a relative indicator for the amount of polymer internalised.
- The percentage of internalised polymer exocytosed by the cell was calculated according to equation (7).

$$\text{Intracellular retention (\%)} = \frac{EX_{K1} \times 100}{ER} \qquad \text{Equation (7)}$$

5.3 Results

5.3.1 Characterisation of parent polymers

The polymer Mw determined experimentally was similar to that provided by the supplier when measured against polysaccharide standards (table 5.3). It can be seen that, as expected, the polydispersity of the linear and branched polymers was greater than estimated for PAMAM dendrimers. All dendrimers displayed a similar dispersity index for all investigated generations. In all cases there were no obvious signs of contaminates at the extremes of the measured Mw (figure 5.2).

Amine content of PAMAM dendrimers determined by NMR was in agreement with the theoretical values (figure 5.3, table 5.4). However, for branched PEI, differences between the theoretical and estimated values were obvious (figure 5.4). The analytical spectrophotometric methods used are only able to determine 1° amine groups. A reasonable correlation between expected and measured amine content was found for PAMAM G2 and G3, but there was significant discrepancy for PAMAM G4 (~ 52 – 73 % of the expected). For branched PEI a correlation between the data obtained by NMR and the ninhydrin assay was evident, with the latter one reaching more than 75 % of the primary amine content determined by NMR. For linear PEI the low abundance of 1° amines was confirmed spectrophotometrically.

5.3.2 Synthesis and characterisation of OG-conjugates

The labelling efficiency and the characteristics of the polymer probes is summarised in table 5.5. Conjugation of OG-SE to PAMAM G4 was successfully achieved under both experimental conditions tested (45 – 71 % yield), but best labelling efficiency was obtained when the reaction was carried out in MeOH (figure 5.5). All subsequent OG-SE conjugations were carried out in this solvent. Best labelling was seen for the branched form of PEI (80 % yield) with subsequently less for linear PEI (73 % yield) and PAMAM G4 (71 % yield) (figure 5.6 – 5.7). The purification method was optimised according to the nature of the polymer.

Table 5.3 Polymer molecular weight characteristics determined by GPC

Polymer	Nominal	Estimated°			Topology
	Mw	Mw	Mn	Polydispersity	
	(g/mol)	(g/mol)		(Mw/Mn)	
Dextran	10,000*	10,311•	4,422•	2.33	Linear
PEI linear	25,000*	21,258♦	6,430♦	3.31	Linear
PEI branched	25,000*	25,324♦	9,723♦	2.61	Branched
PAMAM G4	14,215#	11,245♦	7,404♦	1.52	Dendritic
PAMAM G3	6,909#	6,452♦	4,316♦	1.50	Dendritic
PMAMM G2	3,256#	3,497♦	2,397♦	1.46	Dendritic

* Determined by the manufacturer by laser light scattering

According to (Tomalia et al., 1985)

° Polysaccharide standards

♦ Determined using acetic acid buffer (0.5 M) at 1 ml/min

• Determined using PBS (pH 7.4) at 1 ml/min

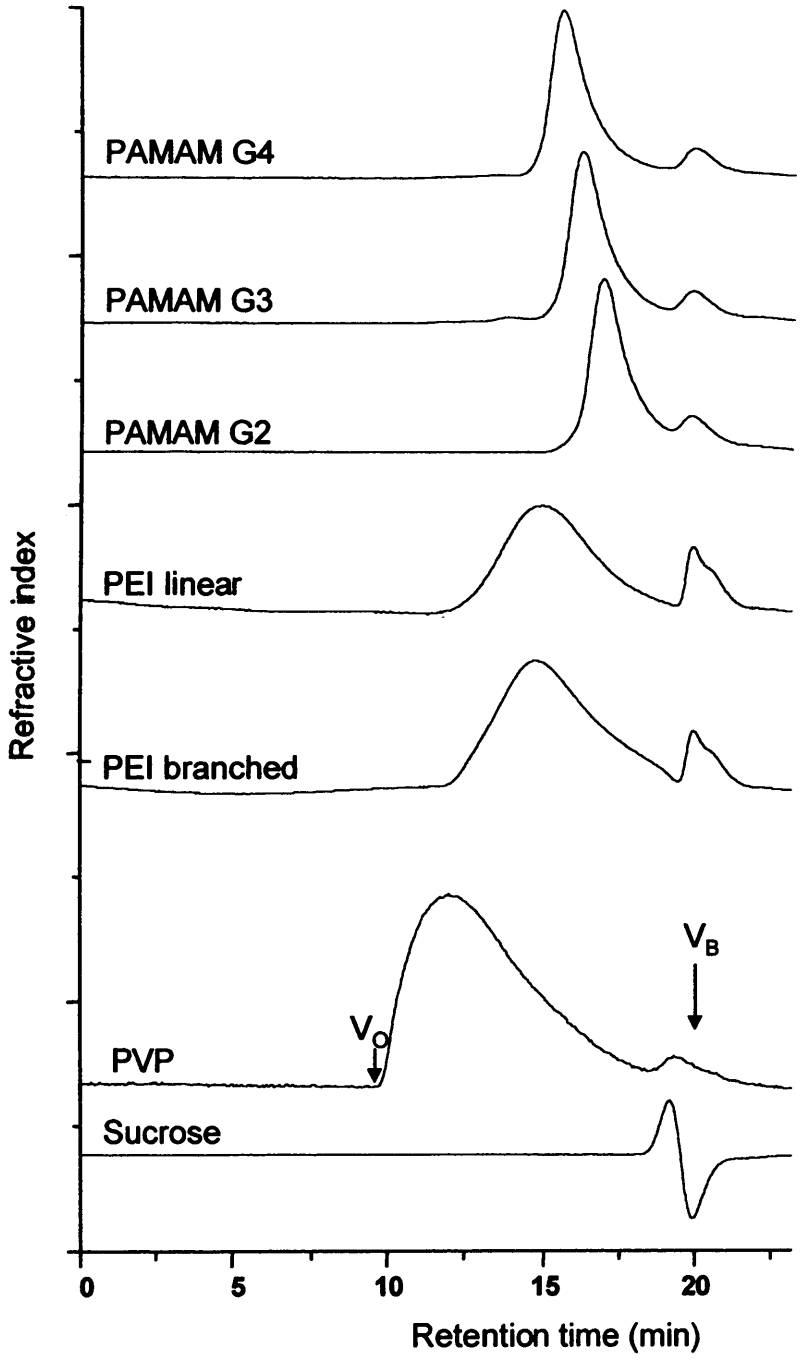

Figure 5.2 Comparison of polymer molecular weight and polydispersity using GPC. Chromatograms for cationic polymer were obtained with Ultrahydrogel columns 1000 and 250 in series using a 0.5 M NaOAc/OHAc as a mobile phase at 1 ml per minute. Void (V_O) and bed volumes (V_B) have been determined using PVP (Mw 1.3 x 10^6 g/mol) and sucrose respectively.

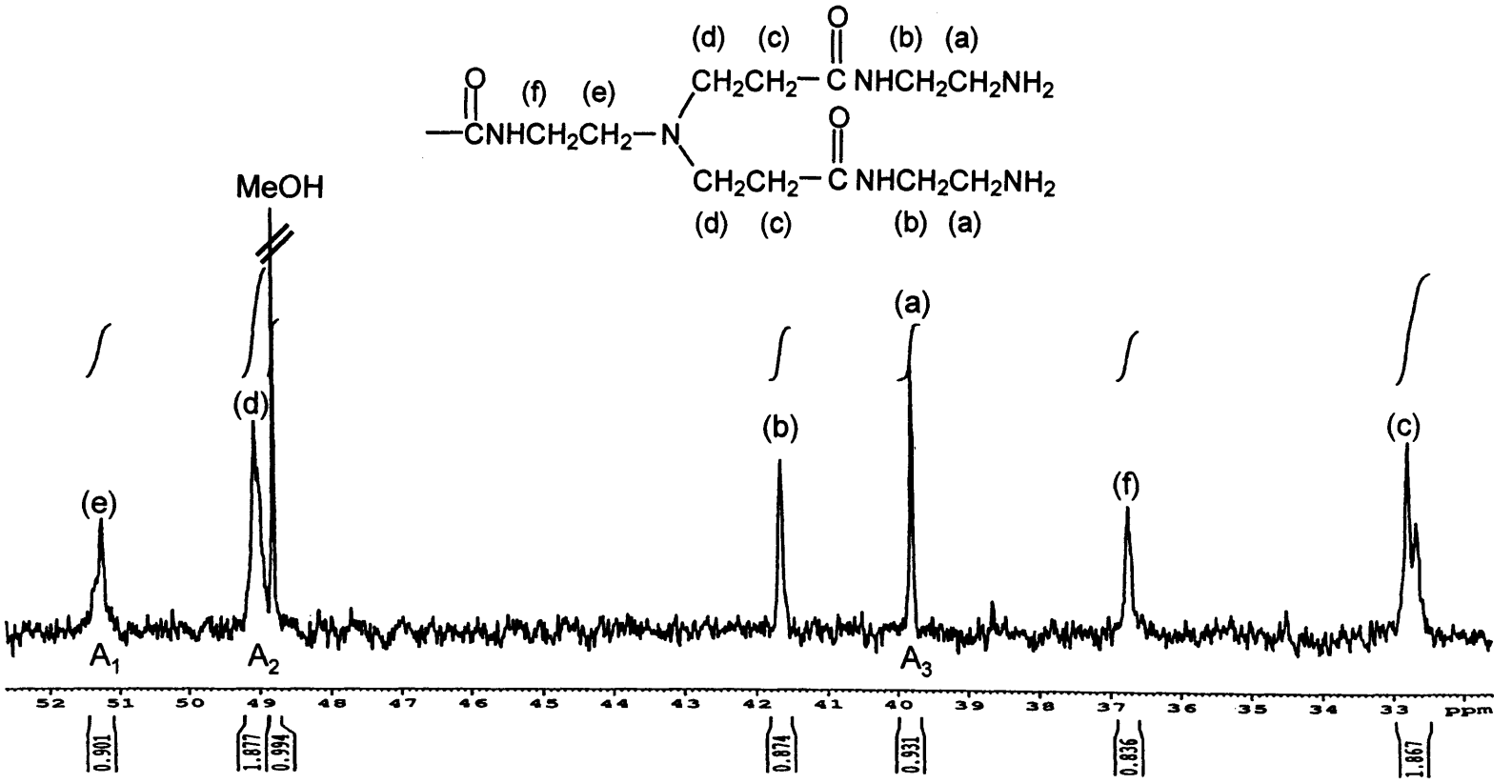

Figure 5.3 Inverse-gated ^{13}C NMR spectrum of PAMAM G4. The spectrum was recorded at 75 MHz in D_20. Signals from different structural elements have been assigned and corresponding peaks are number accordingly. Signal intensities have been integrated as shown. Spectrum is representative for other dendrimers investigated.

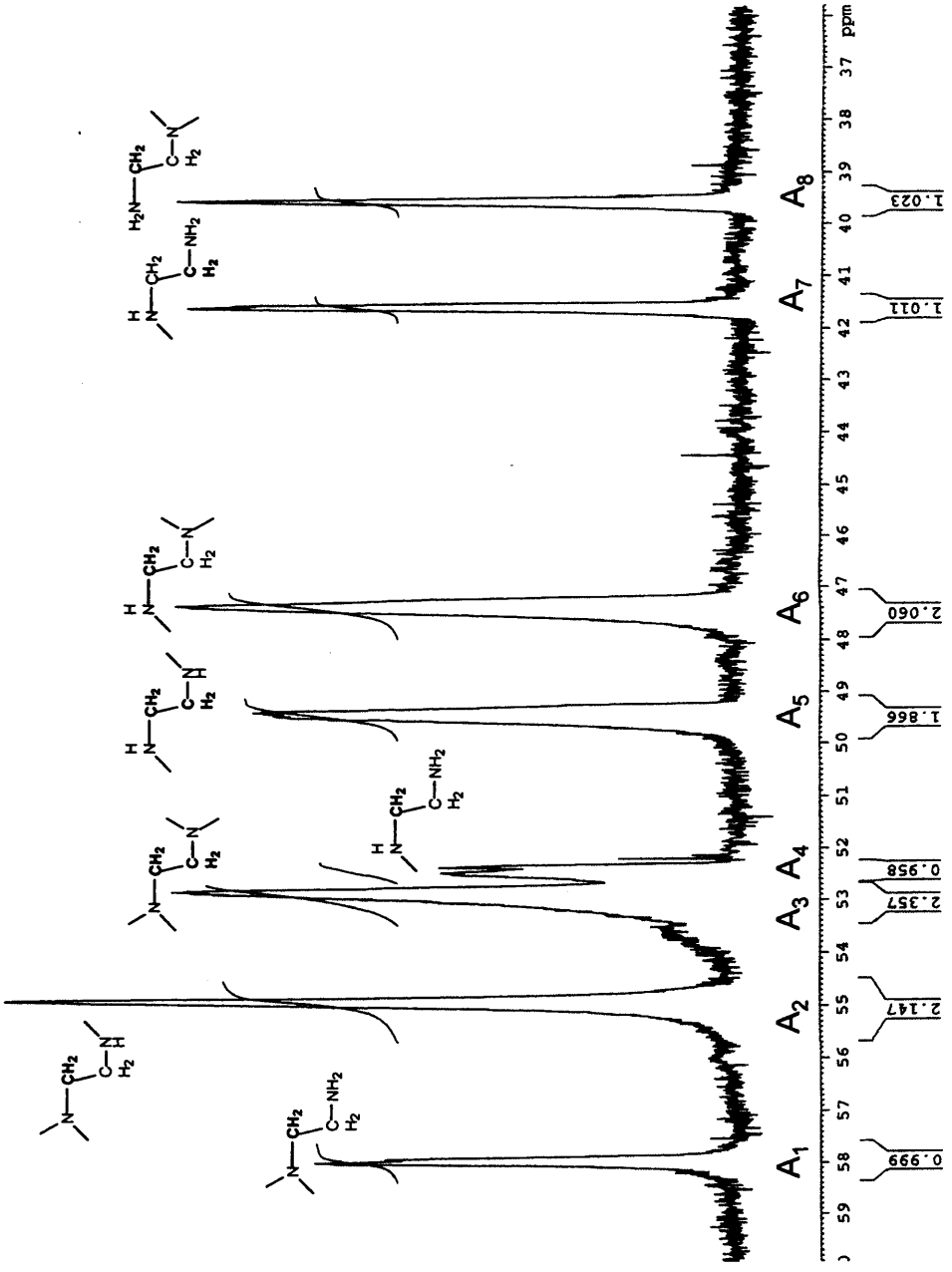

Figure 5.4 Inverse-gated ^{13}C NMR spectrum of branched PEI. The spectrum was recorded at 126 MHz in D_20. Signals from different structural elements have been assigned and corresponding peaks are number accordingly. Signal intensities have been integrated as shown.

Table 5.4 Theoretical and measured 1°, 2° and 3° amine content for PEIs and PAMAM dendrimers.

Polymer	Theoretical amine content*			DB+	^{13}C NMR#			Ninhydrin assay	TNBS assay
	1°	2°	3°		1°	2°	3°	1°	1°
PEI linear	1	580	0	0	ND	ND	ND	5.8 ± 0.4	5.4 ± 0.1
PEI branched	145	290	145	0.50	186	227	168	138.5 ± 6.3	123.3 ± 9.0
PAMAM G2	16	-	14	1.00	16	-	14	14.2 ± 0.8	8.2 ± 0.4
PAMAM G3	32	-	30	1.00	33	-	30	26.0 ± 2.5	20.5 ± 1.9
PAMAM G4	64	-	62	1.00	63	-	63	46.7 ± 2.6	33.3 ± 1.7
PAMAM G2.5	0	-	30	1.00	ND	-	ND	3.8 ± 0.2	0

Results show ± SEM n=3

ND Not determined

* Using theoretical molecular weights

Quantified using inverse-gated NMR

+ Degree of branching calculated according to Frey

Table 5.5 Characteristics of fluorescently labelled polymeric probes

Polymer	Fluorophore	Molar ratio (fluorophore/ polymer)	Labelling efficiency (μg fluorophore/mg polymer) #	Free fluorophore (% of total)*
PAMAM G4	OG	0.45	16.2 (1)	0.6
		0.71	25.6 (2)♣	0.4
PAMAM G3	OG	0.56	41.5 (2)♣	0.2
PAMAM G2	OG	0.50	78.6 (2)♣	0.1
PEI branched	OG	0.80	16.4 (2)♣	0.6
PEI linear	OG	0.73	15.0 (2)♣	0.7
Dextran	FITC	4.00♦	156.3 ♦♣	ND

(1) OG-SE dissolved in DMSO and polymer dissolved in sodium bicarbonate buffer (0.1 M) pH 8.3, allowed to react for 1 h at room temperature under N_2.

(2) OG-SE and polymer dissolved in MeOH, where necessary pH adjusted to ~ 8.5 with triethylamine. Mixture and allowed to react under N_2 for 2 h at room temperature.

Labelling efficiency was estimated unless otherwise stated by integrating peak areas of free and polymer-bound fluorophore using size exclusion chromatograms. Labelling efficiency is expressed as μg of fluorophore/mg of polymer.

* Estimated detection limit of free OG by thin layer chromatography when visualised at 365 nm

♣ Used for trafficking experiments

♦ Supplied by the manufacturer

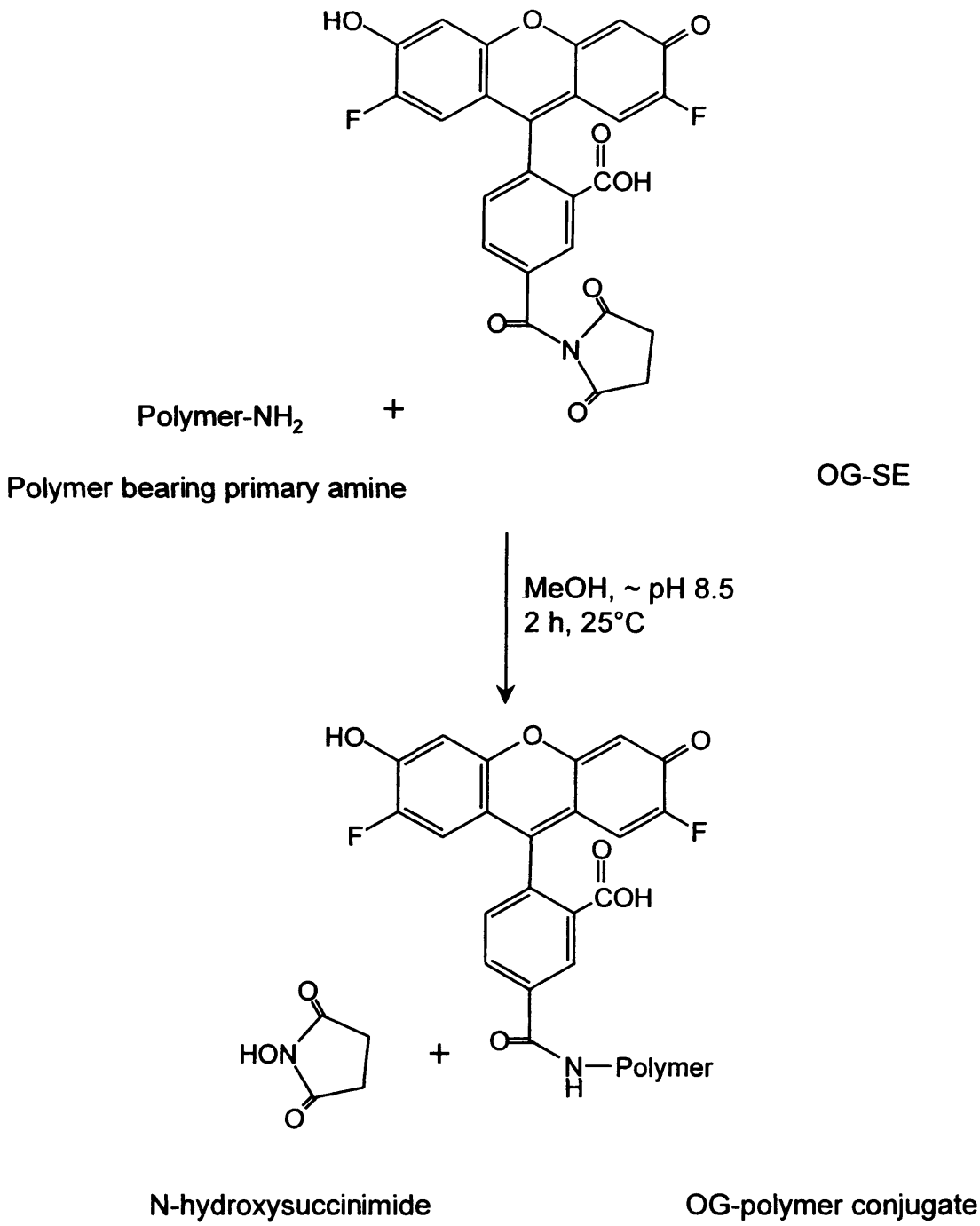

Figure 5.5 Optimised synthesis of OG-polymer conjugates

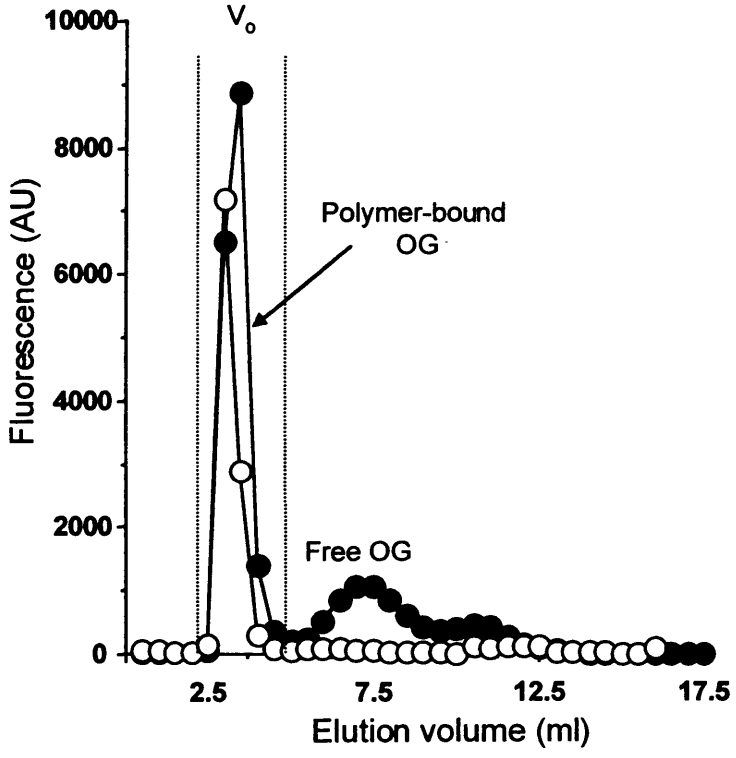

Figure 5.6 Evaluation of reaction yield and purity of branched PEI-OG conjugate using GPC. Representative GPC profiles for crude (●) and purified (O) OG-PEI using a LH20 column and a MeOH/H_20 (60 : 40 containing 0.36 M NaCl) elution buffer.

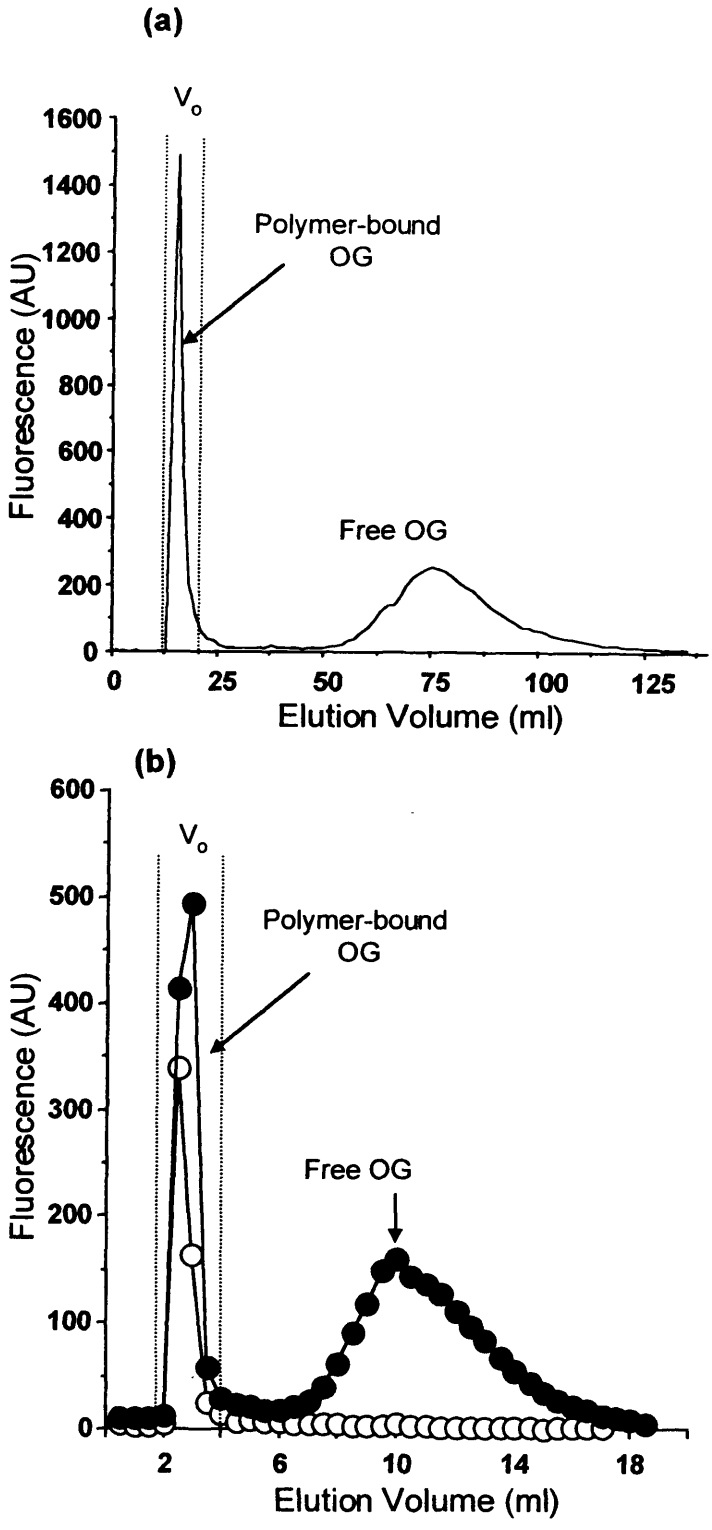

Figure 5.7 Evaluation of reaction yield and purity of OG-PAMAM G4 conjugate using Sephadex G25. Panel (a) elution profile of the crude reaction mixture for polymer-bound and free fluorophore using a 25 cm column and a loading of ~ 2 x 10^{-6} moles of polymer. Panel (b) elution profiles for crude (●) and purified (O) conjugate using a PD10 column and a loading of ~ 2 x 10^{-8} moles of polymer. The molar labelling ratio of OG to PAMAM G4 was estimated as 0.45 and 0.42 for panel (a) and (b) respectively.

5.3.3 Characterisation of polymer conjugates: effect of concentration, buffer and pH on fluorescence.

The emission spectra for all OG conjugates showed a maximum at ~ 520 nm (figure 5.8) though FITC-dextran had a maximum at a slightly lower wavelength (~ 515 nm). FITC-dextran showed a clear linear correlation between concentration and fluorescence quantum yield (figure 5.9). Linear and branched PEI also showed a linear relationship between concentration and fluorescence (figure 5.10). For linear PEI superimposable fluorescence was observed at both pH 7.4/5.4 and pH 6.4/4.0. Highest values were observed for pH 7.4/5.4. For branched PEI similar fluorescence values were observed over the tested pH range. All PAMAM dendrimers showed linear fluorescence at concentrations up to 0.2 μM (figure 5.11 – 5.12). For PAMAM G4 all calibration curves were linear and highest levels of fluorescence were observed at pH 5.4 and second highest levels at pH 4.0 (figure 5.12). Identical fluorescence output was observed at pH 7.4 and pH 6.4 for PAMAM G4. For PAMAM G3 fluorescence was identical over the tested pH range up to a 0.2 μM concentration. At higher concentrations the rank order was pH 5.4 > pH 4.0 > pH 7.4 ≈ pH 5.4 (figure 5.11, panel a). For PAMAM G2 a linear relationship of fluorescence was evident over the tested concentration range at pH 4.0 (figure 5.11, panel b). Highest values were observed at pH 5.4 with subsequently lower ones at pH 6.4 and 7.4.

5.3.4 Cytotoxicity in B16F10 cells

The cytotoxicity of all polymers is shown in figure 5.13 with calculated IC_{50} values summarised in table 5.6. All cationic polymers were cytotoxic. There was a clear generation-dependent toxicity for PAMAM dendrimers (G4 > G3 > G2). Comparable toxicity was seen for both linear and branched PEI (figure 5.13). For OG a reduction in viability was only apparent at the highest concentrations tested and these exceed the concentrations used in the uptake assays (figure 5.14). Visualisation of B16F10 cells exposed to polymers (3 h) using bright-field microscopy confirmed

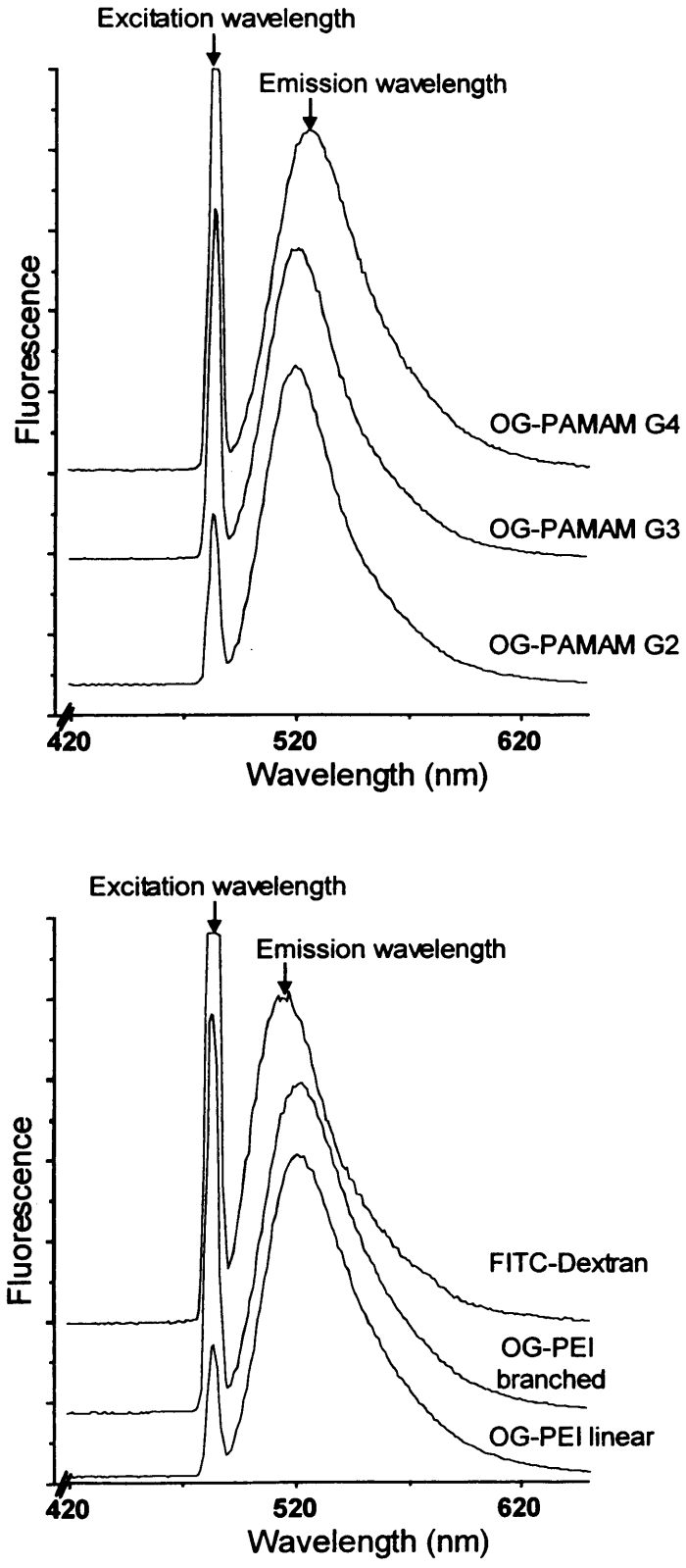

Figure 5.8 Emission spectra for fluorescently labelled polymer conjugates recorded in PBS at pH 7.4. Conjugates were excited at 485 nm (± 4 nm) and emission spectrum was recorded.

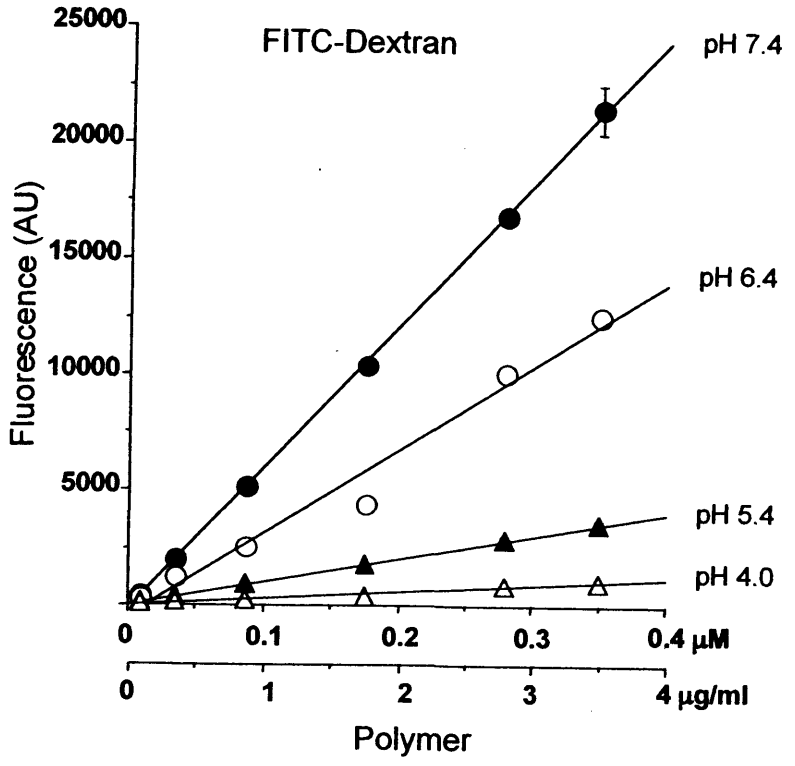

Figure 5.9 Effect of pH and buffer on FITC-dextran fluorescence. Calibration curves for polymer conjugate in PBS (0.1 M) pH 7.4 (●) and 6.4 (○) and citrate buffer (0.1 M) pH 5.4 (▲) and 4.0 (△). (Data represents mean ± SEM n=3, error bars are within plot symbols when not visible).

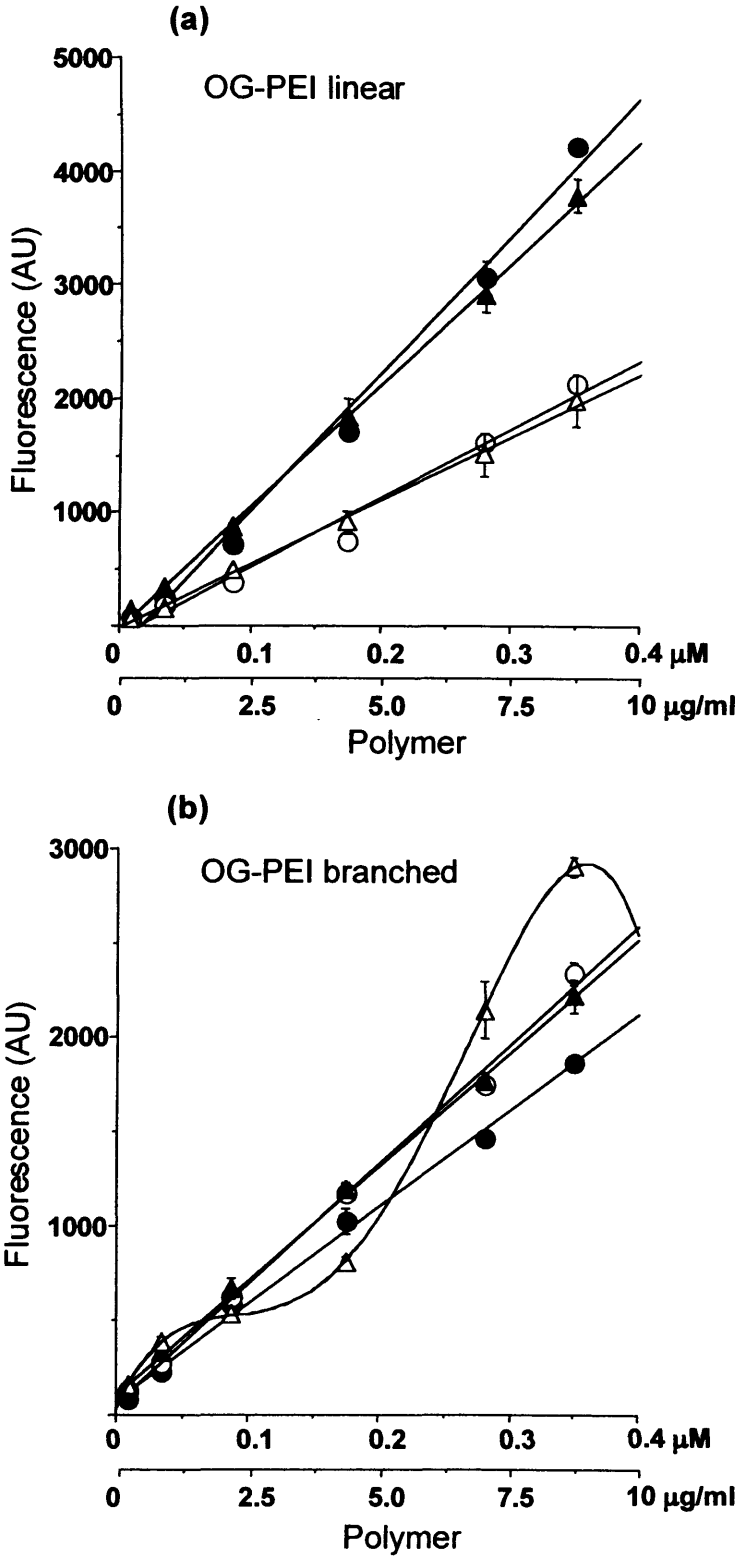

Figure 5.10 Effect of pH and buffer on PEI-OG fluorescence. Panel (a) standard curves for linear PEI, (b) standard curves for branched PEI. Measurements were performed in PBS (0.1 M) pH 7.4 (●) and 6.4 (○) and citrate buffer (0.1 M) pH 5.4 (▲) and 4.0 (△). (Data represents mean ± SEM n=3, error bars are within plot symbols when not visible).

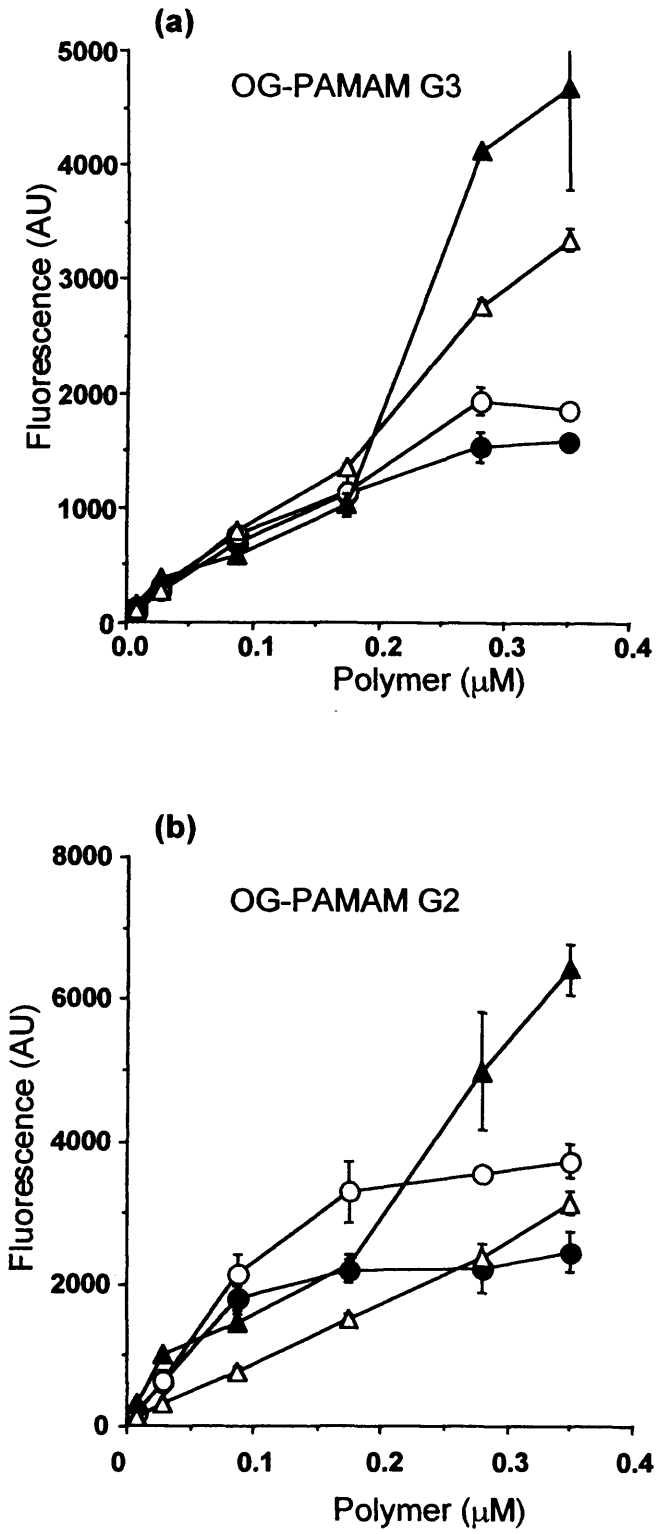

Figure 5.11 Effect of pH and buffer on OG-PAMAM G3 and G2 fluorescence. Measurements were performed in PBS (0.1 M) pH 7.4 (●) and 6.4 (○) and citrate buffer (0.1 M) pH 5.4 (▲) and 4.0 (△). (Data represents mean ± SEM n=3, error bars are within plot symbols when not visible).

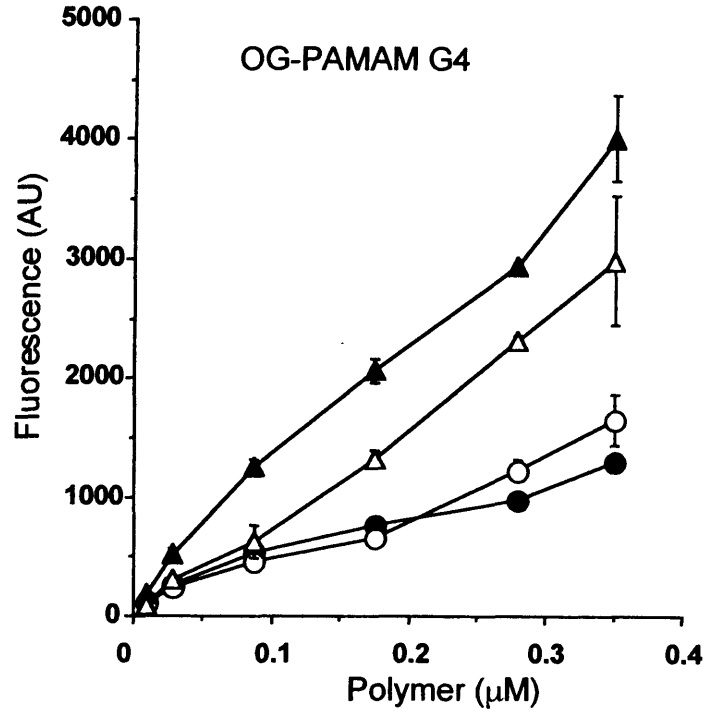

Figure 5.12 Effect of pH and buffer on OG-PAMAM G4 fluorescence. Measurements were performed in PBS (0.1 M) pH 7.4 (●) and 6.4 (○) and citrate buffer (0.1 M) pH 5.4 (▲) and 4.0 (△). (Data represents mean ± S.E.M n=3, error bars are within plot symbols when not visible).

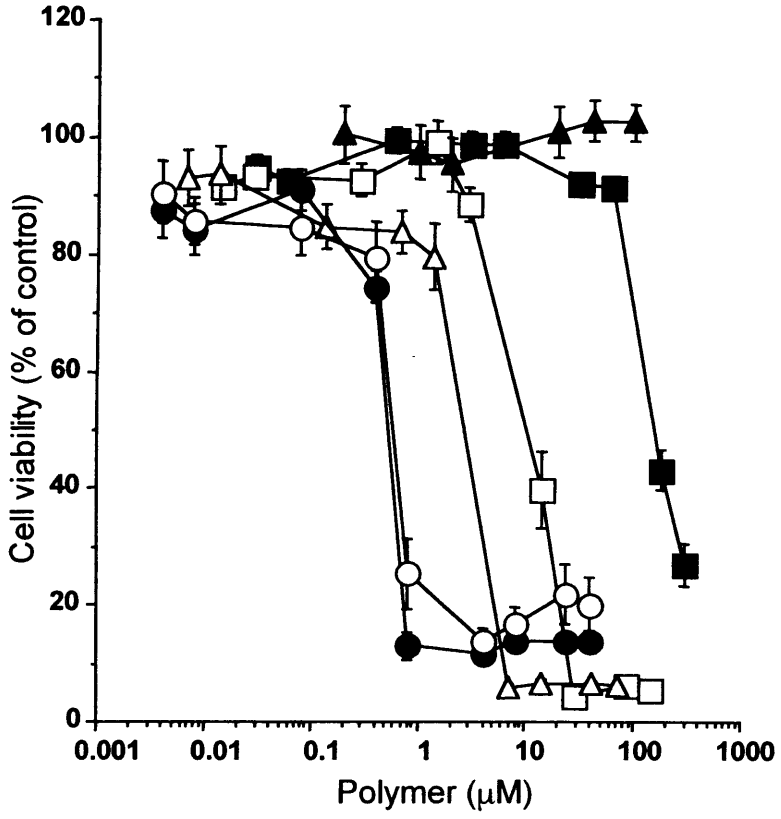

Figure 5.13 Cytotoxicity of cationic polymers and dextran in B16F10 cells. Incubation period was 72 h and cell seeding density 1 x 10^5 cells/ml. Plot symbols are as follows: PAMAM G2 (■), PAMAM G3 (□), PAMAM G4 (△), branched PEI (●), linear PEI (○), dextran (▲). Data are presented as percentage of untreated control cells. (Data represents ± SEM n=18, error bars are within plot symbols when not visible).

Table 5.6 Summary of IC_{50} values for B16F10 cells#

Polymer	IC_{50} values in μM (± SEM)
Dextran	> 100
PAMAM G2	176.6 (20.6)
PAMAM G3	14.3 (2.8)
PAMAM G4	3.6 (0.9)
Branched PEI	0.6 (0.1)
Linear PEI	2.8 (1.8)

Cell viability estimated using the MTT assay following a 72 h exposure to polymers at a seeding density of 1 x 10^5 cells/ml.

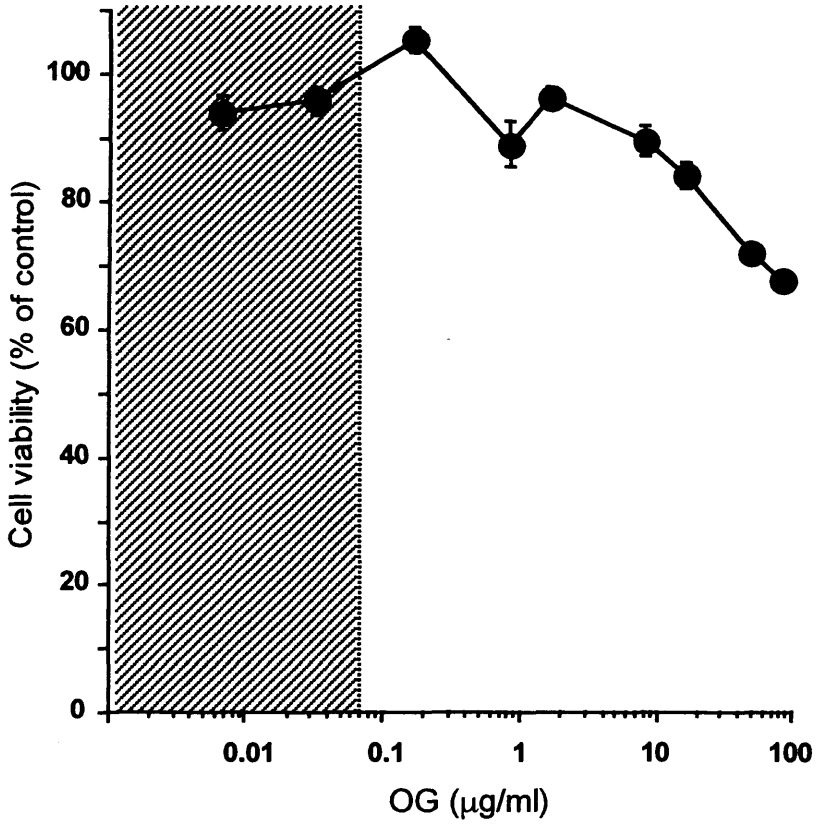

Figure 5.14 Cytotoxicity of OG in B16F10 cells. Incubation period was 72 h and cell seeding density 1 x 10^5 cells/ml. Shaded area corresponds to maximum exposure levels of polymer-bound OG during experiments assuming the presence of one fluorophore per polymer chain. Data are presented as percentage of untreated control cells. (Data represents ± SEM n=6, error bars are within plot symbols when not visible).

the absence of obvious signs of cellular toxicity at polymer concentrations of 1.4 x 10^{-7} M (dummy uptake experiment) (figure 5.15).

5.3.5 Stability of polymer conjugates in vitro and cell-association of fluorescein

At the start OG-PAMAM G4 and linear OG-PEI contained 0.4 % and 0.7 % of free OG respectively. After 3 h, free OG levels were estimated as 8 % and 16 % (figure 5.16). Cell-associated fluorescence of free dye was evaluated with the use of the model fluorophore fluorescein at a molar concentrations 25 fold in excess of concentrations used for uptake studies (figure 5.17). Unwashed cells always showed high cell-associated-fluorescence, which was independent of temperature, whereas washed cells were just above background (figure 5.17).

5.3.6 Pinocytosis and exocytosis of fluorescently labelled polymers measured by flow cytometry

The B16F10 cell association of polymer-OG conjugates over time could be seen from the changes in the flow cytometry profiles (figure 5.18), with excellent peak symmetry for all conjugates. Cell association of FITC-dextran at 37 °C was linear over the 2 h incubation period (figure 5.19). Experiments conducted at 4 °C showed insignificant surface binding. Exocytosis experiments showed a rapid loss of cell-associated fluorescence within 10 min (falling to ~ 60 % of the original value within 10 min) and thereafter only a marginal decrease in fluorescence was evident for the remaining 50 min. Appearance of FITC-dextran in the tissue culture medium over time corroborated these observations (figure 5.20). Insignificant surface binding and extensive recycling was observed for dextran, providing an estimate that only ~ 20 % of internalised polymer was retained intracellular (calculated using equation 7). Furthermore ~ 40 % of total pinocytosed polymer was exocytosed within 10 min from an intracellular pool with a short half-life ($t_{1/2}$ ~ 15 min). Following the rapid release, disappearance of cell-associated fluorescence over the next 50 min was slow ($t_{1/2}$ ~ 120 min). The cellular association of both linear and branched PEIs at 37 °C was linear over the incubation time (figures 5.21 and 5.22). However, in this case

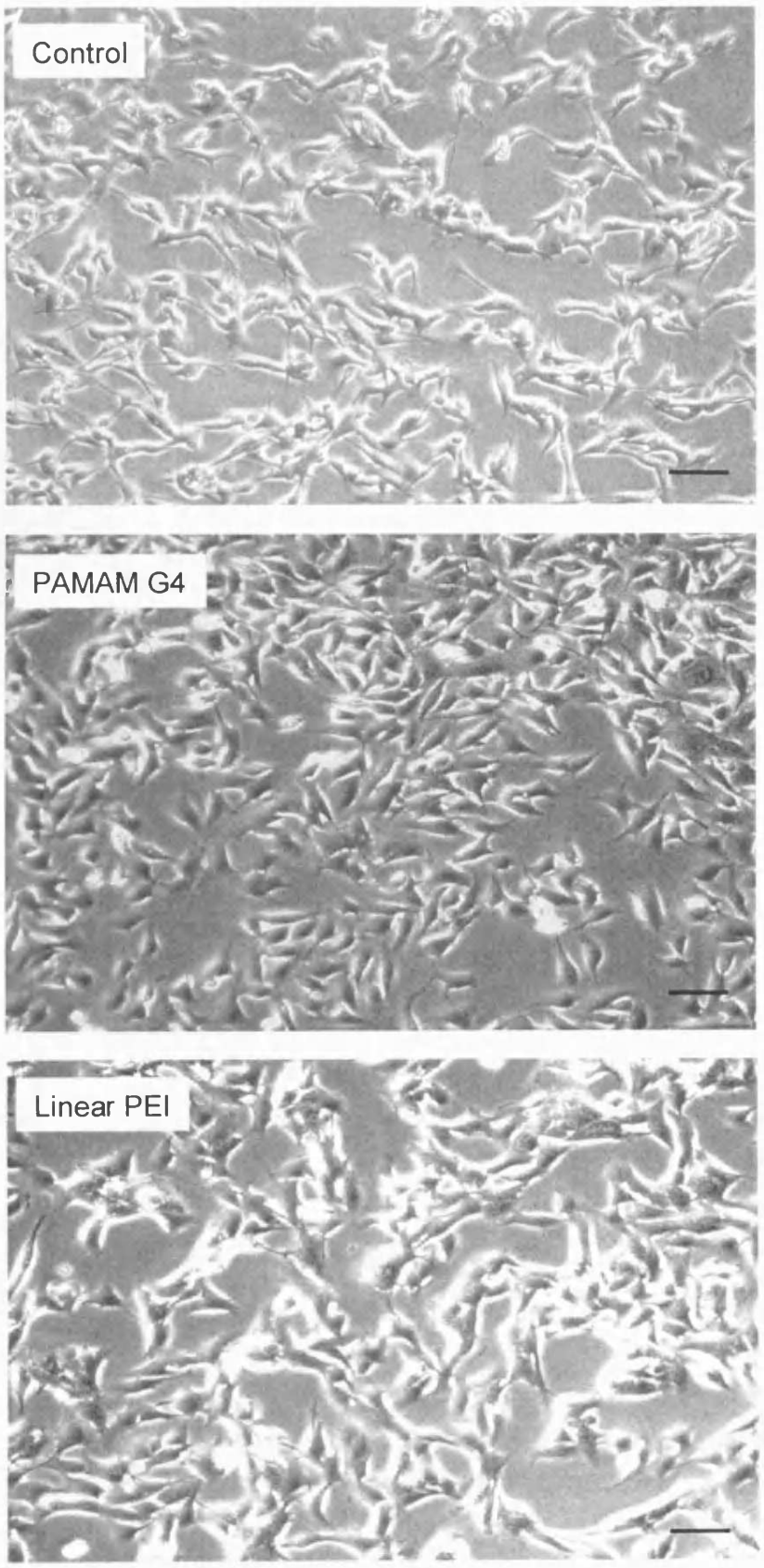

Figure 5.15 Representative bright-field images of B16F10 exposed to cationic polymers for 3 h. Panel (a) control cells, panel (b) cells incubated with PAMAM G4, and panel (c) cells incubated with linear PEI. Scale bar 10 μm.

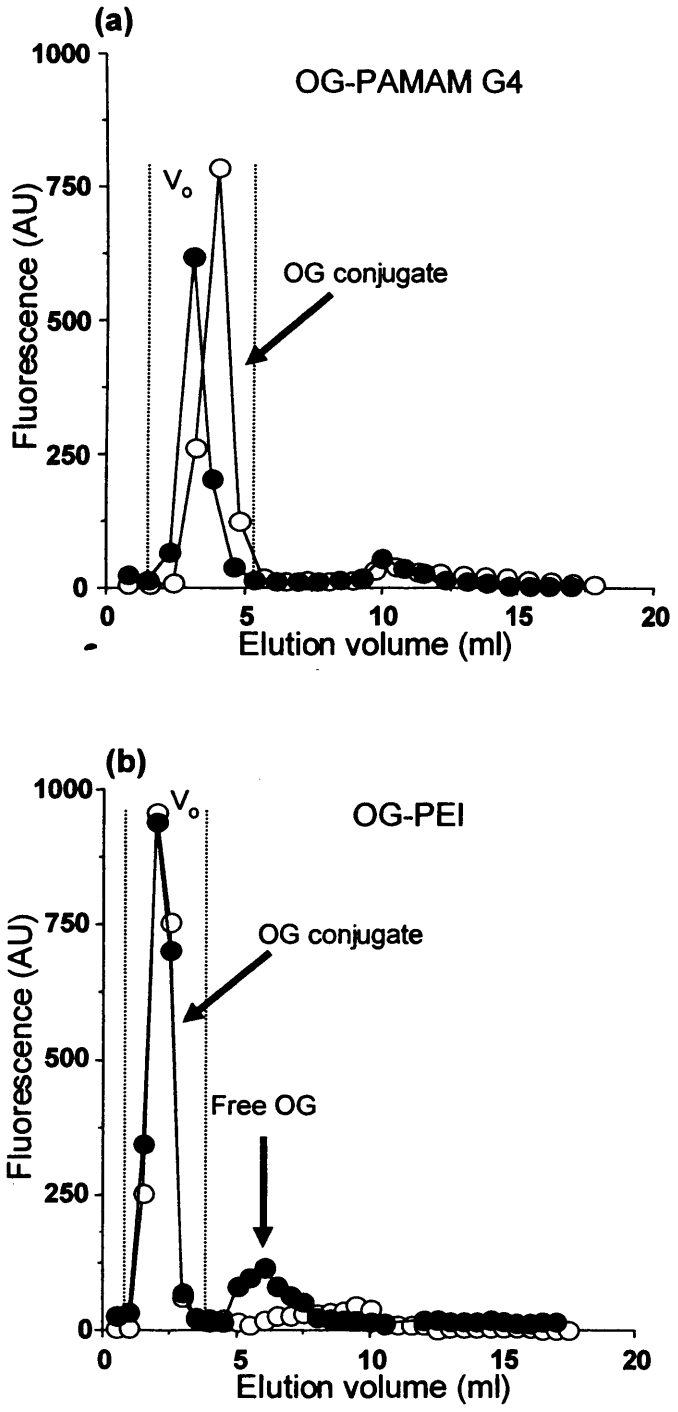

Figure 5.16 GPC profiles of tissue culture medium following incubation with polymer conjugates. B16F10 cells were incubated with conjugate for 3 h. Panel (a) OG-PAMAM G4 at 0 h (O) and 3 h (●), (b) linear OG-PEI at 0 h (O) and 3 h (●). (Data show single representative experiments).

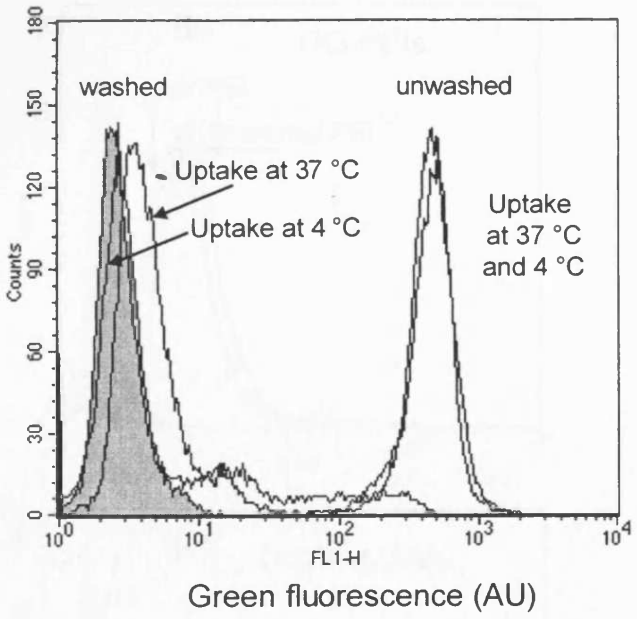

Figure 5.17 Representative histogram profiles obtained by flow cytometry for B16F10 cells exposed to free fluorescein for 2 h at either 37 °C or 4 °C. Dye leakage was evaluated by preparing cells for flow cytometric analysis by either employing or omitting washing steps. Background fluorescence of control cells is shown by filled histogram.

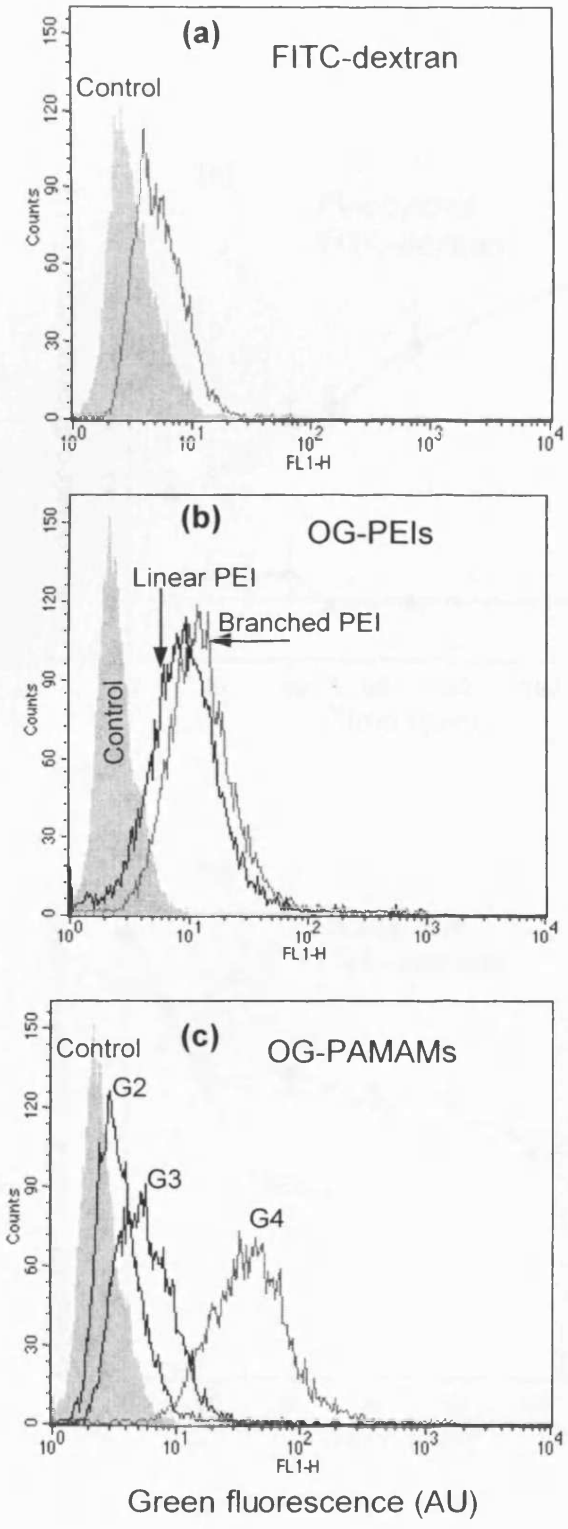

Figure 5.18 Representative histogram profiles obtained by flow cytometry for B16F10 cells exposed to fluorophore labelled polymers for 2 h at 37 °C. Background fluorescent of control cells is shown by filled histograms. Panel (a) FITC-dextran, (b) linear (black line) or branched (grey line) PEI, (c) PAMAM G2 – G4.

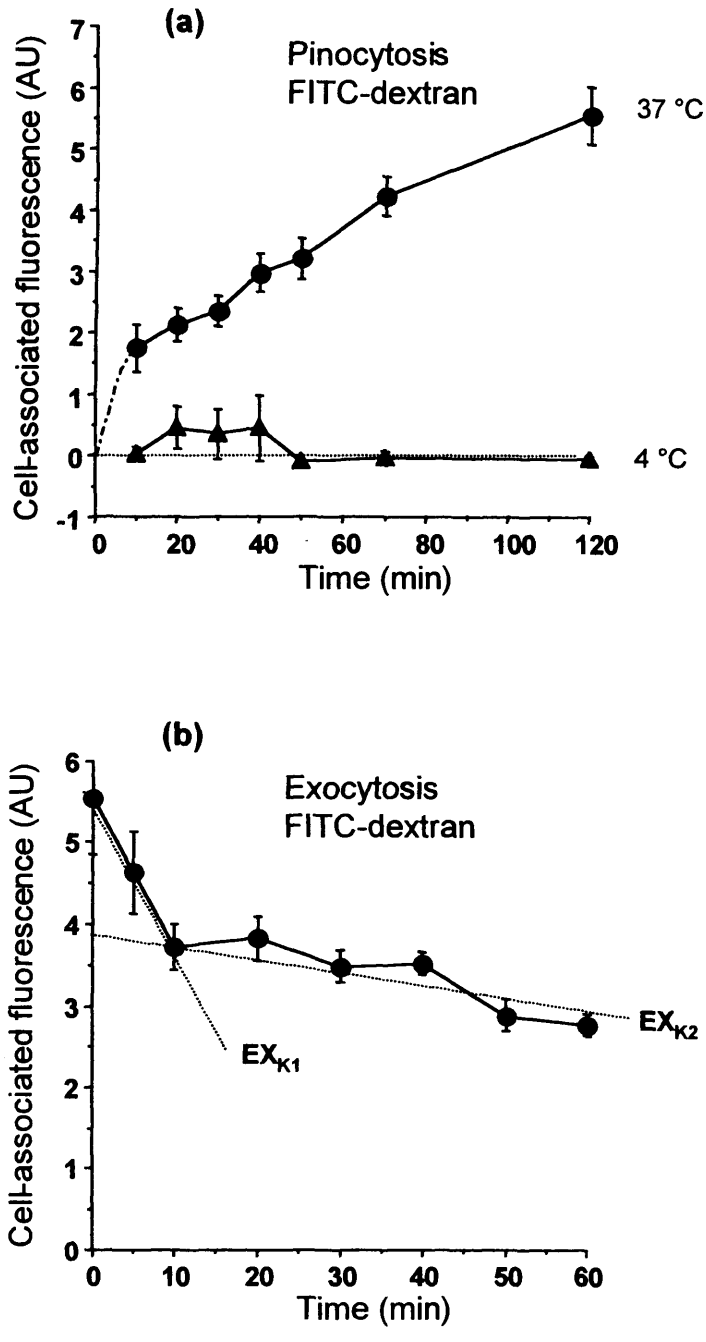

Figure 5.19 Pinocytosis, exocytosis and binding profiles for FITC-dextran in B16F10 cells. Panel (a) 37 °C (●) and 4 °C (▲), panel (b) exocytosis profile following a 2 h uptake period. (Data represents mean ± SEM n=9 for uptake and binding, and n=6 for exocytosis experiments, error bars are within plot symbols when not visible).

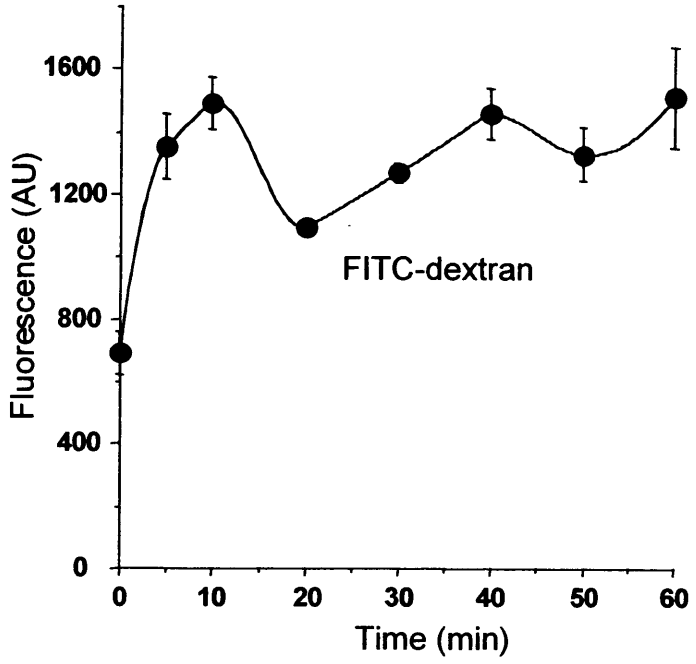

Figure 5.20 Release of FITC-dextran into culture medium during exocytosis phase. (Data represents mean ± SEM n=6, error bars are within plot symbols when not visible).

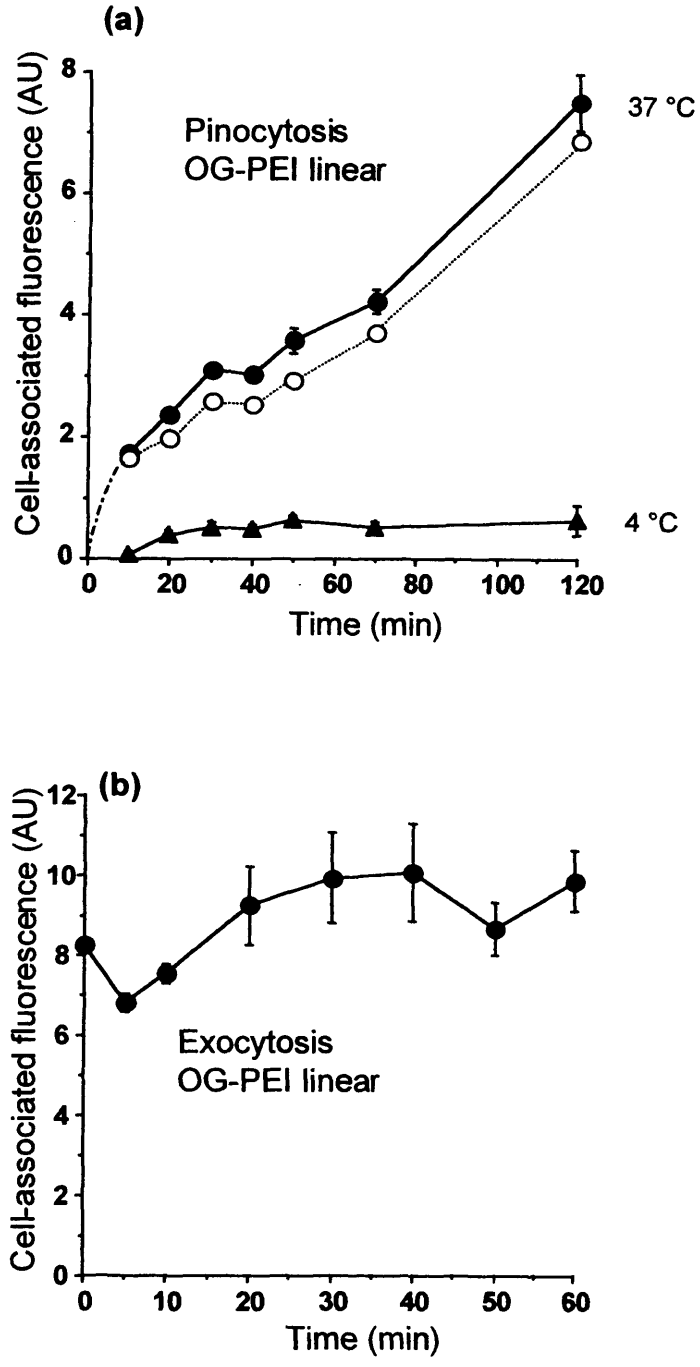

Figure 5.21 Pinocytosis, exocytosis and binding profiles for linear OG-PEI in B16F10 cells. Panel (a) 37 °C (●) and 4 °C (▲), amount of internalised polymer (○) was estimated by subtracting 4 °C binding values form 37 °C uptake profiles. Panel (b) exocytosis profile following a 2 h uptake period. (Data represents ± SEM n=9 for uptake and binding, and n=6 for exocytosis experiments, error bars are within plot symbols when not visible).

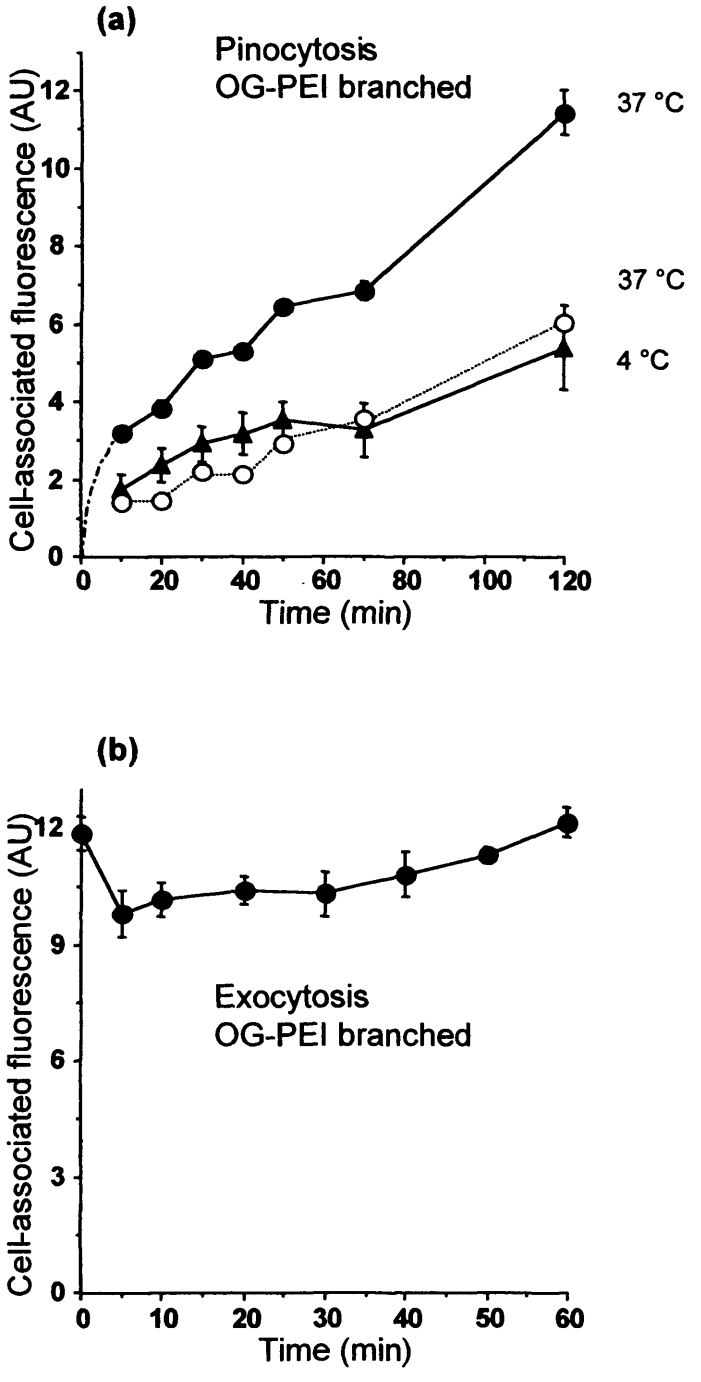

Figure 5.22 Pinocytosis, exocytosis and binding profiles for branched OG-PEI in B16F10 cells. Panel (a) 37 °C (●) and 4 °C (▲), amount of internalised polymer (○) was estimated by subtracting 4 °C binding values form 37 °C uptake profiles. Panel (b) exocytosis profile following a 2 h uptake period. (Data represents ± SEM n=9 for uptake and binding, and n=6 for exocytosis experiments, error bars are within plot symbols when not visible).

studies undertaken at 4 °C indicated significant extracellular binding. For branched PEI this accounted for ~ 58 % of total cell-associated fluorescence. For linear PEI the extent of binding was ~ 13 % of total cell-associated fluorescence. Exocytosis experiments did not reveal obvious signs of changed cellular fluorescence during the 60 min chase for either form of PEI (figure 5.21 and 5.22). The lack of PEI appearance in the culture medium over time corroborated these findings (figure 5.23). The cell association profile of PAMAM G4 resembled that of linear PEI, and extracellular binding contributed ~ 16 % to total cell-associated fluorescence (figure 5.24). Exocytosis experiments did not show signs of reduced cellular fluorescence over time. The lack of PAMAM G4 appearance in the culture medium during the chase corroborated these findings (figure 5.25). The cellular association for PAMAM G3 appeared more biphasic, with rapid cellular uptake (5 – 10 min) and a slower rate for rest of the study (figure 5.26, panel a). Contribution of extracellular binding was on average ~ 20 % of total cell-associated fluorescence. The cell association profile for PAMAM G2 resembled that of PAMAM G4 though with a higher 4 °C surface binding (~ 25 %). When total cell association of polymers was compared over the first 40 min (i.e. using equation 5), maximum rate of internalisation was observed for PAMAM G4 (i.e. using equation 6a), followed by linear and branched PEI achieving 27 % and 36 % of the maximum respectively (figure 5.27). For PAMAM G3 and G2 internalisation rates were significantly lower with 8 % and 4 % of the maximum respectively. Internalisation rate of PAMAM G2 was comparable to FITC-dextran (equation 6b).

5.3.7 Fluorescence microscopy of polymer conjugates

Confocal microscopy examination of live B16F10 cells incubated with FITC-dextran for 1 h revealed clear vesicular labelling with no apparent surface binding (figure 5.28) (N.B. all fluorescent images are also presented in an electronic format to aid visualisation. The CD can be found at the back of the thesis in Appendix II). Maximum projection of confocal slices demonstrated saturated perinuclear fluorescence (figure 5.28, panel b). Live cell images of B16F10 cells incubated with

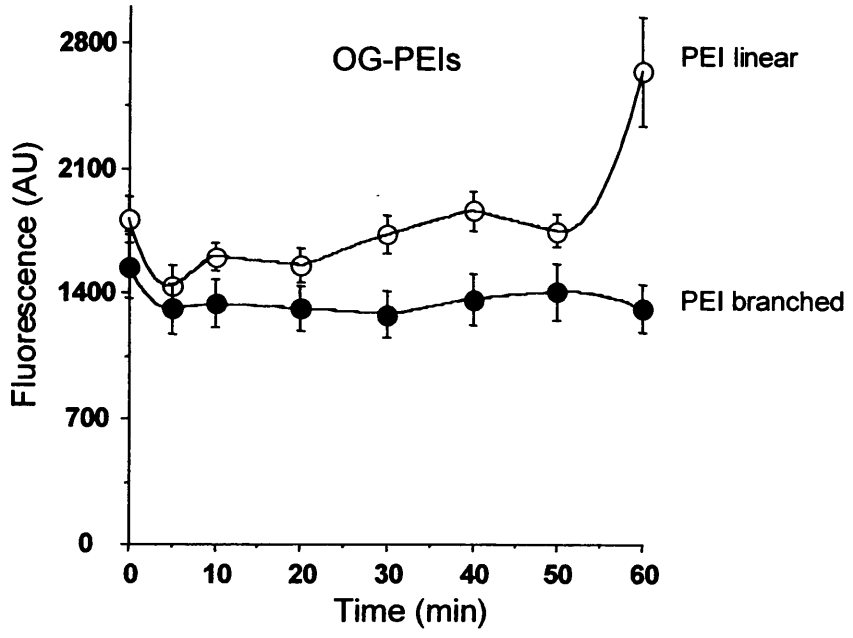

Figure 5.23 Release of linear and branched PEI-OG into culture medium during exocytosis phase. (Data represents mean ± SEM n=6, error bars are within plot symbols when not visible).

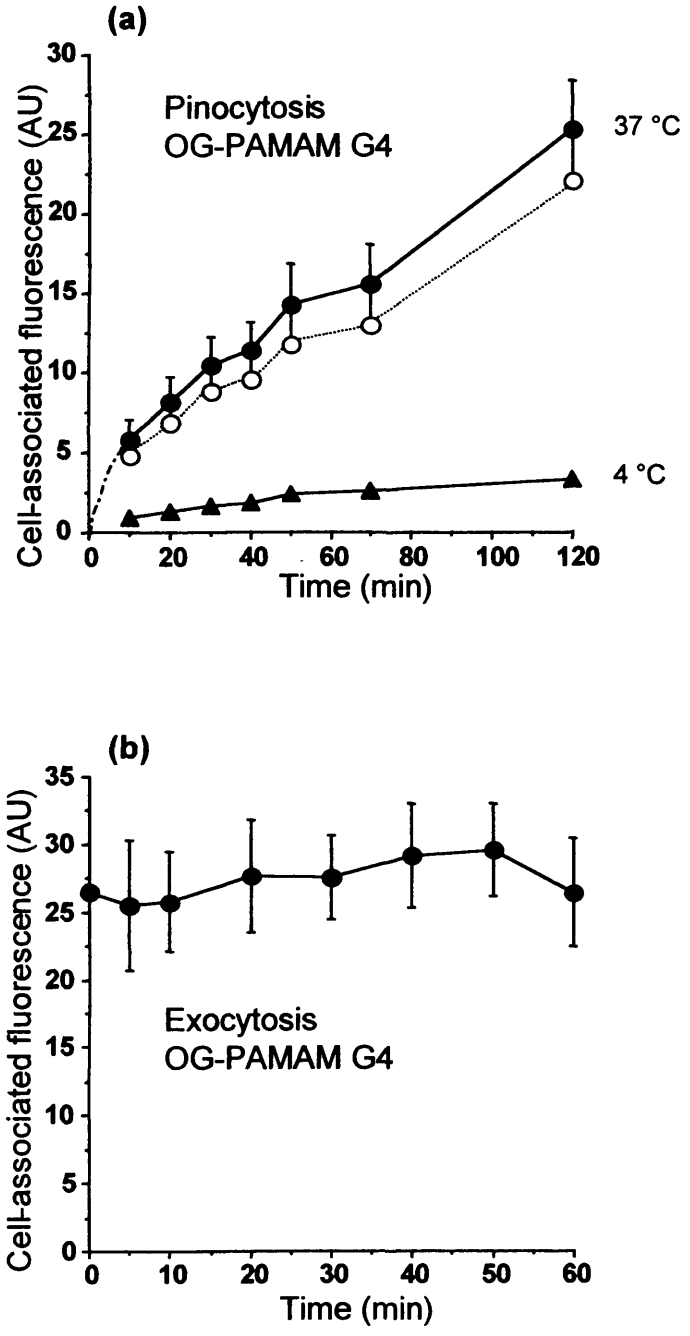

Figure 5.24 Pinocytosis, exocytosis and binding profiles for OG-PAMAM G4 in B16F10 cells. Panel (a) 37 °C (●) and 4 °C (▲), amount of internalised polymer (O) was estimated by subtracting 4 °C binding values form 37 °C uptake profiles. Panel (b) exocytosis profile following a 2 h uptake period. (Data represents ± SEM n=9 for uptake and binding, and n=6 for exocytosis experiments, error bars are within plot symbols when not visible).

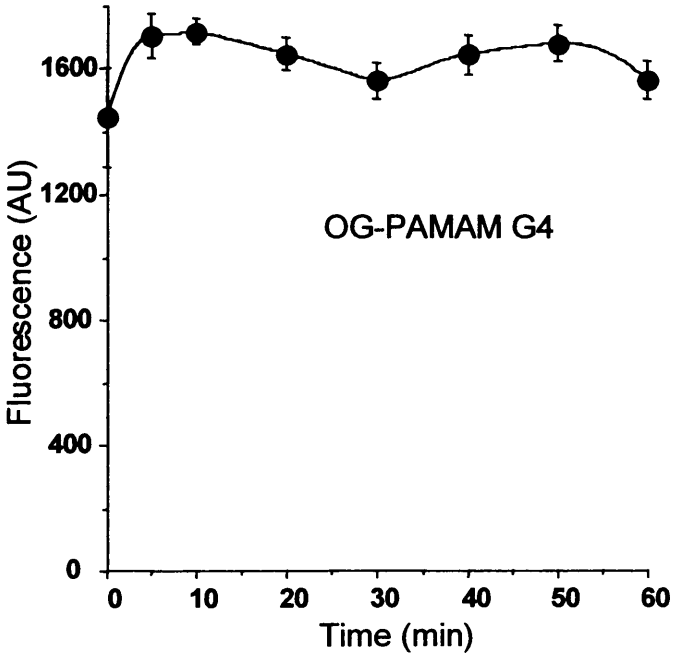

Figure 5.25 Release of OG-PAMAM G4 into culture medium during exocytosis phase. (Data represents mean ± SEM n=6, error bars are within plot symbols when not visible).

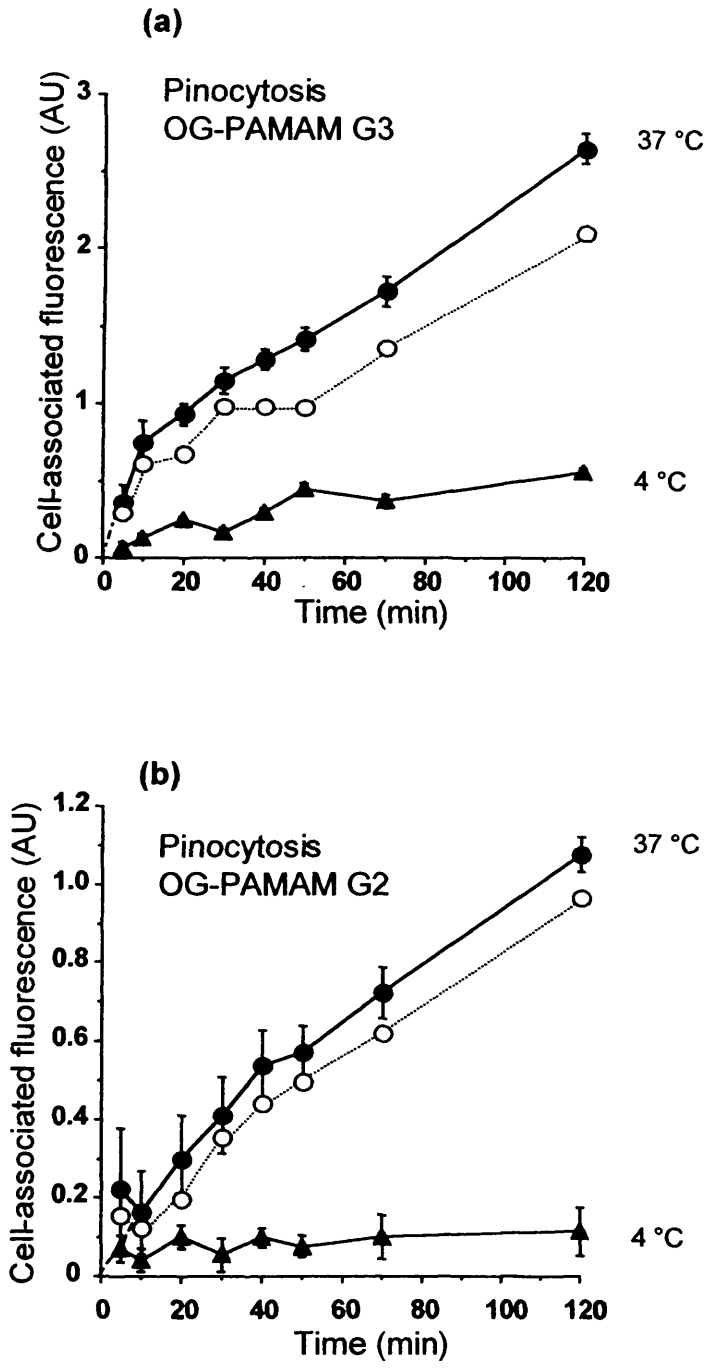

Figure 5.26 Pinocytosis and binding profiles for OG-PAMAMs G3 and G2 in B16F10 cells. The amount of internalised polymer (O) was estimated by subtracting 4 °C binding values (▲) form 37 °C uptake profiles (●). Panel (a) PAMAM G3, panel (b) PAMAM G2. (Data represents ± SEM n=6 for uptake and binding experiments, error bars are within plot symbols when not visible).

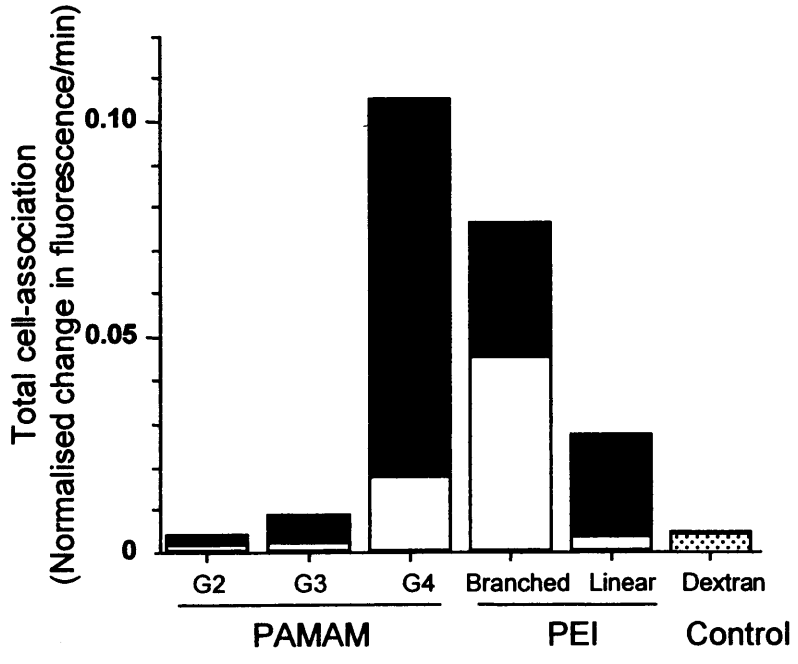

Figure 5.27 Estimated rates of cellular association and internalisation of linear, branched and dendritic polycations in B16F10 cells. Height of bars depicts total rate of cellular accumulation of polymers (cell-association at 37 °C). Black portion of bars corresponds to rate of polymer internalisation. For PAMAMs and PEIs the white portion represents the contribution of external binding (cell-association at 4 °C) to total rate of cellular accumulation. For cationic polymers exocytosis was negligible. For dextran white portion estimates the contribution of exocytosis to total rate of cellular accumulation. For dextran, external binding was negligible.

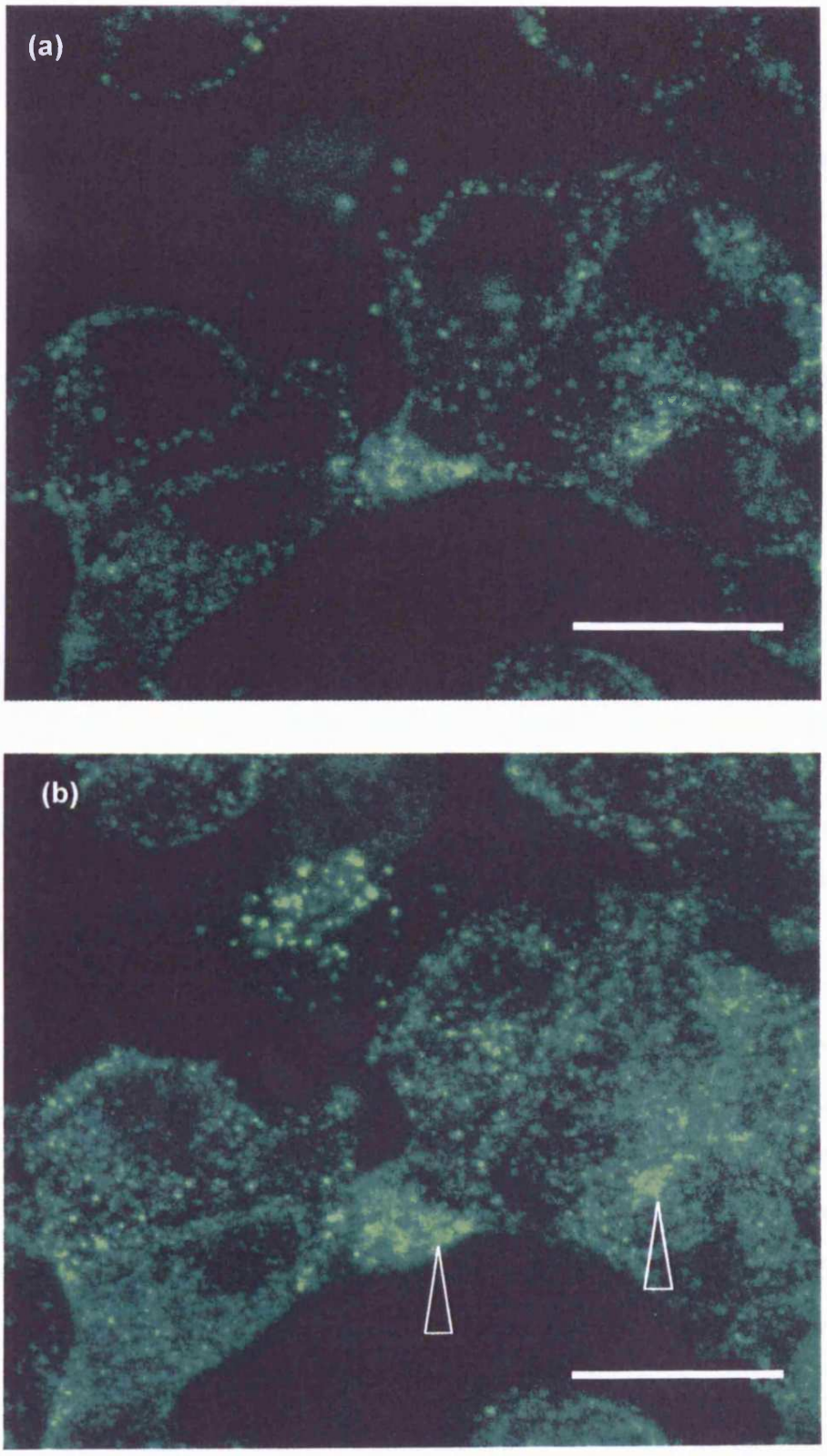

Figure 5.28 Representative confocal images of live B16F10 cells incubated for 1 h with FITC-dextran. Panel (a) single confocal slice, (b) maximum projection of confocal slices (same cells). Arrows point to saturated perinuclear labelling. Scale bar 20 μm.

linear PEI (1 h) showed clear plasma membrane labelling (figure 5.29, panel a) in addition to some vesicular labelling. Maximum projection of fluorescent images of the same set of cells demonstrated vesicular and patched surface labelling (figure 5.29, panel b). Subcellular localisation of branched PEI at 1 h appeared different, with a number of enlarged vesicles with saturated fluorescence (figure 5.30, panel c) and surface binding. B16F10 cells exposed to branched PEI always appeared highly fluorescent. Confocal images of cells incubated with PAMAM G4 for 1 h showed extensive vesicular labelling in addition to low degree surface binding (figure 5.31).

5.3.8 Preliminary studies on the mechanisms of uptake of polymer probes

Comparison between MβCD treated and untreated B16F10 cells incubated with FITC-dextran (1 h) showed a significant reduction (28 %) in the cell-associated fluorescence (figure 5.32). A marginal, but not significant reduction in cell-associated fluorescence was observed following chlorpromazine and wortmannin treatment. B16F10 cells incubated with linear PEI in the presence of MβCD showed a large increase in cell-associated fluorescence (173 %) when compared to control. No significant changes in cell-associated fluorescence were observed following either chlorpromazine or wortmannin treatment when compared to control cells incubated with OG-labelled polymer. For branched PEI, significant reduction (33 %) in cell-associated fluorescence was only evident following MβCD treatment. Marginal, but not significant reduction was seen following chlorpromazine and wortmannin treatment. Inhibitor treated B16F10 cells incubated with PAMAM G4 showed very similar trends observed with branched PEI. For PAMAM G4 a significant reduction (44 %) in cell-associated fluorescence was observed following MβCD treatment when compared to control and only marginal changes when cells were treated with either chlorpromazine or wortmannin.

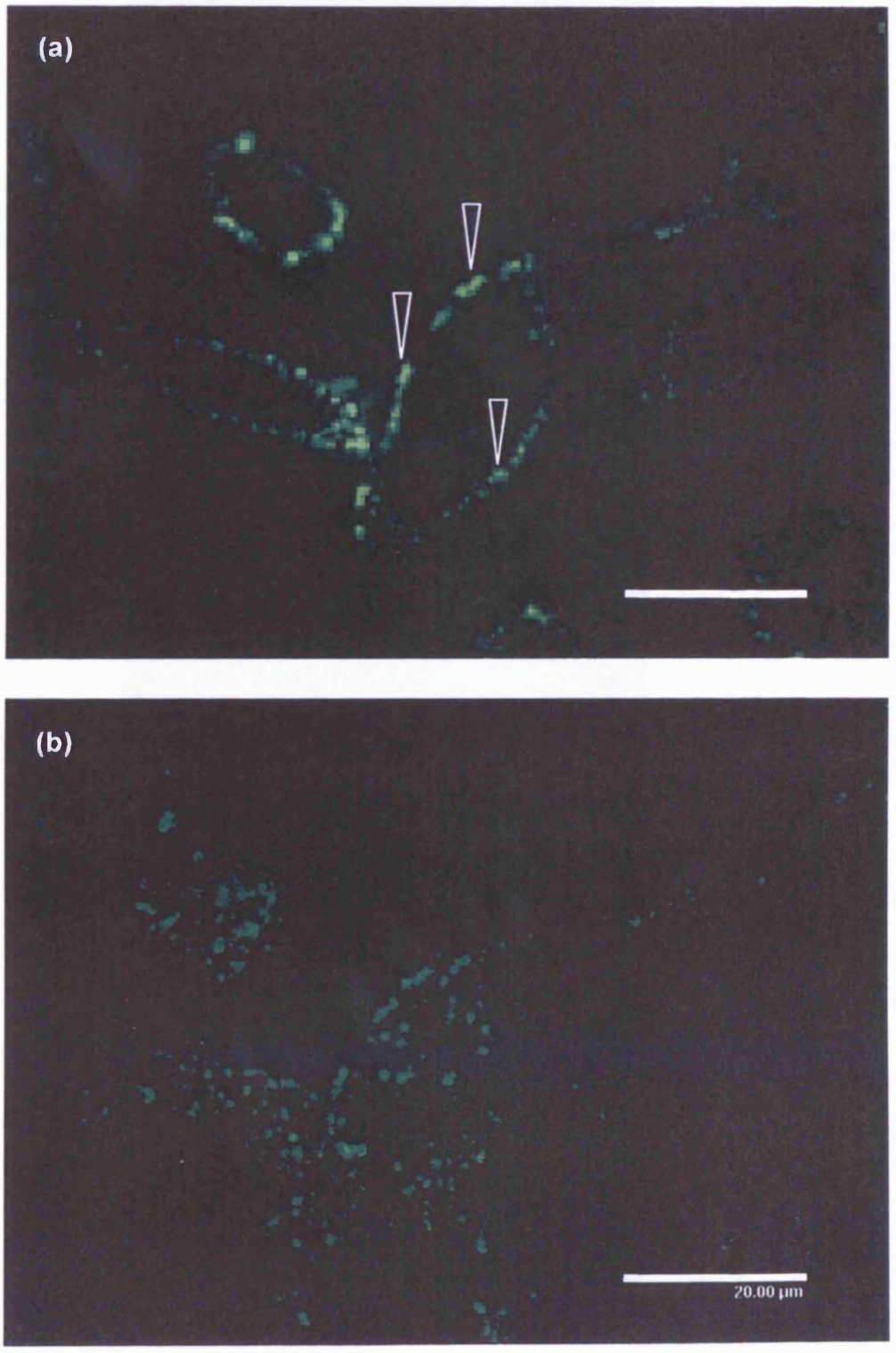

Figure 5.29 Representative confocal images of live B16F10 cells incubated for 1 h with linear OG-PEI. Panel (a) single confocal slice, (b) maximum projection of confocal slices (same cells). Arrows point to characteristic surface binding. Scale bar 20 µm.

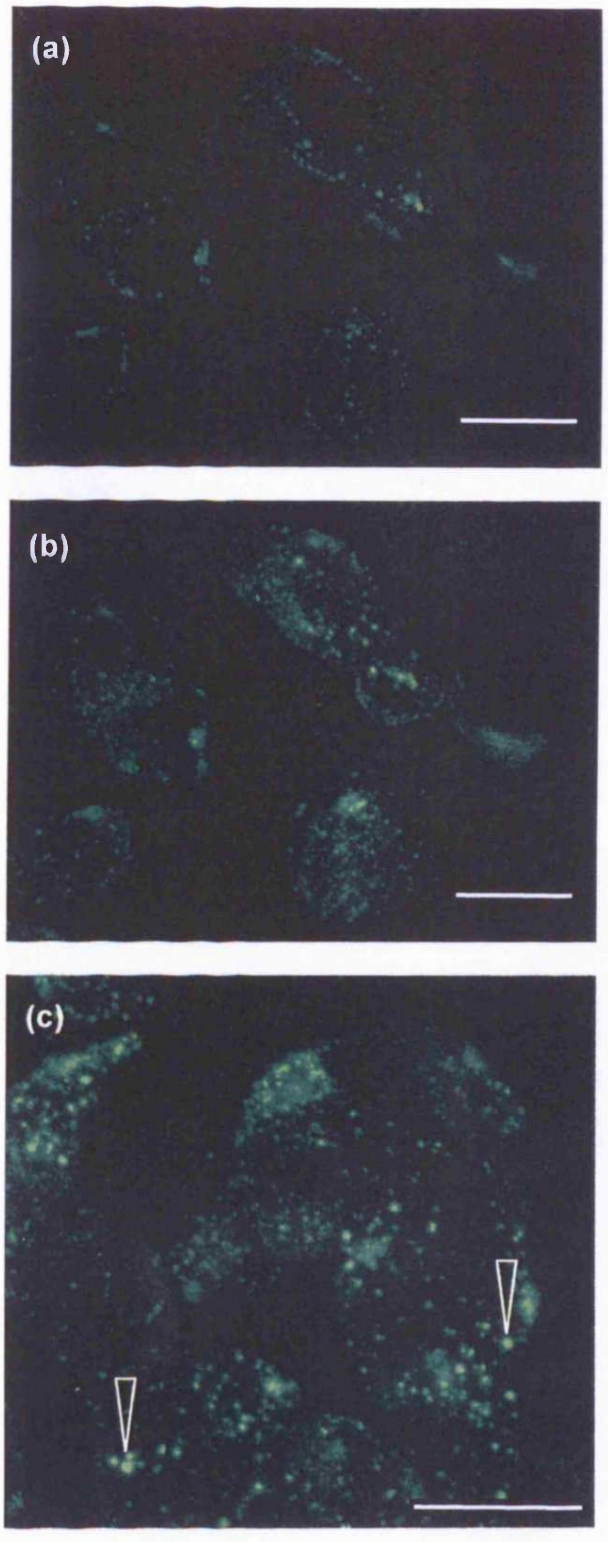

Figure 5.30 Representative confocal images of live B16F10 cells incubated for 1 h with branched OG-PEI. Panel (a) single confocal slice, (b) maximum projection of confocal slices (same cells), (c) maximum projection of confocal slices. Arrows point to swollen vesicular structures. Scale bar 20 μm.

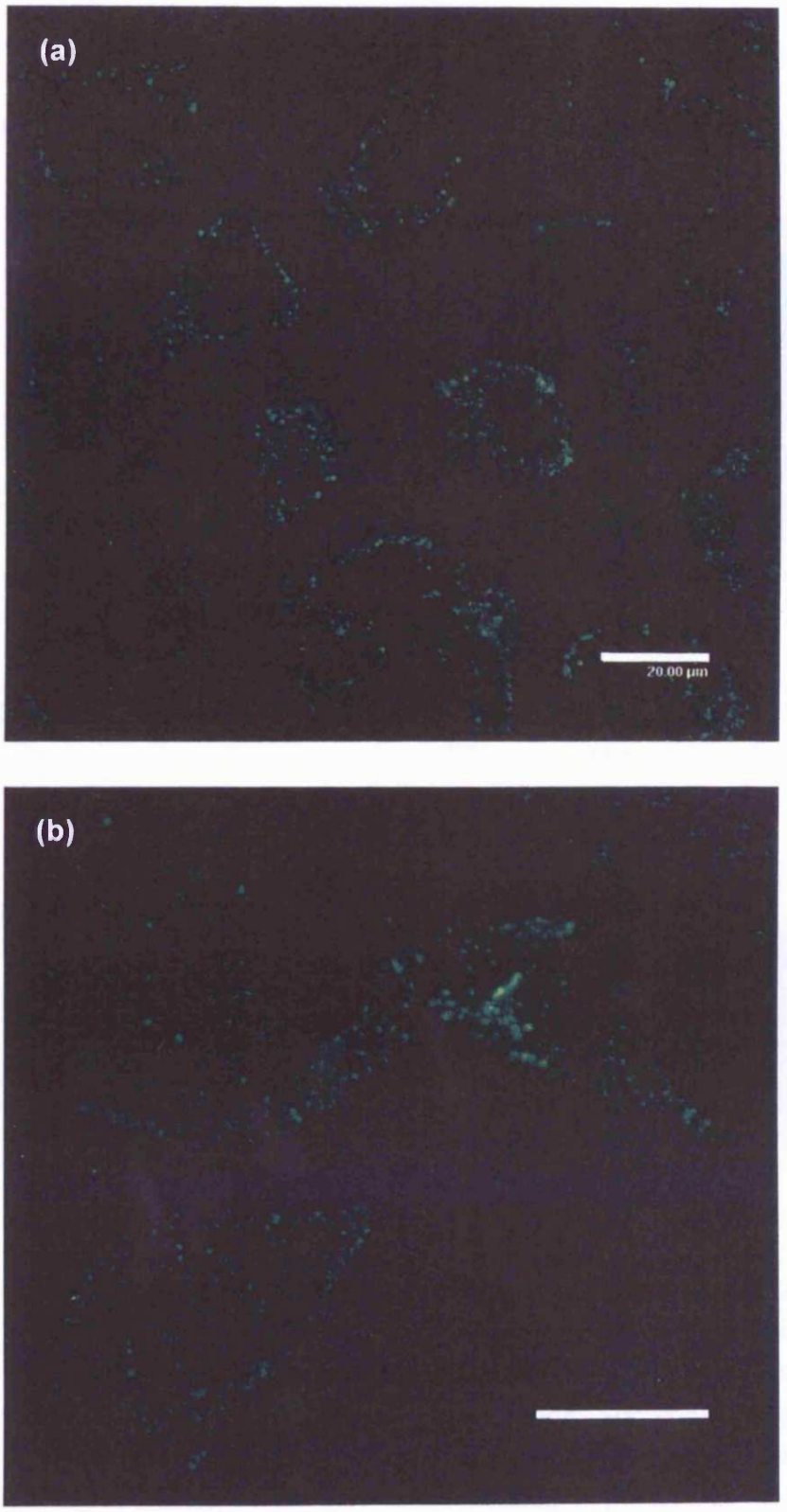

Figure 5.31 Representative confocal images of live B16F10 cells incubated for 1 h with OG-PAMAM G4. Panel (a) single confocal slice, (b) maximum projection of confocal slices. Scale bar 20 µm.

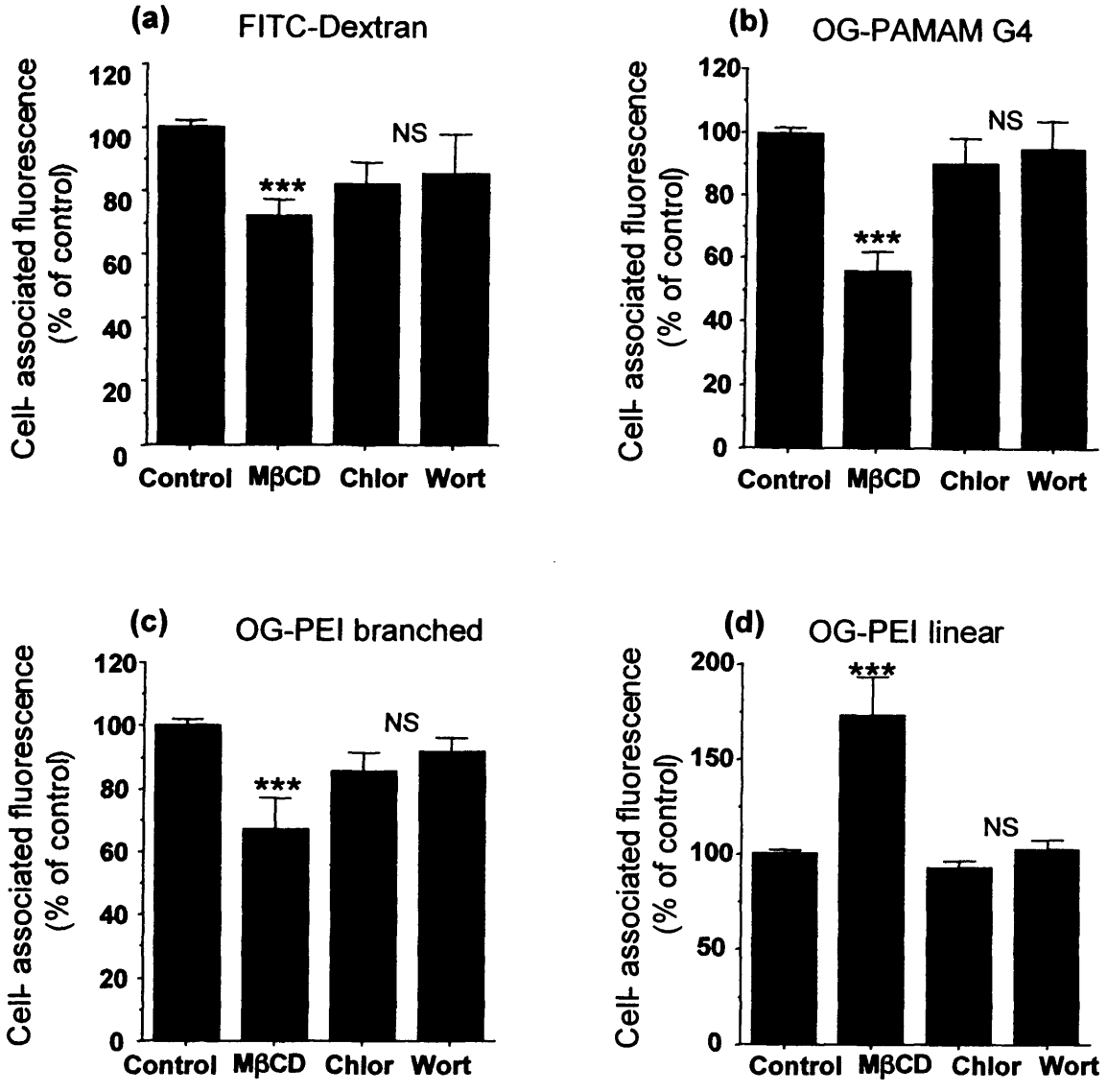

Figure 5.32 Effect of pinocytosis inhibitors on accumulation of fluorescently labelled polymers at 37 °C for 1 h. Results are expressed relative to cell-associated fluorescence in absence of pinocytosis inhibitor. Key: MβCD = methyl-β-cyclodextrin, Chlor = chlorpromazine, Wort = wortmannin. Statistical differences between control and treatment groups were determined at $p \leq 0.1$ - $p \leq 0.01$ (***) using one-way ANOVA and Bonferroni post hoc test. (Data represents mean ± SEM n=4 except wortmannin treatment groups where n=3).

5.4 Discussion

5.4.1 Preliminary characterisation of polymers

Many studies fail to verify the structure and purity of the probes they use in such trafficking experiments (Godbey et al., 1999a). Although it was not possible to use an absolute method, the Mws of all polymers were reasonably consistent with the figures supplied by the manufacturer. The discrepancies could be attributable to the use of chemically different calibration standards to samples. Although the polydispersity of PAMAMs was higher than might be predicted if they were monodisperse, band broadening during GPC analysis could be a contributing factor (Tomalia & Durst, 1993). Characterisation of PAMAM dendrimers by NMR and spectrophotometric assays suggested a defined topology for PAMAMs. For PAMAM G4 experimentally determined results deviated most from expected values. However, experimental errors could be responsible since generation-dependent defects are low for PAMAM G4 (Tomalia et al., 1990), and no obvious degradation products could be seen by GPC (Tang et al., 1996). Likewise for spectrophotometric tests, both branch back-folding and surface crowding (Tomalia et al., 1990) could possibly account for the observations made. Analysis of PEIs by NMR and spectrophotometric methods showed deviations from the predicted structure (Dermer & Ham, 1969) with similar results reported previously (Pierre & Geckle, 1985; Von Harpe et al., 2000).

5.4.2 Synthesis and characterisation of fluorescently labelled polymers

Bicarbonate is recommended by the manufacturer for labelling of proteins with OG (Haugland, 2002), however the use of an aqueous solvent causes hydrolysis of the activated ester reducing reaction yield. Therefore MeOH was used due to good OG-SE/polymer solubility and reduced ester hydrolysis. Reaction conditions were selected to achieve a statistical functionalisation of 1 polymer per OG molecule to minimise possible fluorophore-associated trafficking events (Yoo et al., 1999). It was considered important to estimate OG loading to determine reaction yield and amount of free fluorophore. For all polymers adequate labelling was achieved (lowest yield

50 %) with minimal amounts of free fluorophore (< 1 %) ensuring reliable detection of polymers *in vitro* (table 5.5).

Few studies using fluorescently labelled polymers provide details on the fluorescence characteristics of the conjugates. For all conjugates emission maxima resembled that of the native dye (Haugland, 2002). For FITC-dextran pH-dependent fluorescence was observed (in good agreement with the literature). However, following the conjugation of OG to cationic polymers fluorescence characteristics with respect to pH was somewhat less predictable. It would appear that in part the extent of protonation and buffer composition affected fluorescence. This could be expected since protonation of polymeric amines was affected over the tested pH range (pKa ~ 3.6, ~ 9.7 for 3° and 1° amines respectively) (Suh et al., 1994; Tomalia et al., 1985). Changes in the fluorophore microenvironment due to protonation and buffer composition would be expected to affect fluorescence output, with similar observations reported previously (Xyloyiannis, 2004). Although fluorescence output for all OG-polymer conjugates was affected by changes in pH and/or buffer composition, differences were 4 fold at the most. Therefore comparisons between OG-polymers could be justified.

5.4.3 Cytotoxicity and stability of conjugates in B16F10 cells

Many studies fail to verify the use of non-toxic polymer concentrations when studying cell-association and trafficking (Bieber et al., 2002; Tajarobi et al., 2001). In preliminary cytotoxicity experiments all cationic polymers were cytotoxic with similar observations reported previously for PAMAM dendrimers (Brazeau et al., 1998; Malik et al., 2000; Roberts et al., 1996) and PEIs (Fischer et al., 1999). Therefore polymer concentrations per cell were selected > 40 fold lower than the IC_{50} value. This was qualitatively confirmed with bright-field microscopy due to the absence of polymer-associated toxicity (Godbey et al., 2001). Concentrations of the cationic polymers studied here were also well below the levels required to yield pore

formation in the plasma membrane of viable cells and model bilayers (Hong et al., 2004).

The final study in this series evaluated the stability of selected OG-conjugates, to ensure that only polymer trafficking was monitored. Following the 3 h incubation period free OG was detectable, suggesting that a fraction of fluorophore was released during the incubation period (figure 5.16). The presence of high Mw conjugates after incubation, and the biologically stable amide bond (Banks & Paquette, 1995) between OG and the polymer suggested that free OG originated from unreacted fluorophore. In particular the aromatic ring structure of OG would be expected to permit π-π stacking of free OG with polymer-bound fluorophore, making it difficult to remove during purification. The importance of free fluorophore on cell-associated fluorescence was evaluated with the model compound fluorescein. Studies clearly demonstrated that uptake was passive, and driven by a concentration gradient (figure 5.17). Fluorescein was readily removed during sample preparation. It is therefore reasonable to assume that the presence of small amounts of free OG did not significantly influence observations made in pinocytosis and trafficking studies.

5.4.4 Pinocytosis and exocytosis of fluorescently labelled polymers

Polymers often serve as vectors to achieve selective drug delivery. However, few studies address the basic cellular pharmacokinetics including binding, uptake and exocytosis to provide a biological rationale for their use (Xyloyiannis, 2004). For clarity a diagram of the proposed sequence of events has been included (figure 5.33). Extrapolating the straight line fit for FITC-dextran pinocytosis back to the ordinate, indicated cell-associated fluorescence at time 0 (figure 5.19, panel a). Similar observations for FITC-dextran have been made in other cell lines using flow cytometry (Murphy et al., 1982b; Van Deurs et al., 1984). This "curve-linear" uptake profile, could be due to a number of factors including the progressive accumulation of FITC-dextran in acidic organelles leading to pH and concentration-dependent quenching. However, assays with radioactive labelled probes demonstrated that

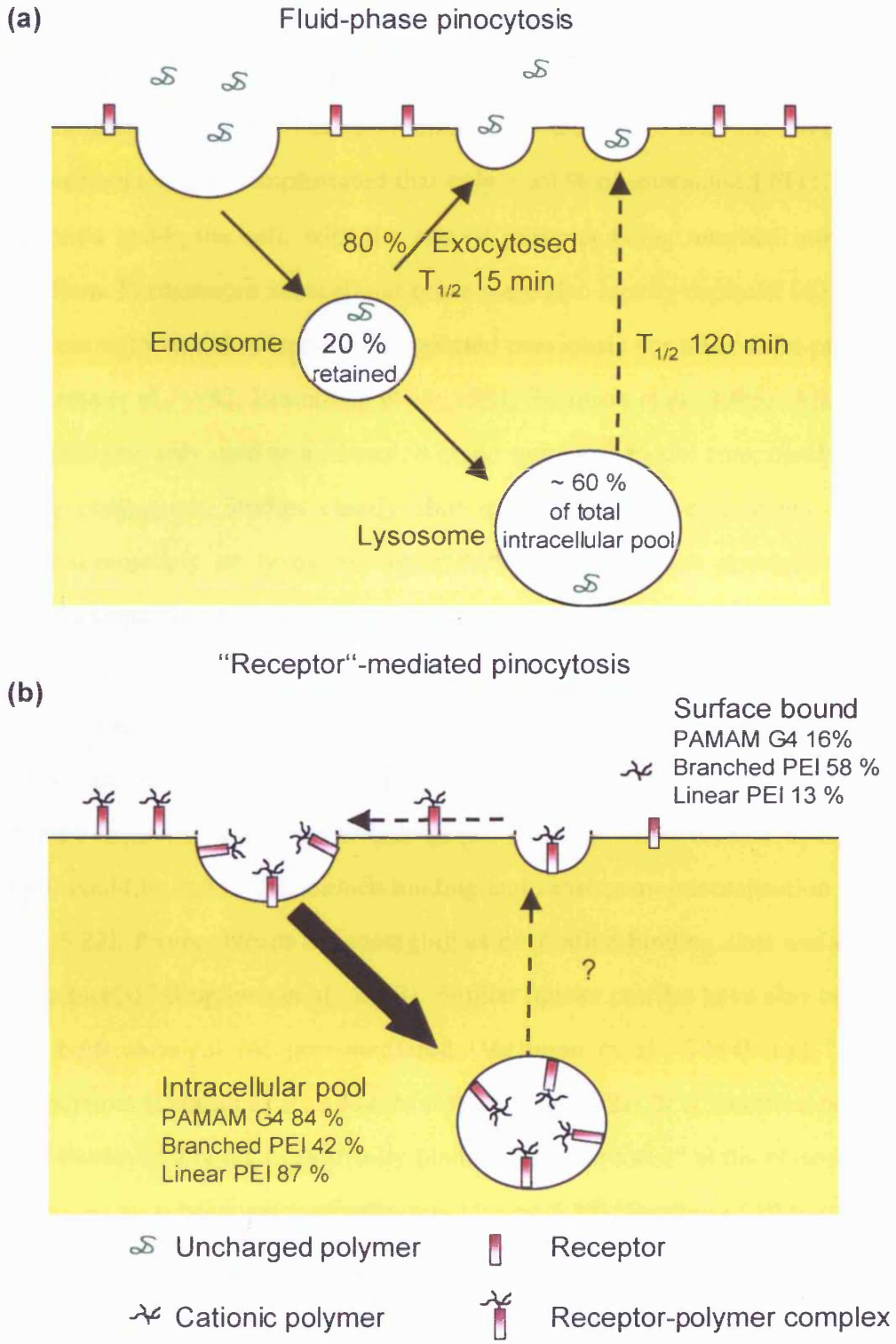

Figure 5.33 Diagram of pinocytosis of linear, branched and dendritic polycations. Panel (a) fluid-phase marker dextran, (b) cationic polymers. Percentages refer to polymer distribution, broke arrows indicate poorly defined pinocytic processes.

cellular accumulation of fluid-phase markers proceeds in a "curve-linear " fashion as the two kinetically distinct processes of pinocytosis and exocytosis reach equilibrium (Besterman et al., 1981; Phaire-Washington et al., 1980). With the aid of exocytosis experiments it was demonstrated that only ~ 20 % of internalised FITC-dextran was retained inside the cell, with the rest of polymer being returned into the culture medium. Furthermore intracellular pools were also rapidly depleted (40 % loss) over 10 min with similar observations reported previously for other fluid-phase markers (Adams et al., 1982; Besterman et al., 1981; Swanson et al., 1985). Although FITC-dextran was only used as a control, it could serve as a model compound for polymer-drug conjugates. Studies clearly showed that polymer conjugates designed for endosomotropic or lysosomotropic delivery could face endogenous "efflux" mechanisms, which minimise cellular accumulation and potentially drug release.

Cell association for both linear and branched PEI was very different from FITC-dextran due to cell surface binding and the absence of PEI release back into the culture medium. The rapid increase in cell associated fluorescence at 37 °C (0 – 10 min) could be due to cell surface binding and subsequent internalisation (figure 5.21 and 5.22). Proteoglycans are emerging as polycation binding sites and could act as "receptor(s)" (Ruponen et al., 2003). Similar uptake profiles have also been reported for both classical receptor-mediated (Mellman et al., 1984) and "adsorptive" pinocytosis (Duncan et al., 1984; Murphy et al., 1982a). It is therefore proposed that PEI displayed a rapid, high affinity binding to "receptor(s)" at the plasma membrane followed by subsequent internalisation (figure 5.33). Binding of PEIs to endosomal membranes has previously been reported (Clamme et al., 2003b) and could explain the absence of exocytosis. However, it is not known if PEI could also participate in recycling while bound to the "receptor(s)". Direct comparisons between linear and branched PEI clearly showed that the rate of internalisation was comparable, although extracellular binding for branched PEI was ~ 5 fold greater. Since the rate of polymer internalisation was significantly greater than for the fluid-phase marker dextran (figure 5.27), it is reasonable to assume that the majority of PEI was

internalised in its bound form. It might therefore be deduced that only a fraction of the occupied binding sites for branched PEI participated in internalisation. However, for linear PEI it might be concluded that the majority of binding sites participated in polymer internalisation. It therefore appears that linear PEI and branched PEI target different binding sites, which were internalised by different routes as shown in figure 5.32. It remains to be seen if additional experiments can confirm this hypothesis.

Fluorescence microscopy of PEI revealed both surface binding and vesicular labelling, corroborating the observations made by flow cytometry. Besides numerous small vesicular structures observed for branched PEI, a number of "enlarged" structures were evident (figure 5.30, panel a). These structures could be endocytic vesicles loaded with PEI experiencing the "proton-sponge effect" (Behr, 1997). Bursting of those vesicles has however not been observed, since it is thought to be a comparatively rare event (Merdan et al., 2001). Linear PEI showed some signs of vesicular labelling, though significantly less than seen for the branched form of PEI. Despite similar fluorescence quantum yields for both forms of PEI, linear PEI appeared to be extensively affected by photo-bleaching during microscopy experiments, possibly leading to poorer vesicular labelling. Nonetheless, overall subcellular distribution appeared different when compared to branched PEI due to distinct, patched plasma membrane labelling with similar observations reported previously in colon carcinoma cells (Wightman et al., 2001).

Both uptake and exocytosis profiles for PAMAM G4 resembled that of linear PEI, and thus also "receptor" binding and internalisation could provide a working model for the observations made (figure 5.24). For PAMAM G4 typical endocytic labelling was evident, with little cell-surface labelling. Similar results have been reported previously with PAMAM G3 (De Long et al., 1997) and PAMAM G4 dendriplexes in human asterocytoma (U251) and HeLa cells respectively. PAMAM G3 and G2 were also investigated in the present study to investigate possible generation-dependent effects. However, only uptake studies were performed since no

exocytosis was observed for any of the other investigated polycations. For PAMAMs G2 and G3 uptake profiles resembled that of PAMAM G4. However, when internalisation rates were compared, generation-dependent uptake was evident (G4 >> G3 > G2) (figure 5.53). The large difference between G4 and G3 (~ 13 fold) could be related to a number of factors including Mw, number of 1° amine groups and transition from an amorphous to a compact globular shape (Rathgeber et al., 2002; Tomalia & Durst, 1993). Comparison of the dendrimers with PEI showed that uptake rates for PAMAM G4 were unprecedented (figure 5.33). A recent study using fluorescently labelled PAMAM G4 (NH_2 surface) and PAMAM G4 (OH surface) also demonstrated high uptake rates into A549 cells (human lung epithelium carcinoma), but considerably slower uptake for hyperbranched polyol (OH surface) (Kannan et al., 2004). It is currently not known which particular feature(s) of PAMAM G4 contributed to this observation. However, it is clear that all cationic polymers showed greater rates of intracellular retention than seen for fluid-phase pinocytosis (figure 5.33).

5.4.5 Preliminary findings on the mechanism of uptake of polymer probes

Increasing awareness of specific cell surface domains interacting with synthetic (Ruponen et al., 2003) and endogenous (Belting et al., 1999) polyamines warranted the use of modulators of pinocytic pathways to investigate the internalisation route of selected polycations. For PAMAM G4, polymer internalisation by B16F10 cells appeared to be in part cholesterol-dependent (44 %) (figure 5.32, panel b). A similar reduction in uptake has been reported for CHO and EA.hy 926 cells (Manunta et al., 2004), however transfection efficiency was reduced by > 90 %. This clearly demonstrated the importance of correct compartmentalisation on therapeutic outcome. Caveolae/raft-mediated uptake routes are attractive due to the neutral pH of caveosomes (Pelkmans et al., 2001), however vesicular escape of the complex by the proposed proton sponge effect (Tang et al., 1996) would be doubtful. For branched PEI only MβCD reduced cellular accumulation significantly (33 %), suggesting that uptake of the polymer is

accomplished predominately by a cholesterol-dependent and clathrin-independent mechanism (figure 5.32, panel c). Similar results have been reported in HeLa cells, where cholesterol depletion with MβCD significantly decreased transfection efficiency (Kopatz et al., 2004). Most surprising were observations made with linear PEI where cholesterol depletion led to a dramatic increase (~ 173 %) in uptake. This is the only example found in the literature where inhibition of a cholesterol-dependent uptake mechanism resulted in increased cellular association of a non-viral vector. Possibly cholesterol depletion up-regulates the intrinsic internalisation route for linear PEI, analogues to the induction of dynamin- and clathrin-independent uptake mechanisms in dynamin mutant HeLa cells (Damke et al., 1995). The proposed different binding sites for branched and linear PEI might explain the differences seen for PEI following MβCD treatment (Belting et al., 2003).

Findings for the mechanism of polycation internalisation should only be regarded as preliminary results. Although inhibitor concentrations and assay procedures were based on published methods, careful tailoring to each cell type is recommended. Thus a number of additional experiments would complement the study by assessing, (a) effect of inhibitors on known ligands such as transferrin, (b) cell-viability following inhibitor treatment, (c) 4 °C binding studies ± inhibitor. Although inhibitors are often portrayed to block specific uptake routes, they are likely to exert a plethora of unwanted effects (e.g. inhibition of endosome fusion) (Clague et al., 1995; Jones et al., 1998). Studies wishing to address the route of polymer internalisation should therefore use a combination of techniques to minimise artefacts.

5.5 Conclusions

All cationic polymers were internalised by "adsorptive" pinocytosis with a maximum rate of internalisation for PAMAM G4, followed by linear and branched PEI achieving 27 % and 36 % of the maximum respectively. Overall extent of extracellular binding was highest for branched PEI accounting for > 50 % of total

cell association and only 13 % for linear PEI. For all dendrimers extracellular binding was 16 – 26 % of the total (G2 > G3 > G4). All cationic polymers lacked significant exocytosis. It appeared that PAMAM G4 was the ideal polymer to maximise intracellular drug delivery with an uptake rate > 130 fold of typical fluid-phase pinocytosis. The extensive exocytosis/recycling of the fluid-phase marker dextran minimised lysosomal accumulation, and could indicate the shortfalls of non-targeted polymer-drug conjugates designed for lysosomotropic delivery. For polycations the interaction with specific membrane component(s) seemed to regulate their cellular uptake mechanisms. Whereas PAMAM G4 and branched PEI were predominately internalised by cholesterol-dependent pathways, internalisation of linear PEI appeared to be independent of clathrin and cholesterol.

Chapter 6

General Discussion

6.1 General Discussion

Critical evaluation of the present study: contribution to science

It is believed that this is the first study to investigate the intracellular trafficking of polymer therapeutics in B16F10 cells by subcellular fractionation. The established quantitative fractionation method in B16F10 cells allowed separation of the major cellular components and thus provides a convenient way to quantify the subcellular distribution of polymer therapeutics (Chapter 3). The present study also addressed some of the fundamental issues such as breakage efficiency and enzyme kinetics (Seib et al., 2003). These elements ensured that distribution patterns of markers and polymer therapeutics were representative for the entire cell population. All recent studies aimed at quantifying the subcellular distribution of polymer therapeutics fail to address these fundamental issues (Nori et al., 2003a; Nori et al., 2003b; Tijerina et al., 2001; Tijerina et al., 2003). Use of polymer-bound and free doxorubicin clearly demonstrated the suitability of the fractionation method to monitor lysosomotropic drug delivery of a clinically relevant anticancer drug conjugate (Chapter 4).

It is interesting to discuss some of the limitations of this subcellular fractionation procedure and opportunities for further developments. It is not possible to differentiate between different endocytic compartments such as EE, LE, and ERC. Since differential centrifugation relies on sufficiently large differences in sedimentation coefficients for separation, a satisfactory separation of the above mentioned organelles can only be achieved with more elaborate centrifugation methods such as gradient centrifugation (Hinton & Mullock, 1993). However, the fractionation procedure can serve as a tool to assess endosomotropic or lysosomotropic delivery since excellent separation of endocytic organelles from the cytosol was accomplished.

At the outset of this PhD it was clear that quantitative methods are needed to define the pinocytic and intracellular trafficking properties of polymers to provide a

biological rationale for the design of second-generation polymer therapeutics. Whilst others have begun to examine pinocytosis and intracellular trafficking of cationic non-viral vectors (table 6.1), it is believed that the adopted methodology of the present study is unique (Chapter 5). It provided the opportunity to compare directly linear, branched and dendritic polycations by monitoring binding, uptake and exocytosis over time. PAMAM G4 appeared to take a special role due to highest rates of internalisation of all investigated polymers (Seib et al., 2004). Recent evidence from a number of other studies with dendrimers also indicated increased cell accumulation (summarised in table 6.1). Taken together with the early reports describing endocytic rates substantially higher for PAMAM dendrimers than for linear, random coil polymers (Wiwattanapatapee et al., 2000), it could be tempting to propose increased uptake for optimised dendritic polymers. It remains to be seen if such generalisation can ever be made.

However, it is interesting to examine some of the challenges associated with the study. Pinocytic properties reported here for polycations have only been studied in B16F10 cells and it is not known if similar observations could be made in other cell types. Furthermore for direct comparisons between polymers, polycations studied here have not been complexed with DNA since only ~ 14 % of polycations are complexed with DNA at commonly used nitrogen-phosphate ratios (Clamme et al., 2003a). Similar simplifications have been applied to studies addressing the influence of non-viral vector size on route of internalisation, where latex beads have been employed as a model for lipoplexes (Rejman et al., 2004). It remains to be seen how well these model systems can predict pinocytosis of non-viral vectors. Polymers were labelled with OG to characterise their pinocytic properties in B16F10 cells by flow cytometry. Although OG can function as a model drug, addition of a hydrophobic molecule can alter polymer conformation in solution. Thus strict reference to the idealised polymeric conformation could be misleading, and possible fluorophore-induced trafficking events can not be ruled out. However, it is worth reiterating that labelling efficiencies for cationic polymers were comparable,

Table 6.1 Recent examples of dendrimer-based drug delivery: transport and subcellular distribution

Polymer	Model system	Probe	Methodology used	Findings	Comment	Reference
PAMAM G0 – 4-NH_2	Madin-Darby canine kidney (MDCK)	Indirect measurements by examining transport of paracellular marker ^{14}C-mannitol	Monolayers (transwells)	Generation-dependent transport reported as G4>>G1 ≈ G0 >G3 >G2.	Does not address possible toxicity-related effects.	(Tajarobi et al., 2001)
PAMAM G0 – 4-NH_2	CaCo-2	^{14}C-Mannitol transepithelial resistance (TEER)	Monolayers (transwells)	G0 – G2 showed time and concentration-dependent transport. Viability of cells reduced at 10 mM at >150 min for G3 – G4.	No generation-dependent transport observed as reported previously.	(El-Sayed et al., 2002)

Table 6.1 Continued

Polymer	Model system	Probe	Methodology used	Findings	Comment	Reference
1, 2 and 4 arm star PEG with G1 or G4 poly(ester) dendron	ECV304 (Endothelial-like cell)	OG	Flow cytometry epifluorescence microscopy	Measurement of endo- and exocytosis rates appeared to be topology-dependent with high intracellular retention for more linear PEG dendrons. High exocytosis rates were observed for the more branched dendrons.	Comprehensive study examined cellular pharmacokinetics. Determined rates, however can not be related to literature as they are fluorescence-based.	(Xyloyiannis, 2004; Xyloyiannis et al., 2003)
PAMAM G3 optional surface modification with ~ 9 lauroyl chains	CaCo-2	FITC Gold	Confocal microscopy flow cytometry monolayers (transwells) electron microscopy	Internalisation and low levels of binding reported for both dendrimers. Localisation of gold labelled dendrimers in endocytic vesicles only.	Previous reports on paracellular transport for these dendrimers not confirmed.	(Jevprasesphant et al., 2004)

Table 6.1 Continued

Polymer	Model system	Probe	Methodology used	Findings	Comment	Reference
PAMAM G4-NH_2 PAMAM G4-OH PAMAM G3 surface modified with ~ 32 PEG_{2000} chains hyperbranched polyol (Perstorp)	A549	FITC	Flow cytometry	Cellular uptake PAMAM G4-NH_2 ≈ PAMAM G4-OH > polyol > PAMAM G3 PEG_{2000}	No data on external binding. Comparison done at different molar concentrations. Does not address possible Mw effects	(Kannan et al., 2004)
Conjugation of propranolol to PAMAM G3 +/- lauroyl chains	CaCo-2	^{14}C-Mannitol permeability TEER	Monolayers (transwells)	Evidence for modified dendrimers to enhance transcellular transport and to overcome drug resistance mechanisms.	Previous reports on paracellular transport for these dendrimers not confirmed.	(D'Emanuele et al., 2004)
Star polymer containing 9 arms of 21-mer antisense ONDs	A431 and U87-MG cells	^{32}P, FITC	Epifluorescence microscopy flow cytometry	Star polymers increased cell-association 100 fold compared to fluid-phase marker. Star polymers showed surface binding and vesicular labelling.	Activity retained despite covalent attachment of ONDs to core.	(Hussain et al., 2004)

and comparisons between polymers were normalised to account for variable fluorescence output (Chapter 5). Furthermore, no attempts were made to calculate absolute cellular levels of polymers. Although fluorescent tags were used in the present study for the reasons detailed in Chapter 5, there are a number of disadvantages associated with their use. Most importantly, the difficulty to provide absolute values when used in biological systems. Therefore endocytic rates determined here could not be compared to literature values typically employing radioisotopes.

Most recent developments: challenges for the field of polymer therapeutics

It has long been recognised that the development of polymer therapeutics requires a multi-disciplinary approach (Duncan & Kopecek, 1984) using polymer chemistry and cell biology. Since the start of this PhD a number of significant advances have been reported in these areas, which are briefly discussed, summarised (table 6.1) and related to the work presented in this thesis.

During the course of these PhD studies, others have begun to investigate the particular extracellular binding sites that interact with polycations and the mechanisms of polymer internalisation. As previously mentioned (section 1.2.1), GAGs have been identified as the main polyplex binding sites, and the presence of GAGs has been positively correlated to gene expression (Belting & Petersson, 1999; Kopatz et al., 2004; Mislick & Bladeschwieler, 1996). However, this process appears to be more complex than first proposed (Lampela et al., 2004; Ruponen et al., 2004). The abundance of specific sub-populations of GAGs present in different cells dictates the success of polyplex-lead transfection. Evidence from experiments investigating the importance of proteoglycan subclasses points towards different uptake routes. Binding to syndecan-1 has been associated with caveolae-mediated uptake (Fuki et al., 2000), yet binding to syndecan-4 leads to internalisation by a caveolin-independent mechanism (Tkachenko & Simons, 2002). These observations could in part explain differences in transfection seen in different cell types. Viruses

can use specific plasma membrane-associated GAGs to control cell entry (Bomsel & Alfsen, 2003) and thus might serve as an inspiration for the design of improved polymeric vectors. Evidence for PAMAM binding to membrane associated GAGs (Sakharov et al., 2003) and "raft"-dependent internalisation of "fractured" PAMAM-DNA complexes (Manunta et al., 2004) already suggests that some polymers act as viral biomimetics. Preliminary results from the current study indicated extracellular binding and internalisation via a "raft"-dependent pathway for PAMAM G4 and branched PEI (Chapter 5) but not for linear PEI, possibly indicate the involvement of different binding sites. It remains to be seen if specific binding sites can be identified and targeted by polymer therapeutics.

"Raft''-dependent uptake route is only one emerging pathway for polymer therapeutics. Although macropinocytosis is regarded as a highly cell type-dependent pinocytic mechanism, uptake of the human immunodeficiency virus (HIV) derived trans-activating factor (TAT) (Wadia et al., 2004) has been attributed to this pathway. It remains to be seen if TAT functionalised polymer therapeutics (Nori et al., 2003b) are also internalised via this route. In the present study macropinocytosis did not appear to regulate uptake of selected cationic polymers by B16F10 cells, though cellular accumulation of lysine-based polyplexes by Hep G2 cells (Goncalves et al., 2004) has partially been attributed to macropinocytosis.

However, targeting a specific uptake route into cells is only one challenge. For instance, recent evidence suggests that CEs and EEs communicate by transient fusion, which allows for the shuttling of cargo from CEs to EEs due to specific cues, such as low pH. More specifically, SV40 and cholera toxin internalised by caveolae-dependent pathway are sorted from CEs, due to selective release and transfer of the toxin to EEs, but the retention of SV40 in CEs (Pelkmans et al., 2004). So the challenge for the field of polymer therapeutics is not only to target the desired route of internalisation but also to ensure the correct routing following internalisation.

Future studies

At the outset of this project it was hoped to select a cationic polymer with a favourable cellular pharmacokinetic profile and to subject it to subcellular fractionation studies to provide quantitative data on the intracellular distribution. Following the careful evaluation and optimisation of the fractionation method and the promising cellular kinetics of PAMAM G4 this goal could now be easily achieved. Reported differences in cellular pharmacokinetics, and preliminary results on the route of internalisation for cationic polymers, warrants further studies into the underlying cellular mechanisms of binding and uptake to help the design of improved polymeric vectors. It is clear from the results presented in this thesis that the subcellular fractionation method can be used in a range of studies wishing to address the intracellular trafficking of polymer therapeutics in a quantitative way. Possible applications of the method are summarised in figure 6.1.

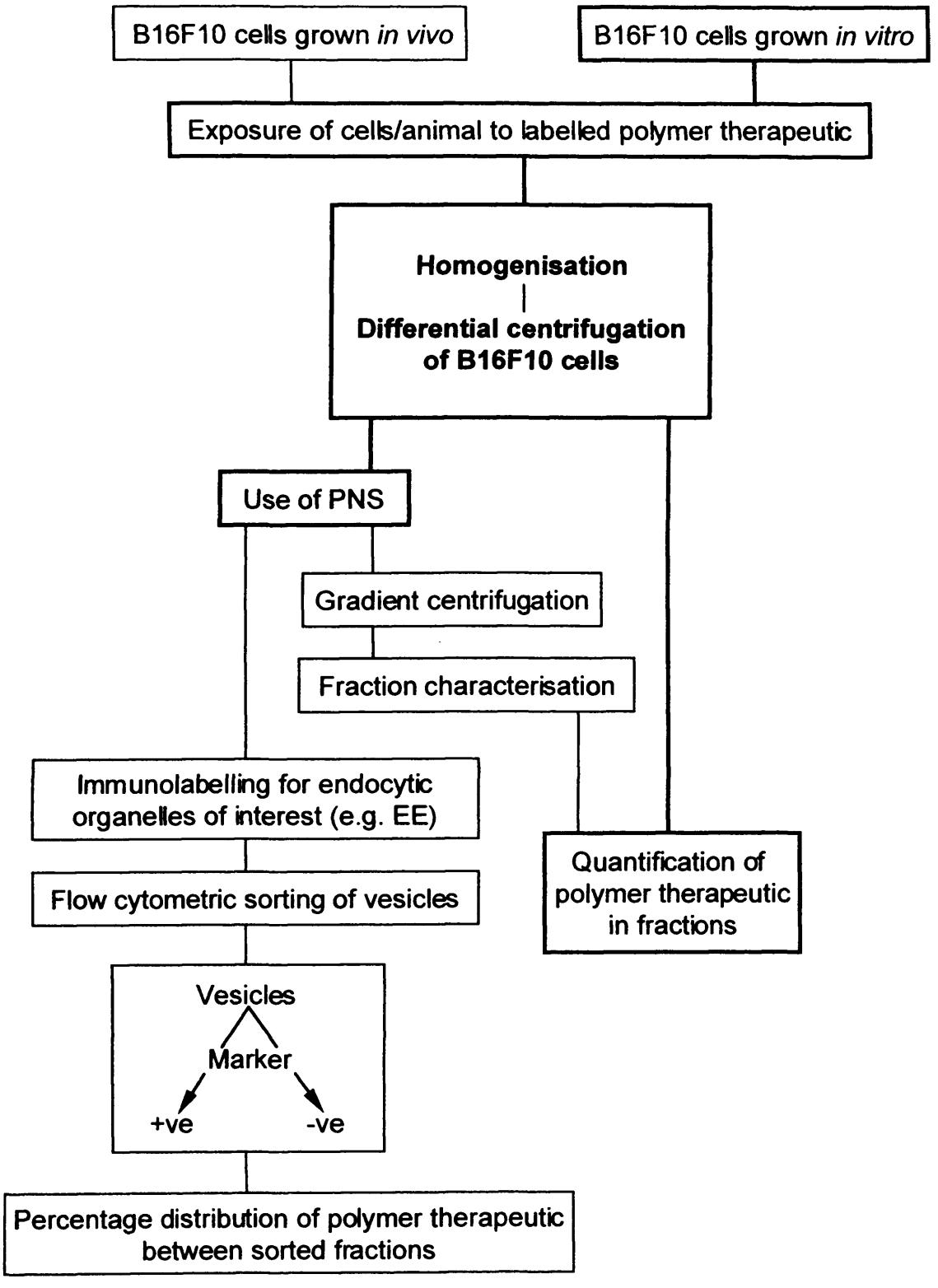

Figure 6.1 Possible applications of subcellular fractionation to trace the intracellular path of polymer therapeutics. Established methods are shown in bold.

References

Aboud-Pirak, E., Sergent, T., Otte-Slachmuylder, C., Abarca, J., Trouet, A. & Schneider, Y.J. (1988). Binding and endocytosis of monoclonal antibody to high molecular weight human milk fat globule membrane-associated antigen by cultured MCF-7 breast carcinoma cells. *Cancer Research*, **48,** 3188-3196.

Adams, C.J., Maurey, K.M. & Storrie, B. (1982). Exocytosis of pinocytic contents by Chinese hamster ovary cells. *Journal of Cell Biology*, **93,** 632-637.

Aguilar, R.C. & Wendland, B. (2005). Endocytosis of membrane receptors: two pathways are better than one. *Proceedings of the National Academy of Sciences of the United States of America*, **102,** 2679-2680.

Ahmed, N.K. (1985). Daunorubicin reductase activity in human normal lymphocytes, myeloblasts and leukaemic cell lines. *European Journal of Cancer and Clinical Oncology*, **21,** 1209-1213.

Akinc, A. & Langer, R. (2002). Measuring the pH environment of DNA delivered using non-viral vectors: implications for lysosomal trafficking. *Biotechnology and Bioengineering*, **78,** 503-508.

Amar-Costesec, A., Beaufay, H., Wibo, M., Thines-Sempoux, D., Feytmans, E., Robbi, M. & Berthet, J. (1974a). Analytical study of microsomes and isolated subcellular membranes from rat liver. II Preparation and composition of the microsomal fraction. *Journal of Cell Biology*, **61,** 201-212.

Amar-Costesec, A., Wibo, M., Thines-Sempoux, D., Beaufay, H. & Berthet, J. (1974b). Analytical study of microsomes and isolated subcellular membranes from rat liver. IV Biochemical, physical and morphological modifications of microsomal components induced by digitonin, EDTA and pyrophosphate. *Journal of Cell Biology*, **62,** 717-745.

Anderson, R.G. & Jacobson, K.A. (2002). A role for lipid shells in targeting proteins to caveolae, rafts, and other lipid domains. *Science*, **296,** 1821-1825.

Anderson, R.G.W., Brown, M.S. & Goldstein, J.L. (1977). Role of the coated endocytic vesicle in the uptake of receptor-bound low density lipoprotein in human fibroblasts. *Cell*, **10,** 351-364.

Apodaca, G. (2001). Endocytic traffic in polarised epithelial cells: role of the actin and microtubule cytoskeleton. *Traffic*, **2,** 149-159.

Appelmans, F., Wattiaux, R. & de Duve, C. (1955). Tissue fractionation studies. 5. The association of acid phosphatase with a special class of cytoplasmic granules in rat liver. *Biochemical Journal*, **59,** 438-445.

Araki, N., Johnson, M.T. & Swanson, J.A. (1996). A role for phosphoinositide 3-kinase in the completion of macropinocytosis and phagocytosis by macrophages. *Journal of Cell Biology*, **135,** 1249-1260.

Aulenta, F., Hayes, W. & Rannard, S. (2003). Dendrimers: a new class of nanoscopic containers and delivery devices. *European Polymer Journal*, **39,** 1741-1771.

Avruch, J. & Hoelzl Wallach, D.F. (1971). Preparation and properties of plasma membrane and endoplasmic reticulum fragments from isolated rat fat cells. *Biochimica et Biophysica Acta*, **233,** 334-347.

Bachur, N.R., Moore, A.L., Bernstein, J.G. & Liu, A. (1970). Tissue distribution and disposition of daunomycin (NSC-82151) in mice: fluorometric and isotopic methods. *Cancer Chemotherapy Reports*, **54,** 89-94.

Bainton, D.F. (1981). The discovery of lysosomes. *Journal of Cell Biology*, **91,** 66S-76S.

Banks, P.R. & Paquette, D.M. (1995). Comparison of three common amine reactive fluorescent probes used for the conjugation to biomolecules by capillary zone electrophoresis. *Bioconjugate Chemistry*, **6,** 447-458.

Baroja, A., de la Hoz, C., Alvarez, A., Vielba, R., Sarrat, R., Arechaga, J. & de Gandarias, J.M. (1998). Polyploidisation and exit from cell cycle as mechanisms of cultured melanoma cell resistance to methotrexate. *Life Sciences*, **62,** 2275-2282.

Beaufay, H., Amar-Costesec, A., Thines-Sempoux, D., Wibo, M., Robbi, M. & Berthet, J. (1974). Analytical study of microsomes and isolated subcellular membranes from rat liver. III. Subfractionation of microsomal fraction by isopycninc and differential centrifugation in density gradients. *Journal of Cell Biology*, **61,** 213-231.

Beaufay, H., Jaques, P., Baudhuin, P., Sellinger, O.Z., Berthet, J. & De Duve, C. (1964). Tissue fractionation studies. 18. Resolution of mitochondrial fractions from rat liver in three distinct populations of cytoplasmic particles by means of density equilibration in various gradients. *Biochemical Journal*, **92,** 184-205.

Behr, J.-P. (1993). Synthetic gene-transfer vectors. *Accounts of Chemical Research*, **26,** 274-278.

Behr, J.-P. (1994). Gene transfer with synthetic cationic amphiphiles: Prospects for gene therapy. *Bioconjugate Chemistry*, **5,** 382-389.

Behr, J.-P. (1997). The proton sponge: a trick to enter cells the viruses did not exploit. *Chimia*, **51,** 34-36.

Behr, J.-P. (2004). PEI's as non-viral vectors for gene delivery- progress towards clinical evaluation. *Proceedings of the 6th International Conference on Polymer Therapeutics: From Laboratory to Clinical Practice, Cardiff*, 12.

Belting, M., Mani, K., Jönsson, M., Cheng, F., Sandgren, S., Jonsson, S., Ding, K., Delcros, J.-G. & Fransson, L.-A. (2003). Glypican-1 is a vehicle for polyamine uptake in mammalian cells. *Journal of Biological Chemistry*, **278,** 47181-47189.

Belting, M., Persson, S. & Fransson, L.-A. (1999). Proteoglycan involvement in polyamine uptake. *Biochemical Journal*, **338,** 317-323.

Belting, M. & Petersson, P. (1999). Protective role of proteoglycans against cationic lipid cytotoxicity allowing optimal transfection efficiency in vitro. *Biochemical Journal*, **342,** 281-286.

Bernfield, M., Kokenyesi, R., Kato, M., Hinkens, M.T., Spring, J., Gallo, R.L. & Lose, E.J. (1992). Biology of the syndecans: a family of transmembrane heparan-sulfate proteoglycans. *Annual Reviews of Cell Biology*, **8,** 365-393.

Bernstein, D.I., Stanberry, L.R., Sacks, S., Ayisi, N.K., Gong, Y.H., Ireland, J., Mumper, R.J., Holan, G., Matthews, B., McCarthy, T. & Bourne, N. (2003). Evaluation of unformulated and formulated dendrimer-based microbicide candidates in mouse and guinea pig models of genital herpes. *Antimicrobial Agents and Chemotherapy*, **47,** 3784-3788.

Berthiaume, E.P., Medina, C. & Swanson, B. (1995). Molecular size-fractionation during endocytosis in macrophages. *Journal of Cell Biology*, **129,** 989-998.

Besterman, J.M., Airhart, J.A., Woodworth, R.C. & Low, R.B. (1981). Exocytosis of pinocytosed fluid in cultured cells: kinetic evidence for rapid turnover and compartmentation. *Journal of Cell Biology*, **91,** 716-727.

Besterman, J.M. & Low, R.B. (1983). Endocytosis: a review of mechanisms and plasma membrane dynamics. *Biochemical Journal*, **210,** 1-13.

Bhatnagar, V., Anjaiah, S., Puri, N., Darshanam, B.N.A. & Ramaiah, A. (1993). pH of melanosomes of B16 murine melanoma is acidic: its physiological importance in the regulation of melanin biosynthesis. *Archives of Biochemistry and Biophysics*, **307,** 183-192.

Bhuyan, B.K., McGovren, J.P. & Crampton, S.L. (1981). Intracellular uptake of 7-con-O-methylnogarol and adriamycin by cells in culture and its relationship to cell survival. *Cancer Research*, **41,** 882-887.

Bickel, U., Yoshikawa, T. & Pardridge, W.M. (2001). Delivery of peptides and proteins through the blood-brain barrier. *Advanced Drug Delivery Reviews*, **46,** 247-279.

Bieber, T., Meissner, W., Kostin, S., Niemann, A. & Elsässer, H.-P. (2002). Intracellular route and transcriptional competence of polyethylenimine-DNA complexes. *Journal of Controlled Release*, **82,** 441-454.

Blanchard, J.C., Schneider, Y.J., Baurain, R. & Trouet, A. (1981). Accumulation, metabolism and subcellular localisation of daunorubicin, doxorubicin and their DNA-complexes in rat heart ventricles. *European Journal of Cancer*, **17,** 297-305.

Blott, E.J. & Griffiths, G.M. (2002). Secretory lysosomes. *Nature Reviews Molecular Cell Biology*, **3,** 122-131.

Bomsel, M. & Alfsen, A. (2003). Entry of viruses through the epithelial barrier: pathogenic trickery. *Nature Reviews Molecular Cell Biology*, **4,** 57-68.

Bosman, A.W., Janssen, H.M. & Meijer, E.W. (1999). About dendrimers: structure, physical properties, and applications. *Chemical Reviews*, **99,** 1665-1688.

Boussif, O., Lezoualc'H, F., Zanta, M.A., Mergny, M.D., Scherman, D., Demeneix, B. & Behr, J.-P. (1995). A versatile vector for gene and oligonucleotide transfer into cells in culture and *in vivo*: Polyethylenimine. *Proceedings of the National Academy of Sciences of the United States of America*, **92,** 7297-7301.

Brazeau, G.A., Attia, S., Poxon, S. & Hughes, J.A. (1998). *In vitro* myotoxicity of selected macromolecules used in non-viral gene delivery. *Pharmaceutical Research*, **15,** 680-684.

Bretaudiere, J.-P. & Spillman, T. (1984). Alkaline phosphates. In *Methods of Enzymatic Analysis*, Bergmeyer, H.U., Bergmeyer, J. & Graßl, M. (eds), Vol. 4. pp. 75-82. Verlag Chemie: Weinheim.

Brocchini, S. & Duncan, R. (1999). Pendent drugs, release from polymers. In *Encyclopaedia of Controlled Drug Delivery*, Mathiowitz, E. (ed) pp. 786-816. Wiley: New York.

Brown, M.D., Schätzlein, A. & Uchegbu, I.F. (2001). Gene delivery with synthetic (non viral) carriers. *International Journal of Pharmaceutics*, **229,** 1-21.

Buckmaster, M.J., Braico, J.D.L., Ferris, A.L. & Storrie, B. (1987). Retention of pinocytosed solute by CHO cell lysosomes correlates with molecular weight. *Cell Biology International Reports*, **11,** 501-507.

Buhleier, E., Wehner, W. & Vögtle, F. (1978). Cascade- and nonskid-chain-like syntheses of molecular cavity topologies. *Synthesis*, 155-158.

Cardelli, J. (2001). Phagocytosis and macropinocytosis in *Dictyostelium*: Phosphoinositide-based processes, biochemically distinct. *Traffic*, **2,** 311-320.

Casciola-Rosen, L.A.F. & Hubbard, A.L. (1991). Hydrolases in intracellular compartments of rat liver cells. *Journal of Biological Chemistry*, **266,** 4341-4347.

Chen, J., Gamou, S., Takayanagi, A. & Shimizu, N. (1994). A novel gene delivery system using EGF receptor-mediated endocytosis. *FEBS Letters*, **338,** 167-169.

Chen, Q.-R., Zhang, L., Luther, P.W. & Mixson, A.J. (2002). Optimal transfection with the HK polymer depends on its degree of branching and the pH of endocytic vesicles. *Nucleic Acid Research*, **30,** 1338-1345.

Chen, Q.-R., Zhang, L., Stass, S.A. & Mixson, A.J. (2001). Branched co-polymers of histidine and lysine are efficient carriers of plasmids. *Nucleic Acid Research*, **29,** 1334-1340.

Clague, M.J. (1998). Molecular aspects of the endocytic pathway. *Biochemical Journal*, **336,** 271-282.

Clague, M.J., Thorpe, C. & Jones, A.T. (1995). Phosphatidylinositol 3-kinase regulation of fluid phase endocytosis. *FEBS Letters*, **367,** 272-274.

Clamme, J.-P., Azoulay, J. & Mely, Y. (2003a). Monitoring of the formation and dissociation of polyethylenimine/DNA complexes by two photon fluorescence correlation spectrospcopy. *Biophysical Journal*, **84,** 1960-1968.

Clamme, J.-P., Krishnamoorthy, G. & Mely, Y. (2003b). Intracellular dynamics of the gene delivery vehicle polyethylenimine during transfection: investigation by two-photon fluorescence correlation spectroscopy. *Biochimica et Biophysica Acta*, **1617,** 52-61.

Claude, A. (1946). Fractionation of mammalian liver cells by differential centrifugation. II Experimental procedures and results. *Journal of Experimental Medicine*, **84,** 61-89.

Conibear, E. (2002). An ESCRT into the endosome. *Molecular Cell*, **10,** 215-216.

Conner, S.D. & Schmid, S.L. (2003). Regulated portals of entry into the cell. *Nature*, **422,** 37-44.

Cotten, M., Längle-Rouault, F., Kirlappos, H., Wagner, E., Mechtler, K., Zeneke, M., Beug, H. & Birnstiel, M.L. (1990). Transferrin-polycation-mediated introduction of DNA into human leukaemic cells: stimulation by agents that affect the survival of transfected DNA or modulate transferrin receptor levels. *Proceedings of the National Academy of Sciences of the United States of America*, **87,** 4033-4037.

Couchman, J.R. (2003). Syndecans: proteoglycan regulators of cell-surface microdomains? *Nature Reviews Molecular Cell Biology*, **4,** 926-936.

D'Emanuele, A., Jevprasesphant, R., Penny, J. & Attwood, D. (2004). The use of a dendrimer-propranolol prodrug to bypass efflux transporters and enhance oral bioavailability. *Journal of Controlled Release*, **95,** 447-453.

Daly, L.E. & Bourke, G.J. (2000). Interpretation and uses of medical statistics pp. 27-31. Blackwell Sciences: Oxford.

Damke, H., Baba, T., van der Bliek, A.M. & Schmid, S.L. (1995). Clathrin-independent pinocytosis is induced in cells overexpressing a temperature sensitive mutant of dynamin. *Journal of Cell Biology*, **131**, 69-80.

Danhauser-Reidl, S., Hausmann, E., Schick, H.D., Bender, R., Dietzfelbinger, H., Rastetter, J. & Hanauske, A.R. (1993). Phase-I clinical and pharmacokinetic trial of dextran conjugated doxorubicin (AD-70, DOX-OXD). *Investigational New Drugs*, **11**, 187-195.

Dautry-Varsat, A. (2001). Clathrin-independent endocytosis. In *Endocytosis*, Marsh, M. (ed) pp. 26-57. Frontiers in Molecular Biology. Oxford University Press: Oxford.

Dawson, R.M.C., Elliot, D.C., Elliot, W.H. & Jones, K.M. (1986). *Data for Biochemical Research*. Clarendon Press: Oxford.

De Diesbach, P., Berens, C., N'Kuli, F., Monsigny, M., Sonveaux, E., Wattiez, R. & Courtoy, P.J. (2000). Identification, purification and partial characterisation of an oligonucleotide receptor in membranes of Hep G2 cells. *Nucleic Acid Research*, **28**, 868-874.

De Diesbach, P., N'Kuli, F., Berens, C., Sonveaux, E., Monsigny, M., Roche, A.-C. & Courtoy, P.J. (2002). Receptor-mediated endocytosis of phosphodiester oligonucleotides in the HepG2 cell line: evidence for non-conventional intracellular trafficking. *Nucleic Acid Research*, **30**, 1512-1521.

De Duve, C., de Barsy, T., Poole, B., Trouet, A., Tulkens, P. & Van Hoof, F. (1974). Lysosomotropic agents. *Biochemical Pharmacology*, **23**, 2495-2531.

De Duve, C., Pressman, B.C., Gianetto, R., Wattiaux, R. & Appelmans, F. (1955). Tissue fractionation studies. 6. Intracellular distribution patterns of enzymes in rat-liver tissue. *Biochemical Journal*, **60,** 604-617.

De Long, R., Stephenson, K., Loftus, T., Fisher, M., Alahari, S., Nolting, A. & Juliano, R.L. (1997). Characterisation of complexes of oligonucleotides with polyamidoamine starburst dendrimers and effects on intracellular delivery. *Journal of Pharmaceutical Sciences*, **86,** 762-764.

De Vries, P., Bhatt, R., Stone, I., Klein, P. & Singer, J. (2001). Optimisation of CT-2106: a water-soluble poly-L-glutamic acid (PG)- camptothecin conjugate with enhanced *in vivo* anti-tumour efficacy. *Clinical Cancer Research (Supplement)*, **7,** #101.

Dermer, O.C. & Ham, G.E. (1969). Polymerisation and polymers of aziridines. In *Ethylenimine and other Aziridines. Chemistry and Applications* pp. 315-358. Academic Press: New York.

Deshpande, M.C., Davies, M.C., Garnett, M.C., Williams, P.M., Armitage, S.P., Bailey, L., Vamvakaki, M., Armes, S.P. & Stolnik, S. (2004). The effect of poly(ethylene glycol) molecular architecture on cellular interaction and uptake of DNA complexes. *Journal of Controlled Release*, **97,** 143-156.

Diment, S., Eidelman, M., Rodriguez, G.M. & Orlow, S.J. (1995). Lysosomal hydrolases are present in melanosomes and are elevated in melanising cells. *Journal of Biological Chemistry*, **270,** 4213-4215.

Duncan, R. (1987). Selective endocytosis of macromolecular drug carriers. In *Controlled drug delivery*, Robinson, J.R. & Lee, V.H.L. (eds) pp. 581-621. Marcel Dekker: New York.

Duncan, R. (1999). Polymer conjugates for tumour targeting and intracytoplasmic delivery. The EPR effect as a common gateway? *Pharmaceutical Science Technology Today*, **11**, 441-449.

Duncan, R. (2000). Polymer therapeutics into the 21st century. In *Controlled Drug Delivery Designing Technologies for the Future*, Park, K. & Mrsny, R.J. (eds), Vol. 752. pp. 350-363. American Chemical Society: Washington DC.

Duncan, R. (2003a). The dawning era of polymer therapeutics. *Nature Reviews Drug Discovery*, **2**, 347-360.

Duncan, R. (2003b). Polymer-drug conjugates. In *Handbook of anticancer drug development*, Budman, D.R., Calvert, A.H. & Rowinsky, E.K. (eds) pp. 239-260. Lippincott Williams & Wilkins: New York.

Duncan, R. (2004). Nanomedicines in action. *The Pharmaceutical Journal*, **273**, 485-488.

Duncan, R. (2005). *N*-(2-Hydroxypropyl)methacrylamide copolymer conjugates. In *Polymeric Drug Delivery Systems*, Kwon, G.S. (ed) pp. 1-92. Marcel Dekker: New York.

Duncan, R., Cable, H.C., Lloyd, J.B., Rejmanova, P. & Kopecek, J. (1982). Degradation of side-chains of N-(2-hydroxypropyl)methacrylamide copolymer by lysosomal thiol-proteinases. *Bioscience Reports*, **2**, 1041-1046.

Duncan, R., Cable, H.C., Reijmanova, R., Kopecek, J. & Lloyd, J.B. (1984). Tyrosinamide residue enhances pinocytic capture of N-(2-hydroxypropyl)methacrylamide copolymers. *Biochimica et Biophysica Acta*, **799**, 1-8.

Duncan, R., Dimitrijevic, S. & Evagorou, E.G. (1996). The role of polymer conjugates in the diagnosis and treatment of cancer. *S T P Pharma Sciences*, **4,** 237-263.

Duncan, R., Gac-Breton, S., Kean, R., Musila, R., Sat, Y.N., Satchi, R. & Searle, F. (2001). Polymer-drug conjugates, PDEPT and PELT: basic principles for design and transfer from laboratory to clinic. *Journal of Controlled Release*, **74,** 135-146.

Duncan, R., Hume, I., Kopeckova, P., Ulbrich, K., Strohalm, J. & Kopecek, J. (1989). Anticancer agents coupled to N-(2-hydroxypropyl)methacrylamide copolymers. 3. Evaluation of adriamycin conjugates against mouse leukaemia L1210 *in vivo*. *Journal of Controlled Release*, **10,** 51-63.

Duncan, R., Hume, I., Yardley, H.J., Flanagan, P.A., Ulbrich, K., Subr, V. & Strohalm, J. (1991). Macromolecular prodrugs for use in targeted cancer chemotherapy: melphalan, covalently coupled to N-(2-hydroxypropyl)methacrylamide copolymers. *Journal of Controlled Release*, **15,** 121-136.

Duncan, R. & Kopecek, J. (1984). Soluble synthetic polymers as potential drug carriers. **57,** 51-101.

Duncan, R. & Pratten, M.K. (1985). Pinocytosis: Mechanism and regulation. In *Mononuclear Phagocytosis. Physiology and Pathology*, Jessup, D. (ed) pp. 27-51. Elsevier Science Publishers B.V. (Biomedical Devision).

Duncan, R., Pratten, M.K., Cable, H.C., Ringsdorf, H. & Lloyd, J.B. (1981a). Effect of molecular size of ^{125}I-labelled poly(vinylpyrrolidone) on its pinocytosis by rat visceral yolk sacs and rat peritoneal macrophages. *Biochemical Journal*, **196,** 49-55.

Duncan, R., Rejmanova, P., Kopecek, J. & Lloyd, J.B. (1981b). Pinocytic uptake and intracellular degradation of N-(2-hydroxypropyl)methacrylamide copolymers. A potential drug delivery system. *Biochimica et Biophysica Acta*, **678,** 143-150.

Duncan, R., Seymour, L.W., O'Hare, K.B., Flanagan, P.A., Wedge, S., Hume, I., Ulbrich, K., Strohalm, J., Subr, V., Spreafico, F., Grandi, M., Ripamonti, M., Farao, M. & Suarato, A. (1992). Preclinical evaluation of polymer-bound doxorubicin. *Journal of Controlled Release*, **19,** 331-346.

Duncan, R., Seymour, L.C.W., Scarlett, L., Lloyd, J.B., Rejmanova, P. & Kopecek, J. (1986). Fate of N-(2-hydroxypropyl)methacrylamide copolymers with pendent galactosamine residues after intravenous administration to rats. *Biochimica et Biophysica Acta*, **880,** 62-71.

Duvvuri, M., Gong, Y., Chatterji, D. & Krise, J.P. (2004). Weak base permeability characteristics influence the intracellular sequestration site in the multidrug-resistant human leukaemic cell line HL-60. *Journal of Biological Chemistry*, **279,** 32367-32372.

Edidin, M. (2001). Shrinking patches and slippery rafts: scales of domains in the plasma membrane. *Trends in Cell Biology*, **11,** 492-496.

Eichman, J.D., Bielinska, A.U., Kukowska-Latallo, J.F. & Baker, Jr. (2000). The use of PAMAM dendrimers in the efficient transfer of genetic material into cells. *Pharmaceutical Science Technology Today*, **3,** 232-244.

Eisenthal, R. & Danson, M.J. (1992). *Enzyme Assays: A Practical Approach*. The Practical Approach Series. Oxford University Press: Oxford.

El-Sayed, M., Ginski, M., Rhodes, C. & Ghandehari, H. (2002). Transepithelial transport of polyamidoamine dendrimers across Caco-2 cell monolayers. *Journal of Controlled Release*, **81,** 355-365.

Elias, H.-G. (1997). History. In *An introduction to polymer science* pp. 4-9. VCH Verlagsgesellschaft: Weinheim.

Engqvist-Goldstein, A.E.Y. & Drubin, D.G. (2003). Actin assembly and endocytosis: from yeast to mammals. *Annual Reviews of Cell Development and Biology*, **19,** 287-332.

Esfand, R. & Tomalia, D.A. (2001). Polyamidoamine (PAMAM) dendrimers: from biomimicry to drug delivery and biomedical applications. *Drug Discovery Today*, **6,** 427-436.

Evans, W.H. (1992). Isolation and characterisation of membranes and cell organelles. In *Preparative Centrifugation: A Practical Approach*, Rickwood, D. (ed) pp. 233-270. The Practical Approach Series. Oxford University Press: Oxford.

Felgner, P.L., Barenholz, Y., Behr, J.-P., Cheng, S.H., Cullis, P., Huang, L., Jessee, J.A., Seymour, L.W., Szoka, F.C.J., Thierry, A.R., Wagner, E. & Wu, G. (1997). Nomenclature for synthetic gene delivery systems. *Human Gene Therapy*, **8,** 511-512.

Fidler, I.J. (1973). Selection of successive tumour lines for metastasis. *Nature New Biology*, **242,** 148-149.

Fidler, I.J. (1975). Biological behaviour of malignant melanoma cells correlated to their survival *in vivo*. *Cancer Research*, **35,** 218-224.

Fischer, D., Bieber, T., Li, Y., Elsässer, H.-P. & Kissel, T. (1999). A novel non-viral vector for DNA delivery based on low molecular weight, branched polyethylenimine: effect of molecular weight on transfection efficiency and cytotoxicity. *Pharmaceutical Research*, **16,** 1273-1279.

Florence, A.T. & Hussain, N. (2001). Transcytosis of nanoparticle and dendrimer delivery systems: evolving vistas. *Advanced Drug Delivery Reviews*, **50,** S69-S89.

Forrest, M.L. & Pack, D.W. (2002). On the kinetics of polyplex endocytic trafficking: implications for gene delivery vector design. *Molecular Therapy*, **6,** 57-66.

Fotin, A., Cheng, Y., Sliz, P., Grigorieff, N., Harrison, S.C., Kirchhausen, T. & Walz, T. (2004). Molecular model for a complete clathrin lattice from electron cryomicroscopy. *Nature*, **432,** 573-579.

Fuki, I.V., Meyer, M.E. & Williams, K.J. (2000). Transmembrane and cytoplasmic domains of syndecan mediate a multi-step endocytic pathway involving detergent-insoluble membrane rafts. *Biochemical Journal*, **351,** 607-612.

Funhoff, A.M., van Nostrum, C.F., Koning, G.A., Schuurmans-Nieuwenbroek, N.M., Crommelin, D.J.A. & Hennink, W.E. (2004). Endosomal escape of polymeric gene delivery complexes is not always enhanced by polymers buffering at low pH. *Biomacromolecules*, **5,** 32-39.

Garnett, M.C. (1999). Gene-delivery systems using cationic polymers. *Critical Reviews in Therapeutic Drug Carrier Systems*, **16,** 147-207.

Gaus, K., Gratton, E., Kable, E.P.W., Jones, A.S., Gelissen, I., Kritharides, L. & Jessup, W. (2003). Visualising lipid structure and raft domains in living cells with

two-photon microscopy. *Proceedings of the National Academy of Sciences of the United States of America*, **100,** 15554-15559.

Gewirtz, D.A. (1999). A critical evaluation of the mechanism of action proposed for the antitumour effects of the anthracycline antibiotics adriamycin and daunorubicin. *Biochemical Pharmacology*, **57,** 727-741.

Gianasi, E., Buckley, R.G., Latiga, J., Wasil, M. & Duncan, R. (2002). HPMA copolymers platinates containing dicarboxylato ligands. Preparation, characterisation and *in vitro* and *in vivo* evaluation. *Journal of Drug Targeting*, **10,** 549-556.

Gianasi, E., Wasil, M., Evagorou, E.G., Keddle, A., Wilson, G. & Duncan, R. (1999). HPMA copolymer platinates as novel antitumour agents: *in vitro* properties, pharmacokinetics and antitumour activity *in vivo*. *European Journal of Cancer*, **35,** 994-1002.

Gieseler, F., Biersack, H., Brieden, T., Manderscheid, J. & Nüßler, V. (1994). Cytotoxicity of anthracyclines: correlation with cellular uptake, intracellular distribution and DNA binding. *Annals of Hematology*, **69,** S13-S17.

Godbey, W.T., Wu, K.K. & Mikos, A.G. (1999a). Polyethylenimine and its role in gene delivery. *Journal of Controlled Release*, **60,** 149-160.

Godbey, W.T., Wu, K.K. & Mikos, A.G. (1999b). Tracking the intracellular path of polyethylenimine/DNA complexes for gene delivery. *Proceedings of the National Academy of Sciences of the United States of America*, **96,** 5177-5181.

Godbey, W.T., Wu, K.K. & Mikos, A.G. (2001). Polyethylenimine-mediated gene delivery affects endothelial cell function and viability. *Biomaterials*, **22,** 471-480.

Goncalves, C., Mennesson, E., Fuchs, R., Gorvel, J.-P., Midoux, P. & Pichon, C. (2004). Macropinocytosis of polyplexes and recycling of plasmid via the clathrin-dependent pathway impair the transfection efficiency of human hepatocarcinoma cells. *Molecular Therapy*, **10,** 373-385.

Graham, J.M. (1993). The identification of subcellular fractions from mammalian cells. In *Methods in Molecular Biology, Biomembrane Protocols: I. Isolation and Analysis*, Graham, J.M. & Higgins, J.A. (eds), Vol. 19. pp. 1-18. Humana Press Inc: Totowa.

Graham, J.M. (1997). Homogenisation of tissues and cells. In *Subcellular Fractionation: A Practical Approach*, Graham, J.M. & Rickwood, D. (eds) pp. 1-30. The Practical Approach Series. Oxford University Press: Oxford.

Grayson, S.M. & Fréchet, J.M.J. (2001). Convergent dendrons and dendrimers: from synthesis to applications. *Chemical Reviews*, **101,** 3819-3867.

Greenwald, R.B., Pendri, A., Bolikal, D. & Gilbert, C.W. (1994). Highly water soluble taxol derivatives- 2'-polyethyleneglycolesters as potential prodrugs. *Bioorganic and Medicinal Chemistry Letters*, **4,** 2465-2470.

Griffiths, G., Back, R. & Marsh, M. (1989). A quantitative analysis of the endocytic pathway in baby hamster kidney cells. *Journal of Cell Biology*, **109,** 2703-2720.

Griffiths, P.C., Khayat, Z., Wan, K.-W., King, S.M., Grillo, I., Schweins, R., Ferruti, P., Franchini, J. & Duncan, R. (2004). Understanding the mechanism of action of polyamidoamines as endosomolytic polymers: correlation of physicochemical and biological properties. *Biomacromolecules*, **5,** 1422-1427.

Gruenberg, J. & Stenmark, H. (2004). The biogenesis of multivesicular endosomes. *Nature Reviews Molecular Cell Biology*, **5**, 317-323.

Grundelfinger, E.D., Kessels, M.M. & Qualmann, B. (2003). Temporal and spatial co-ordination of exocytosis and endocytosis. *Nature Reviews Molecular Cell Biology*, **4**, 127-139.

Gumbleton, M. (2001). Caveolae as potential macromolecule trafficking compartments within alveolar epithelium. *Advanced Drug Delivery Reviews*, **49**, 281-300.

Hailstones, D., Sleer, L.S., Parton, R.G. & Stanley, K.K. (1998). Regulation of caveolin and caveolae by cholesterol in MDCK cells. *Journal of Lipid Research*, **39**, 369-379.

Harris, J.M. & Chess, R.B. (2003). Effect of pegylation on pharmaceuticals. *Nature Reviews Drug Discovery*, **2**, 214-221.

Haugland. (2002). Fluorophores and their amine-reactive probes. In *Handbook of Fluorescent Probes and Research Products*, Haugland (ed) pp. 11-78. Molecular Probes: Eugene.

Helenius, A., Mellman, I., Wall, D. & Hubbard, A. (1983). Endosomes. *Trends in Biochemical Sciences*, **8**, 245-250.

Helin, V., Gottikh, M., Mishal, Z., Subra, F., Malvy, C. & Lavignon, M. (1999a). Cell cycle-dependent distribution and specific inhibitory effect of vectorised antisense oligonucleotides in cell culture. *Biochemical Pharmacology*, **58**, 95-107.

Helin, V., Gottikh, M., Mishal, Z., Subra, F., Malvy, C. & Lavignon, M. (1999b). Uptake and intracellular distribution of oligonucleotides vectorised by PAMAM dendrimers. *Nucleosides and Nucleotides*, **18,** 1721-1722.

Hell, S.W. (2003). Toward fluorescence nanoscopy. *Nature Biotechnology*, **21,** 1347-1355.

Herborn, C.U., Barkhausen, J., Paetsch, I., Hunold, P., Mahler, M., Shamsi, K. & Nagel, E. (2003). Coronary arteries: contrast-enhanced MR imaging with SH L 643A- experience in 12 volunteers. *Radiology*, **229,** 217-223.

Hermanson, G.T. (1996). In *Bioconjugate Techniques* pp. 136-145. Academic Press: San Diego.

Hinton, R.H. & Mullock, B.M. (1993). Isolation of subcellular fractions. In *Enzyme Assays: A Practical Approach*, Eisenthal, R. & Danson, M.J. (eds) pp. 31-69. Oxford University Press: Oxford.

Hölter, D., Burgath, A. & Frey, H. (1997). Degree of branching in hyperbranched polymers. *Acta Polymerica*, **48,** 30-35.

Hong, S., Bielinska, A.U., Mecke, A., Keszler, B., Beals, J.L., Shi, X., Balogh, L., Orr, B.G., Baker, J.R., JR & Holl, M.M.B. (2004). Interaction of poly(amidoamine) dendrimers with supported lipid bilayers and cells: hole formation and the relation to transport. *Bioconjugate Chemistry*, **15,** 774-782.

Hovorka, O., St'astny, M., Etrych, T., Subr, V., Srohalm, J., Ulbrich, K. & Rihova, B. (2002). Differences in the intracellular fate of free and polymer-bound doxorubicin. *Journal of Controlled Release*, **80,** 101-117.

Hovorka, O., Strohalm, J., Zacharcenko, M., Etrych, T., Subr, V., Ulbrich, K. & Rihova, B. (2004). Intracellular destiny of HPMA based non-targeted polymeric prodrugs. *Proceedings of the International Symposium for Controlled Release of Bioactive Materials*, **31**, #190.

Hussain, M., Shchepinov, M.S., Sohail, M., Benter, I.F., Hollins, A.J., Southern, E.M. & Akhtar, S. (2004). A novel anionic dendrimer for improved cellular delivery of antisense oligonucleotides. *Journal of Controlled Release*, **99**, 139-155.

Ilangumaran, S. & Hoessli, D.C. (1998). Effects of cholesterol depletion by cyclodextrin on the sphingolipid microdomains of the plasma membrane. *Biochemical Journal*, **335**, 433-440.

Jaiswal, J.K., Goldman, E.R., Mattoussi, H. & Simon, S.M. (2004). Use of quantum dots for live cell imaging. *Nature Methods*, **1**, 73-78.

Jaiswal, J.K. & Simon, S.M. (2004). Potentials and pitfalls of fluorescent quantum dots for biological imaging. *Trends in Cell Biology*, **14**, 497-504.

Jensen, K.D., Kopeckova, P., Bridge, J.H.B. & Kopecek, J. (2001). The cytoplasmic escape and nuclear accumulation of endocytosed and microinjected HPMA copolymers and a basic kinetic study in Hep G2 cells. *American Association of Pharmaceutical Scientists*, **4**, U69-U82.

Jevprasesphant, R., Penny, J., Attwood, D. & D'Emanuele, A. (2004). Transport of dendrimer nanocarriers through epithelial cells via the transcellular route. *Journal of Controlled Release*, **97**, 259-267.

Johannes, L. & Lamaze, C. (2002). Clathrin-dependent or not: is it still the question? *Traffic*, **3**, 443-451.

Jones, A.T., Gumbleton, M. & Duncan, R. (2003). Understanding endocytic pathways and intracellular trafficking: a prerequisite for effective design of advanced drug delivery systems. *Advanced Drug Delivery Reviews*, **55**, 1353-1357.

Jones, A.T., Mills, I.G., Scheidig, A.J., Alexandrov, K. & Clague, M.J. (1998). Inhibition of endosome fusion by wortmannin persists in the presence of activated rab5. *Molecular Biology of the Cell*, **9**, 323-332.

Kannan, S., Kolhe, P., Raykova, V., Glibatec, M., Kannan, R.M., Lieh-Lai, M. & Bassett, D. (2004). Dynamics of cellular entry and drug delivery by dendritic polymers into human lung epithelial carcinoma cells. *Journal of Biomaterials Science. Polymer Edition*, **15**, 311-330.

Kapuscinski, J. & Skoczylast, B. (1977). Simple and rapid fluorimetric method for DNA microassay. *Analytical Biochemistry*, **83**, 252-257.

Kataoka, K., Kwon, G.S., Yokoyama, M., Okano, T. & Sakurai, Y. (1993). Block copolymer micelles as vehicles for drug delivery. *Journal of Controlled Release*, **24**, 119-132.

Kean, R. (2002). HPMA copolymer-aminoellipticine conjugates: mechanism of action. *PhD Thesis University of London*.

Klemm, A.R., Young, D. & Lloyd, J.B. (1998). Effects of polyethylenimine on endocytosis and lysosomal stability. *Biochemical Pharmacology*, **56**, 41-46.

Knox, W.E. (1976). Appendices I and II. Analyses of rat tissues. In *Enzyme Patterns In Fetal, Adult and Neoplastic Rat Tissues*, Knox, W.E. (ed) pp. 254-332. S Karger: London.

Kopatz, I., Remy, J.-S. & Behr, J.-P. (2004). A model for non-viral gene delivery: through syndecan adhesion molecules and powered by actin. *The Journal of Gene Medicine*, **6,** 769-776.

Kopecek, J., Kopeckova, P., Minko, T. & Lu, Z.-R. (2000). HPMA copolymer-anticancer drug conjugates: design, activity, and mechanism of action. *European Journal of Pharmaceutics and Biopharmaceutics*, **50,** 61-81.

Kopitz, J., Kisen, G.O., Gordon, P.B., Bohley, P. & Seglen, P.O. (1990). Non-selective autophagy of cytosolic enzymes by isolated rat hepatocytes. *Journal of Cell Biology*, **111,** 941-953.

Kos, J. & Lah, T.T. (1998). Cysteine proteinases and their endogenous inhibitors: target proteins for prognosis, diagnosis and therapy in cancer (review). *Oncology Reports*, **5,** 1349-1361.

Kovar, M., Kovar, L., Subr, V., Etrych, T., Ulbrich, K., Mrkvan, T., Loucka, J. & Rihova, B. (2004). HPMA copolymers containing doxorubicin bound by a proteolytically or hydrolytically cleavable bond: comparison of biological properties *in vitro*. *Journal of Controlled Release*, **99,** 301-314.

Kudelka, A.P., Verschraegen, C.F., Loyer, E., Wallace, S., Gershenson, D.M., Han, J., Ho, L., Garzone, P.D., Warner, M., Bolton, M.G. & Kavanagh, J.J. (2002). Preliminary report of a phase I study of escalating dose PG-paclitaxel (CT-2103) and fixed dose cisplatin in patients with solid tumours. *Proceedings of the American Society of Clinical Oncology*, #2146.

Kukowska-Latallo, J.F., Bielinska, A.U., Johnson, J., Spindler, R., Tomalia, D.A. & Baker, J.R., JR. (1996). Efficient transfer of genetic material into mammalian cells

using Starburst polyamidoamine dendrimers. *Proceedings of the National Academy of Sciences of the United States of America*, **93,** 4897-4902.

Kumazawa, E. & Ochi, Y. (2004). DE-310, a novel macromolecular carrier system for the camptothecin analogue DX-8951f: potent antitumour activities in various murine tumour models. *Cancer Science*, **95,** 168-175.

Lamaze, C., Dujeancourt, A., Baba, T., Lo, C.G., Benmerah, A. & Dautry-Varsat, A. (2001). Interleukin 2 receptors and detergent-resistant membrane domains define a clathrin-independent endocytic pathway. *Molecular Cell*, **7,** 661-671.

Lampela, P., Soininen, P., Puttonen, K.A., Ruponen, M., Urtti, A., Männistö, M. & Raasmaja, A. (2004). Effect of cell-surface glycosaminoglycans on cationic carrier combined with low-MW PEI-mediated gene transfection. *International Journal of Pharmaceutics*, **284,** 43-52.

Langer, R. (1998). Drug delivery and targeting. *Nature*, **392,** S5-S10.

Larson, D.R., Zipfle, W.R., Williams, R.M., Clark, S.W., Bruchez, M.P., Wise, F.W. & Webb, W.W. (2003). Water-soluble quantum dots for multiphoton fluorescence imaging *in vivo*. *Science*, **300,** 1434-1436.

Laurent, N., Wattiaux-De Coninck, S., Mihaylova, E., Leontieva, E., Warnier-Pirotte, M.-T., Wattiaux, R. & Jadot, M. (1999). Uptake by rat liver and intracellular fate of plasmid DNA complexed with poly-L-lysine or poly-D-lysine. *FEBS Letters*, **443,** 61-65.

LaVan, D., McGuire, T. & Langer, R. (2003). Small-scale systems for *in vivo* drug delivery. *Nature Biotechnology*, **21,** 1184-1191.

Le, P.U., Guay, G., Altschulter, Y. & Nabi, I.R. (2002). Caveolin-I is a negative regulator of caveolae-mediated endocytosis to the endoplasmic reticulum. *Journal of Biological Chemistry*, **277,** 3371-3379.

Lecocq, M., Wattiaux-De Coninck, S., Laurent, N., Wattiaux, R. & Jadot, M. (2000). Uptake and intracellular fate of polyethylenimine *in vivo*. *Biochemical and Biophysical Research Communications*, **278,** 414-418.

Leighton, F., Poole, B., Beaufay, H., Baudhuin, P., Coffey, J.W., Fowler, S. & de Duve, C. (1968). The large-scale separation of peroxisomes, mitochondria, and lysosomes from the livers of rats injected with triton WR-1339. Improved isolation procedures, automated analysis, biochemical and morphological properties of fractions. *Journal of Cell Biology*, **37,** 482-513.

Li, C., Dong-Fang, Y., Newman, R.A., Cabral, F., Stephens, C., Hunter, N., Milas, L. & Wallace, S. (1998). Complete regression of well-established tumours using a novel water-soluble poly(L-glutamic acid)-paclitaxel conjugate. *Cancer Research*, **58,** 2404-2409.

Li, Y., Tseng, Y.D., Kwon, S.Y., D'Espaux, L., Bunch, J.S., Mceuen, P.L. & Luo, D. (2004). Controlled assembly of dendrimer-like DNA. *Nature Materials*, **3,** 38-42.

Liu, S.-H., Mallet, W.G. & Brodsky, F.M. (2001). Clathrin-mediated endocytosis. In *Endocytosis*, Marsh, M. (ed) pp. 1-25. Frontiers in Molecular Biology. Oxford University Press: Oxford.

Lloyd, J.B. (2000). Lysosomal membrane permeability: implications for drug delivery. *Advanced Drug Delivery Reviews*, **41,** 189-200.

Loadman, P.M., Bibby, M.C., Double, J.A., Al-Shakhaa, W. & Duncan, R. (1999). Pharmacokinetics of PK1 and doxorubicin in experimental colon tumour models with differing response to PK1. *Clinical Cancer Research*, **5,** 3682-3688.

Londos-Gagliardi, D., Aubel-Sadron, G., Maral, R. & Trouet, A. (1980). Subcellular localisation of daunorubicin in sensitive and resistant Ehrlich ascites tumour cells. *European Journal of Cancer*, **16,** 849-854.

Londos-Gagliardi, D., Zenebergh, A. & Aubel-Sadron, G. (1979). Analytical fractionation of homogenates from Ehrlich ascites tumour cells. *Bulletin Societes Chimiques Belges*, **88,** 99-105.

Lopez-Saura, P., Trouet, A. & Tulkens, P. (1978). Analytical fractionation of cultured hepatoma cells (HTC Cells). *Biochimica et Biophysica Acta*, **543,** 430-449.

Lopez-Saura, P., Tulkens, P. & Trouet, A. (1972). Characterisation of subcellular constituents of hepatoma cultured cells (HTC cells). *Archives Internationales de Physiologie et de Biochimie*, **80,** 977-978.

Luzio, J.P., Rous, B.A., Bright, N.A., Pryor, P.R., Mullock, B.M. & Piper, R.C. (2000). Lysosome-endosome fusion and lysosome biogenesis. *Journal of Cell Science*, **113,** 1515-1524.

Maeda, H. (1994). Polymer conjugated macromolecular drugs for tumour-specific targeting. In *Polymeric site-specific pharmacotherapy*, Domb, A.J. (ed) pp. 95-116. John Wiley & Sons Ltd: New York.

Malik, N., Evagorou, E.G. & Duncan, R. (1999). Dendrimer-platinate: a novel approach to cancer chemotherapy. *Anti-Cancer Drugs*, **10,** 767-776.

Malik, N., Wiwattanapatapee, R., Klopsch, R., Lorenz, K., Frey, H., Weener, J.W., Meijer, E.W., Paulus, W. & Duncan, R. (2000). Dendrimers: relationship between structure and biocompatibility *in vitro*, and preliminary studies of the biodistribution of ^{125}I-labelled polyamidoamine dendrimers *in vivo*. *Journal of Controlled Release*, **65**, 133-148.

Maniak, M. (2001). Macropinocytosis. In *Endocytosis*, Marsh, M. (ed) pp. 78-93. Frontiers in Molecular Biology. Oxford University Press: Oxford.

Manunta, M., Tan, P.H., Sagoo, P., Kashefi, K. & George, A.J.T. (2004). Gene delivery by dendrimers operates via a cholesterol-dependent pathway. *Nucleic Acid Research*, **32**, 2730-2739.

Mariani, M. & Supino, R. (1990). Morphological alterations induced by doxorubicin in B16 melanoma cells. *Cancer Letters*, **51**, 209-212.

Marks, M.S. & Seabra, M.C. (2001). The melanosome: membrane dynamics in black and white. *Nature Reviews Molecular Cell Biology*, **2**, 738-748.

Masquelier, M., Braurain, R. & Trouet, A. (1980). Cellular pharmacology of amino acid derivatives of daunorubicin. *Current Chemotherapy and Infectious Disease Proceeding 11th ICC and 19th ICAAC American Society of Microbiology*, 1688-1690.

Maxfield, F.R. & McGraw, T.E. (2004). Endocytic recycling. *Nature Reviews Molecular Cell Biology*, **5**, 121-132.

McCarthy, T., Karellas, P., Henderson, S., Giannis, M., O'Keefe, D., Matthews, B., Braggs, B., Paull, J., Heery, G., Krippner, G. & Holan, G. (2004). Design and preclinical development of dendrimer based topical microbicides for HIV and STI

prevention. *Proceedings of the 6th International Conference on Polymer Therapeutics: From Laboratory to Clinical Practice, Cardiff*, #22.

McCormick, L.A., Seymour, L.W. & Duncan, R. (1986). Interaction of cationic N-(2-hydroxypropyl)methacrylamide copolymer with rat visceral yolk sacs cultured *in vitro* and rat liver *in vivo*. *Journal of Bioactive and Compatible Polymers*, **1**, 4-19.

Mellman, I. (1996). Endocytosis and molecular sorting. *Annual Reviews of Cell Development and Biology*, **12**, 575-625.

Mellman, I., Plutner, H. & Ukkonen, P. (1984). Internalisation and rapid recycling of macrophage Fc receptors tagged with monovalent antireceptor antibody: possible role of a prelysosomal compartment. *Journal of Cell Biology*, **98**, 1163-1169.

Meltzer, A.D., Tirrell, D.A., Jones, A.S., Inglefield, P.T., Hedstrand, D.M. & Tomalia, D.A. (1992). Chain dynamics in polyamidoamine dendrimers. A study of ^{13}C NMR relaxation parameters. *Macromolecules*, **25**, 4541-4548.

Merdan, T., Kunath, K., Fisher, D., Kopecek, J. & Kissel, T. (2001). Intracellular processing of polyethylenimine/ribozyme complexes can be observed in living cells by using confocal laser scanning microscopy and inhibitor experiments. *Pharmaceutical Research*, **19**, 140-146.

Minko, T., Kopeckova, P. & Kopecek, J. (2000). Efficacy of chemotherapeutic action of HPMA copolymer-bound doxorubicin in a solid tumour model of ovarian carcinoma. *International Journal of Cancer*, **86**, 108-117.

Minko, T., Kopeckova, P., Pozharov, V. & Kopecek, J. (1998). HPMA copolymer bound adriamycin overcomes MDR1 gene encoded resistance in a human ovarian carcinoma cell line. *Journal of Controlled Release*, **54**, 223-233.

Mislick, K.A., Baldeschwieler, J.D., Kayyem, J.F. & Meade, T.J. (1995). Transfection of folate-polylysine DNA complexes: evidence for lysosomal delivery. *Bioconjugate Chemistry*, **6,** 512-515.

Mislick, K.A. & Bladeschwieler, J.D. (1996). Evidence for the role of proteoglycans in cationic-mediated gene transfer. *Proceedings of the National Academy of Sciences of the United States of America*, **93,** 12349-12354.

Mitchell, D.J., Kim, D.T., Steinman, L., Fathman, C.G. & Rothbard, J.B. (2000). Polyarginine enters cells more efficiently than other polycationic homopolymers. *Journal of Peptide Research*, **56,** 318-325.

Möllering, H., Wahlefeld, A.W. & Michal, G. (1978). Visualisation of NAD(P)-dependent reactions. In *Principles of enzymatic analysis*, Bergmeyer, H.U. & Gawehn, K. (eds) pp. 88-93. Verlag Cehmie: Weinheim.

Moore, S. (1968). Amino acid analysis: Aqueous dimethyl sulfoxide as solvent for ninhydrin reaction. *Journal of Biological Chemistry*, **243,** 6281-6283.

Mosmann, T. (1983). Rapid colorimetric assay for cellular growth and survival: application of proliferation and cytotoxicity assays. *Journal of Immunological Methods*, **65,** 55-63.

Mostov, K.E. & Simister, N.E. (1985). Transcytosis. *Cell*, **43,** 389-390.

Mostov, K.E., Verges, M. & Altschulter, Y. (2000). Membrane traffic in polarised epithelial cells. *Current Opinion in Molecular Therapeutics*, **12,** 483-490.

Mounkes, L.C., Zhong, W., Cipres-Palacin, G., Heath, T.D. & Debes, R.J. (1998). Proteoglycans mediate cationic liposome-DNA complex-based gene delivery *in vitro* and *in vivo*. *Journal of Biological Chemistry*, **273**, 26164-26170.

Mukherjee, A., Ghosh, R.N. & Maxfield, F.R. (1997). Endocytosis. *Physiological Reviews*, **77**, 759-803.

Mullock, B.M., Bright, N.A., Fearon, C.W., Gray, S.R. & Luzio, J.P. (1998). Fusion of lysosomes with late endosomes produces a hybrid organelle of intermediate density and is NSF dependent. *Journal of Cell Biology*, **140**, 591-601.

Munro, S. (2003). Lipid rafts: Elusive or illusive? *Cell*, **115**, 377-388.

Murphy, R.F., Jorgensen, E.D. & Cantor, C.R. (1982a). Kinetics of histone endocytosis in Chinese hamster ovary cells. *Journal of Biological Chemistry*, **257**, 1695-1701.

Murphy, R.F., Powers, S., Verderame, M., Cantor, C.R. & Pollack, R. (1982b). Flow cytofluorometric analysis of insulin binding and internalisation by Swiss 3T3 cells. *Cytometry*, **2**, 402-406.

Nabi, I.R. & Le, P.U. (2003). Caveolae/raft-dependent endocytosis. *Journal of Cell Biology*, **161**, 673-677.

Nakanishi, T., Fukushima, S., Okamoto, K., Suzuki, M., Matsumura, Y., Yokoyama, M., Okano, T., Sakurai, Y. & Kataoka, K. (2001). Development of polymer micelle carrier systems for doxorubicin. *Journal of Controlled Release*, **74**, 295-302.

Nichols, B. (2003). Caveosomes and endocytosis of lipid rafts. *Journal of Cell Science*, **116**, 4707-4714.

Nichols, B.J. (2002). A distinct class of endosomes mediates clathrin-independent endocytosis to the Golgi complex. *Nature Cell Biology*, **4,** 374-378.

Nichols, B.J. & Lippincott-Schwartz, J. (2001). Endocytosis without clathrin coats. *Trends in Cell Biology*, **11,** 406-412.

Noel, G., Peterson, C., Trouet, A. & Tulkens, P. (1978). Uptake and subcellular localisation of daunorubicin and adriamycin in cultured fibroblasts. *European Journal of Cancer*, **14,** 363-368.

Noel, G. & Trouet, A. (1976). Fate of DNA and its complexes with daunorubicin and adriamycin in rat fibroblasts. *Archives Internationales de Physiologie et de Biochimie*, **85,** 189-191.

Nori, A., Jensen, K.D., Tijerina, M., Kopeckova, P. & Kopecek, J. (2001). Tat-conjugated synthetic macromolecules facilitate cytoplasmic drug delivery to human ovarian carcinoma cells. *Bioconjugate Chemistry*, **14,** 44-50.

Nori, A., Jensen, K.D., Tijerina, M., Kopeckova, P. & Kopecek, J. (2003a). Subcellular trafficking of HPMA copolymer-Tat conjugates in human ovarian carcinoma cells. *Journal of Controlled Release*, **91,** 53-59.

Nori, A., Jensen, K.D., Tijerina, M., Kopeckova, P. & Kopecek, J. (2003b). Tat-conjugated synthetic macromolecules facilitate cytoplasmic drug delivery to human ovarian carcinoma cells. *Bioconjugate Chemistry*, **14,** 44-50.

Novikoff, A.B., Albala, A. & Biempica, L. (1968). Ultrastructural and cytochemical observations on B-16 and Harding-Passey mouse melanomas. *Journal of Histochemistry and Cytochemistry*, **16,** 299-319.

Nowotnik, D.P. (2004). Preclinical development and Phase I results with HPMA copolymer platinates. *Proceedings of the 6th International Conference on Polymer Therapeutics: From Laboratory to Clinical Practice, Cardiff*, #25.

OBA & RAC. (2004). *Office of Biotechnology Activities (OBA) and Recombinant DNA Advisory Committee (RAC) Human Gene Transfer Protocols*, http://www4.od.nih.gov/oba/rac/documents1.htm.

Ogris, M., Steinlein, P., Kursa, M., Mechtler, K., Kircheis, R. & Wagner, E. (1998). The size of DNA/transferrin-PEI complexes is an important factor for gene expression in cultured cells. *Gene Therapy*, **5**, 1425-1433.

Ohkuma, S. & Poole, B. (1978). Fluorescence probe measurement of the intralysosomal pH in living cells and the perturbation of pH by various agents. *Proceedings of the National Academy of Sciences of the United States of America*, **75**, 3327-3331.

Omelyanenko, V., Kopeckova, P., Gentry, C. & Kopecek, J. (1998). Targetable HPMA copolymer-adriamycin conjugates. Recognition, internalisation, and subcellular fate. *Journal of Controlled Release*, **53**, 25-37.

Orlandi, P.A. & Fishman, P.H. (1998). Filipin-dependent inhibition of cholera toxin: evidence for toxin internalisation and activation through caveolae-like domains. *Journal of Cell Biology*, **141**, 905-915.

Orlow, S.J. (1995). Melanosomes are specialised members of the lysosomal lineage of organelles. *Journal of Investigative Dermatology*, **105**, 3-7.

Orlow, S.J., Boissy, R.E., Moran, D.J. & Pifko-Hirst, S. (1993). Subcellular distribution of tyrosinase and tyrosinase-related protein-1: implications for melanosomal biogenesis. *Journal of Investigative Dermatology*, **100,** 55-64.

Ormerod, M.G. (2000). Further applications to cell biology. In *Flow Cytometry*, Ormerod, M.G. (ed) pp. 249-260. Practical Approach Series. Oxford University Press: Oxford.

Patton, J.S. (1996). Mechanisms of macromolecular absorption by the lungs. *Advanced Drug Delivery Reviews*, **19,** 3-36.

Pattrick, N., Ferruti, P. & Duncan, R. (2001). Demonstration of polyamidoamine-mediated lysosomal membrane perturbation after administration to rats *in vivo*. *Proceedings of the International Symposium for Controlled Release of Bioactive Materials*, **28,** 864-865.

Pearse, B.M.F. (1975). Coated vesicle from pig brain: purification and biochemical characterisation. *Journal of Molecular Biology*, **97,** 93-98.

Pelkmans, L., Bürli, T., Zerial, M. & Helenius, A. (2004). Caveolin-stabilised membrane domains as multifunctional transport and sorting devices in endocytic membrane traffic. *Cell*, **118,** 767-780.

Pelkmans, L. & Helenius, A. (2003). Insider information: what viruses tell us about endocytosis. *Current Opinion in Cell Biology*, **15,** 414-422.

Pelkmans, L., Kartenbeck, J. & Helenius, A. (2001). Caveolar endocytosis of simian virus 40 reveals a new two-step vesicular-transport pathway to the ER. *Nature Cell Biology*, **3,** 473-483.

Pelkmans, L., Püntener, D. & Helenius, A. (2002). Local actin polymerisation and dynamin recruitment in SV40-induced internalisation of caveolae. *Science*, **296,** 535-539.

Peterson, C., Noel, G., Zenebergh, A. & Trouet, A. (1979). Uptake of the daunorubicin-DNA complex in cultured fibroblasts. *Cancer Chemotherapy and Pharmacology*, **2,** 3-6.

Peterson, C. & Trouet, A. (1978). Transport and storage of daunorubicin and doxorubicin in cultured fibroblasts. *Cancer Research*, **38,** 4645-4649.

Pfeffer, S.R. (1996). Transport vesicle docking: SNAREs and associates. *Annual Reviews of Cell Development and Biology*, **12,** 441-461.

Pfeffer, S.R. (2003). Membrane domains in the secretory and endocytic pathways. *Cell*, **112,** 507-517.

Phaire-Washington, L., Wang, F. & Silverstein, S.C. (1980). Phorbol myristate acetate stimulates pinocytosis and membrane spreading in mouse peritoneal macrophages. *Journal of Cell Biology*, **86,** 634-640.

Pierre, T.S. & Geckle, M. (1985). ^{13}C-NMR analysis of branched polyethylenimine. *Journal of Macromolecular Science. Chemistry*, **A22,** 877-887.

Pollard, H., Remy, J.-S., Loussouran, G., Demolombe, S., Behr, J.-P. & Escande, D. (1998). Polyethylenimine but not cationic lipids promotes transgene delivery to the nucleus in mammalian cells. *Journal of Biological Chemistry*, **273,** 7507-7511.

Poole, B. & Tiltman, K.J. (1978). Differences in secretion of the proteinase cathepsin B at the edges of human breast carcinomas and fibroadenomas. *Nature*, **273**, 545-547.

Poxon, S.W., Mitchell, P.M., Liang, E. & Hughes, J.A. (1996). Dendrimer delivery of oligonucleotides. *Drug Delivery*, **3**, 255-261.

Pratten, M.K., Duncan, R. & Lloyd, J.B. (1980). Adsorptive and passive pinocytic uptake. In *Coated Vesicles*, Ockelford, C.F. & A, W. (eds) pp. 181-212. Cambridge University Press: Cambridge.

Puri, V., Watanabe, R., Singh, R.D., Dominguez, M., Brown, J.C., Wheatley, C.L., Marks, D.L. & Pagano, R.E. (2001). Clathrin-dependent and -independent internalisation of plasma membrane sphingolipids initiates two Golgi targeting pathways. *Journal of Cell Biology*, **154**, 535-547.

Raposo, G. & Marks, M.S. (2002). The dark side of lysosome-related organelles: specialisation of the endocytic pathway for melanosome biogenesis. *Traffic*, **3**, 237-248.

Rathgeber, S., Monkenbusch, M., Kreitschmann, M., Urban, V. & Brulet, A. (2002). Dynamics of star-burst dendrimers in solution in relation to their structural properties. *Journal of Chemical Physics*, **117**, 4047-4062.

Regoeczi, E., Chindemi, P.A. & Dabanne, M.T. (1982). Dual nature of the hepatic lectin pathway for human asialotransferrin type 3 in the rat. *Journal of Biological Chemistry*, **257**, 5431-5436.

Rejman, J., Oberle, V., Zuhorn, I.S. & Hoekstra, D. (2004). Size-dependent internalisation of particles via the pathways of clathrin- and caveolae-mediated endocytosis. *Biochemical Journal*, **377,** 159-169.

Remy-Kristensen, A., Clamme, J.-P., Vuilleumier, C., Kuhry, J.-G. & Mely, Y. (2001). Role of endocytosis in the transfection of L929 fibroblasts by polyethylenimine/DNA complexes. *Biochimica et Biophysica Acta*, **1514,** 21-32.

Richard, J.P., Melikov, K., Vives, E., Ramos, C., Verbeure, B., Gait, M.J., Chernomordik, L.V. & Lebleu, B. (2003). Cell-penetrating peptides. A re-evaluation of the mechanism of cellular uptake. *Journal of Biological Chemistry*, **278,** 585-590.

Richardson, S., Ferruti, P. & Duncan, R. (1999a). Poly(amidoamine)s as potential endosomolytic polymers: evaluation *in vitro* and body distribution in normal and tumour-bearing animals. *Journal of Drug Targeting*, **6,** 391-404.

Richardson, S.C.W., Kolbe, H.V.J. & Duncan, R. (1999b). Potential of low molecular mass chitosan as a DNA delivery system: biocompatibility, body distribution and ability to complex and protect DNA. *International Journal of Pharmaceutics*, **178,** 231-243.

Rickwood, D. (1992). Appendix 4: Marker enzymes and chemical assays for the analysis of subcellular fractions. In *Preparative Centrifugation: A Practical Approach*, Rickwood, D. (ed) pp. 369-387. Oxford University Press: Oxford.

Ringsdorf, H. (1975). Structure and properties of pharmacological active polymers. *Journal of Pharmaceutical Science Polymer Symposium*, **51,** 135-153.

Ringsdorf, H. (2004). Hermann Staudinger and the future of polymer research jubilees- beloved occasions for cultural piety. *Angewandte Chemie International Edition in English*, **43,** 1064-1076.

Roberts, J.C., Bhalgat, M.K. & Zera, R.T. (1996). Preliminary biological evaluation of polyamidoamine (PAMAM) Starburst dendrimers. *Journal of Biomedical Materials Research*, **30,** 53-65.

Rodal, S.K., Skretting, G., Garred, O., Vilhardt, F., van Deurs, B. & Sandvig, K. (1999). Extraction of cholesterol with methyl-beta-cyclodextrin perturbs formation of clathrin-coated endocytic vesicles. *Molecular Biology of the Cell*, **10,** 961-974.

Rodman, J.S. & Wandinger-Ness, A. (2000). Rab GTPases coordinate endocytosis. *Journal of Cell Science*, **113,** 183-192.

Rogers, K.E., Carr, B.I. & Tokes, Z.A. (1983). Cell surface-mediated cytotoxicity of polymer-bound adriamycin against drug-resistant hepatocytes. *Cancer Research*, **43,** 2741-2748.

Roth, T.F. & Porter, K.R. (1964). Yolk protein uptake in the oocyte of mosquito *aedes aegyti* L. *Journal of Cell Biology*, **20,** 313-332.

Rozhin, J., Robinson, D., Stevens, M.A., Lah, T.T., Honn, K.V., Ryan, R.E. & Sloane, B.F. (1987). Properties of plasma membrane-associated cathepsin B-like cysteine proteinase in metastatic B16 melanoma variants. *Cancer Research*, **47,** 6620-6628.

Rozhin, J., Wade, R.L., Honn, K.V. & Sloane, B.F. (1989). Membrane-associated cathepsin L: a role in metastasis of melanomas. *Biochemical and Biophysical Research Communications*, **164,** 556-561.

Ruponen, M., Honkakoski, P., Rönkko, S., Pelkonen, J., Tammi, M. & Urtti, A. (2003). Extracellular and intracellular barriers in non-viral gene delivery. *Journal of Controlled Release*, **93,** 213-217.

Ruponen, M., Honkakoski, P., Tammi, M. & Urtti, A. (2004). Cell-surface glycosaminoglycans inhibit cation-mediated gene transfer. *The Journal of Gene Medicine*, **6,** 405-414.

Ruponen, M., Rönkko, S., Honkakoski, P., Pelkonen, J. & Tammi, M. (2001). Extracellular glycosaminoglycans modify cellular trafficking of lipoplexes and polyplexes. *Journal of Biological Chemistry*, **276,** 33875-33880.

Ruponen, M., Ylä-Herttuala, S. & Urtti, A. (1999). Interaction of polymeric and liposomal gene delivery systems with extracellular glycosaminoglycans: physicochemical and transfection studies. *Biochimica et Biophysica Acta*, **1415,** 331-341.

Ryser, H.J.-P. (1967). A membrane effect of basic polymers dependent on molecular size. *Nature*, **215,** 934-936.

Ryser, H.J.-P. & Hancock, R. (1965). Histones and basic polyamino acids stimulate the uptake of albumin by tumour cells in culture. *Science*, **150,** 501-503.

Ryser, H.J.-P. & Shen, W.-C. (1978). Conjugation of methotrexate to poly(L-lysine) increases drug transport and overcomes drug resistance in cultured cells. *Proceedings of the National Academy of Sciences of the United States of America*, **75,** 3867-3870.

Sabbatini, P., Brown, J., Aghajanian, C., Hensley, M.L., Pezzulli, S., O'Flaherty, C., Lovegren, M., Funt, S., Warner, M., Mitchell, P., Bolton, M.G., Spriggs, D. & Duggan, B. (2002). A phase I/II study of PG-paclitaxel (CT-2103) in patients (pts)

with recurrent ovarian, fallopian tube, or peritoneal cancer. *Proceedings of the American Society of Clinical Oncology*, #871.

Sakharov, D.V., Jie, A.F.H., Filippov, D.V., Bekkers, M.E.A., van Boom, J.H. & Rijken, D.C. (2003). Binding and retention of polycationic peptides and dendrimers in the vascular wall. *FEBS Letters*, **537,** 6-10.

Samuel, B.U., Hearn, B., Mack, D., Wender, P., Rothbard, J., Kirisits, M.J., Mui, E., Wernimont, S., Roberts, C.W., Muench, S.P., Rice, D.W., Prigge, S.T., Law, A.B. & McLeod, R. (2003). Delivery of antimicrobials into parasites. *Proceedings of the National Academy of Sciences of the United States of America*, **100,** 14281-14286.

Sarafian, V., Jadot, M., Wattiaux-De Coninck, S. & Wattiaux, R. (1997). Biological functions of lysosomal membrane-associated glycoproteins. *Biomedical Reviews*, **8,** 119-125.

Sat, Y.N. (1999). Factors that influence tumour targeting by the enhanced permeability and retention (EPR) effect. *PhD Thesis University of London*.

Schindler, M., Grabski, S., Hoff, E. & Simon, S.M. (1996). Defective pH regulation of acidic compartments in human breast cancer cells (MCF-7) is normalised in adriamycin-resistant cells (MCF-7adr). *Biochemistry*, **35,** 2811-2817.

Schmaljohann, D., Komber, H. & Voit, B.I. (1999). Conversion dependence of the structural units and the degree of branching of a hyperbranched polyester based on 4,4-bis-(4'-hydroxyphenyl)pentanoic acid determined by NMR spectroscopy. *Acta Polymerica*, **50,** 196-204.

Schmid, S.L. (1997). Clathrin-coated vesicle formation and protein sorting: an integrated process. *Annual Reviews of Biochemistry*, **66,** 511-548.

Schnitzer, J.E. (2001). Caveolae: from basic trafficking mechanisms to targeting transcytosis for tissue-specific drug and gene delivery *in vivo*. *Advanced Drug Delivery Reviews*, **49**, 265-280.

Schoemaker, N.E., van Kesteren, C., Rosing, H., Jansen, S., Swart, M., Lieverst, J., Fraier, D., Breda, M., Pellizzoni, C., Spinelli, R., Grazia Porro, M., Beijnem, J.H., Schellens, J.H.M. & ten Bokkel Huinink, W.W. (2002). A phase I and pharmacokinetic study of MAG-CPT, a water-soluble polymer conjugate of camptothecin. *British Journal of Cancer*, **87**, 608-614.

Schomburg, D., Salzmann, M. & Stephen, D. (1993). Succinate dehydrogenase. In *Enzyme Handbook Class 1.2-1.4 Oxidoreductases*, Vol. 6. pp. 1-5. Spriner-Verlag: Berlin.

Schomburg, D. & Stephen, D. (1995). L-Lactate dehydrogenase. In *Enzyme Handbook Class 1.1 Oxidoreductases*, Vol. 9. pp. 1-8. Springer-Verlag: Berlin.

Schröter, C.J., Braun, M., Englert, J., Beck, H., Schmid, H. & Kalbacher, H. (1999). A rapid method to separate endosome from lysosomal contents using differential centrifugation and hypotonic lysis of lysosomes. *Journal of Immunological Methods*, **227**, 161-168.

Schulz, J., Burris, H.A., Redfern, C., Mitchell, P., Warner, M. & Bolton, M.G. (2002). Phase II study of CT-2103 in patients with colorectal cancer having recurrent disease after treatment with a 5-fluorouracil-containing regimen. *Proceedings of the American Society of Clinical Oncology*, #2330.

Schwartz, A.L. (1991). Trafficking of asialoglycoproteins and the asialoglycoprotein receptor. *Targeted Diagnosis and Therapy*, **4**, 3-39.

Seaman, M.N.J. & Luzio, J.P. (2001). Lysosomes and other late compartments of the endocytic pathway. In *Endocytosis*, Marsh, M. (ed) pp. 111-148. Frontiers in Molecular Biology. Oxford University Press: Oxford.

Seib, F.P., Hann, A., Jones, A.T. & Duncan, R. (2003). Establishing a quantitative subcellular fractionation method in B16F10 cells; use to monitor the intracellular trafficking of polymer therapeutics. *Proceedings of the International Symposium for Controlled Release of Bioactive Materials*, **30,** #520.

Seib, F.P., Jones, A.T. & Duncan, R. (2004). Endocytic capture and intracellular trafficking: effect of polymer architecture. *Proceedings of the International Symposium for Controlled Release of Bioactive Materials*, **31,** #717.

Seiji, M., Shimao, K., Birbeck, M.S.C. & Fitzpatrick, T.B. (1963). Subcellular localisation of melanin biosynthesis. *Annals New York Academy of Sciences*, **100,** 497-533.

Seymour, L.W., Ferry, D.R., Anderson, D., Hesslewood, S., Julyan, P.J., Poyner, R., Doran, J., Young, A.M., Burtles, S. & Kerr, D.J. (2002). Hepatic drug targeting: Phase I evaluation of polymer-bound doxorubicin. *Journal of Clinical Oncology*, **20,** 1668-1676.

Seymour, L.W., Miyamoto, Y., Maeda, H., Brereton, M., Strohalm, J., Ulbrich, K. & Duncan, R. (1995). Influence of molecular weight on passive tumour accumulation of a soluble macromolecular drug carrier. *European Journal of Cancer*, **31A,** 766-770.

Seymour, L.W., Ulbrich, K., Steyger, P.S., Brereton, M., Subr, V., Strohalm, J. & Duncan, R. (1994). Tumour tropism and anti-cancer efficiency of polymer-based

doxorubicin prodrugs in the treatment of subcutaneous murine B16F10 melanoma. *British Journal of Cancer*, **70,** 636-641.

Sgouras, D. & Duncan, R. (1990). Methods for the evaluation of biocompatibility of soluble synthetic polymers which have potential for biomedical use: 1- Use of the tetrazolium-based colorimetric assay (MTT) as a preliminary screen for evaluation of *in vitro* cytotoxicity. *Journal of Materials Science: Materials in Medicine*, **1,** 61-68.

Shaffer, S.A., Baker Lee, C., Nudelman, E., Kumar, A., Coon, M., Stone, I., de Vries, P. & Singer, J.W. (2002). Metabolism of poly-L-glutamic acid (PG) paclitaxel (CT-2103); proteolysis by lysosomal cathepsin B and identification of intermediate metabolites. *Proceedings of the American Association of Cancer Research*, **43,** #2067.

Shaffer, S.A. & Singer, J.W. (2004). Poly-L-glutamic acid (PG) drug conjugates: elucidation of cellular distribution and metabolism through *in vitro* and *in vivo* studies. *Proceedings of the 6th International Conference on Polymer Therapeutics: From Laboratory to Clinical Practice, Cardiff*, #21.

Shen, W.-C. & Ryser, H.J.-P. (1978). Conjugation of poly-L-lysine to albumin and horseradish peroxidase: novel method of enhancing the cellular uptake of proteins. *Proceedings of the National Academy of Sciences of the United States of America*, **75,** 1872-1876.

Shen, W.-C. & Ryser, H.J.-P. (1979). Poly(L-lysine) and poly(D-lysine) conjugates of methotrexate: different inhibitory effect on drug resistant cells. *Molecular Pharmacology*, **16,** 614-622.

Shepherd, V.E., Soos, M.A. & Siddle, K. (1995). Inhibitors of phosphoinositide 3-kinase block exocytosis but not endocytosis of transferrin receptors in 3T3-L1 adipocytes. *Biochemical and Biophysical Research Communications*, **211,** 535-539.

Sigismund, S., Woelk, T., Puri, C., Maspero, E., Tacchetti, C., Transidico, P., Di Fiore, P.P. & Polo, S. (2005). Clathrin-independent endocytosis of ubiquitinated cargoes. *Proceedings of the National Academy of Sciences of the United States of America*, **102,** 2760-2765.

Simon, S.M., Roy, D. & Schindler, M. (1994). Intracellular pH and the control of multidrug resistance. *Proceedings of the National Academy of Sciences of the United States of America*, **91,** 1128-1132.

Simons, K. & Ikonen, E. (1997). Functional rafts in cell membranes. *Nature*, **387,** 569-572.

Singer, J.W. (2004). Poly-L-glutamic acid (PG) drug conjugates: an overview of development from the bench to phase III. *Proceedings of the 6th International Conference on Polymer Therapeutics: From Laboratory to Clinical Practice, Cardiff*, #1.

Skovsgaard, T. (1977). Transport and binding of daunorubicin, adriamycin, and rubidazone in Ehrlich ascites tumour cells. *Biochemical Pharmacology*, **26,** 215-222.

Sloane, B.F., Dunn, J.R. & Honn, K.V. (1981). Lysosomal cathepsin B: correlation with metastatic potential. *Science*, **212,** 1151-1153.

Sloane, B.F., Honn, K.V., Sadler, J.G., Turner, W.A., Kimpson, J.J. & Taylor, J.D. (1982). Cathepsin B activity in B16 melanoma cells: a possible marker for metastatic potential. *Cancer Research*, **42,** 980-986.

Sloane, B.F., Rozhin, J., Johnson, K., Taylor, H., Crissman, J.D. & Honn, K.V. (1986). Cathepsin B: association with plasma membrane in metastatic tumours. *Proceedings of the National Academy of Sciences of the United States of America*, **83,** 2483-2487.

Sludden, J., Boddy, A.V., Griffin, M.J., Robson, L., Todd, R., Cassidy, J., Bissett, D., Main, M., Brannan, M.D., Elliott, S., Verrill, M. & Calvert, H. (2001). Phase I and pharmacological study of CT-2103, a poly(L-glutamic acid)-paclitaxel conjugate. *Proceedings of the American Association of Cancer Research*, **42,** #2883.

Smith, P.K., Krohn, R.I., Hermanson, G.T., Mallia, A.K., Gartner, F.H., Provenzano, M.D., Fujimoto, E.K., Goeke, N.M., Olson, B.J. & Klenk, D.C. (1985). Measurement of protein using bicinchoninic acid. *Analytical Biochemistry*, **150,** 76-85.

Snyder, S.L. & Sobocinski, P.Z. (1975). An improved 2,4,6-trinitrobenzenesulfonic acid method for the determination of amines. *Analytical Biochemistry*, **64,** 284-288.

Sosnowski, B.A., Gonzalez, A.M., Chandler, L.A., Büchler, Y.J., Pierce, G.F. & Baird, A. (1996). Targeting DNA to cells with basic fibroblast factor (FGF2). *Journal of Biological Chemistry*, **271,** 33647-33653.

Spragg, S.P. & Steensgaard, J. (1992). Theoretical aspects of practical centrifugation. In *Preparative Centrifugation: A Practical Approach*, Rickwood, D. (ed) pp. 1-42. Oxford University Press: Oxford.

Steinman, R.M., Mellman, I.S., Muller, W.A. & Cohn, Z.A. (1983). Endocytosis and the recycling of plasma membrane. *Journal of Cell Biology*, **96,** 1-27.

Stinchcombe, J., Bossi, G. & Griffiths, G.M. (2004). Linking albinism and immunity: the secrets of secretory lysosomes. *Science*, **305,** 55-59.

Stiriba, S.-E., Frey, H. & Haag, R. (2002). Dendritic polymers in biomedical applications: from potential to clinical use in diagnostics and therapy. *Angewandte Chemie International Edition in English*, **41,** 1329-1334.

Stirling, J. (1983). Beta-N-acetylhexosaminidase. In *Methods of Enzymatic Analysis*, Bergmeyer, H.U., Bergmeyer, J. & Graßl, M. (eds), Vol. 4. pp. 269-277. Verlag Chemie: Weinheim.

Stockert, R.J. (1995). The asialoglycoprotein receptor: relationships between structure, function, and expression. *Physiological Reviews*, **75,** 591-609.

Subr, V., Srohalm, J., Ulbrich, K., Duncan, R. & Hume, I. (1992). Polymers containing enzymatically degradable bonds, XII. Effect of spacer structure on the rate of release of daunomycin and adriamycin from poly(N-(2-hydroxypropyl)-methacrylamide) copolymer drug carriers *in vitro* and antitumour activity measured *in vivo*. *Journal of Controlled Release*, **18,** 123-132.

Subtil, A., Gaidarov, I., Kobylarz, K., Lampson, M.A., Keen, J.H. & McGraw, T.E. (1999). Acute cholesterol depletion inhibits clathrin-coated pit budding. *Proceedings of the National Academy of Sciences of the United States of America*, **96,** 6775-6780.

Suh, J., Paik, H.-J. & Hwang, B.K. (1994). Ionisation of polyethylenimine and polyallylamine at various pH's. *Bioorganic Chemistry*, **22,** 318-327.

Suh, J., Wirtz, D. & Hanes, J. (2003). Efficient active transport of gene nanocarriers to the cell nucleus. *Proceedings of the National Academy of Sciences of the United States of America*, **100,** 3878-3882.

Supino, R., Mariani, M., Colombo, A., Prosperi, E., Croce, A.C. & Bottiroli, G. (1992). Comparative studies on the effects of doxorubicin and differentiation

inducing agents on B16 melanoma cells. *European Journal of Cancer*, **28A**, 778-783.

Suzuki, M., Matsukawa, A., Kato, T., Sakamoto, N., Takahashi, K., Takimoto, C., LoRusso, P., Soepenberg, O., Wente, M., Friess, H., Kamida, M., Langman, S., de Jager, R., Wanders, J., Verweij, J. & Rowinsky, E. (2004). Results of DE-310 (macromolecular carrier conjugated DX-8951) phase I studies. *Proceedings of the 6th International Conference on Polymer Therapeutics: From Laboratory to Clinical Practice, Cardiff*, #26.

Swaan, P.W. (1998). Recent advances in intestinal macromolecular drug delivery via receptor-mediated transport pathways. *Pharmaceutical Research*, **15**, 826-834.

Swanson, J.A. & Watts, C. (1995). Macropinocytosis. *Trends in Cell Biology*, **5**, 424-428.

Swanson, J.A., Yirinec, B.D. & Silverstein, S.C. (1985). Phorbol esters and horseradish peroxidase stimulate pinocytosis and redirect the flow of pinocytosed fluid in macrophages. *Journal of Cell Biology*, **100**, 851-859.

Tajarobi, F., El-Sayed, M., Rege, B.D., Polli, J.E. & Ghandehari, H. (2001). Transport of polyamidoamine dendrimers across Madin-Darby canine kidney cells. *International Journal of Pharmaceutics*, **215**, 263-267.

Talieri, M., Papadopoulou, S., Scorilas, A., Xynopoulos, D., Arnogianaki, N., Plataniotis, G., Yotis, J. & Agnanti, N. (2004). Cathepsin B and cathepsin D expression in the progression of colorectal adenoma to carcinoma. *Cancer Letters*, **205**, 97-106.

Tang, M.X., Redemann, C.T. & Szoka, F.C.J. (1996). *In vitro* gene delivery by degraded polyamidoamine dendrimers. *Bioconjugate Chemistry*, **7**, 703-714.

Terwogt, J.M.M., ten Bokkel Huinink, W.W., Schellens, J.H.M., Schot, M., Mandjes, I.A.M., Zurlo, M.G., Rocchetti, M., Rosing, H., Koopman, F.J. & Beijnem, J.H. (2001). Phase I clinical and pharmacokinetic study of PNU166945, a novel water-soluble polymer-conjugated prodrug of paclitaxel. *Anti-Cancer Drugs*, **12**, 315-323.

Thanou, M. & Duncan, R. (2003). Polymer-protein and polymer-drug conjugates in cancer therapy. *Current Opinion in Investigational Drugs*, **4**, 701-709.

Tijerina, M., Kopeckova, P. & Kopecek, J. (2001). The effects of subcellular localisation of N-(2-hyrdoxypropyl)methacrylamide copolymer-Mce_6 conjugates in a human ovarian carcinoma. *Journal of Controlled Release*, **74**, 269-273.

Tijerina, M., Kopeckova, P. & Kopecek, J. (2003). Correlation of subcellular compartmentalisation of HPMA copolymer-Mce_6 conjugates with chemotherapeutic activity in human ovarian carcinoma cells. *Pharmaceutical Research*, **20**, 728-737.

Tipton, K.F. (1992). Principles of enzyme assay and kinetic studies. In *Enzyme Assays: A Practical Approach*, Rickwood, D. & Hames, B.D. (eds) pp. 1-58. The practical approach series. Oxford University Press: Oxford.

Tkachenko, E. & Simons, M. (2002). Clustering induces redistribution of syndecan-4 core protein into raft membrane domains. *Journal of Biological Chemistry*, **277**, 19946-19951.

Tokes, Z.A., Rogers, K.E. & Rembaum, A. (1982). Synthesis of adriamycin-coupled polyglutaraldehyde microspheres and evaluation of their cytostatic activity.

Proceedings of the National Academy of Sciences of the United States of America, **79,** 2026-2030.

Tolleshaug, H., Chindemi, P.A. & Regoeczi, E. (1981). Diacytosis of human asialotransferrin type 3 by isolated rat hepatocytes. *Journal of Biological Chemistry*, **256,** 6526-6528.

Tomalia, D.A., Baker, H., Dewald, J., Hall, M., Kallos, G., Martin, S., Roeck, J., Ryder, J. & Smith, P. (1985). A new class of polymers: Starburst-dendritic macromolecules. *Polymer Journal*, **17,** 117-132.

Tomalia, D.A. & Durst, H.D. (1993). Genealogically directed synthesis: starburst/cascade dendrimers and hyperbranched structures. In *Topics in Current Chemistry*, Weber, E., Dewar, M.J.S., Dunitz, J.D., Hafner, K., Ito, S., Lehn, J.-M., Raymond, K.N., Rees, C.W., Thiem, J. & Vögtle, F. (eds), Vol. 165. pp. 193-313. Springer-Verlag: Berlin.

Tomalia, D.A., Naylor, A.M. & Goddard, W.A. (1990). Starburst dendrimers: molecular-level control of size, shape, surface chemistry, topology, and flexibility from atoms to macroscopic matter. *Angewandte Chemie International Edition in English*, **29,** 138-175.

Tritton, T.R. (1991). Cell surface actions of adriamycin. **49,** 293-309.

Trouet, A., Deprez-de Campeneere, D. & De Duve, C. (1972). Chemotherapy through lysosomes with a DNA-daunorubicin complex. *Nature New Biology*, **239,** 110-112.

Trouet, A. & Jolles, G. (1984). Targeting of daunorubicin by association with DNA or protein: a review. *Seminars in Oncology*, **11,** S64-S72.

Trouet, A. & Tulkens, P. (1981). Intracellular penetration and distribution of antibiotics: the basis for an improved chemotherapy of intracellular infections. In *The Future of Antibiotherapy and Antibiotic Research*, Ninet, L., Bost, P.E., Bouanchaud, D.H. & Florent, J. (eds) pp. 337-349. Academic Press: London.

Tulkens, P., Beaufay, H. & Trouet, A. (1974). Analytical fractionation of homogenates from cultured rat embryo fibroblasts. *Journal of Cell Biology*, **63,** 383-401.

Tulkens, P. & Trouet, A. (1978). The uptake and intracellular accumulation of aminoglycoside antibiotics in lysosomes of cultured rat fibroblasts. *Biochemical Pharmacology*, **27,** 415-424.

Tuma, P.L. & Hubbard, A.L. (2003). Transcytosis: crossing cellular barriers. *Physiological Reviews*, **83,** 871-932.

Tuvim, M.J., Adachi, R., Hoffenberg, S. & Dickey, B.F. (2001). Traffic control: Rab GTPases and the regulation of interorganellar transport. *News of Physiological Science*, **16,** 56-61.

Uchegbu, I.F., Ringsdorf, H. & Duncan, R. (1996). The lower critical solution temperature of doxorubicin polymer conjugates. *Proceedings of the International Symposium for Controlled Release of Bioactive Materials*, **23,** #791.

UKCCCR. (2000). UKCCCR guidelines for the use of cell lines in cancer research. *British Journal of Cancer*, **82,** 1495-1509.

Ulbrich, K. & Subr, V. (2004). Polymeric anticancer drugs with pH-controlled activation. *Advanced Drug Delivery Reviews*, **56,** 1023-1050.

Vale, R.D. (2003). The molecular motor toolbox for intracellular transport. *Cell*, **112**, 467-480.

Van Deurs, B., Röpke, C. & Thorball, N. (1984). Kinetics of pinocytosis studied by flow cytometry. *European Journal of Cell Biology*, **34**, 96-102.

Vasanthakumar, G. & Ahmed, N.K. (1986). Comparative uptake, retention and cytotoxicity of daunorubicin by human myeloid cells. *Biochemical Pharmacology*, **35**, 1185-1190.

Vasey, P.A., Kaye, S.B., Morrison, R., Twelves, C., Wilson, P., Duncan, R., Thomson, A.H., Murray, L.S., Hilditch, T.E., Murray, T., Burtles, S., Fraier, D., Frigerio, E. & Cassidy, J. (1999). Phase I clinical and pharmacokinetic study of PK1 N-(2-hydroxypropyl)methacrylamide copolymer doxorubicin): First member of a new class of chemotherapeutic agents: drug-polymer conjugates. *Clinical Cancer Research*, **5**, 83-94.

Vassault, A. (1983). Lactate dehydrogenase. In *Methods of Enzymatic Analysis: Enzymes I Oxidoreductases, Transferases*, Bergmeyer, U., Bergmeyer, J. & Graßl, M. (eds), Vol. 3. pp. 118-126. Methods in Enzymatic analysis. Verlag Chemie: Basel.

Vicent, M.J., Paul, A., Griffiths, P.C. & Duncan, R. (2004). Using small angle neutron scattering (SANS) to evaluate the conformation of PK1 and PK2: a potential explanation for their clinical behaviour. *Proceedings of the 6th International Conference on Polymer Therapeutics: From Laboratory to Clinical Practice, Cardiff*, #50.

Vigevani, A. & Williamson, M.J. (1980). Doxorubicin. In *Analytical Profiles of Drug Substances*, Florey, K. (ed), Vol. 9. pp. 246-274. Academic Press: London.

Von Harpe, A., Petersen, H., Li, Y. & Kissel, T. (2000). Characterisation of commercially available and synthesised polyethylenimines for gene delivery. *Journal of Controlled Release*, **69,** 309-322.

Voura, E., Jaiswal, J.K., Mattoussi, H. & Simon, S.M. (2004). Tracking metastatic tumour cell extravasation with quantum dot nanocrystals and fluorescence emission-scanning microscopy. *Nature Medicine*, **10,** 993-998.

Wade, N., Bryant, N.J., Connolly, L.M., Simpson, R., Luzio, J.P., Piper, R.C. & James, D.E. (2001). Syntaxin 7 complexes with mouse Vsp10p tail interactor 1b, syntaxin 6, vesicle-associated membrane protein (VAMP)8, and VAMP7 in B16 melanoma cells. *Journal of Biological Chemistry*, **276,** 19820-19827.

Wadia, J.S., Stan, R.V. & Dowdy, S.F. (2004). Transducible TAT-HA fusogenic peptides enhances escape of TAT-fusion proteins after lipid raft macropinocytosis. *Nature Medicine*, **10,** 310-315.

Wagner, E. (1999). Application of membrane-active peptides for non-viral gene delivery. *Advanced Drug Delivery Reviews*, **38,** 279-289.

Wang, L.-H., Rothberg, K.G. & Anderson, R.G.W. (1993). Miss-assembly of clathrin lattices on endosomes reveals a regulatory switch for coated pit formation. *Journal of Cell Biology*, **123,** 1107-1117.

Watson, J.D. & Crick, F.H.C. (1953). Molecular structure of nucleic acids. A structure for deoxyribose nucleic acid. *Nature*, **171,** 737-738.

Wattiaux, R., Jadot, M., Dubois, F., Misquith, S. & Wattiaux-De Coninck, S. (1995). Uptake of exogenous DNA by rat liver: Effect of cationic lipids. *Biochemical and Biophysical Research Communications*, **213,** 81-87.

Wattiaux, R., Jadot, M., Laurent, N., Dubois, F. & Wattiaux-De Coninck, S. (1996). Cationic lipids delay the transfer of plasmid DNA to lysosomes. *Biochemical and Biophysical Research Communications*, **227,** 448-454.

Wattiaux, R., Laurent, N., Wattiaux-De Coninck, S. & Jadot, M. (2000). Endosomes, lysosomes: their implication in gene transfer. *Advanced Drug Delivery Reviews*, **41,** 201-208.

Watts, C. (1985). Rapid endocytosis of the transferrin receptor in the absence of bound transferrin. *Journal of Cell Biology*, **100,** 633-637.

Wedge, S. (1991). Mechanism of action of polymer anthracyclines: potential to overcome multidrug resistance. *PhD Thesis Keele University.*

Wedge, S.R., Duncan, R. & Kopeckova, P. (1991). Comparison of the liver subcellular distribution of free daunomycin and that bound to galactosamine targeted N-(2-hydroxypropyl)methacrylamide copolymers, following intravenous administration in the rat. *British Journal of Cancer*, **63,** 546-549.

Whitesides, G.M. (2003). The 'right' size in nanobiotechnology. *Nature Biotechnology*, **21,** 1161-1165.

Wightman, L., Kircheis, R., Rössler, V., Carotta, S., Ruzicka, R., Kursa, M. & Wagner, E. (2001). Differential behaviour of branched and linear polyethylenimine for gene delivery *in vitro* and *in vivo*. *The Journal of Gene Medicine*, **3,** 362-372.

Williams, K.E., Kidston, E.M., Beck, F. & Lloyd, J.B. (1975). Quantitative studies of pinocytosis. I. Kinetics of uptake of [^{125}I]polyvinylpyrrolidone by rat yolk sac cultured *in vitro*. *Journal of Cell Biology*, **64,** 113-121.

Wiwattanapatapee, R., Carreno-Gomez, B., Malik, N. & Duncan, R. (2000). Anionic PAMAM dendrimers rapidly cross adult rat intestine *in vivo*: A potential oral delivery system? *Pharmaceutical Research*, **17,** 991-998.

Wu, G.Y. & Wu, C.H. (1987). Receptor-mediated *in vitro* gene transformation by a soluble DNA carrier system. *Journal of Biological Chemistry*, **262,** 4429-4432.

Xyloyiannis, M. (2004). Poly(ethylene glycol) (PEG)-poly(ester) dendritic hybrids: biocompatibility and effect of architecture on cellular pharmacokinetics. *PhD Thesis University of Wales*.

Xyloyiannis, M., Padilla de Jesus, O.L., Frechet, J.M.J. & Duncan, R. (2003). PEG-dendron architecture influences endocytic capture and intracellular trafficking. *Proceedings of the International Symposium for Controlled Release of Bioactive Materials*, **30,** #149.

Yan, S., Sameni, M. & Sloane, B.F. (1998). Cathepsin B and human tumor progression. *Biological Chemistry*, **379,** 113-123.

Yoo, H. & Juliano, R.L. (2000). Enhanced delivery of antisense oligonucleotides with fluorophore-conjugated PAMAM dendrimers. *Nucleic Acid Research*, **28,** 4225-4231.

Yoo, H., Sazani, P. & Juliano, R.L. (1999). PAMAM dendrimers as delivery agents for antisense oligonucleotides. *Pharmaceutical Research*, **16,** 1799-1804.

Zaro, J.L. & Shen, W.C. (2003). Quantitative comparison of transduction and endocytosis of oligopeptides. *Biochemical and Biophysical Research Communications*, **307,** 241-247.

Zenebergh, A., Baurain, R. & Trouet, A. (1984). Cellular pharmacology of detorubicin and doxorubicin in L1210 cells. *European Journal of Cancer and Clinical Oncology*, **20**, 115-121.

Zenebergh, A., Schneider, Y.-J. & Trouet, A. (1981). Enzymatic characterisation and analytical fraction of L1210 cells. *Biochimie*, **63**, 411-418.

Zhou, B.-K., Boissy, R.E., Pifko-Hirst, S., Moran, D.J. & Orlow, S.J. (1993). Lysosome-associated membrane protein-1 (LAMP-1) is the melnocyte vesicular membrane glycoprotein band II. *Journal of Investigative Dermatology*, **100**, 110-114.

Zuhorn, I.S., Kalicharan, R. & Hoekstra, D. (2002). Lipoplex-mediated transfection of mammalian cells occurs through the cholesterol-dependent clathrin-mediated pathway of endocytosis. *Journal of Biological Chemistry*, **277**, 18021-18028.

Appendix I

Appendix I

Abstracts

F.P. Seib, A.T. Jones and R. Duncan (2004). Endocytic capture and intracellular trafficking: Effect of polymer architecture. *Proceedings of the International Symposium of Controlled Release of Bioactive Materials* **31**: #717

F.P. Seib, M. Xyloyiannis, N. Pattrick, N. Malik, R. Wiwattanapatapee and R. Duncan (2004) Intracellular trafficking of polymeric nanomedicines. *National Science week: Britain's Young Scientists, Engineers and Technologists, House of Commons, London*

F.P. Seib, A. Hann, A.T. Jones and R. Duncan (2003). Establishing a quantitative subcellular fractionation method in B16F10 cells; Use to monitor the intracellular trafficking of polymer therapeutics. *Proceedings of the International Symposium of Controlled Release of Bioactive Materials* **30**: #520

Primary Publications

F.P. Seib, A.T. Jones and R. Duncan (2004). Establishing a quantitative subcellular fractionation method in B16F10 cells to monitor the intracellular trafficking of polymer-bound and free doxorubicin. *Journal of Controlled Release* (To be submitted)

F.P. Seib, A.T. Jones and R. Duncan (2004). Pinocytosis of linear, branched and dendritic polycations. *Journal of Controlled Release* (To be submitted)

Appendix II

Endocytosis and Trafficking of
Polymer Therapeutics in Melanoma Cells
F. Philipp Seib

Fluorescent Images

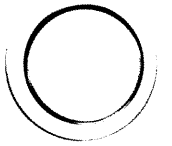

2005
Centre for Polymer Therapeutics
Cardiff University
United Kingdom